Modelling aeciospore release, dispersal and disease transmission to inform wheat rust management

Vanessa Bueno Sancho

A thesis submitted to the University of East Anglia for the degree of Doctor of Philosophy

John Innes Centre
September 2020

Abstract

Wheat rust pathogens have been threatening agriculture all through history and they currently cause big economic loses every year. Investigating how these pathogens are able to spread and the key aspects of host-pathogen dynamics is vital for the design of appropriate control strategies. Two of the most damaging pathogens that require more careful monitoring are *Puccinia graminis tritici* (*Pgt*), that causes wheat stem rust, and *Puccinia striiformis* f. sp. *tritici* (*Pst*), cause of wheat yellow rust. Here, I have studied the process of aeciospore dispersal for *Pgt*, beginning with aeciospore release. Aeciospore release was recorded using high-speed videography and the velocity of ejection was estimated. Aeciospores are observed to release in clusters to achieve greater distances and their ejection is not affected by the temperatures tested here (5-37ºC). Humidity is the key factor in aeciospore release, and it leads to their increase in volume, which was also measured in this thesis. A model of how this occurs is also proposed here. The dispersal process of *Pgt* aeciospores is also investigated, by evaluating the number of aeciospores that can be produced in barberry bushes. A Gaussian Plume model is used to predict how far aeciospores can travel, including real-time weather data gather using an API. This model was included into a user-friendly website to make the model accessible to the widest demographic. This tool can help identify the barberry bushes that present a higher risk and thus prioritise them for careful monitoring. Finally, the dynamics of *Pst* population in the UK at a field level is studied here. To do so, I developed a quick method for genotyping *Pst*-infected wheat samples collected from the field to determine which race they belong to. Using this method, I analysed samples collected all through the wheat growing season (December-June) for two consecutive years (2015-16 and 2016-17). Results indicate that one race (Warrior -) has become predominant in the UK and that seasonality for different races is observed. However, the presence of Pst races in one season was not indicative of prevalence of the same race in following seasons. In summary, this thesis provides tools to improve wheat rust management, both for stem and yellow rust at different levels. First, by trying to predict *Pgt* aeciospore release and dispersal to avoid future epidemics and secondly, with a quick genotyping method that can lower the costs of yellow rust surveillance.

People are the most important resource in science

Vanessa Bueno Sancho[1]
[1]John Innes Centre, UK. vbuens@gmail.com

Introduction

Doing a PhD is never easy, but it helps when you have scientists near you willing to read your thesis, care for you and guide you through the difficult path of research (and mathematics) [1,2,3]. However, there are many other factors conducive to a successful (i.e. completed) thesis. After four years of research, my observations and conclusions are portrayed here.

Methods

Acknowledgements are ordered by date of occurrence, when possible.

Results and Discussion

Surrounding yourself by experts leads to better science

The contents of this thesis would not have been possible had I been deprived of the colleagues with whom I was blessed. The first steps in the lab are never easy, hence I can never endorse enough the best teacher that spared 48 hours prior leaving for Switzerland and all the subsequent hours solving my enquiries [4]. Likewise, the mentor who guided me in my first LSF steps, R and even statistics, while teaching me all I know about wheat [5]. Having a referent scientist nearby helped me learn review papers and even understand *popgen* (ish) [6].

Summer students help you increase your mentoring skills while doing your work, both things you find displeasing such as infecting plants/designing primers [7] or dull such as spore counting [8]. The help of angels fallen from the sky, especially when doing fieldwork shall never be forgotten [9]. Sample collectors are sometimes underrated but driving long distances to gather the most needed material is not a trivial task [10,11,12]. As Mr. R. Feynman stated in his thesis, no attempt is made at mathematical rigor here. But if there ever was, credit belongs to my modelling mentors [3,13,27]. As an enthusiast of imaging, my greatest gratitude goes towards the team of experts that achieved the astonishing pictures included in this document [14]. Last, but definitely not least, discussions not only provide ideas but help clear one's mind. To all the brilliant minds who shared their time listening and providing the most needed advice [4,5,6,15,16].

The importance of a support system

Some people will never know the big part they took in this work. Even if not directly, to them I owe the strength that I needed to get to where I am.

The originals that were there since the beginning [4,5,6] and all the colleagues that brightened my days [16], with their craziness [17] and support. Office hours and lunch/tea breaks have been crucial in my well-being. Sharing memes has become the greatest form of support [18,19,25]. Much support is needed from people who are at your same stage [18,20], and I'll never forget our nights with Ross [20]. When away from home, flatmates become your family and mine made my days much better [21].

Science can darken even the brightest of days, and inspirations are needed on those days to remind you the reason why everything started [3,22]. Life consists of sharing moments with people that are (hopefully) at your same stage. Thus, this also goes to you with whom I managed to share few moments of happiness [23].

Also, to my future dog, who never left my mind during these four years and reminded me the things that truly matter in life [24].

Por ultimo, agradecer al Comité por amenizarme los largos días de trabajo [25]. Y en especial a las 4 maravillas, por todo su apoyo incondicional, no solo durante estos 4 años, sino durante los últimos 20 y los siguientes 60 (con suerte) [26]. A mis padres [27], por dármelo todo (el interés en las matemáticas incluido), por su paciencia y apoyo incondicional. No habría llegado hasta aquí sin vosotros. Y a mi hermana, la primera Dr. Bueno [28], mi modelo a seguir y la razón por la que he acabado en ciencia.

Conclusion

People who got to know me during these past four years are aware of my disappointment towards the academic system. I have witnessed reprehensible behaviour from people at all stages (but sadly, more frequent in seniors) and I can only hope that this changes in the future.

Science is the greatest tool of humanity, it has given us knowledge, entertainment and even life. I believe that studying nature (or technology) to contribute to the world is the most noble profession. However, science is impossible without humility. I'd only wish scientists were more aware of that. My love for science will forever remain, despite of where I am. I wish one day this emotion can be expanded to Academia too.

There's a stranger staring at the ceiling, rescuing a tiger from a tree. The pictures in her head are always dreaming, each of them means everything to me [29].

References

[1] Dr. Diane Saunders.

[2] Prof. Richard Morris.

[3] Dr. Mark Blyth.

[4] Dr. Nicola M. Cook.

[5] Dr. Pilar Corredor Moreno.

[6] Dr. Antoine Persoons.

[7] Francesca Minter.

[8] Morgan Gerrity.

[9] Phoebe Davey.

[10] Dr. Christopher Judge.

[11] Dr. Elizabeth Orton.

[12] Dr. Clare Lewis.

[13] Dr. Nick Cunniffe.

[14] Photography team: Kim Findlay, Elaine Barclay, Phil Robinson.

[15] Dr. Guru Radhakrishnan.

[16] Past and present members of the lab: Andrey, Ashley, Ayako, Cassandra, Clare, Elizabeth, Fran, Jessica, Morgan, Phoebe, Rebecca, Tamsin, Tom.

[17] Rebecca Doherty / Becky / Chewbecky

[18] Dr. Samuel Vega Estevez

[19] Dr. Thomas Adams

[20] Cassandra Jensen

[21] Mottramers: Roger, Estela, Eli

[22] Nicholas P. Money, Arthur Henry Reginald Buller, Daniel Kahneman.

[23] You know who you are, and I shall preserve thee in my memory forever

[24] My beautiful future dog/s

[25] Eduardo Marco, Sergio Fes, Diego Torrome. Y las cuatro maravillas [26].

[26] Pilar Calvo Ballano, Elena Ceacero Gamez, Alicia Diaz Franc, Julia Doñate Cuartero.

[27] Maria Rosa Sancho Andrés, Julián Bueno Remacha.

[28] Dr. Jessica Bueno Sancho.

[29] Blink-182.

Table of Contents

Table of Figures

Table of Tables

Abbreviations

API	Application Programming Interface
BGRI	Borlaug Global Rust Initiative
BIC	Bayesian Information Criterion
BR	Brown Rust
DAPC	Discriminant Analysis of Principal Components
DNA	Deoxyribonucleic acid
ELISA	Enzyme-Linked Inmmunosorbent Assay
GBS	Genotyping by sequencing
GP	Gaussian Plume
GRRC	Global Rust Reference Center
HS	High-Speed
HSD	Turkey's Honestly Significant Difference
KASP	Kompetitive Allele Specific PCR
LAI	Leaf Area Index
LAMP	Loop-Mediated Isothermal Ampification
ML	Machine Learning
MVC	Model-View-Controller
NIAB	National Institute of Agricultural Botany
NGS	Next Generation Sequencing
PCR	Polymerase Chain Reaction
PDF	Probability Density Function
Pg	*Puccinia graminis*
Pst	*Puccinia striiformis* f. sp. *tritici*
Pt	*Puccinia triticina*
Re	Reynolds number
RH	Relative Humidity

RNA	Ribonucleic acid
SEM	Scanning Electron Microscopy
S.D.	Standard Deviation
S.E.	Standard Error
SNP	Single Nucleotide Polymorphism
SPRI	Solid-Phase Reversible Immobilisation
SR	Stem Rust
TEM	Transfer Electron Microscopy
UAV	Unmanned Aerial Vehicle
UK	United Kingdom
UKCPVS	United Kingdom Crop Pathogen Virulence Survey
YR	Yellow Rust

Chapter 1:
General Introduction

Chapter 1 General Introduction

1.1 The importance of wheat and other cereal crops

The demand for crop production is ever rising as the world population increases and meat, dairy and biofuel consumption becomes more prevalent (Ray, Mueller, West, & Foley, 2013). By 2050, predictions of a global population of more than 10 billion[1] people mean that an extra 200,000 billion calories per annum are needed (Daniel P. Bebber & Gurr, 2015). Cereal crops currently provide around 25 % of the total protein intake of humankind, and wheat in particular provides around 20 % of the total calories consumed worldwide (FAO, 2019). Wheat is grown on more area than any other crop, occupying 22 % of the cultivated area worldwide (Leff, Ramankutty, & Foley, 2004). In the United Kingdom (UK), around 70 % of the total land area is reserved for horticultural and arable crops. More than 20 % of this land is devoted to cereal crops, with wheat and barley being the most predominant (DEFRA, 2016).

The increasing crop demand could imply an expansion of the arable land area, although studies show that it is more sustainable to improve crop yields instead of clearing more land for agriculture (Ray, Ramankutty, Mueller, West, & Foley, 2012). However, crop yields are not only no longer improving, but are in constant danger due to both abiotic and biotic factors. Abiotic factors include global warming, water crises and land degradation and biotic factors comprise pests and pathogens such as insects, viruses, bacteria, fungi and oomycetes (Daniel P. Bebber & Gurr, 2015). These can cause large yield losses, with up to 50 % of all global potential wheat yield being lost to diseases every year (Oerke & Dehne, 2004). Examples of this include the suni bug (*Eurygaster integriceps*) that affects developing countries (Dizlek & Özer, 2016), the wheat yellow mosaic virus (K. Singh, Wegulo, Skoracka, & Kundu, 2018), or *Septoria* spp. (Fones & Gurr, 2015). Out of all these biotic factors, pest and pathogens are the greatest threat to food security, accounting for approximately 21% of crop loses (Savary et al., 2019). On top of this, the distribution of crop pest and pathogens is currently changing and many pathogens have recently expanded their range to new locations which can lead to an even bigger loss of crop yields over time (Bebber, 2015).

[1] Note: the use of "billion" in this thesis corresponds to 1,000 million, as oppose to 1,000,000 million as it is the case in most of continental Europe and Spanish-speaking countries.

1.2 Wheat rusts diseases: a major threat to wheat production

1.2.1 A threat since the beginning of agriculture

One of the main pests that affect wheat are rust diseases caused by filamentous fungi from the order Pucciniales, division Basidiomycota (Oerke & Dehne, 2004). Rusts are obligate biotrophic plant pathogens and many of them infect agriculturally important crops such as wheat, barley, oat, soybean and coffee (Helfer, 2014). Rust diseases are one of the most economically significant diseases in wheat, causing losses of around 1 billion $USD every year (Beddow et al., 2015). There are three major wheat rusts: stem (black) rust, leaf (brown) rust and stripe (yellow) rust, caused by *Puccinia graminis* f. sp. *tritici (Pgt)*, *Puccinia triticina* (*Pt*) and *Puccinia striiformis* f. sp. *tritici* (*Pst*) respectively (Figueroa, Hammond-Kosack, & Solomon, 2018).

Out of all the three rusts, stem rust (SR) has had the greatest importance historically, causing large epidemics in most parts of the world. It has been a major problem since the beginning of agriculture, when Romans sacrificed animals to protect their crops, praying to the stem rust god 'Robigus'. Since then, it has been prevalent in the Middle East, Europe, America, Australia, New Zealand, all of Africa and Asia (Ravi P. Singh et al., 2008). In more recent history, SR was considered a disease of lower significance in most parts of the world largely due to the use of resistant wheat varieties (Shank 1994). However, the emergence of a new race called Ug99 in Uganda in 1998 raised the alarm as it carried virulence to one of the main resistance genes used in wheat (Ravi P. Singh et al., 2011). Since then, variants of this race have merged and propagated to Central Asia and the Middle East. More recently, one of these races termed Digalu has been found in several European countries (Olivera Firpo et al., 2017; Olivera et al., 2015).

Even though less attention has been paid to brown rust (BR), it is the most globally distributed of all the rusts, being present in all wheat production areas in the world (Aoun et al., 2020). This disease is more severe in warmer climates such as Central Asia, the Mediterranean Great Plains in north America and South America (M. Liu, Rodrigue, & Kolmer, 2014). With climate change and the arrival of milder summers, *Pt* is however increasing its prevalence in areas previously too cold.

Yellow rust (YR) is also present in most wheat growing areas, being found today in more than 60 countries (Duan et al., 2010). Before the 2000s, the *Pst* global population was distributed into seven *Pst* races mainly based on geographical origin (Thach, Ali, de Vallavieille-Pope, Justesen, & Hovmøller, 2016). However, recently more aggressive races have appeared, adapted to warmer climates, which has led to a geographical expansion of

this pathogen (Beddow et al., 2015; Milus, Seyran, & McNew, 2006). Now, it is reported to be the most economically damaging wheat rust today and therefore it needs to be constantly monitored to avoid epidemics (Hodson, 2011; Schwessinger, 2016).

1.2.2 Wheat rust life cycle

All three wheat rust pathogens have complicated heteroecious life cycles that include five types of spores: urediniospores, teliospores, basidiospores, pycniospores and aeciospores (**Figure 1.1**), and two plant hosts: wheat (*Triticum aestivum*) and an alternate *Berberis* host for *Pgt* and *Pst*, with common barberry (*Berberis vulgaris*) being especially notable due to its high level of susceptibility to *Pgt* and widespread occurrence. *Pt* however has different alternate hosts, mainly from the *Ranunculaceae* family (**Table 1.1**), depending on geographical location (Samborski, 1985). While the alternate hosts of *Pgt* and *Pt* were discovered almost a century ago (A P Roelfs, Singh, & Saari, 1992), the alternate host of *Pst* had remained a mystery until lately (Jin, 2011).

Table 1.1. Primary and alternate hosts of wheat rust pathogens. Adapted from (A P Roelfs et al., 1992; R P Singh, Huerta-Espino, & Roelfs, 2002).

Pathogen	Disease	Predominant primary Host	Alternate Host
Puccinia striiformis f. sp. *tritici*	Stripe (yellow) rust	Wheat	*Berberis* spp, *Mahonia* spp
Puccinia graminis f. sp. *tritici*	Stem (black) rust	Wheat	*Berberis* spp, *Mahonia* spp
Puccinia triticina	Leaf (brown) rust	Wheats, triticale	*Thalictrum, Anchusa, Isopyrum, Clemantis*

The presence of the alternate host is required to complete the sexual cycle, whereas when these pathogens infect wheat (the so-called 'primary host'), they undergo asexual reproduction with the production of urediniospores (Xue, Chi, Shu-zhen, & Zuo-fu, 2012). When a urediniospore lands on the surface of a susceptible wheat leaf, it germinates and enters the underlying tissue through open stomata. Inside of the host, the pathogen forms haustoria through which it is able to get nutrients and secrete effector proteins to manipulate the host immune response (Panstruga & Dodds, 2009). During this asexual phase on wheat, the fungus produces haploid dikaryotic urediniospores with two haploid

nuclei that can mutate independently leading to high levels of heterozygosity (Mogens S Hovmøller, Sørensen, Walter, & Justesen, 2011). Around two weeks after the infection starts, the pathogen will re-emerge on the wheat leaf surface, disrupting the tissue, with the formation of pustules called uredia that are responsible for the name of this disease, as the colour resembles rust on metal. Each one of these pustules contains thousands of urediniospores that will be expelled, leading to reinfection cycles of wheat in just one season. These cycles can continue during spring and summer until the host senesces or until environmental conditions are not optimal (R P Singh et al., 2002).

At the end of the growing season, the pathogen can form telia and produce dikaryotic teliospores (**Figure 1.1**). These spores merge their nuclei (karyogamy) and then undergo meiosis with sexual recombination that generates genetic diversity, producing four haploid basidiospores that will infect the alternate host (W. Chen, Wellings, Chen, Kang, & Liu, 2014). After the infection of the alternate host is successful, the pathogen will form pycnia on the leaf, producing haploid pycniospores that can be either + or -. Pycniospores from one matting type will be transferred to hyphae of the opposite mating type to then merge and develop into aecia (Schwessinger, 2016). Each cluster of aecia is formed by several aecium, with every aecium (or aecial-cup) containing a different genotype. This process can happen several times, giving rise to several aecia that are genetically different. The aeciospores contained in the aecial-cups are then able to infect wheat (the 'primary host'), which will restart the asexual stage, in which the fungus can cycle for long periods. Even though the complete life cycle of wheat rusts includes two hosts and a sexual stage, the sexual cycle does not always occur and can be geographically restricted. In fact, to date, sexual reproduction of *Pst* has only been reported to take place in the near Himalayan region, where the genetic diversity of isolates is much higher compared to other regions (M. S. Hovmøller et al., 2016). In the rest of the world, including Europe, Africa, Americas, Australasia or the Middle East, the pathogen is reported to only undergo asexual reproduction (Ali et al., 2014). On the other hand, sexual reproduction for *Pgt* is much more widespread (Berlin, 2017). For *Pt*, sexual reproduction has not been widely reported, since this pathogen population has been shown to be highly clonal for a long time (McCallum, Seto-Goh, & Xue, 2017).

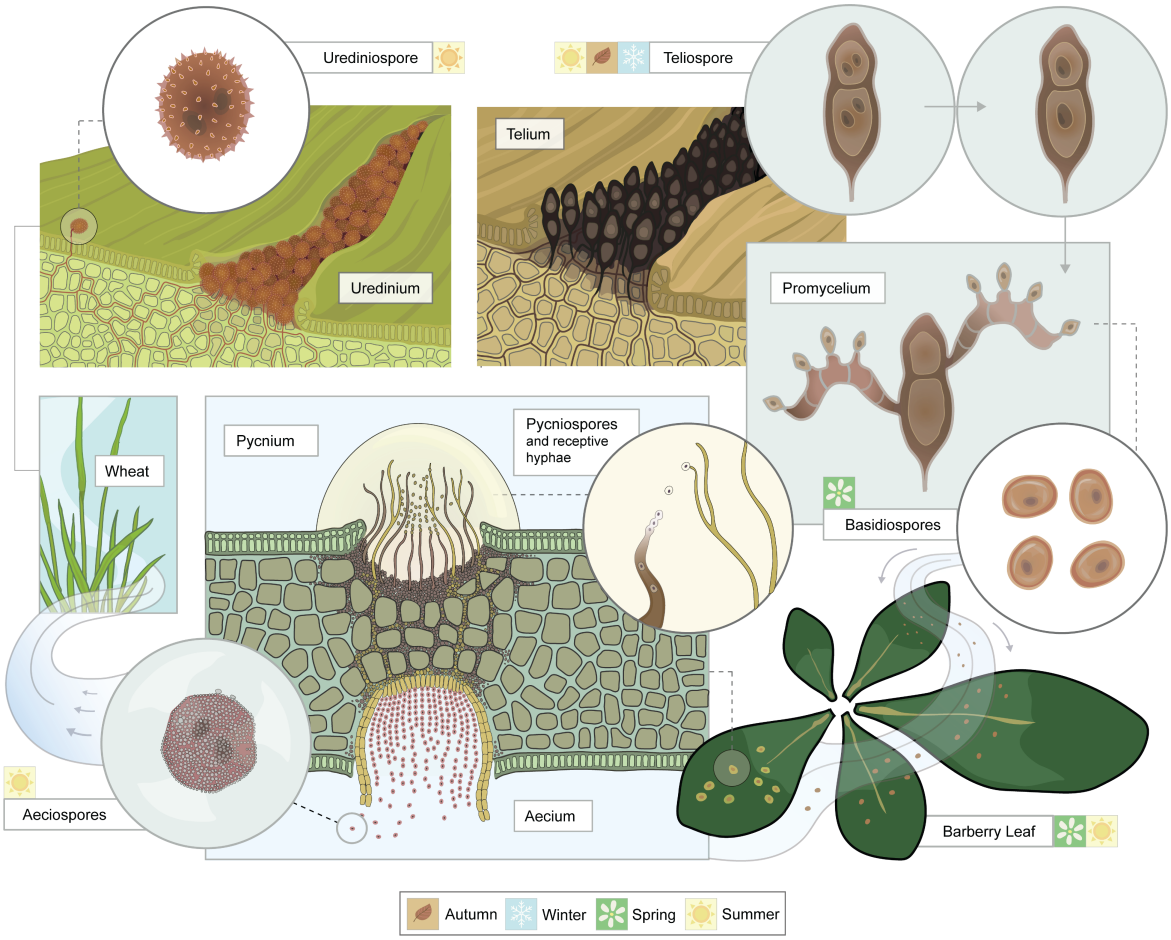

Figure 1.1. Life cycle of the wheat yellow or stem rust pathogens. The asexual cycle carried out in wheat leads to production of urediniospores (n+n) and teliospores (2n) at the end of the season. The nuclei of the teliospores merges and undergoes meiosis to produce basidiospores (n) that will go and infect barberry. In the alternate host, the pathogen will produce pycniospores (n) that will merge and produce aecium containing aeciospores (2n) that can infect wheat thus re-starting the cycle. Image extracted from (Bueno-Sancho, Lewis, & Saunders, 2020).

1.2.3 Environmental factors affecting wheat rust diseases

Climate conditions are critical for the development of all plant diseases, but they are particularly relevant in the case of wheat rusts (Jon S. West, Townsend, Stevens, & Fitt, 2012). Seasonal variables such as temperature affect both the pathogen life cycle and host growth, modifying infection rates and the length of the latency period (X. M. Chen, 2005). There are three main factors that have an important effect on the rate of success of these pathogens: humidity, temperature and wind (X. M. Chen, 2005). Firstly, humidity is required for infection of the host, spore germination and survival, which is why wheat rusts are typically found in moist-weather regions, as the rate of infection increases under high moisture conditions. Urediniospores usually need at least 1-3 hours of humidity to germinate directly and 6-8 hours of dew period for the infection process to take place (X. M. Chen, 2005). Germination temperatures are distinct for the different wheat rusts, with *Pgt* and *Pt* ranging between 2 – 30 ºC, with an optimum of 15-24 ºC for *Pgt* and an optimum of 20 ºC for *Pt* (Junk, Kouadio, Delfosse, & El Jarroudi, 2016; Prank, Kenaley, Bergstrom, Acevedo, & Mahowald, 2019; A P Roelfs et al., 1992). For *Pst* urediniospores to germinate, temperatures typically ranged from 3-20 ºC, with an optimum of 10-15 ºC, which is lower than for *Pgt* and *Pt* (A P Roelfs et al., 1992; R. Singh, Mahmoudpour, Rajkumar, & Narayana, 2017). However, from the 2000s, *Pst* isolates have been found in warmer climates with reported optimum germination temperature of 18ºC, explaining their adaptation to higher temperatures (X. M. Chen, 2005). These are important factors that affect the development of wheat rust and thus have to be taken into account when developing control strategies.

1.3 Controlling fungal diseases remains a challenge

Wheat rust management has been done mainly through the use of resistant varieties and fungicide application. Breeding to incorporate resistance genes has been very useful in controlling wheat rusts (Chaves et al., 2013). However, fungal pathogens are able to overcome resistance quickly if it is encoded by a single resistance gene (Ayliffe, Singh, & Lagudah, 2008). A more durable resistance can be achieved by stacking several resistance genes in wheat varieties, but the discovery of resistance genes to include into commercial cultivars is a lengthy and costly process that sometimes can also lead to a decrease in yield (Oliver & Hewitt, 2014; Wulft & Moscou, 2014). On the other hand, fungicides are commonly used by farmers and their application is a great tool to help control several fungal diseases at once (Hirooka & Ishii, 2013). However, fungicides are very expensive, and pathogens are able to acquire resistance which can cause severe yield losses (Olivera Firpo et al., 2017). The high cost of these strategies sometimes cannot be assumed at large scales and selection

of an appropriate scale for fungicide application is needed. This can present a challenge due to cryptic information about spread of infection (C. a Gilligan, Truscott, & Stacey, 2007). Thus, understanding pathogen transmission and disease development is key to design both appropriate surveillance systems and control strategies to avoid further spread (R. K. Meentemeyer et al., 2011).

1.3.1 Models can be used to optimise disease management strategies

Managing a plant disease presents a great challenge because the resources are usually limited and determining when, where and how to invest these precious resources typically requires a high knowledge of epidemic dynamics (Cunniffe, Cobb, Meentemeyer, Rizzo, & Gilligan, 2016). Control of epidemics includes understanding the scale of management, early detection of the disease and removal of infected plants, as well as prevention of the epidemics itself (C. a Gilligan et al., 2007). However, detection of the pathogen is not always easy as they frequently have long incubation periods that lead to cryptic information, making it difficult to stop the disease before it spreads (Cunniffe, Koskella, et al., 2015). Therefore, finding cost-effective strategies that can either control or eradicate pathogen spread is necessary. Mathematical modelling can help build better management systems by using knowledge on disease spread to generate predictive models of disease dynamics.

Previously developed models have focused on (i) disease control, (ii) design of surveillance programs or (iii) risk forecasting. Firstly, disease control based on breeding programs has been modelled to improve their efficiency (Cooper et al., 2009). Models have also been developed to evaluate fungicide resistance dynamics and to detect the best spraying strategy to avoid the appearance of resistance (Hobbelen, Paveley, Oliver, & Van Den Bosch, 2013; van den Bosch & Gilligan, 2008). Different spraying methods can be easily tested by simulation modelling to optimise disease control (Dammer, Wollny, & Giebel, 2008; Elderfield, Lopez-Ruiz, Van Den Bosch, & Cunniffe, 2018). Modelling has also helped detect the optimal point of chemical control usage needed to maintain sufficient crop yields while keeping the fungicide costs low (Caffi & Rossi, 2018; Silva Junior et al., 2016; Teng, Blackie, & Close, 1978). Secondly, mathematical modelling can also help improve surveillance by selecting sites to monitor based on information from models, which has proved to be more accurate than randomly choosing sites (Cunniffe, Stutt, DeSimone, Gottwald, & Gilligan, 2015). Indeed, surveillance programs have already been designed to manage plant pest invasions using Bayesian modelling (Stanaway, Mengersen, & Reeves, 2011). Thirdly, risk forecasting has been a huge help in managing plant disease epidemics (Gaydos, Petrasova, Cobb, & Meentemeyer, 2019; Shah, Paul, De Wolf, & Madden, 2019). Models can therefore provide very useful information to improve management strategies of plant diseases.

In fact, modelling has been previously applied to the study of plant diseases such as the Sudden oak death in the US to investigate the effect of different management systems on disease spread (Cunniffe et al., 2016). They found that increasing the management of the disease at the beginning of the epidemic can improve control, and that selection of plants for removal using models enhanced the successful management of disease. This is a clear example of how models can optimise management of an established plant disease and how model-based optimisation of resources during disease management can enhance the probability of success (Cunniffe et al., 2016). The UK Government is in fact already using epidemiological models to predict the progression of tree diseases such as Chalara dieback of ash, and also *Phytophthora ramorum* and *Phytophthora kernoviae*, pathogens that are responsible for several diseases that can lead even to their death. The models for these pathogens monitor their spread and likely future impacts (National Statistics, 2015). Effective methods for plant disease management are necessary and mathematical models that are able to characterise pathosystems and subsequently predict their dynamics can be very useful to optimise control efficiency.

1.4 The process of modelling plant diseases

Mathematical models applied to study disease development can be generally classified into two types: descriptive or conceptual. The first ones are based on generalization of experimental results. These can also be predictive models if they help forecast the occurrence and severity of a disease (El Jarroudi et al., 2017). Conceptual models on the other hand explain specific events or processes in the development of the disease/epidemics (van Maanen & Xu, 2003).

Modelling a disease is a complex process and several aspects need to be considered. First of all, the initial production of the inoculum in the first infection. Then the dispersal of the inoculum, which will be defined by a dispersal kernel that measures the dynamics of the pathogen (Kot, Lewis, & Driessche, 1996). Finally, the subsequent probability of infection after dispersal. In addition, models can include parameters such as host susceptibility, pathogen reproduction and landscape composition. Production of inoculum can either be described as a stochastic process (R. K. Meentemeyer et al., 2011) or be defined based on known parameters that are related to environmental conditions (C. A. Gilligan & Van Den Bosch, 2008). Understanding how inoculum is produced and released is also important when studying the process of disease development (Gregory, 1968). Dispersal of the pathogen can be separated into local and long-distance (R. K. Meentemeyer et al., 2011). In the case of wheat rusts, local dispersal is usually driven by wind and/or rain, whereas long distance dispersal can be associated with both global wind currents and anthropogenic

activities due to movement of infected materials or spores in clothing (C. R. Wellings, 2007). However, long-distance spread is very difficult to measure, and it is generally excluded from the simpler models (R. Meentemeyer, Rizzo, Mark, & Lotz, 2004). The posterior probability of infection once the pathogen has been disseminated will depend not only on the dispersal process but also other factors such as weather conditions, host susceptibility and pathogen aggressiveness.

1.4.1 Dispersal kernel estimation

One of the main key challenges when studying the dynamics of a disease is to determine the dispersal kernel, that is, the probability distribution of the distance travelled by the pathogen responsible for the disease (Nathan, Klein, Robledo-Arnuncio, & Revilla, 2012). Estimation of dispersal kernels is a complex process. Defining a dispersal kernel presents three main challenges related to the uncertainty of the process. First of all, the risk of falling under over-simplifications of the model by disregarding important variables (variation of environment, or population). Second of all, determining the parameters for the model. Finally, dispersal has an intrinsic stochastic nature that enhances the difficulty to be determined (Clark, Lewis, McLachlan, & HilleRisLambers, 2003). Kernels are defined as the probability density function (PDF) of a distribution and its shape varies regarding several factors such as the navigation capacities of the pathogen (how it can spread), the landscape composition or biotic interactions (Nathan et al., 2008). The 'fatness' of the distribution tail, that defines how fast the PDF decreases towards zero, is also an important aspect to consider since it is directly related to population dynamics. Nevertheless, sometimes the differences between one dispersal kernel or another are minor and can only be detected by improving the observation design, which entails a huge increase in the sampling time and costs (Nathan et al., 2012). Besides, assuming dispersal kernels are constant throughout the season is a mistake and it is more realistic to include meteorological or geographical variables (Cunniffe, Koskella, et al., 2015; Rieux et al., 2014).

1.4.2 Environmental conditions also play a crucial role in dispersal

Finding the right balance between details in the model and oversimplification is often challenging. There are temporal heterogeneities during the year that need to be taken into account, like environmental changes between seasons that can either initiate or end an epidemic (Hamelin, Bisson, Desprez-Loustau, Fabre, & Mailleret, 2016). Climatic factors not only affect the development of the disease within the plant, but also the spread of the pathogen and how it will infect the host after primary infection (X. M. Chen, 2005). For example, dispersal can be greatly affected by humidity, as in the case for wheat rust

pathogens. Under humid conditions, urediniospores tend to cluster that can adhere strongly to the leaf, increasing the infection frequency. Rain also helps the pathogen spread by releasing spores directly in the field (Rapilly, 1979). If at the end of the summer the weather is dry and hot, urediniospores that are produced on late-harvested wheat will be able to survive the summer (Sharma-Poudyal, Chen, & Rupp, 2014). That would mean that they will be able to infect wheat planted in early autumn. Despite the apparent importance of rain and temperature in dispersion, wind is the main driver for spore dispersal since it transports them to the next host. In addition, it can dry urediniospores, reducing germination but increasing the possibilities of spore survival (Geagea et al., 2000). The type and direction of the wind can directly indicate the scale of epidemics of wheat rusts, and how early they can occur (Rapilly, 1979). Thus, including environmental variables when modelling disease dispersal is crucial to be able to represent the full picture of the process.

1.4.3 Modelling in an agricultural landscape

Landscape properties are known to have an impact on pathogen behaviour and how disease spreads. Despite its high influence on plant diseases, they are usually ignored when building epidemiological models (Hess et al., 2002). However, landscape composition can affect the inoculum density, the pathogen dynamics, pathogen occurrence, the genetic structure of the pathogen population, pathogen genetic diversity and pathogen dispersal (Plantegenest, Le May, & Fabre, 2007). For example, the host density in the landscape (and the frequency of different kinds of patches in an area) determines not only the amount of inoculum, but is also a limiting factor for disease spreading, existing a threshold under which a pathogen cannot infect a population (Otten & Gilligan, 2006). Presence of different phylogenetic-related hosts (such as the primary and the alternate host) in the same landscape can also vary the pathogen behaviour in several ways. An alternative host can decrease the disease prevalence or, on the contrary, be used as a reservoir for the pathogen to survive until the conditions for spreading are optimal, increasing disease prevalence (Plantegenest et al., 2007). Likewise, high levels of host genetic diversity alter the structure of pathogen populations, leading to large genetic diversity in the pathogen which increases the probabilities of emergence of a virulent race (Gérard, Husson, Pinon, & Frey, 2006; Papaïx, Goyeau, Du Cheyron, Monod, & Lannou, 2011). This is particularly important for *Pst*, since its high levels of genetic diversity have led to long-distance migration and overcoming of resistance genes (M. S. Hovmøller, Justesen, & Brown, 2002). Moreover, different strains of the pathogen can influence the spread of each other, and this information is key to predict disease dynamics. Different races can have different behaviour in the same host and therefore competition between them affects the dispersal of the disease (Hamelin et al.,

2016). Therefore, it is crucial to understand the landscape composition as it directly affects disease dynamics and its study allows us to (i) design better strategies for crop protection by taking into account its characteristics (Plantegenest et al., 2007) and (ii) rearrange landscape structures to reduce the initial risk and thus disease spread (Peter Skelsey, Rossing, Kessel, & van der Werf, 2010).

1.5 Mathematical modelling to control wheat rust diseases

Many mathematical models have been applied to wheat rusts to study several aspects including inoculum production and release, disease dispersal patterns and epidemic forecasting based on environmental factors. Disease development has been investigated through models of latent period duration for SR (Hernandez Nopsa & Pfender, 2014). The release and posterior dispersal of *Pst* urediniospores by raindrop impact has also been modelled (Kim, Park, Gruszewski, Schmale, & Jung, 2019). Spore dispersal by wind has been examined for both *Pst* (El Jarroudi et al., 2020) and *Pt* urediniospores (Pfender, Graw, Bradley, Carney, & Maxwell, 2006). Models of spore dissemination have indeed helped forecast YR disease risk (Newlands, 2018) and predict YR epidemics in the US (Sharma-Poudyal et al., 2014). Spore transport models have also facilitated the investigation of migration routes for *Pgt* and helped build an understanding regarding when and how so many spores could be dispersed in the Middle East, East Africa and Central/South Asia (Meyer, Burgin, Hort, Hodson, & Gilligan, 2017). Models of spore deposition have been able to predict severity of leaf rust disease (Scott A. Isard & Chamecki, 2015).

However, weather factors have shown to be key in disease development and most forecasting models have focused on this aspect (El Jarroudi et al., 2017; Luo & Zeng, 1995). Thus, environmental factors that affect key processes such as initial infection, latent period and infectious period have been taken into account to develop disease progression models for BR (Rossi, Racca, Giosue', Pancaldi, & Alberti, 1997). Models of YR show that temperature, dew period and light quantity are the key factors for disease progression (Rodríguez-Moreno, Jiménez-Lagunes, Estrada-Avalos, Mauricio-Ruvalcaba, & Padilla-Ramírez, 2020). Several models have also been developed more recently to predict disease based on these environmental conditions for both YR (El Jarroudi et al., 2017, 2020) and BR (Junk et al., 2016). The effect of climate change has also been investigated thanks to mathematical modelling to predict the incidence and severity of SR and BR (Launay et al., 2020; Prank et al., 2019). Despite the wide range of models that have been developed for wheat rust diseases, most of them are focused on urediniospores and there is a lack of information about aeciospore release and dispersal. Furthermore, most disease

transmission models ignore the pathogen population which can be a key factor in dispersal (Papaïx et al., 2011).

1.6 Introduction to the current study

Wheat rust diseases continue to pose a great threat to global food security and the lack of durable resistance genes plus the possible increase in fungicide resistance only enhance the risk of these diseases. Understanding pathogen transmission that leads to these diseases is therefore key to create better control strategies. Mathematical modelling can help increase our knowledge about a system when other empirical methods fall short. In this thesis, I aimed to gain a better understanding of transmission of wheat rust pathogens to inform wheat rust management, focusing on the following aspects:

1. Studying the process of aeciospore release by inspecting the key factors in the process and developing a model that describes the likely mechanism.
2. Evaluating the risk of barberry bushes near wheat fields by modelling aeciospore dispersal and developing an accessible tool for the wheat community.
3. Investigating the dynamics of the *Pst* population in the UK and developing a system to identify *Pst* races in a quick and inexpensive manner.

Chapter 2:

Decrypting the aeciospore release mechanism in Puccinia graminis

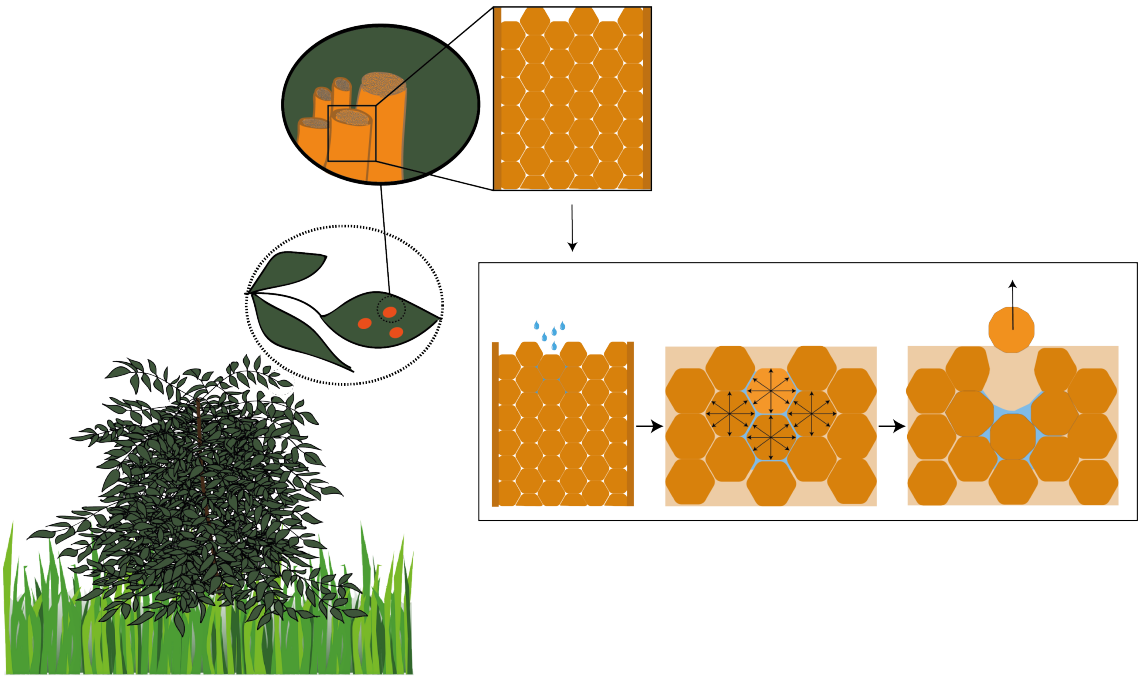

Chapter 2 Decrypting the aeciospore release mechanism in *Puccinia graminis*

2.1 Abstract

Understanding the process of how spores get released can give us an insight into when infection occurs and thereby help manage epidemics. Here I have investigated the mechanism of aeciospore discharge in *Puccinia graminis*, the fungus responsible for stem rust. High-speed videography was used to determine the release velocities of aeciospores and their full trajectory after ejection was recorded. The distance that aeciospores travelled after release was investigated under different temperature conditions and no difference was observed, indicating that temperatures within the range 5-37 ºC have minimal effect in aeciospore release. Aeciospores were found to be released in clusters to achieve greater distances (up to 7 cm). A significant increase in volume of aeciospores was observed when immersed in water, which confirms the hypothesis that aeciospores round-off under high RH conditions and this can lead to aeciospore release. A mathematical model was developed including the information gathered in this chapter that fits with observations of launch speeds. The results obtained here provide the first model of the aeciospore release mechanism and further support that water availability is the key factor in *Puccinia graminis* aeciospore release.

2.2 Introduction

2.2.1 Importance of studying spore release

For most fungal pathogens the process of dispersion starts with spores being liberated from their parental tissue with the final aim of infecting another susceptible host (Mahaffee & Stoll, 2016). Spore release is a vital step in the life cycle of fungi and is an important process to consider when evaluating disease outbreaks. Understanding the conditions that induce spore release is crucial to comprehend how many fungal pathogens spread. For instance, the mechanism of spore release can give us information about when spores are more likely to be found in the air and therefore initiate infections (Gregory, 1968). For example, fungi releasing spores under decreasing vapor pressure conditions tend to be found during early mornings (Chang, Blenis, & Hiratsuka, 1989), while fungi that depend on water for release are more likely to release at night (Hirst, 1953). Ascospores from *Mycosphaerella pinodes*

have been found to be liberated just before the dew period so they get deposited and can germinate when moisture is higher (Carter, 1963). The spore release mechanism has also been reported to affect disease symptoms, as in the case of *Mycosphaerella musicola* (Jones, 2003). This pathogen presents line or tip-spotting lesions depending on how their spores have been released (Meredith, 1973).

As epidemics are frequently proportional to the initial inoculum that is produced in the source, knowledge of the conditions under which the number of spores released increases can aid forecasting of epidemics (Gregory, 1961). For effective dispersal, fungi have to release a vast number of spores as the probability of a successful infection is low (Galante, Horton, & Swaney, 2011). Reducing this initial inoculum, for example by removing infected individuals, has been reported to be an effective way of controlling epidemics (White & Gilligan, 2006). Understanding the environmental conditions that would lead to a high rate of spore release can also be used to time fungicide application for more effective usage, as has been shown for *Leptosphaeria maculans* (West et al., 2002) and *Erysiphe necator* (Thiessen, Neill, & Mahaffee, 2017). Thus, understanding when and how spores are released can give us an insight into when a disease is more likely to occur, and the mechanisms involved, which can aid in the prediction and management of disease epidemics.

2.2.2 Fungal spores must overcome the boundary layer for effective dispersal

After air-borne spores are liberated, to be dispersed further they have to be carried by wind currents. When wind moves near a surface, the friction with the surface reduces the wind velocity until it reaches a null speed. This creates a layer of almost still air called the "boundary layer" whose thickness can vary depending on the surface (Schlichting & Gersten, 2000). Due to the small size of most fungal spores, even weak winds are able to carry spores long distances (Alastair McCartney, 1994). However, to reach the turbulent free wind stream a spore must first overcome the adhesive forces of this thin laminar boundary layer of still air that is found near the surface (**Figure 2.1 A**).

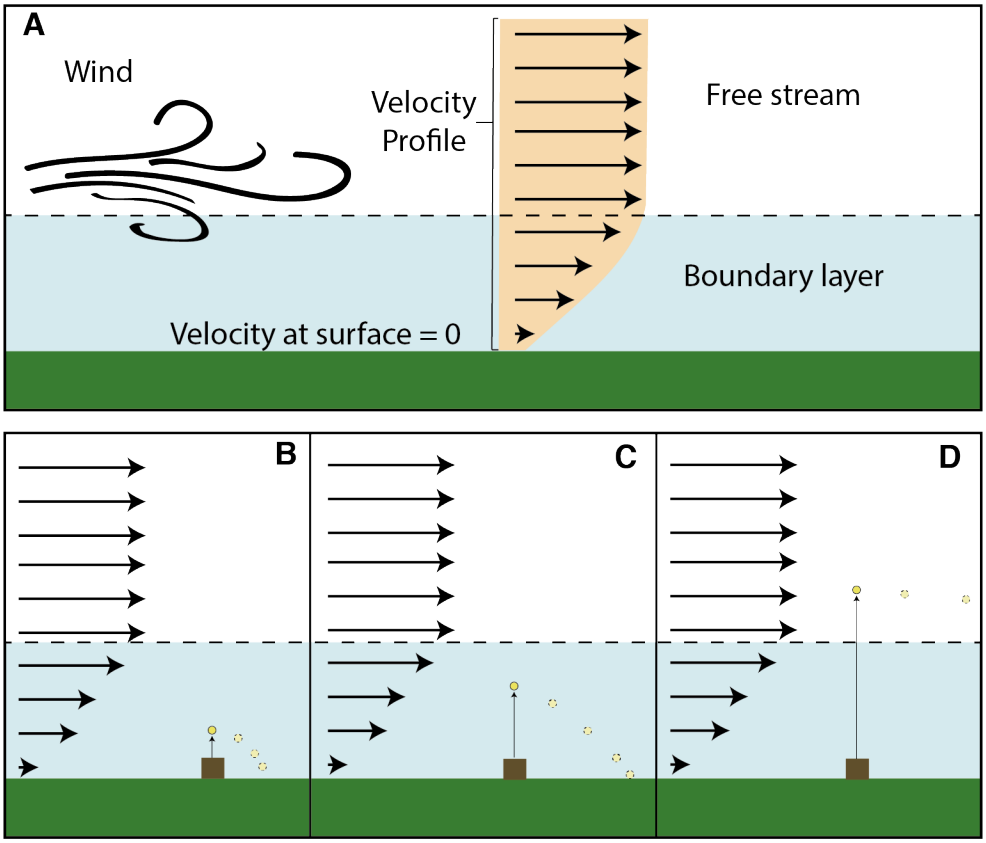

Figure 2.1. Fungal spores have to cross the boundary layer to reach the free air stream and be carried by the wind. A) Wind velocity decreases as it approaches a surface until reaching 0, creating a boundary layer of relatively still air. **B, C)** If spores can't cross the boundary layer, they will fall back somewhere very close to the initial place of liberation. **D)** If they enter the free stream, they can be carried by the wind more easily due to their small size. Inspired by (NASA, n.d.).

When a spore enters the air, force acts opposite to the motion of the spore, causing it to decelerate very quickly (Fischer, Stolze-Rybczynski, Cui, & Money, 2010). This force is commonly called aerodynamic drag (or air resistance) and is usually divided into two components: viscous and pressure drag. The Reynolds number (Re) is a ratio between the inertial and viscous forces and thus represents the importance of each force under certain conditions (Fox & McDonald, 1994). At large Re, the pressure drag would dominate (the case of macroscopic objects such as animals or plants), and at low Re, the viscous drag would be more relevant (Alexander, 2017). The latter is the case for spores entering the air and this drag can be represented as a viscous drag coefficient (ζ) that is linearly proportional to the spore size. This drag can be used to estimate the maximum distance (d) the spore can travel following the equation (Pringle, Brenner, Fritz, Roper, & Seminara, 2017):

$$d = V_{spore}\frac{m}{\zeta} \tag{2.1}$$

with the ratio mass-air drag (m/ζ) being equivalent to (assuming a spherical spore):

$$\frac{m}{\zeta} = \frac{2}{9}\frac{a^2\rho_{spore}}{\mu} \tag{2.2}$$

where m is the mass of the spore, a is the radius of the spore, ρ_{spore} is the density if the spore (considered roughly constant) and μ is the viscosity of the medium (in the case of the air, at 15 ºC: 1.81 x 10^{-5} kg/m/s). Knowing the initial release velocities, the maximum distance that a spore can travel under the effect of the viscous drag can be calculated with the following formula, under the assumption of single spores being released:

$$d = V_{spore}\frac{2}{9}\frac{a^2\rho_{spore}}{\mu} \tag{2.3}$$

For a spore to cross the boundary layer, the distance travelled should be higher than the thickness of the boundary layer (**Figure 2.1 B-D**). Thus, to be able to travel a distance large enough to enter the free air, fungi can act on several factors, as indicated in the formula. They can (i) increase spore velocity during release (Fritz, Seminara, Roper, Pringle, & Brenner, 2013), (ii) decrease the thickness of the boundary layer (Kinjo & Zang, 2001) or (iii) minimise the drag, for example by creating spores with drag-minimising shapes (Roper, Pepper, Brenner, & Pringle, 2008) or by coordinating spore ejection (Roper et al., 2010). However, minimising the drag by increasing mass would complicate subsequent wind dispersal. To overcome this, fungi such as *Ascobolus immerses* are able to cross the boundary layer by releasing spores as a conjugated mass that then disarticulate into single spores to

facilitate subsequent wind dispersal (Buller, 1909). Given the necessity of fungal spores to be dispersed as far as possible, fungi have developed all kinds of mechanisms to liberate their spores taking into account the barriers that they have to overcome.

2.2.3 Types of spore release in fungi

Spore liberation has been widely studied in fungi and their mechanisms for this process vary greatly depending on the species. Since spore propagation is the ultimate goal of fungi, they have developed specific mechanisms adapted to their environmental conditions to make sure spores are able to be dispersed as far as possible (Roper et al., 2010).

However, many species have not acquired any mechanical process to ensure spores enter the free air stream, and instead they rely on external factors. This type of mechanism is classified as "passive liberation" and it relies on external agents assisting spore dissemination (Alastair McCartney, 1994). Examples of passive liberation mechanisms include: shedding of spores under gravity or in convection currents like *Botrytis cinerea* (Chastagner, Ogawa, & Manji, 1978; Dobbs, 1942), spores being blown away by the wind like in the case of *Puccinia* urediniospores or moulds (Viljanen-Rollinson, Parr, & Marroni, 2007) (**Figure 2.2 A**). Another example is falling raindrops that create kinetic energy when they impact the plant and can help spore dispersal (Kim et al., 2019). This is the case of "puffball" mushrooms that need external forces (such as rain or small animals) to assist spores release (**Figure 2.2 B**). Certain fungi rely heavily on animals for the dispersal of their spores. This is the case of *Anthurus archeri* (also called stinkhorn) that contains spores in a "foul-smelling, sticky slime" that attract insects. When insects land on the fungus, spores get stuck to their body and then are transported (**Figure 2.2 C**). This is also the mechanism of *Puccinia monoica*, that mimics flowers in shape, fragrance and even nectar reward to attract insects (Raguso & Roy, 1998). Pycniospores of rust fungi are also believed to be carried by insects from barberry leaves (Kolmer, 2013). The spores of other fungi such as *Tuber melanosporum* are dispersed on faeces after passing through the digestive track of animals like wild boards or rodents (Piattoni, Oir, Morara, Iotti, & Zambonelli, 2013) (**Figure 2.2 D**). Despite the high number of fungi that have passive mechanisms, relying on external factors reduces the likelihood of success in spore propagation.

As an alternative strategy, many fungi have therefore developed active mechanisms of spore release to increase efficiency of dispersal (Ingold, 1999). These generally rely on the availability of water for the fungus, although some fungi have mechanisms that are independent of weather. The fruit-body will usually develop after a period of rain and then either discharge spores over a short time period or dry and start release when it gets re-

wet (Gregory, 1961). One very well studied process of active spore release is the ballistospore discharge mechanism in Basidiomycetes by the formation of the so-called "Buller's drop" (Buller, 1909). This process is divided into 3 steps. First, water condenses at the hilar appendix, forming the Buller's drop, and at the surface of the spore, forming the adaxial drop. Condensation then leads both drops to expand and fuse on the spore surface (**Figure 2.2 E**). This causes a redistribution of mass that gives momentum to the spore, ejecting the spore from the sterigma (Fischer, Stolze-Rybczynski, Cui, et al., 2010).

Another very well-known example of active liberations is the "squirt-gun" mechanism that is used by Ascomycetes where the ascus swells and ejects spores into the air (Trail, 2007). This process appears to be driven by osmosis (Money & Webster, 1989). When the accumulation of osmolytes inside the ascus leads to water passing through the membrane by osmosis, turgor pressure increases until reaching a critical pressure of 0.31-1.54 MPa (Money, 1994). This causes spores to be discharged violently with the liquid content from the ascus (**Figure 2.2 F)**. This type of explosive spore discharge has also been observed in other species such as Zygomycetes (e.g. *Pilobolus Crystallinus*), whose spores get released due to osmotic turgor pressure (Tuthill, 2005). Another active release mechanism, frequently observed in fungi imperfecti (Meredith, 1963), is cavitation-based. This occurs under dry conditions when cells dehydrate and their membrane shrinks, causing cell walls to cave inwards. This entails a deformation of the structure and increment in negative pressure that produces the emergence of a gas bubble (**Figure 2.2 G)**. The appearance of the cavitation bubble results in a release of the wall tension, which makes the structure return to its original shape (Sakes et al., 2016). Another interesting observed phenomenon of spore release in the Entomophthorales order is the rounding-off of turgid cells (Hughes, Cole, & Kendrick, 2007; Ingold, 1934) usually under high humidity. This is also thought to be the case for rust aeciospores, although the details are yet not clear (Buller, 1950).

Passive Liberation

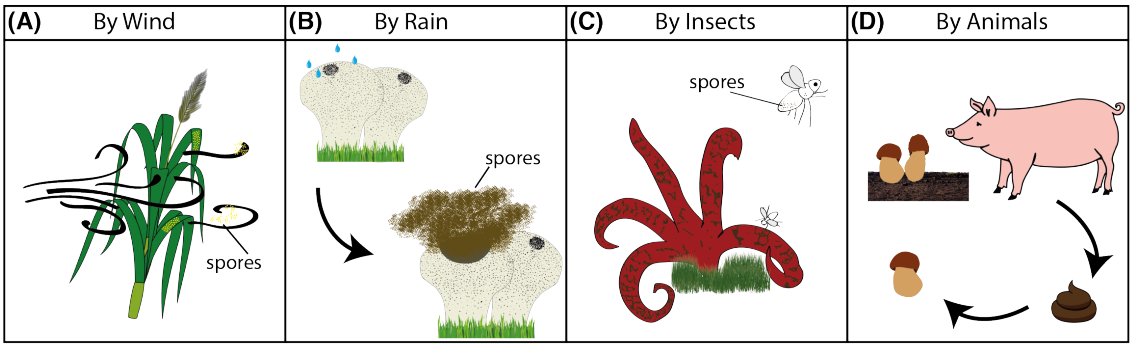

Active Liberation

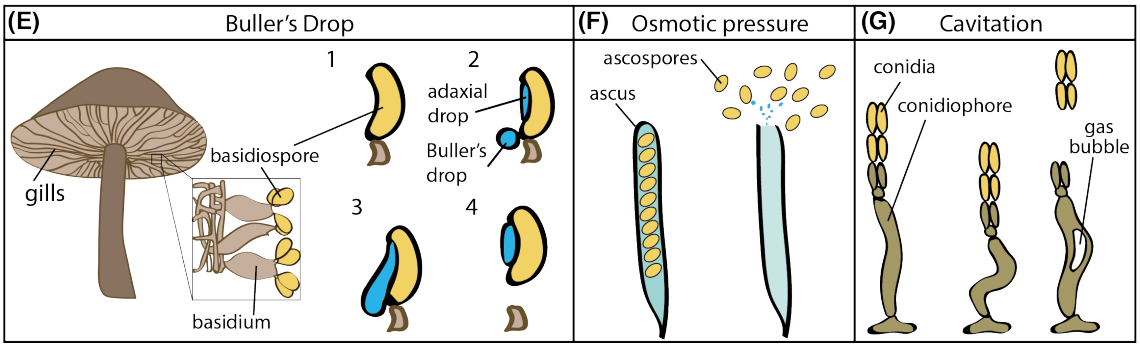

Figure 2.2. Spore release can be classified into 'passive' or 'active' liberation. Passive liberation can occur by **(A)** wind (Kim et al., 2019), **(B)** rain (Dixon, 1963), **(C)** insects (Burk, Flegler, & Hess, 1982) or **(D)** animals (Piattoni et al., 2013). Examples of active liberation include: **(E)** Buller's drop for basidiomycota (Buller, 1909; Stolze-rybczynski et al., 2009), **(E)** ascospore release by osmotic pressure (Trail, 2007) and **(F)** cavitation-based (Sakes et al., 2016). Drawings in F and G are adapted from (Sakes et al., 2016).

2.2.4 Aeciospore release in rusts

The production and dispersal of different types of spores produced by *Puccinia* rust fungi have been highly studied partly because of their economic importance (Helfer, 2014). Out of the five types of spores that *Puccinia* rust fungi produce, aeciospores are the ones carrying genotypes generated after the sexual cycle is completed through infection of *Berberis* as mentioned in the introduction (Berlin, Samils, & Andersson, 2017). Thus, the importance of aeciospores in the life cycle of these fungi makes them very interesting to study.

Aeciospores are formed inside fungal structures known as cluster cups or aecia that are formed on the abaxial side of barberry leaves. Different morphological types of aecia have been found in several rust species, that vary in a number of factors such as spore ontogeny or presence of intercalary cells (Sato & Sato, 1985). In the case of *Puccinia graminis* (*Pg*), the type of aecium is called aecidioid aecia that are cylindrical cup-like structures in which aeciospores are tightly packed forming rows (**Figure 2.3 A-B**). These aecia have a firm wall of cells called peridium that is formed by a one-cell layer of peridial cells (Singh, 1969). These peridial cells are usually hexagonal with walls of different thickness: a thinner one on the inner face and a thicker one of up to 8 μm in the outer face (Mims, Littlefield, & Heath, 1980) (**Figure 2.3 D**).

At the bottom of the aecial cups, basal cells (or aeciosporophores) (**Figure 2.3 C**) are in charge of forming aeciospore mother cells, also named aeciospore initials (**Figure 2.3 E**). These subsequently divide into a large aeciospore and a small disjuncture cell (or intercalary cell) (Rijkenberg & Truter, 1974)**.** These wedge-shaped intercalary cells occur in between aeciospores and eventually disintegrate to give place to the mature aeciospores (**Figure 2.3 F-I**). Mature aeciospores display knob-like ornamentation on their surface called verrucose o verrucae. The shape of this verrucose has been reported to vary for different rust fungi and can be used as a way of distinguishing between species (Lee & Kakishima, 1999; Wahyuno, Kakishima, & Ono, 2002). Aeciospores can also contain large granules on their surface in certain species, like *Pg* (**Figure 2.3 G-H**), whose function is unknown. However, this also varies between species, as it is not found in *Puccinia triticina* or *Puccinia coronata* (Gold, Littlefield, & Statler, 1979). It has been suggested that these granules can help in the process of spore release, but this has not been confirmed (Mims et al., 1980).

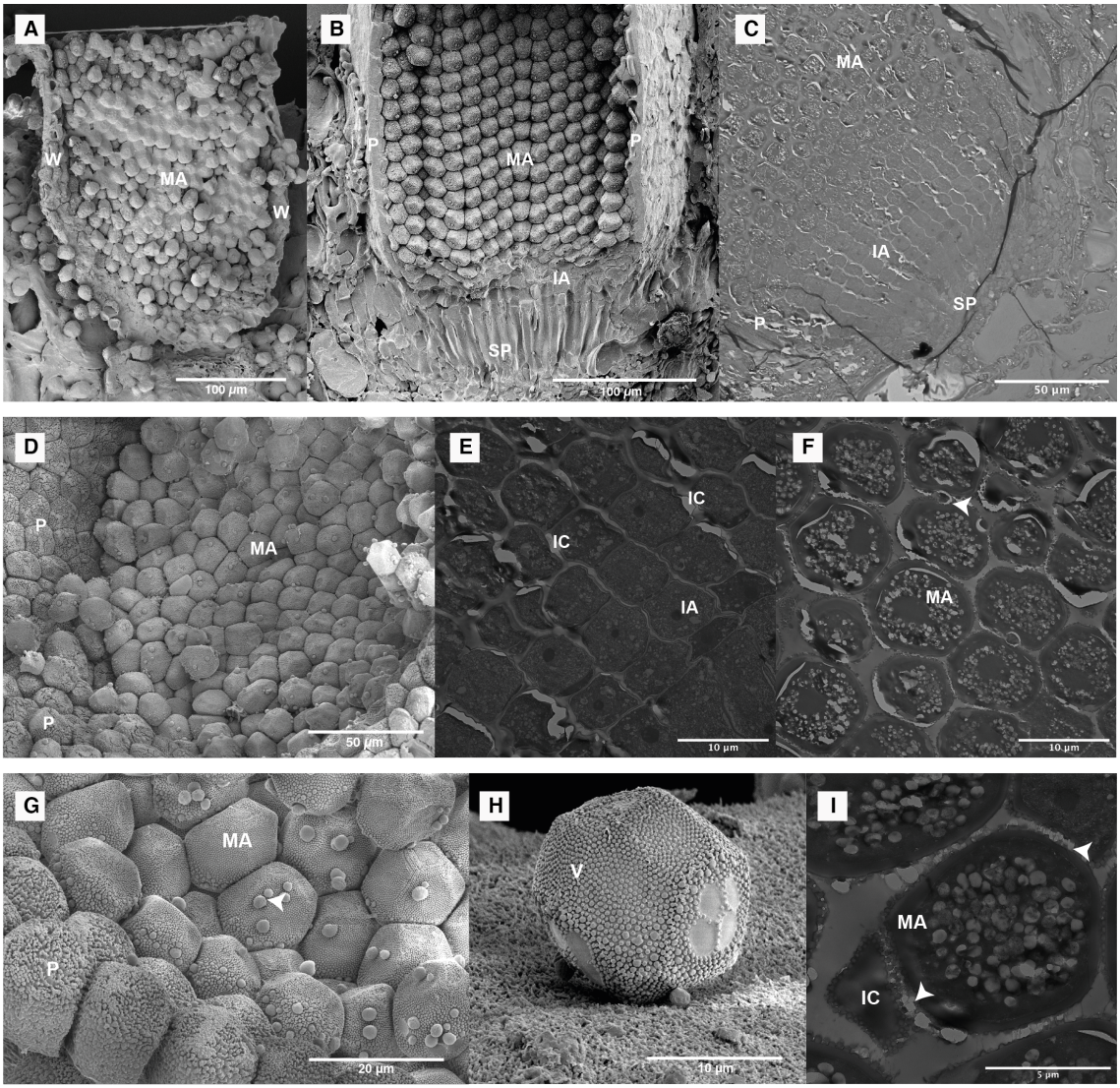

Figure 2.3. Aeciospores are tightly packed inside of aecial cups. (A) SEM images show aeciospores highly packed inside of aecial cups, forming rows **(B)**. **(C)** TEM imaging shows immature aeciospores are formed at the bottom of the cup and mature aeciospores are found towards the top. **(D)** At the top of the cup, mature aeciospores can be seen tightly packed together without any apparent order. TEM imaging of immature **(E)** and mature **(F)** aeciospores illustrates the little space between spores inside the cup. **(G)** A closer look at aeciospores shows they contain verrucae in their surface **(H)**. **(I)** Verrucae is found all around aeciospores and between each other. W: Cup Wall; P: Peridium cells; SP; Aeciosporophore; MA: Mature Aeciospores; IA: Immature Aeciospores; IC: Intercalary Cell; V: verrucae; arrow: verrucae granules. SEM images were taken by Kim Findlay and TEM by Elaine Barclay (John Innes Centre) as described in methods (sections **2.3.6** and **2.3.7** respectively).

Aeciospore discharge is thought to occur under high relative humidity (RH) conditions in Pucciniales containing aecidioid aecia. However, for some rust species with a different type of aecia (called roestelia), liberation has been associated with a decrease in humidity as in *Gymnosporangium juniperi-virginianae*. This fungus has the capacity to close its aecia when humidity is high and under low humidity, the outer layer of the peridial cells shrinks, causing the roestelia to open (Pady, Kramer, & Clary, 1969). This is due to the hygroscopic nature of its peridial cells that allows roestelia to open and close (fracture-release mechanism), unlike aecidioid aecia that once their peridium breaks, it remains open. This has however not been observed in all fungi that produce roestelia, since other *Gymnosporangium*, such as *G. clavipes*, are reported to release at 90% RH and as a possible consequence of the rounding-off of aeciospores after water intake (Pady et al., 1969). This is the same process that is believed to occur in Pucciniales, whose aeciospores are thought to be released when they expand into a spherical shape under high RH (Kramer, Pady, Clary, & Haard, 1968). Despite these indications, the actual mechanism of aeciospore release for *Puccinia* fungi remains unknown (Buller, 1958).

2.2.5 High speed videography can be used to observe spore release

The development of high-speed (HS) videography has given the opportunity to observe spore release in many species, such as *Adiantum peruvianum* (Poppinga, Haushahn, Warnke, Masselter, & Speck, 2015), *Selaginella martensii* (Schneller, Gerber, & Zuppiger, 2008) and in *Sphagnum* (Sundberg, 2010). In fungi, HS cameras have been used for a long time to observe the mechanism of discharge (Gregory, 1949). It has allowed the examination in detail of the process of ballistospore discharge in Basidiomycota via the Buller's drop (Noblin, Yang, & Dumais, 2009) and 'squirt-gun' in Ascomycota and Zygomycota (Yafetto et al., 2008). Videos recorded with a HS camera have also been used to predict trajectories of ballistospores for several basidiomycetes (M. W. F. Fischer, Stolze-Rybczynski, Cui, et al., 2010). Observing the process of spore discharge can thus help elucidate the mechanism of release (Dressaire, Yamada, Song, & Roper, 2016). HS videography offers an excellent opportunity to study aeciospore release since, despite the many studies, the actual process has not been previously observed due to the high velocity of discharge invisible to the human eye (Coons, 1910).

In this chapter, I have investigated how aeciospores are being released from aecial cups in *Pg*, the fungus responsible for Stem Rust (SR) and propose a model to explain how the release mechanism could take place. To do so, I used HS videography to observe the active release of *Pg* aeciospores and estimate the velocity at which they are ejected. In addition, I assessed how far away aeciospores initially travel after ejection and the effect of

temperature and water absorption in the release process. Using these data, I propose a model of how aeciospores may be actively released from aecial cups.

2.3 Methods

2.3.1 Sample collection

Barberry (*B. vulgaris*) leaves showing symptoms of SR infection were collected during the summer period of 2018 and 2019 from Chalk Road, Brandon, United Kingdom. Samples were collected from several common barberry bushes (cultivar is unknown) with the help of Phoebe Davey, Morgan Gerrity, Elizabeth Orton and Clare Lewis (Saunders Lab). After collection leaves were placed in boxes or 9 mm petri dishes and transported back to the laboratory.

2.3.2 Aeciospore release video recording

Leaf fragments containing aecia were attached to a cuvette using Vaseline. The cuvette was held in place with a clamp between two spotlights to improve the clarity of the video. A Photron SAX2 mono high-speed camera (Slowmo Ltd, England) was used to record the spore release at maximum magnification (3,000 fps at 1025x1024 pixels resolution). To record the videos, the Photron Fastcam Viewer software was used on a DELL laptop running Windows 7. To induce aeciospore release for recording, the aecial cups were sprayed with water. This was done with the help of Phoebe Davey, Morgan Gerrity and Elizabeth Orton (Saunders Lab).

2.3.3 Aeciospore velocity calculation from videos

To estimate the velocity at which aeciospores are released, I took the first frame before an aeciospore was released and the subsequent frame. Using ImageJ, the coordinates of the position of the spore were calculated for each one of the two frames. Aeciospores were assumed to follow a straight line between those two positions and the distance travelled by the spore was estimated. The distance was then divided by the time between frames (0.0003 seconds) to calculate the launch speed. The same process was followed for each frame to determine the velocity of the spore at every point during its trajectory and thus investigate how the velocity changes over time. The video stills for each frame were then overlaid together using ImageJ (Images > Stack > Images to Stack) to acquire a picture of the full trajectory that the aeciospores followed after release.

2.3.4 Distance reached by aeciospores after release

To examine how far aeciospores can be released in a closed environment, leaf fragments containing aecia were attached to the wall of a 100 mm squared petri dish using Vaseline (**Figure 2.4 A**). Before attaching the lesions, they were placed on water to induce spore release. A microscope slide with 2 % water agar on top was placed in front of the leaf fragment to catch the released aeciospores (**Figure 2.4 B**). The aecial cups were then sprayed with water to increase humidity and the dish was left at 18 ºC for 18 hours. The aeciospores that were released from the cups were deposited on the agar and then observed under an inverted Leica DMi1 microscope with a scale to determine how far they had travelled (**Figure 2.4 C, D**). To investigate whether temperature had an effect on spore release, this experiment was carried out under different temperatures: 5 ºC, 10 ºC, 18 ºC, 25 ºC, 30 ºC, 33 ºC and 37 ºC. A Tukey's honestly significant difference (HSD) post hoc test was performed to compare distances reached by released aeciospores in each condition.

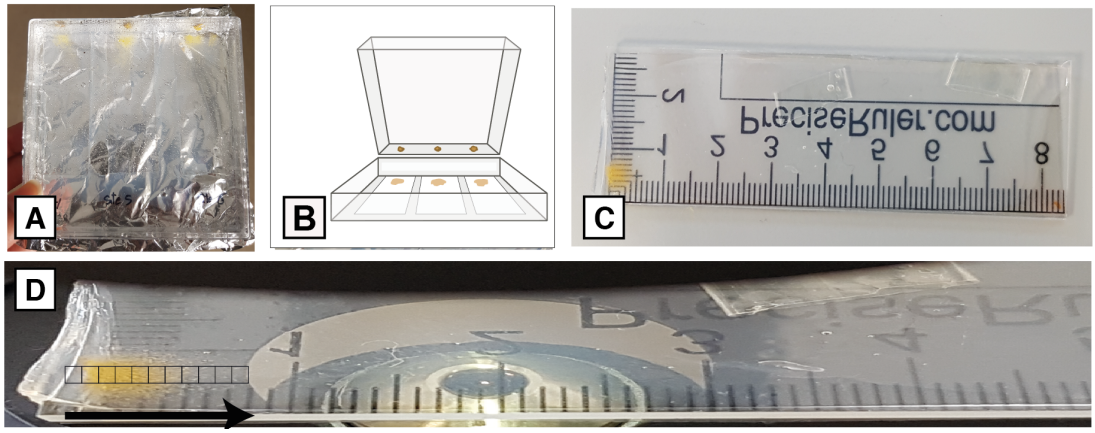

Figure 2.4. Preparation of experiment to estimate distance reached by aeciospores. (A) A 10 cm square plate containing three lesions and three microscope slides, the image shows the plate after release. **(B)** Lesions were positioned on the wall of the plate lid in front of the microscope slides to collect the released aeciospores on the slides, as shown in the drawing. **(C)** After release, slides were placed on a transparent scale to measure distance of release. **(D)** Slides with the scale were then observed in the microscope.

2.3.5 Water absorption of aeciospores

To record the rate of aeciospore expansion when absorbing water, dry aeciospores were placed on a microscope slide. An inverted microscope Leica DMi1 (Leica, Milton Keynes, UK) was used for this experiment. While recording with the microscope at 40x amplification, a droplet of 0.1 µL of water was added on top of the aeciospore. Video stills were taken prior to adding the water until aeciospore expansion was complete. These video stills were used to estimate the rate of aeciospore increase by calculating the area of aeciospores before the

water was added and after they had expanded, and the time for both stills was recorded. Area was measured using ImageJ by contouring the aeciospore and selecting the option 'Measure'.

To quantify the precise increase in size of aeciospores after water intake, the size of dried aeciospores and those immersed in water was measured. Released aeciospores were collected and air dried for at least 2 hours. Aeciospores were then mounted in water (hydrated) or 100 % glycerol (dehydrated) to simulate dry conditions. Using a Zeiss LSM780 confocal microscope, pictures of the spores in glycerol and in water were taken by Elizabeth Orton (Saunders lab) using an excitation wavelength of 405 nm. Afterwards, I estimated the area of aeciospores in the images using ImageJ by contouring the aeciospore and selecting the option 'Measure' that estimates the area. To calculate the diameter, three measurements were taken using ImageJ: diagonal, vertical and horizontal. The three measurements were then averaged.

2.3.6 Scanning Electron Microscopy of aeciospores and fungal structures

Samples were mounted on aluminium stubs using Tissue Tek^{R} (BDH Laboratory Supplies, Poole, England). The stubs were then immediately plunged into liquid nitrogen slush at approximately − 210 °C to cryopreserve the material. The samples were transferred onto the cryostage of an ALTO 2500 cryotransfer system (Gatan, Oxford, England) attached to a Zeiss Supra 55 VP FEG scanning electron microscope (Zeiss SMT, Germany) or the same type of cryo-system on an FEI Nova NanoSEM 450 (FEI, Eindhoven, The Netherlands). Sublimation of surface frost was performed at − 95 °C for ~ 3 min before the samples were sputter coated with platinum for 2 min at 10 mA, at colder than − 110 °C. After sputter-coating, the samples were moved onto the cryo-stage in the main chamber of the microscope, held at − 125 °C. The samples were imaged at 3 kV and digital TIFF files were stored. Both sample preparation and image capture were performed by Kim Findlay (John Innes Centre).

2.3.7 Transfer Electron Microscopy of aeciospores and fungal structures

Barberry leaves showing symptoms of SR infection were cut out and placed in a solution of 2.5 % (v/v) glutaraldehyde in 0.05 M sodium cacodylate, pH 7.3 and left overnight at room temperature. The fixative was washed out by three successive 10-minute washes in 0.05 M sodium cacodylate and samples were post-fixed in 1 % (w/v) OsO_4 in 0.0 M sodium cacodylate for one hour at room temperature. The osmium fixation was followed by three, 15-minute washes in distilled water before beginning the ethanol dehydration series (30 %, 50 %, 70 %, 95 %, 100 % ethanol, for approximately one hour in each solution). Once fully

dehydrated, the samples were gradually infiltrated with LR White resin (London Resin Company, Reading, Berkshire) by successive changes of resin: ethanol mixtures at room temperature as follows; 1:1 for 1 hour, 2:1 for 1 hour, 3:1 for 1 hour, 100 % resin for 1 hour then 100 % resin for 16 hours. After a fresh resin change for a further 8 hours, the samples were transferred into gelatine capsules full of fresh LR White and placed at 60 ºC for 16 hours to polymerize. The material was sectioned with a diamond knife using a Leica UC6 ultramicrotome (Leica, Milton Keynes, UK). Ultrathin sections of approximately 90 nm were picked up on formvar/carbon coated 200 mesh copper grids. The sections were stained with 2 % (w/v) uranyl acetate for 1 hour and 1 % (w/v) lead citrate for 1 minute, washed in distilled water and then air dried. The grids were viewed in a FEI Talos 200C transmission electron microscope (FEI UK Lrd, Cambridge, UK) at 200 kV and imaged using a Gatan OneView 4K x 4K digital camera (Gatan, Cambridge, UK) to record DM4 files. Both sample preparation and image capture were performed by Elaine Barclay (John Innes Centre).

2.3.8 Aeciospore release model

The mathematical model was developed with the help of Dr. Mark Blyth (University of East Anglia), who performed all mathematical operations. The programming software MATLAB and Maple were used for mathematical calculations. The full description of the model is included in Annexe section **6.1**.

2.4 Results

2.4.1 *Pg* aeciospores are released at variable velocities that decrease rapidly after ejection

To study the release of *Pg* aeciospores from aecial cups located on the abaxial surface of barberry leaves, we used a high-speed camera to record videos of aeciospore release. Spore ejection was recorded at 3,000 fps and the consequent 80 videos were analysed to measure the velocity of discharge. To ensure accuracy in the velocity measurements, 31 out of the initial 80 videos were selected for analysis where the trajectory of the aeciospore remained in focus and followed a straight line (**Figure 2.5 A-C,D-F**). If spores were perceived to be released diagonally or out of focus, the measurement would not be precise, and the video was discarded. For each of the selected videos, we took the first frame and measured how much the spore had travelled in the timeframe (0.0003 s) (**Figure 2.5 G**). Release velocities were observed from 0.094 m/s up to 0.754 m/s, with a median of 0.24 m/s (**Figure 2.5 H**). The variability in initial discharge velocities was observed in videos of several aeciospores being ejected at the same time at different speeds. Despite the different values of release speed, all of them were in range of tens of cm/s, which shows that there is consistency in

the observations. This is likely to be a consequence of the release mechanism that allows for a degree of variability.

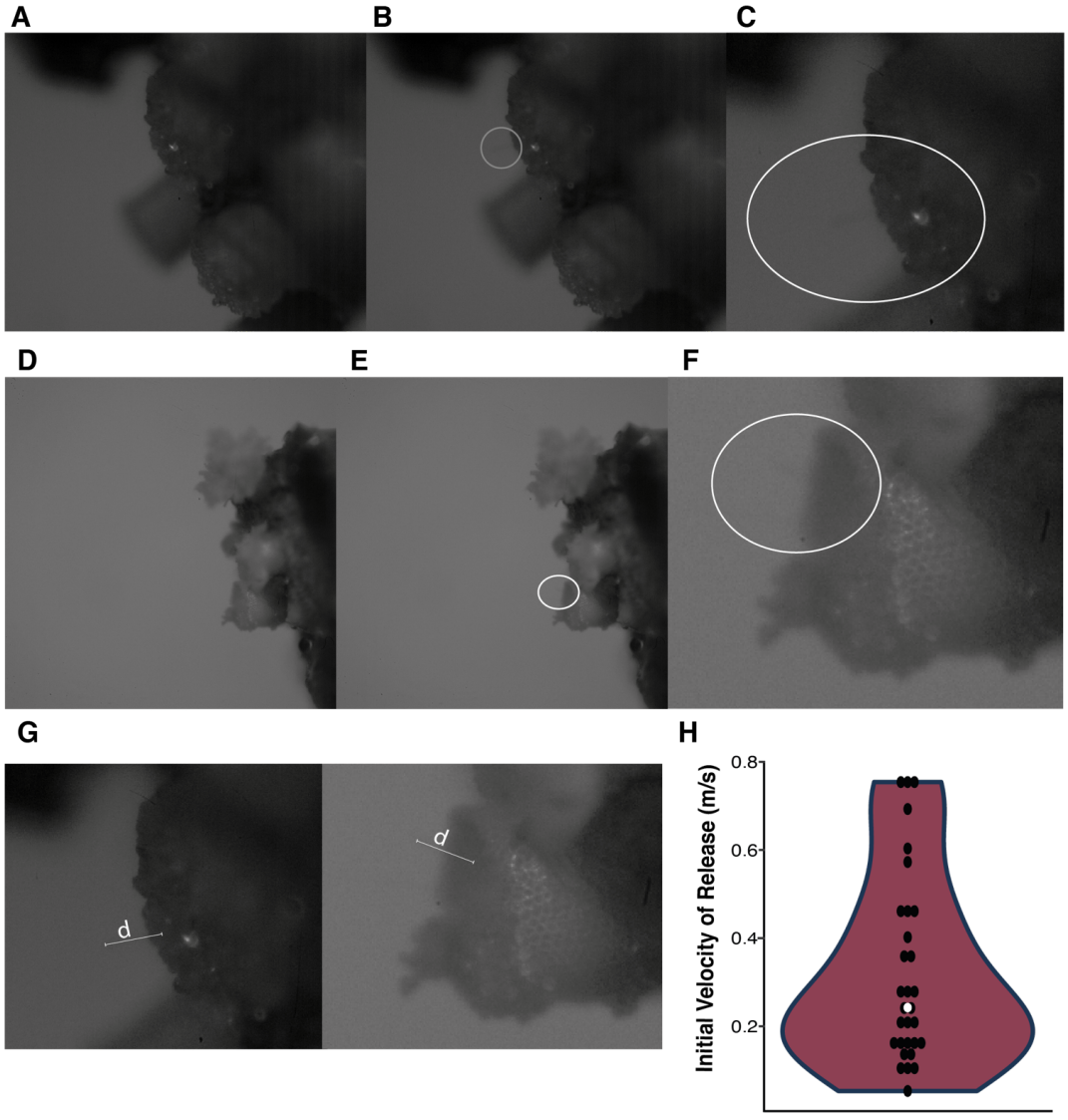

Figure 2.5. *Pg a*eciospores are actively released at a median of 0.24 m/s. A total of 31 videos of aeciospore release were recorded with a HS camera at 3,000 frames per second. To estimate the initial velocity, the first two frame of each video were taken (**A, D**: first frames; **B, E**: second frames; **C, F**: zoom of the second frame; white circle indicates moving spore). **(G)** An estimate of initial velocity was determined by measuring the distance that the spore travelled in the time between the two frames for a total of 31 videos of aeciospore release and dividing this by the timeframe (0,0003 seconds). **(H)** Initial velocities ranged from 0.094 m/s to 0.754 m/s, with a median of 0.24 m/s.

The recorded videos were analysed frame by frame to measure the velocity across time and to study how it changed during the aeciospore trajectory. Velocity was estimated from the point of release until the aeciospores decelerated completely and started falling down. As shown in **Figure 2.6 A**, aeciospores showed rapid deceleration over time due to the drag force that air exerts on the aeciospore (Pringle et al. 2017). This leads to the distance travelled by the aeciospore across time to reach a plateau when the aeciospores decelerate. When their velocity reached almost 0 m/s, spores ceased to move and started falling (**Figure 2.6 B**). This deceleration can be observed in the aeciospore trajectories (**Figure 2.6 C**) in which when the spore's velocity reaches 0 m/s and it fell downwards freely. The distance that the spores reached after ejection was related to the initial velocity recorded as those with greater velocity travelled further away before falling. The full trajectories of spores had been previously predicted for several fungi (Fischer, Stolze-Rybczynski, Cui, et al., 2010) but, to our knowledge, they had never been observed and recorded for *Puccinia* rust fungi.

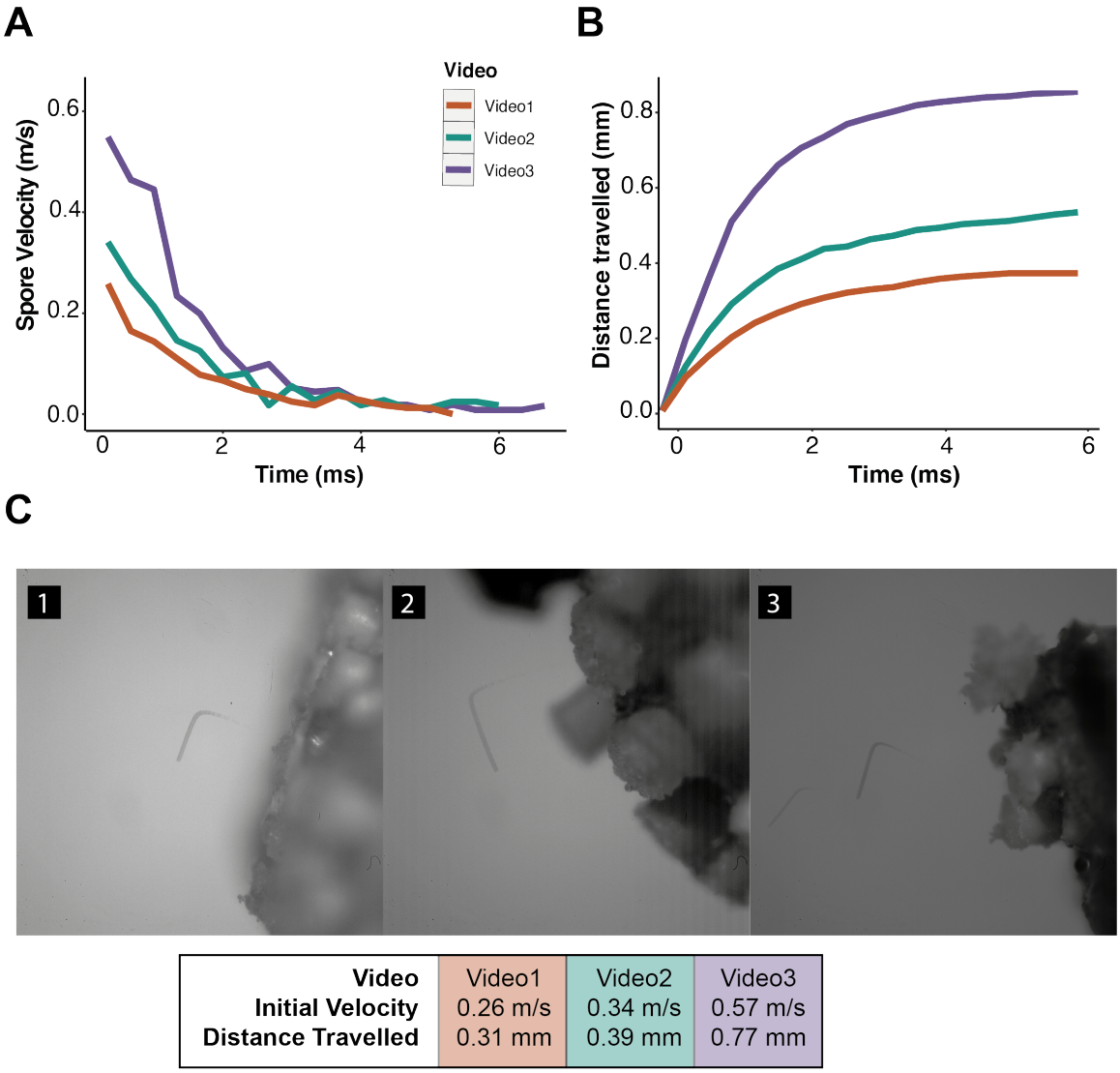

Video	Video1	Video2	Video3
Initial Velocity	0.26 m/s	0.34 m/s	0.57 m/s
Distance Travelled	0.31 mm	0.39 mm	0.77 mm

Figure 2.6. *Pg* aeciospore initial release velocity decreases rapidly after ejection. Aeciospore release videos were analysed frame by frame to estimate the velocity and distance travelled from ejection until fall. **(A)** Aeciospore velocity decreased rapidly after ejection due to drag forces. **(B)** Distance travelled by the aeciospore across time decreased rapidly until reaching a plateau when they cease to move and start falling. **(C)** Full trajectories show how aeciospores only start falling after their velocity reaches 0 m/s. Aeciospores released at higher velocities travelled further (Video 3).

2.4.2 Distance that aeciospores travel can be used to predict initial velocity

We can estimate the maximum distance reached by an aeciospore if the initial release velocity is known, with the following formula (Pringle et al. 2017):

$$d = V_{spore} \frac{2}{9} \frac{a^2 \rho_{spore}}{\mu} \quad (2.4)$$

Where a is the radius of the spore, ρ_{spore} is the density of the spore and μ is the viscosity of the medium, i.e. the air. The radius of the *Pg* aeciospore has been determined previously to be around 10 μm, with a density of 882 kg/m^3, assuming an spherical aeciospore (Gregory, 1961) and the dynamic viscosity of air is 1.81 x 10^{-5} kg/m/s. Substituting these values into the previous equation, we can see the following relationship between the maximum distance (d) travelled and the velocity of the aeciospore:

$$d = 0.00109\, V_{spore} \quad (m) \quad (2.5)$$

The relationship above could also be used to infer the initial velocity of aeciospore release if the maximum distance travelled is known, by simple reversing the equation as follows:

$$V_{expected} = \frac{d_{reached}}{0.00109} \quad (m/s) \quad (2.6)$$

Using this equation, I could estimate the theoretical velocity ($V_{expected}$) at which *Pg* aeciospores were released by knowing the initial distance aeciospores travelled following release. Since the real maximum distance that aeciospores reached could not be accurately estimated (since aeciospores left the plane before reaching the floor), the point at which aeciospores started falling was determined where their velocity was 0 m/s. At this point it was assumed that they would fall freely vertically until reaching the floor if they were not caught in an air current. The linear distance reached by *Pg* aeciospores was estimated assuming the floor would have been at the same altitude of release.

From the recorded videos, I measured the distance reached as described and then calculated the theoretical expected velocity using the equation above. Then I compared it with the observed release velocity (**Figure 2.7**). A total of 20 videos were analysed and are shown in the graph for simplicity. For most videos the difference between the expected maximum distance travelled and the observed value was very small. The dissimilarity between the expected and observed distance was sometimes greater for aeciospores that were released in pairs thus increasing the value of a, which affects the drag and thus the above relationship changes. However, overall the observed and expected values remained close, indicating that, when taking into account the effect of the drag on the aeciospore, the initial velocity of release can be estimated if the maximum distance travelled is known.

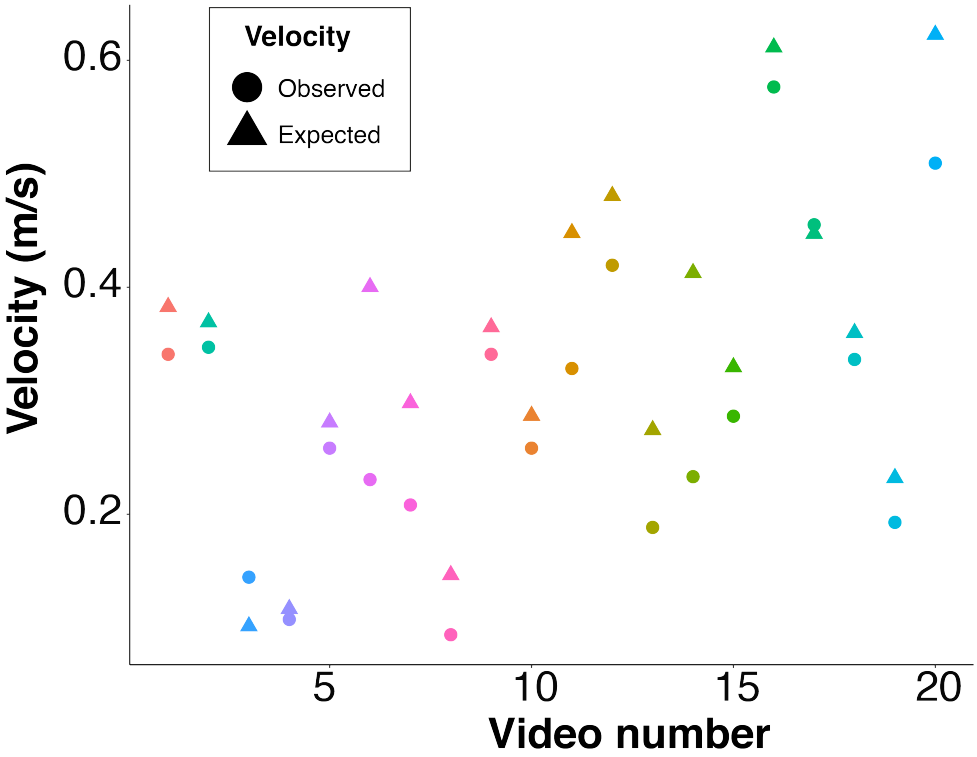

Figure 2.7. The distance travelled by *Pg* aeciospores can be used to predict their initial ejection velocity. *Pg* aeciospore release velocity was estimated using the distance travelled by the aeciospore (expected), compared to the measured release velocity (observed). A total of 20 videos were included in this analysis, and for all of them the observed and expected velocity were very close, indicating initial distance reached by *Pg* aeciospores can indeed be used predict the initial velocity of release. Colours represent the different videos used for this calculation.

2.4.3 Distance that *Pg* aeciospores initially travel after ejection remains constant over a range of temperatures

To elucidate the mechanism of *Pg* aeciospore release, I wanted to confirm whether water is the main factor influencing aeciospore liberation or whether temperature could affect it too. To investigate whether temperature has an effect on *Pg* aeciospore release, I evaluated the distance that *Pg* aeciospores can reach under a range of temperatures in a closed environment. To do so, I attached aecial cups to the wall of a square dish containing microscope slides with agar on top. I then left the square dishes in darkness under different temperatures: at 5 ºC, 10 ºC, 18 ºC, 25 ºC, 30 ºC, 33 ºC and 37 ºC. After 18 hours, slides were evaluated under the microscope to measure the maximum distance that *Pg* aeciospores had travelled. Six independent biological replicates were carried out for each one of the temperatures, except for 33 ºC and 37 ºC where only three replicates were utilised. *Pg* aeciospore release followed the same pattern in all experiments where there was a high spore density close to the source and then they progressively became more dispersed (**Figure 2.8**). I recorded the distance until which a high density of aeciospores was found (more than 100 aeciospores/0.2 mm^2), a medium aeciospore density (10-100 aeciospores in 0.2 mm^2) and the final maximum distance where aeciospores (single or groups) were found, defined as "last spores found". Images representing each one of these conditions can be observed in **Figure 2.8**. These three categories were defined to test whether temperature had an effect on the distance that the majority of aeciospores were able to reach and also on the maximum total distance that aeciospores could reach.The red line represents the three distances that were recorded in the example from **Figure 2.8**. These distances are the maximum distance at which each one of these three conditions could still be observed (i.e. more than 100 aeciospores, 10-100 aeciospores and the maximum distance at which aeciospores were found). They were recorded for each one of the range of temperatures used and plotted for comparison (**Figure 2.9**).

The maximum distance until which *Pg* aeciospores were found at a high density fluctuated from 0.55 cm to 1.63 cm (average of 1.09 cm) across all temperatures. The maximum distance until which a medium aeciospore density was seen ranged from 0.88 cm to 2.38 cm (average 1.42 cm). The total maximum distance that aeciospores were able to reach varied greatly, from 1.06 cm (at 37 ºC) to 7.12 cm (at 25 ºC), with an average of 2.40 cm. In general, distances recorded under each condition were very variable. Slight variation was apparent in **Figure 2.9**, with aeciospores travelling less for example at 5 ºC and 37ºC and more at 18 ºC and 25 ºC. Therefore, an HSD post hoc test was performed to check for significant differences between temperatures. No statistically significant differences ($p >$

0.01) were observed, indicating that the given temperature range does not have a substantial effect on initial aeciospore distances following ejection in a closed environment. This suggests that the range of temperatures tested here does not seem to have a role in the release of aeciospores from aecial cups in stem rust, which supports the hypothesis that the main driver of *Pg* aeciospore release is water.

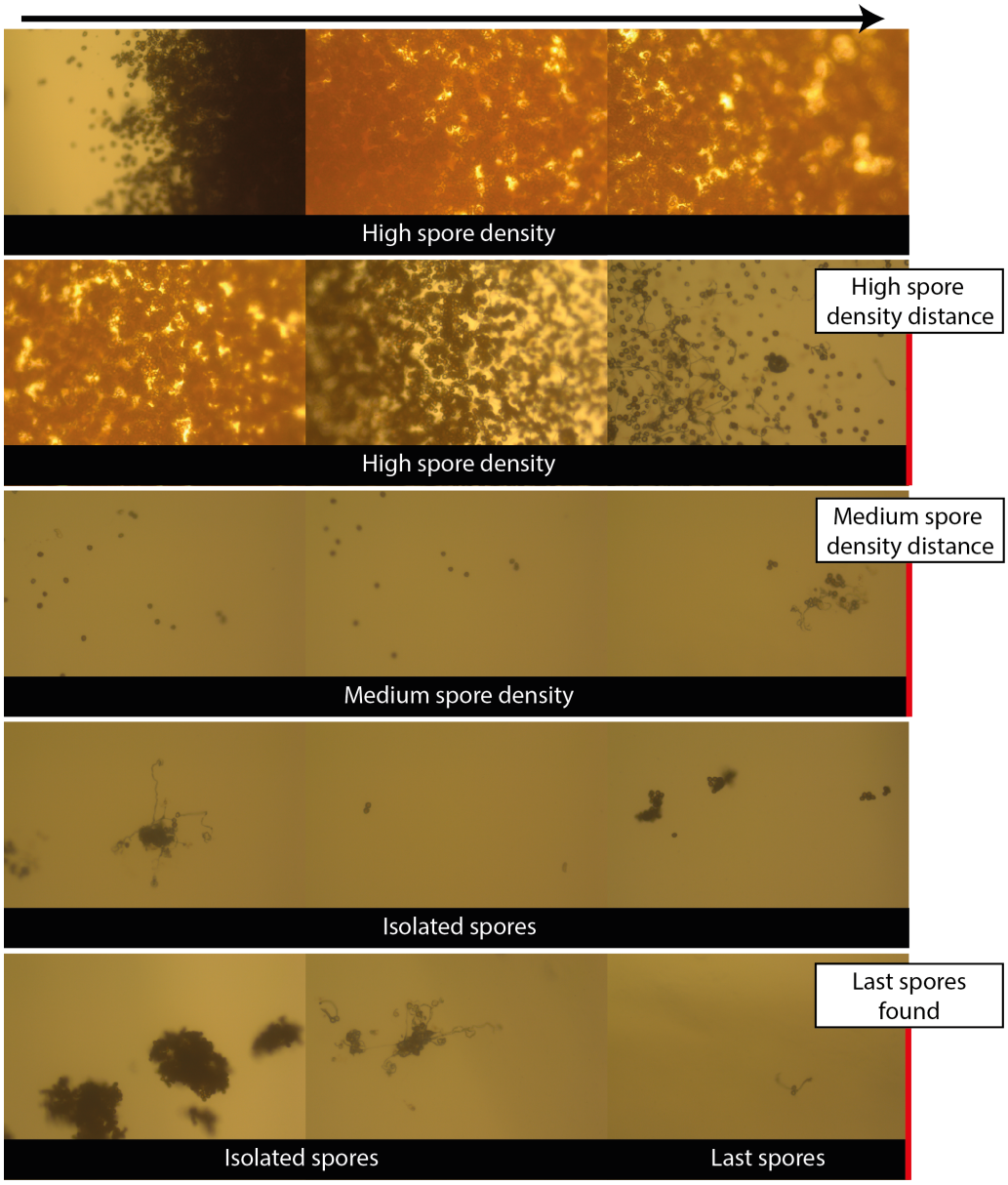

Figure 2.8. Microscope slides were observed to determine the distance reached by *Pg* aeciospores after release. The slides were divided into three conditions: high aeciospore density (>100 aeciospores/0.2 mm^2), medium aeciospore density (10-100 aeciospores/0.2 mm^2) and isolated aeciospores. The maximum distance at which all of these three conditions were observed was recorded for each sample. The red line indicated the distance representing the end of "high aeciospore density", "medium aeciospore density" and the point at which the last aeciospore was found.

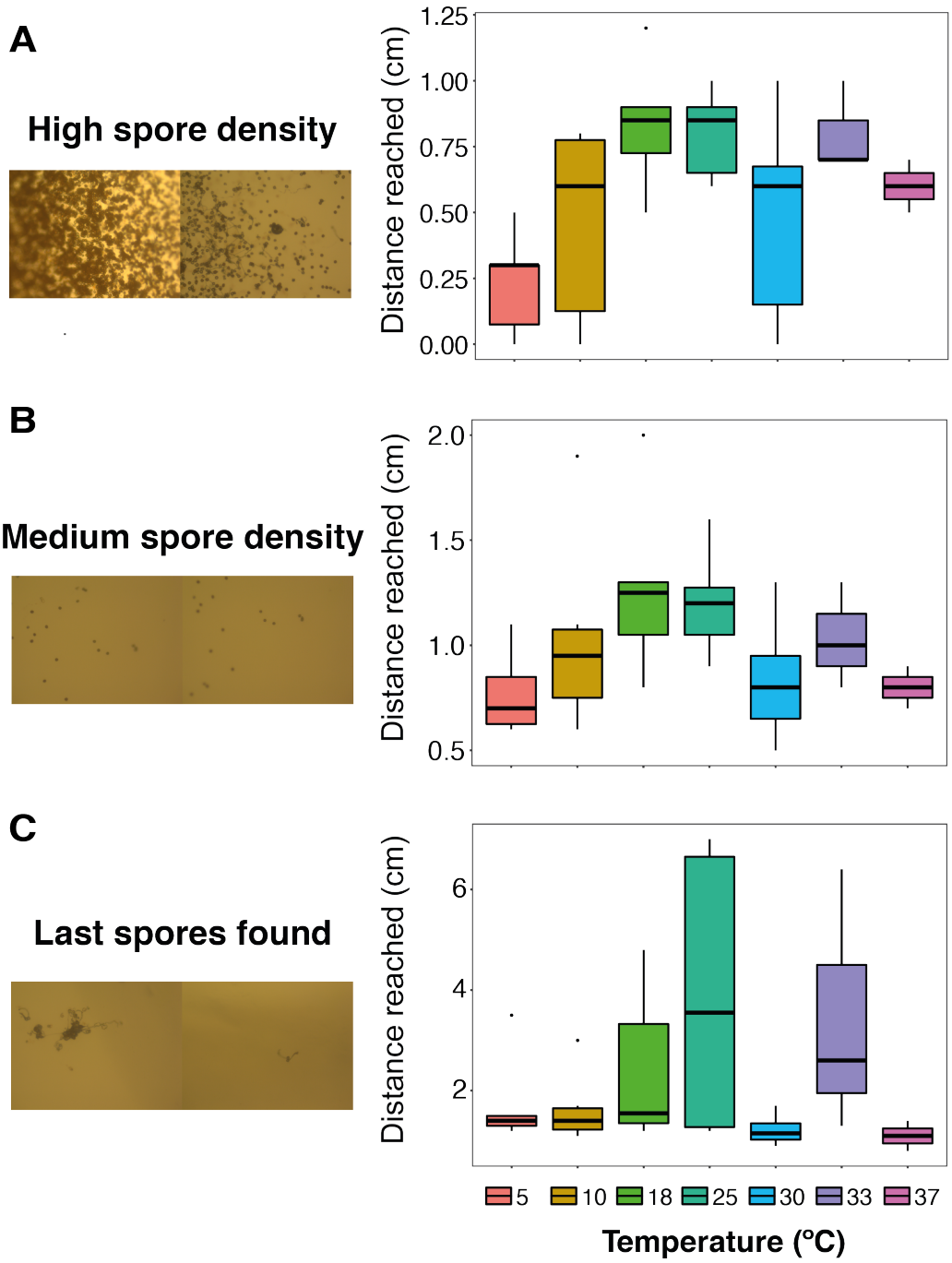

Figure 2.9. Temperature does not significantly affect distance reached by aeciospores. Maximum distance reached by aeciospores released from aecial cups was studied under different temperatures (5 ºC, 10 ºC, 18 ºC, 25 ºC, 30 ºC, 33 ºC and 37 ºC). The maximum distance at which aeciospores were found at a **(A)** high density (>100 aeciospores in 0.2 mm^2), **(B)** medium density (10-100 aeciospores/0.2 mm^2) and **(C)** the total maximum distance reached by isolated aeciospores was recorded for each temperature and compared. Images on the left represent each one of the three situations. Differences in temperature were not statistically significant ($p < 0.01$; HSD post hoc test) for any of the experiments.

2.4.4 Expected release velocities based on distance of single *Pg* aeciospores are higher than observed velocities by HS videography.

Since the distances observed in the previous experiment were much higher than that those reached by aeciospores in the recorded videos, I investigated the release velocity needed for aeciospore to achieve those distances. Using the relationship between maximum distance and initial velocity previously defined (equation **2.6**), I could estimate the initial velocity that was needed for aeciospores to reach the distances observed in the previous experiment. A total of 51 experiments were included, with 6 biological replicates for 5, 10, 25 and 30 ºC, 3 biological replicates for 33 ºC and 37 ºC and 21 biological replicates at 18 ºC. For each temperature I calculated the mean distance until a high density of aeciospores was found and the maximum distance at which an aeciospore was found (**Figure 2.10 A**). As it can be observed, the mean high aeciospore density ranged between 0-1 cm while the maximum distance at which an aeciospore was found fluctuated from 1.4 to 7 cm. These values were used to estimate the expected release velocity with equation **2.4**. The results are displayed in **Figure 2.10 B**. For distances at which a high density of aeciospores is found, the expected velocities ranged from 2 to 8 m/s, which are one order of magnitude higher than that observed in the high-speed recordings of aeciospore release. Furthermore, when estimating the velocities needed for aeciospores to reach the maximum distance at which they were found, the expected velocities reached tens of meters per second, which is 100 times greater than that observed with the HS camera. This implies that in order to reach that distance, single aeciospores would have to be ejected at velocities two orders of magnitude higher than what was observed. The disparity between the range of observed ejected velocities recorded and the expected velocities could indicate issues with the input values used in the formula for predicting the initial velocity.

It was noted that many aeciospores were identified in clumps and as aeciospore radius is a core property of the formula used (equation **2.3**), this parameter has a high effect on the estimated initial velocity. If all the values in the equation are maintained, increasing the value of the radius would greatly decrease the expected velocity. This is applicable for a radius of any object travelling under the effect of the drag as described in the formula. For instance, if hypothetically the radius of the aeciospore doubled, the expected velocity would decrease by a factor of 4 (equation **2.7**). If it tripled, the velocity would decrease by a factor of 9 etc. Consequently, if aeciospores aggregate in groups as shown in **Figure 2.11**, the "radius" of the group would be much higher than that of a single aeciospore, and a lower release velocity would be needed for them to achieve the same distance.

$$V_{spore} = \frac{1}{a^2}\frac{9\mu}{2d\,\rho_{spore}} \rightarrow \frac{1}{(2a)^2}\frac{9\mu}{2d\,\rho_{spore}} = \frac{1}{4a^2}\frac{9\mu}{2d\,\rho_{spore}} \qquad (2.7)$$

To reach a distance of more than 1 cm, a spore group with a radius of 30 µm would only need an initial velocity of 1 m/s (dashed line in **Figure 2.11**), which is what was observed in the HS videos. Aeciospore clusters with a 50 µm radius could then reach higher distances (3-7 cm) with velocities closer to those observed by HS videography (~ 1 m/s).

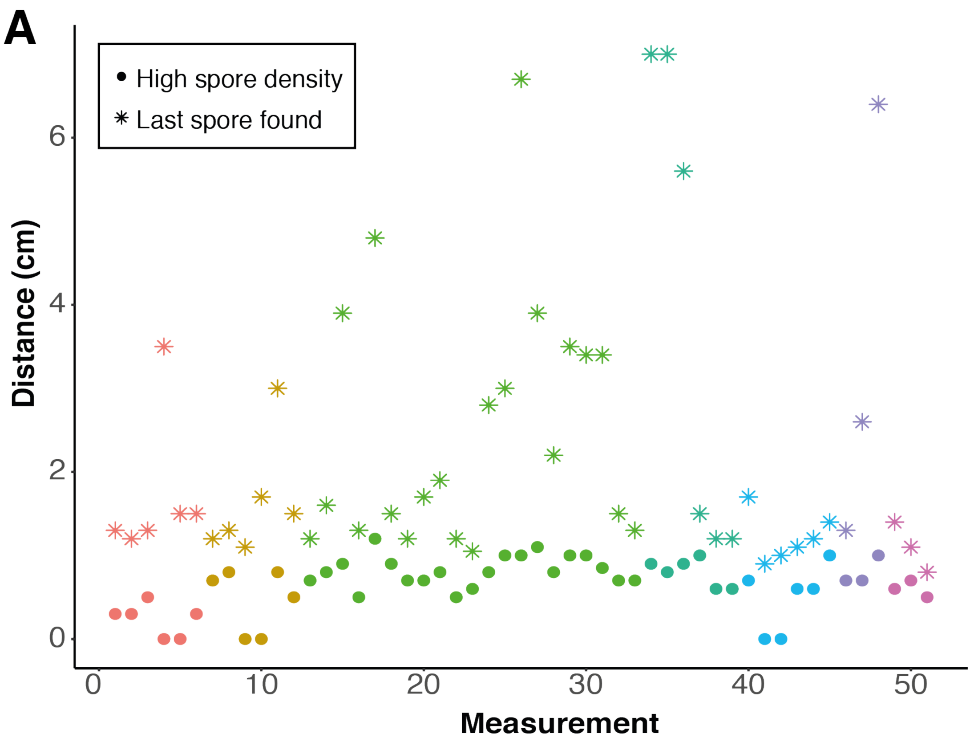

B

	Temperature (°C)	Distance (cm)	Expected velocity (m/s)
Mean distance until which a high density of spores was found	5	0.23	2.11
	10	0.46	4.22
	18	0.82	7.53
	25	0.8	7.34
	30	0.48	4.41
	33	0.8	7.35
	37	0.6	5.51
Maximum distance at which a spore was found	5	3.5	32.14
	10	3	27.55
	18	6.7	61.53
	25	7	64.29
	30	1.7	15.61
	33	6.4	58.78
	37	1.4	12.86

Figure 2.10. Predicted *Pg* aeciospore release velocities are higher than observed in high-speed videography. (A) For each temperature, the mean distance until which a high density of aeciospores was found (•) and the maximum distance at which an aeciospore was found (*) were computed. Colours represent the different temperatures. **(B)** Initial aeciospore velocity was predicted from the observed maximum distance *Pg* aeciospores travelled. Predicted velocities for a single aeciospore reached up to 64.29 m/s.

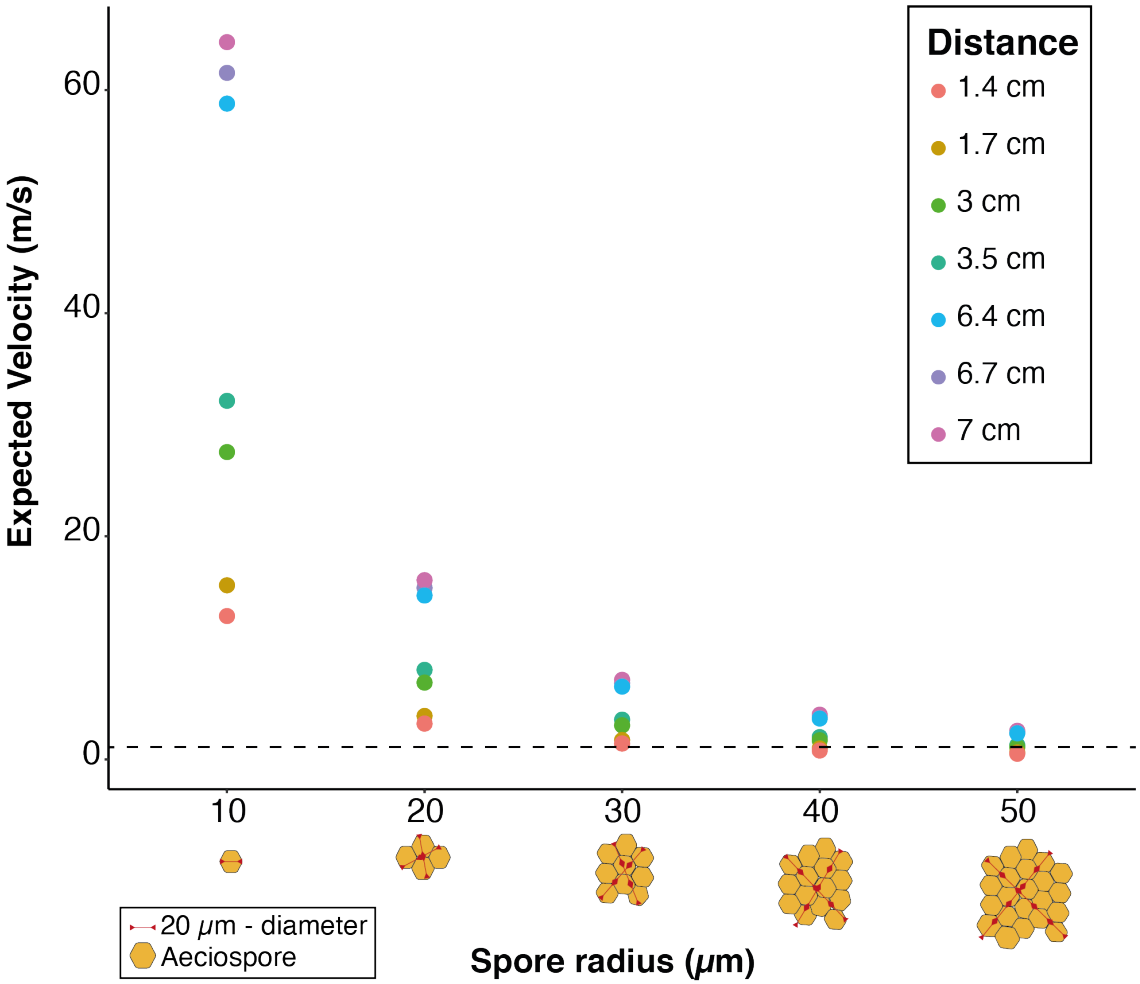

Figure 2.11. Increasing the radius of a spore would decrease the initial velocity needed to reach the same distance. The predicted velocity of release for *Pg* aeciospores to reach the maximum distances observed was plotted for different values of *a* (radius of the aeciospore). Radius of aeciospore is determined to be approximately 10 μm (hence the diameter is 20 μm, red line), but if this value increases, the predicted velocity decreases. The value of the radius in the formula can increase by aeciospores clustering together into groups that have a radius equal to 2, 3, 4 or 5 times the real aeciospore radius. Aeciospores grouped as shown underneath the x-axis would thus be able to travel the same distance with a lower velocity.

2.4.5 Aeciospores are released in groups to achieve greater distances

The discrepancy detected in the previous section between the expected velocity of single aeciospores and the observed ones using the HS camera suggests aeciospores could not achieve great distances at the observed velocities. However, aeciospores aggregating together into groups to increase their radius would reduce the effect of drag, which would help them achieve greater distances. To further investigate this hypothesis, I examined the impact of aeciospore aggregation on distances reached by these clusters.

SEM imaging of *Pg* aeciospores shows that aeciospores are frequently found in rows, both inside and outside of the aecial cups after release (**Figure 2.12 A**). This suggests that aeciospores are being released in rows, with the bond between aeciospores facilitated by the verrucose that aeciospores contain on their surface (**Figure 2.12 B**). This is consistent with the theory that they are ejected in groups to achieve greater distances. Moreover, when aeciospores were found at larger distances (more than 4-5 cm), they were rarely identified as single aeciospores, but rather as groups clustered together (**Figure 2.12 D**). Aeciospores also seemed to have a trend of being found in bigger clusters at the furthest distances, although this was not always observed. Aeciospores found at 1.9 cm appeared to be in rows of 3-4 spores, at 2.6 cm a big cluster of tens of aeciospores was found and at 7 cm, aeciospores were observed to be in a block of hundreds of aeciospores. As the likelihood of aeciospores being released one by one into the same space is extremely low, it can be concluded that these aeciospores were initially released as clusters. Having showed how the increase in diameter of the object travelling (i.e. the aggregation of aeciospores) would influence the maximum distance reached, it can be deduced that these aeciospores could have been released at the lower velocities observed with the HS videography (~ 1 m/s). Furthermore, HS videography also showed that groups of aeciospores, released at the same velocity are able to achieve greater distances. In **Figure 2.12 E**, groups of aeciospores released at the same time and velocity are observed to maintain a velocity for longer when they had a larger radius due to aggregation. Groups of four aeciospores (red circle) are observed to achieve greater distances than rows of 2-3 aeciospores (green circle) in **Figure 2.12 E**.

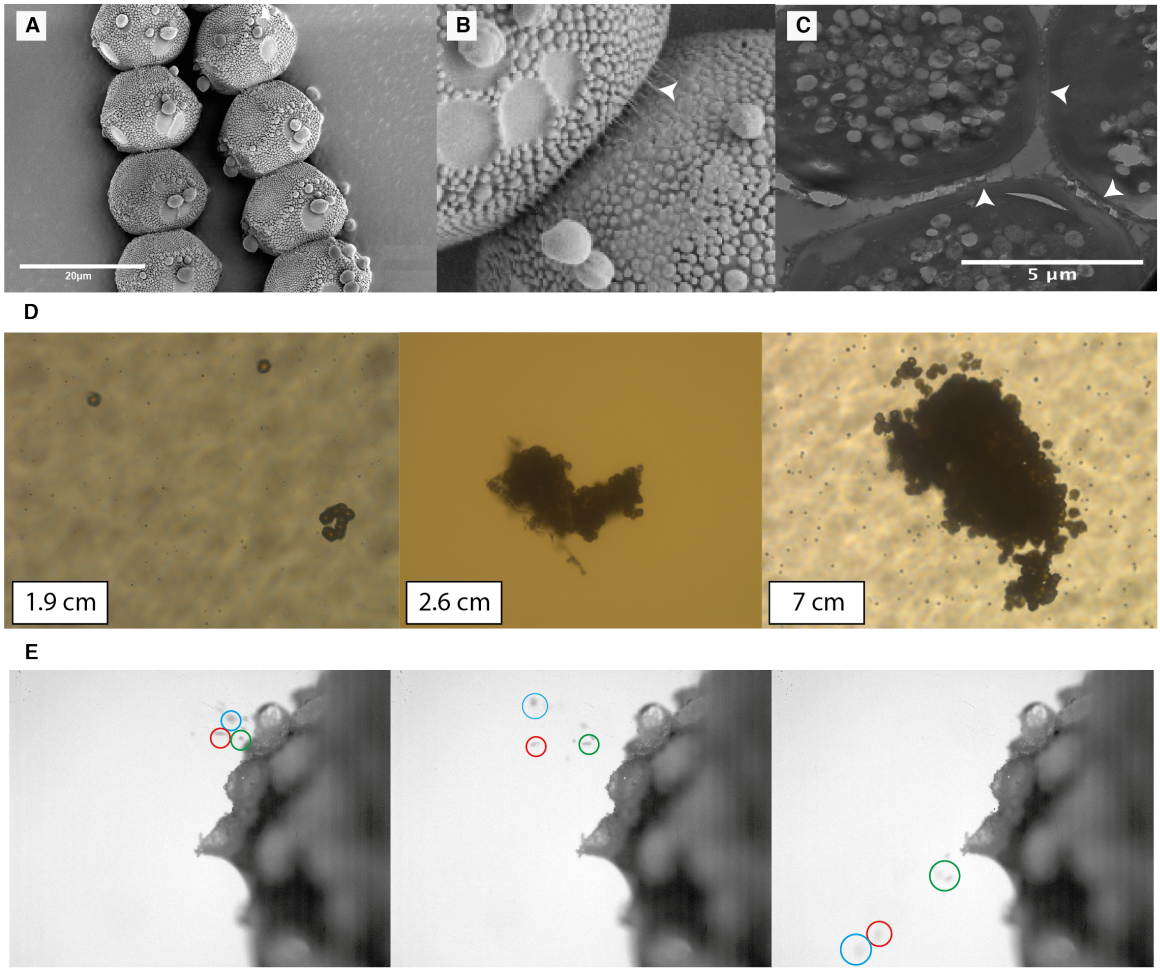

Figure 2.12. *Pg* aeciospores could be released in clusters to achieve greater initial distances. (A) *Pg* aeciospores are frequently found in rows after release. **(B)** SEM and **(C)** TEM imaging shows verrucose that acts to potentially adhere aeciospores together. **(D)** *Pg* aeciospores that reached greater initial release distances were most commonly found in clusters of several aeciospores, with more aeciospores grouping the further they were found. Images are shown of aeciospore clusters identified at 1.9, 2.6, and 7 cm. **(E)** Larger groups of aeciospores (blue circle) released at the same time and with equal initial velocity reached greater distances than groups of four aeciospores (red circle) and rows of two/three aeciospores (green circle).

2.4.6 *Pg* aeciospores are able to absorb water to increase volume

As it has been reported that high RH is an important factor in aeciospore release and after confirming that water is likely to be the main factor in aeciospore release, I examined the behaviour of aeciospores under high RH conditions, i.e. when water is freely available. To investigate whether aeciospores were able to absorb water, we isolated an aeciospore in a microscope slide and added 0.1µl of water. Immediately after adding the droplet, the spore started increasing in volume due to water absorption. As it can be observed in **Figure 13A**, the dry aeciospore shows a polyhedral shape (perceived as a hexagon in this particular image) whereas the aeciospore rounds up after absorbing water (**Figure 2.13 B**). The video stills in **Figure 2.13 A-B** show the aeciospore before adding the droplet of water, at 5.56 seconds of the video, and the aeciospore displaying a spherical shape after absorbing water, at 10.58 seconds. This indicates that it took the aeciospore 5.02 seconds to become fully rounded. The capacity of aeciospores of absorbing water means that under high RH, aeciospores inside an aecial-cup could increase in volume after water intake. Considering how tightly packed aeciospores are inside cluster cups, if the increase in volume is high enough, it could increase the pressure inside of the cups, possibly leading to its release.

To calculate the exact increase in size of aeciospores after hydration, I estimated the volume that aeciospores have in dry conditions (simulated by immersing them in glycerol) and then compared them to aeciospores that had been immersed in water (i.e. in a high RH environment) (**Figure 2.13 C-D**). This way, I could estimate the theoretical increase that aeciospores can achieve when water is freely available. The images taken were then analysed and the diameter and area measured. To estimate the diameter, aeciospores were measured horizontally, vertically and in diagonal and I calculated the average of all three. This was particularly important for aeciospores immersed in glycerol that have a more irregular shape. A total of 26 measurements were carried out for those aeciospores in glycerol and 33 for those immersed in water. Aeciospores immersed in glycerol showed an average diameter of 13.6 µm (± 0.59 S.D.) and when they were in water, they had an average diameter of 18.55 µm (± 2.08 S.D.). This implies an increase of 4.95 µm in diameter from when aeciospores are dry (glycerol) to when they absorb water. As the S.D. shows, aeciospores immersed in water exhibited a higher variability than those in glycerol, with aeciospores displaying a diameter ranging from 15.83 µm to 22.99 µm. Still the difference in volume between the two conditions was statistically significant, $p < 0.01$; 2-tailed p-test (**Figure 2.13 E**). Likewise, an increase in the area was observed, with aeciospores having an area of 142.34 µm (± 11.09 S.D.) when immersed in glycerol and of 262.40 (± 59.41 S.D.) µm when immersed in water (**Figure 2.13 F**). This represents an increase of 120.06 µm (p-

value < 0.01; 2-tailed p-test). As shown in **Figure 2.3 A**, aeciospores appear to be tightly packed inside of the aecial cup and an increase in volume due to hydration would increase the pressure inside of the cup. Therefore, it is reasonable to infer that aeciospores could be ejected due to the increase in pressure that the expansion of aeciospore volume would produce on surrounding aeciospores. Hence, we decided to develop a model of spore release that utilised this knowledge to explain the potential *Pg* aeciospore release mechanism.

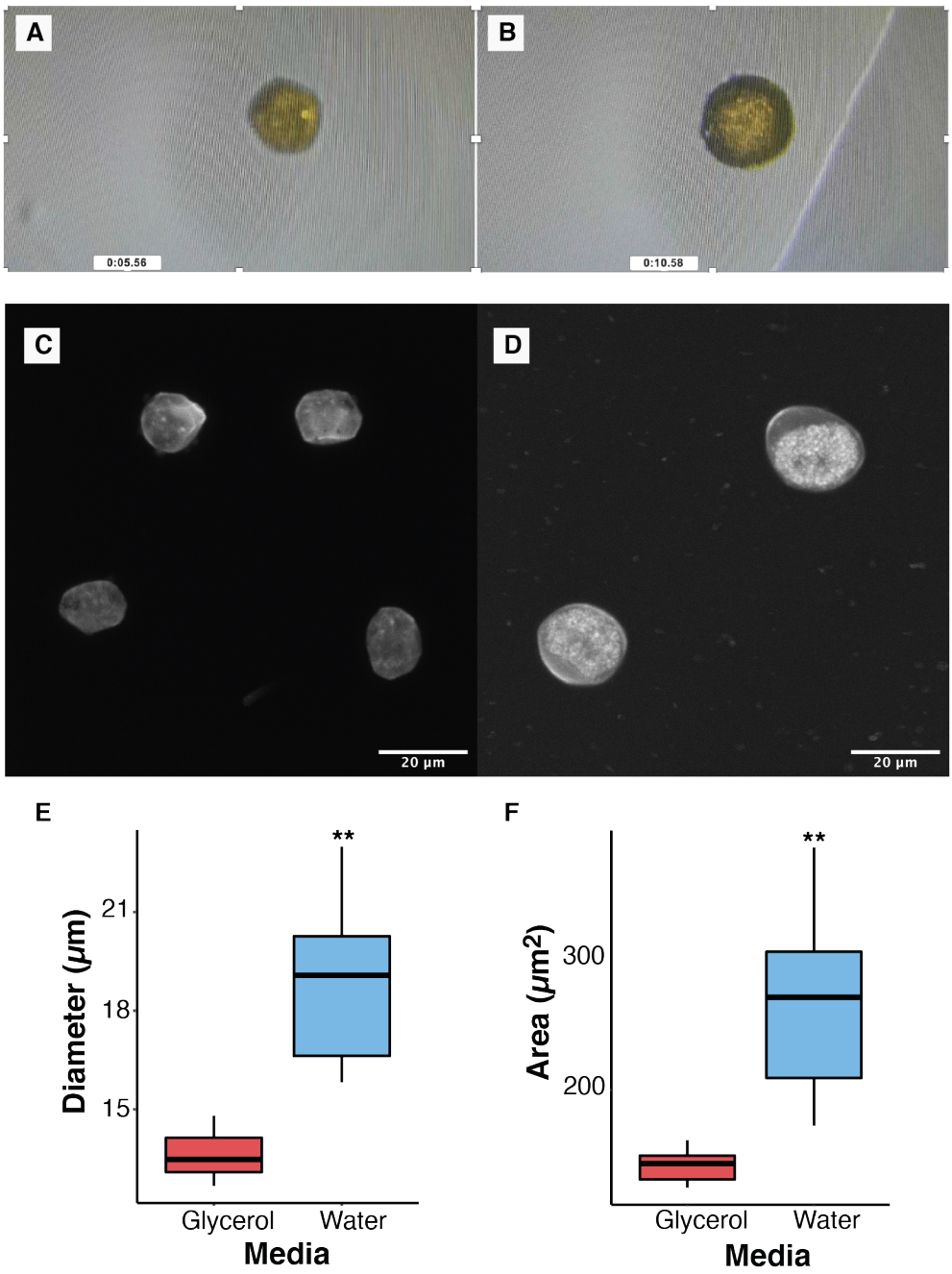

Figure 2.13. *Pg* aeciospores increase in volume significantly when immersed in water. (A) Video still before and **(B)** after hydration show an increase in volume. Aeciospores were immersed in glycerol **(C)** and water **(D)** and observed under confocal microscopy to compare their diameter before and after hydration. **(F)** Aeciospores showed an average diameter of 15.6 ± 0.59 µm in glycerol and 18.55 ± 2.08 µm in water. **(F)** Aeciospores displayed an average section area of 142.34 ± 11.09 µm in glycerol and 262.40 ± 59.51 µm in water. Aeciospores thus display a statistically significant increase both in diameter (4.95 µm increase) and area (increase of 120.06 µm). Asterisks denote statistically significant differences (**: $p < 0.01$; 2-tailed t-test).

2.4.7 Proposed model of aeciospore release in *Puccinia graminis*

As previously stated, aeciospores are found tightly packed in rows inside of aecial cups and have been observed to increase significantly in volume when in contact with water. This expansion can cause an increase of pressure that could lead to aeciospore liberation. Following this principle, a mathematical model was developed in collaboration with Dr. Mark Blyth (UEA) to explain this process. The model proposes that after hydration the interspore gaps become perfused with water so that each aeciospore becomes coated with a thin lubrication film. This film acts in two important ways: first, it substantially lowers the shear force between aeciospores that opposed translation, and second it tolerates a substantial load similar to a slider bearing. The result is that a single aeciospore can impose a substantial force on its neighbouring aeciospores (modelled here as two diverging walls), this force being mediated by the lubrication film (**Figure 2.14**). Aeciospores are modelled as cuboids whose sides are parallel to the walls of neighbouring spores. When the aeciospore expands due to water intake, the gap between aeciospores is reduced, which could generate a 'squeeze-film' effect whereby a force is generated along the axis of symmetry. The aeciospore would then acquire momentum in the *x* direction and would be ejected from the aecial-cup at a velocity V. Two parameters were key for the model and were estimated here. First, the rate at which aeciospores increase its radius, i.e. the rate at which the space between neighbouring aeciospores close. Second, the initial size of the gap between aeciospores.

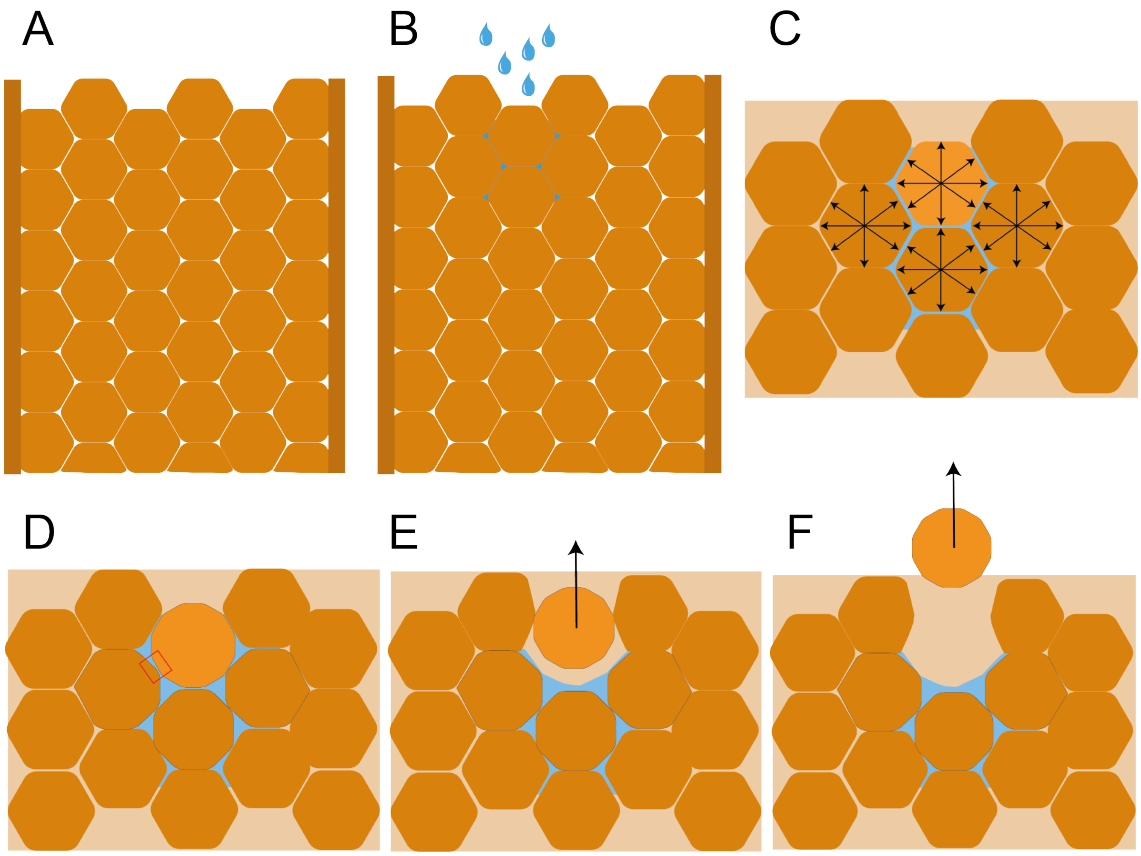

Figure 2.14. Diagram of *Pg* aeciospore release mechanism. (A) Aeciospores are highly packed forming rows in aecial-cups. **(B)** When water is splashed on the cups, aeciospores absorb water and increase their volume **(C)**. This increments the pressure inside the cup, and the water acts as a lubrication film **(D)** that leads spores to be discharged outside of the cup **(E, F).**

To estimate the rate of increase in radius after aeciospores absorb water, the cross-sectional area was estimated before and after immersing them in water. Calling this *A(t)*

$$A = \pi r^2$$

Where r(t) is the radius of the spore. Differentiating with respect to *t,* and substituting *r*

$$\frac{dA}{dt} = 2\pi r \frac{dr}{dt} = 2\sqrt{A\pi}\frac{dr}{dt}$$

Hence

$$\frac{dr}{dt} = \frac{1}{2\sqrt{A\pi}}\frac{dA}{dt}$$

The rate at which the area changes is approximated by the difference between the cross-sectional area before and after divided by the time that took for aeciospores to increase in volume, i.e.

$$\frac{dA}{dt} \approx \frac{A_{after} - A_{before}}{T}$$

and

$$A \approx \frac{1}{2}(A_{after} + A_{before})$$

A total of 6 measurements from videos (**Figure 2.13 A**) were done, resulting on a median value of the rate of water absorption for aeciospores (dr/dt) of 0.56 s^{-1}.

To calculate the size of the gap between aeciospores, TEM images were used to measure the space that exists between neighbouring aeciospores. Measurements were taken from the bottom, medium and top of the aecial cup to get a representation of the possible space size that can be occur between neighbouring aeciospores within the cap. A total of 138 measurements were taken, resulting in an average of 1.96 μm, with a minimum of 0.462 μm and a maximum of 7.464 μm, near the top of the cup (**Figure 2.15**). Thus, an average of 1.96 $x10^{-6}$ m was used for the value of the initial gap size in the model.

A detailed explanation of the model is included in (**Annexe 6.1**). A range of predicted ejected velocities was estimated that fluctuates between 0.1-0.7 m/s, as it was observed using HS videography. Since some of the parameters included in the model were rough estimates, the predicted values of the launch speed should be treated with caution. The order of magnitude of the estimate is however within the range of what was observed, and thus the model is consistent with the experimental data gathered.

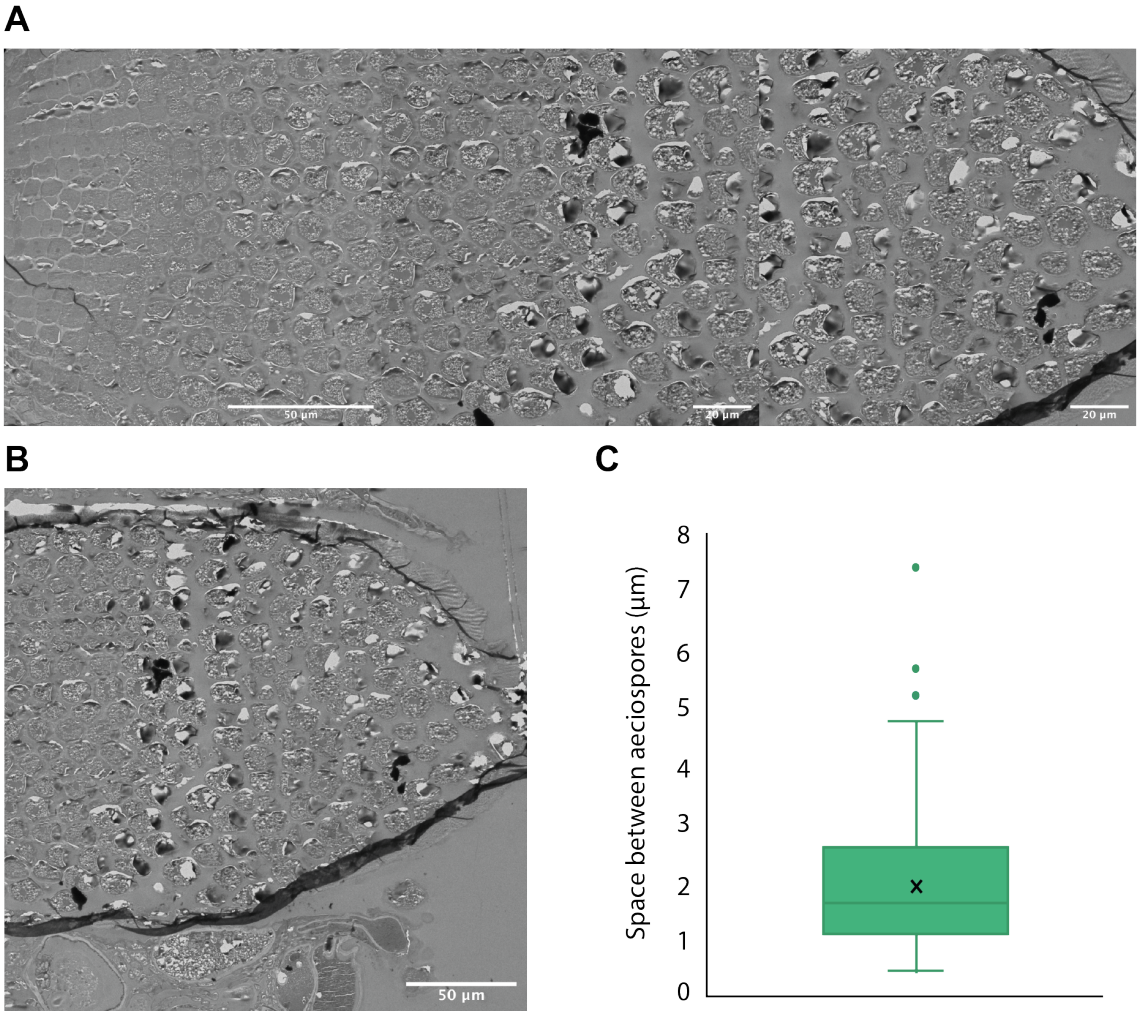

Figure 2.15 The space between aeciospores was measured using TEM. (A, B) A total of 138 measurements were taken using TEM images from the bottom, middle and top of the aecial cup. **(C)** The size of the gap between neighbouring aeciospores varied between 0.462 up to 7.464 µm, with an average of 1.96 µm.

2.5 Discussion

2.5.1 High-speed videography allows us to determine aeciospore launch speed

Release mechanisms of fungal spores have been studied for a long time (Micheli, 1729) and before HS videography was used, estimates of release velocities were carried out using various methods (Ingold & Hadland, 1959; Page & Kennedy, 1964). However, these were not very accurate, and the use of HS videography has permitted the measurement of launch speeds unambiguously (Yafetto et al., 2008). In this chapter, I used a HS camera to record the release of *Pg* aeciospores from aecial-cups. To my knowledge, this is the first time that aeciospore discharge has been observed in detail and recorded. Ejection velocities calculated here oscillated between 0.1-0.7 m/s, with a median of 0.2 m/s. These values are similar to that observed in other Basidiomycota when releasing basidiospores via the Buller's drop mechanism (**Table 2.1**). However, it is considerably slower than the observed for ascospores (in Ascomycota) released using the squirt-gun mechanism (14-21 m/s, **Table 2.1**). For *B. ranarum*, that uses a rounding-off mechanism (Ingold, 1934), launch speeds were also higher than what was observed for aeciospores.

Table 2.1. Spore launch speeds for a range of fungi. Discharge velocities for a range of fungi using different mechanism of spore release. Values vary slightly between species even with the same mechanism.

Species	Launch Speed (m/s)	Mechanism	Reference
Ascobolus immersus	14	Squirt-gun	(Yafetto et al., 2008)
Podospora anserina	21	Squirt-gun	(Yafetto et al., 2008)
Basidiobolus ranarum	4	Rounding-off	(Yafetto et al., 2008)
Armillaria tabescens	0.6	Buller's drop	(Fischer et al., 2010)
Gymnosporangium juniper-virginianae	1.1	Buller's drop	(Fischer et al., 2010)
Auricularia auricula	0.8	Buller's drop	(Noblin et al., 2009)
Aleurodiscus gigasporus	0.53	Buller's drop	(Fischer et al., 2010)
Pilobolus kleinii	9	Squirt-gun	(Yafetto et al., 2008)

Looking at the ultrastructure of spores and the fruiting body can help elucidate release mechanisms (Meredith, 1973). In terms of aeciospores, it was suggested that the granules on the surface of aeciospore had a role in aeciospore discharge (Gregory, 1961). These granules are thought to aid in a similar way that a marble would help a tennis ball leap high

into the air: “if a tennis ball is pressed down against a table and released, it would barely leave the table, but if it is pressed down over a marble on the table, it would be released high” (Savile, 1954). This has yet to be confirmed, since no differences in discharge distances were found between species that either contain or lack these plugs. A correlation has however been observed between aeciospore size and distance travelled, with larger spores being released further (12-13.5 mm for *P. podophylli* versus 3-6 mm *P. andropogonis*) (Savile, 1954). These differences could be explained by the effect of drag, which would be smaller in larger spores, thus allowing them to travel further. A way to evaluate the role of granules in aeciospore discharge would be to estimate the velocity of aeciospore discharge for fungi with and without these plugs and compare both launch speeds to see if initial speed increases when granules are found. Surface roughness is known to have an effect in particle motion during collisions and also in adhesive interactions (Wilson, Dini, & Van Wachem, 2017). An increasing grain size has been observed to help maintain kinetic energy for certain materials (Sandeep, Luo, & Senetakis, 2020). Thus, large granules in the surface of aeciospores might indeed have a role, even if their occurrence is not intentional but only a by-product of verrucose formation.

Velocity of release had been calculated in the past for several fungi using distance of release (Fischer et al., 2004; Trail, Gaffoor, & Vogel, 2005). However, these methods were limited by drag assumptions. The estimation of the effect of the drag in small particles is not trivial and much work has been done in this field (Purcell, 1977; Vogel, 2005). The equation used here proved to be accurate when predicting spore launch speeds using the distance travelled (Pringle et al. 2017). The effect of drag in the aeciospores after leaving the aecial-cup can be observed in their trajectories. Trajectories of ballistospores had been previously predicted (Fischer et al., 2010), however, to my knowledge the full trajectory of the spore from release until fall had never been shown before for any other rust fungi.

2.5.2 *Pg* aeciospores are released in groups to achieve greater distances

Distances reached by aeciospores after release observed in the videos differed with that observed after leaving them to release for a few hours in a closed environment. Observations with the high-speed camera showed spores travelling around 0.11-0.77 mm (median: 0.4 mm) before starting to fall. Nonetheless, distance travelled under different temperature conditions ranged from a maximum of 5.5 mm up to 71.2 mm. This maximum value is considerably higher than that previously reported, which was 3 - 7 mm (Savile, 1954), although these values from the literature are presumably for single aeciospores.

Release of *Pg cluster-bombs* had already been reported and found to reach up to 1 cm (Coons, 1910). Here, aeciospore clusters were mostly found reaching distances above 2 cm, and a maximum of 7.12 cm. These results suggest that aeciospores could be grouping together as a way of achieving greater distances when being released. This is a very well observed behaviour in fungi (Ingold, 1928, 1939). Grouping spores would increase the mass-air drag (m/ζ) ratio which would allow spores to travel further. This could however affect the posterior spore dispersal since small and light objects can be carried more easily in the wind (Pringle et al. 2017). Observations of clusters after release revealed that single aeciospores were sometimes found near these clusters, which could indicate that aeciospores might also be able separate after release to achieve greater distances. The capacity of aeciospores to cluster could help them achieve greater distances which as a consequence will enable them to propagate further to reach their primary host (wheat in the case of *Puccinia graminis* f. sp. *tritici*). If aeciospores are then able to disperse, it will help them start an infection and thus continue their life cycle.

2.5.3 Temperature does not seem to have a direct effect in the mechanism of *Pg* aeciospore release

Understanding the variables that influence spore discharge can help predict and control disease dynamics (Fourie, Schutte, Serfontein, & Swart, 2013). Environmental factors are known to affect highly spore release (Mims et al., 1980). Some of these include (i) temperature, as it's the case of basidiospore release of *Paxillus panuoides* (McCracken, 1987), (ii) humidity (Johansson, Lönnell, Rannik, Sundberg, & Hylander, 2016) or (iii) light, as shown for for *Venturia inaequalis* (Brook, 1969), or even alternating light/dark as for *Chondrostereum purpureum* (Spiers, 1985). Although in most cases, spore release is not affected by just one variable, but it is a combination of several factors (Grove, 1991). In the case of *Pg* aeciospores, release has been associated mainly with high levels of RH. Here, aeciospore release was observed under different temperature conditions and no significant differences were found between experiments. This suggests that the range of temperatures tested here (5 to 37 ºC) does not have a role in spore release and does not affect how far away aeciospores are discharged. Although certain pattern can be observed, with an increase in distance reach at 18-25ºC, variation is too high between replicates, so further work would be required. Besides, aecial and leaf stage of samples was not considered here, and future work would include testing differences in release under different temperatures with samples collected at the same stage of infection.

Periodicity in spore liberation is a commonly observed and well reported phenomenon (Pady, Kramer, & Clary, 1967; Stępalska & Wołek, 2009). Many fungal spores are believed

to have cycles of release associated with numerous factors (Kadowaki, Leschen, & Beggs, 2010). These factors can be related to weather conditions that trigger spore release, but that is not the case for all pathogens (Hirst, 1953). Periodicity in aeciospore discharge was previously reported for *Puccinia andropogonis* (Pady et al., 1967). Observations in several rust species confirmed aeciospores were more frequently found at night-time (Kramer et al., 1968). However, these peaks in release not only coincided with periods of high RH, but spore release was also observed during daytime rains. Studies of liberation periods in *Gymnosporangium* showed a clear correlation between high RH or rain and aeciospore release (Pady et al., 1969). Periodicity observed previously can therefore be biased by environmental factors, which would indicate that water availability is the key requirement for spore release. Here, aeciospore release was always observed after spraying them directly with water or placing the lesion on water to induce water intake. This, together with the lack of effect of the range of temperatures tested here, contributes to the hypothesis that water absorption by aeciospore is a prominent factor influencing their ejection from the aecial cups (Kramer et al., 1968).

2.5.4 The increase in *Pg* aeciospores via water absorption likely contributes to spore discharge

Water absorption by aeciospores has been previously reported (Mims et al., 1980). Aeciospores were observed to increase in volume when sprayed with water (Kramer et al., 1968). Here, I measured the precise increase in area and diameter of aeciospores when immersed in water. The rate at which aeciospores are able to expand was also determined using videography. This expansion of up to 5 µm (almost half of their initial diameter) could indeed increase the pressure in aecial-cups which would lead them to take-off, as previously determined (Kramer et al., 1968). Spore liberation based on cell turgidity has been observed in other species, such as in *Peronossclerospora philippinensis* (Downy mildew of maize) (Weston, 1923) and *Basidiobolus ranarum* (Ingold, 1934). This kind of release, even if the norm for *Pg* aeciospores, does not occur in all rust fungi, as it is the case of *Gymnosporangium Juniperi-virginianea* that needs dry conditions for spores to escape (Pady et al., 1969). To illustrate how this may happen, we built a mathematical model that includes the details observed in aeciospore release. Predictions with mathematical models should be taken with caution, especially when parameters are an approximation (Breckling, 2002). However, modelling can help us represent a biological mechanism and prove whether it is plausible (Fischer et al., 2010). The model developed here gives a plausible explanation to the hypothesis of aeciospore release mechanism. An assumption is made regarding the film that forms between aeciospores, for which no clear evidence has been obtained.

Presumably, if water enters the aecial cup and there are gaps occurring between aeciospores, it can be assumed that water would perfuse between the gaps, hence forming said film. However, this does not imply that this is the definite mechanism of how aeciospore release occurs, since other mechanisms could be plausible. In fact, other models were considered previous to the one described in this thesis, such as a 'spring-release' mechanism (Ilton et al., 2018). For said model, the elasticity of aeciospores would be a key parameter and its calculation would have been necessary. Future work would include this, using Atomic Force Microscopy, as done for other fungi such as *Aspergillus nidulans* (Zhao, Schaefer, & Marten, 2005). Measuring the force needed to break the bond between aeciospores would also be a nice addition to the model, and a good way to test whether the force being produced with the proposed model would be enough to break said bond (Noblin, Yang, & Dumais, 2009). Here, it is proposed that water availability is the only requirement for aeciospore release. This model could be adapted to other rust fungi by substituting the key parameters included in the model, such as H_0 (the initial gap), δ (the rate of radius increase) and λ (the diameter of the aeciospore). These last two parameters might not differ in close *Puccinia* species, although the differences in aeciospore morphology among rust species suggests that h_0 could vary which would affect the velocity of release (Lee & Kakishima, 1999; Mims et al., 1980; Zwetko & Blanz, 2012). The model developed here is a good representation of how ejection could occur by just the effect of rounding-off after water absorption.

2.6 Conclusion

High-speed videography was used to study the mechanism of aeciospore discharge in *Puccinia graminis*. Aeciospores were observed to have a median launch speed of 0.24 m/s that decreases rapidly due to the effect of drag. Aeciospores were able to reach distances of up to 7 cm, higher than previously reported. Aeciospores travelling more than 2 cm were found forming clusters which could be a mechanism to achieve greater distances. Aeciospore release was observed to be independent from the temperature range tested and triggered largely by water availability. Water intake led aeciospores to increase their volume significantly, up to a diameter increase of 5 μm. This expansion generates an increment in pressure inside of the aecial cups that may lead to their expulsion. The mechanism of release was modelled using lubrication theory that proved to be a plausible method, with predicted velocities being similar to that observed. This suggest that the hypothesis that water availability is the key factor in aeciospore release is reasonable and this information could potentially be used to predict aeciospore ejection in the field.

Chapter 3:

Modelling *Pgt* aeciospore dispersal after release from barberry bushes

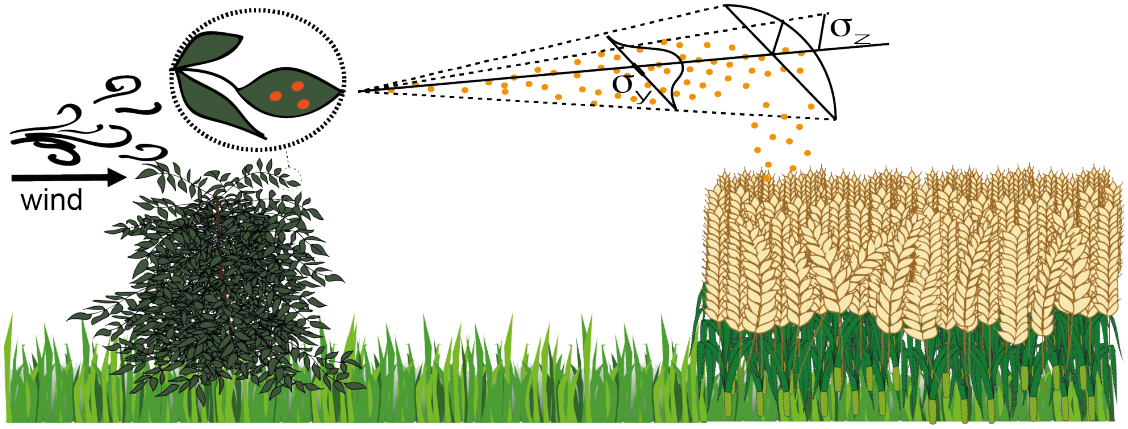

Chapter 3 Modelling *Pgt* aeciospore dispersal after release from barberry bushes

3.1 Abstract

Like many rust pathogens, the wheat stem rust pathogen, *Puccinia graminis* f. sp. *tritici*, requires two hosts to complete its life cycle, with asexual reproduction taking place on wheat and sexual reproduction completed on various *Berberis spp.*, where recombination can give place to novel virulent genotypes. Historically the removal of common barberry (*B. vulgaris*) that is highly susceptible to stem rust infection reduced the intensity of stem rust epidemics by breaking the *Pgt* cycle. However, recently barberry planting has reinitiated, and new stem rust foci of infection have been reported in western Europe. Therefore, there is a deep sense of urgency to establish the role of common barberry in harbouring and enhancing the diversity of wheat rusts in the UK. Mathematical modelling can help us assess the risk of planting barberry near wheat fields by using dispersal models to investigate how far away aeciospores could travel. Two key measurements are needed to generate accurate dispersal models: (i) the amount of inoculum being produced and (ii) environmental factors that influence dispersal and survival of spores. Here, I examined the number of aeciospores contained in infected barberry leaves, with an average of 7,111 aeciospores found per aecial cup and 8.29 cups/mm^2 within an aecium. The effect of temperature (5-30 ºC) on source strength was also evaluated and no effect was observed, although only 2.96 % of predicted aeciospores were actually found to be released. This information was used in a Gaussian Plume Model to predict how far aeciospores could travel from barberry bushes. A user-friendly webapp that includes real-time weather data was then developed to make the model accessible to the widest demographic. This tool can help evaluate the threat of barberry bushes that are infected with stem rust in spreading inoculum to adjacent wheat fields and identify those that need careful monitoring.

3.2 Introduction

3.2.1 The risk of barberry bushes

Out of all the wheat rust, *Puccinia graminis tritici* (*Pgt*), that causes stem rust (SR), has been causing severe epidemics since the beginning of agriculture (Arya & Perelló, 2010). As mentioned in the introduction, this pathogen has a complex life cycle that includes two plant

hosts: a cereal crop (wheat or barley) where it undergoes asexual reproduction and an alternate host (barberry) that is necessary to carry out sexual reproduction (Jin, 2011). Common barberry (*Berberis vulgaris*) bushes were brought to Europe from Asia and were frequently used as field hedges because of their density and sharp spines (Barnes, Saunders, & Williamson, 2020). The relation of *Pgt* with common barberry bushes has been observed for a long time, before the role of the alternate host was fully understood. European farmers soon realised that growing barberries near cereals caused SR epidemics in their fields. This led to a law being passed in Rouen (France) to forbid the growing of SR-susceptible barberry bushes in 1660, more than 200 years before DeBary showed that rust infecting barberry in spring was the same that infected cereals later in summer (Pipal, 1918). The eradication of common barberry was shown to be an effective method to stop SR epidemics on wheat and led to almost its complete extinction in many European countries (Berlin, Djurle, Samils, & Yuen, 2012; Alan P. Roelfs, 2010). Likewise, in the US, eradication programs to remove common barberry from 1918-1980s managed to reduce the intensity of wheat SR epidemics and the number of *Pgt* races (Wang, Wan, & Chen, 2015).

However, legislation to restrict barberry planting in western Europe has long since lapsed and planting of this popular shrub has reinitiated alongside reports in recent years of new SR foci of infection after many decades of absence (Saunders, Pretorius, & Hovmøller, 2019). In the UK, SR was recorded in 2013 on wheat for the first time in 60 years (Lewis et al., 2018). The isolate found, that belonged to the 'Digalu' race, was reported to be able to infect over 80 % of current UK wheat varieties. Isolates from the same race had also been found in 2013 in Germany and Denmark (Lewis et al., 2018). In 2017, an outbreak of wheat SR was reported in Sweden, near an area where common barberry had been re-established (Berlin, 2017). This repopulation of common barberry has given SR a chance to survive between crop seasons through the production of overwintering teliospores that will in turn produce basidiospores when they germinate, being then able to infect susceptible barberry. Once the pathogen is on the alternate host, it can complete sexual reproduction and recombine which could originate novel genotypes and races (Berlin et al., 2012). *Pgt* aeciospores containing these new genotypes can be carried by the wind and reach wheat fields nearby, occupying a new niche through novel virulence phenotypes. Once they infect wheat, they can produce more inoculum that can then be dispersed to wheat fields further away, which has the potential to lead to a large SR epidemic in the UK.

Common barberry, apart from an alternate host for *Pgt* and other *Puccinia graminis* (*Pg*) *formae speciales*, is an essential habitat for various species, such as the barberry carpet moth (*Pareulype berberata*). Larvae of this moth rely on this bush as a food source and thus

common barberry eradication drove the barberry carpet moth to near extinction (Waring, 2004). Hence, there is a need for a balance between increasing the population of this species by re-planting barberry bushes and managing the risk that SR can pose to UK agriculture. In order to address this problem, it is crucial to understand how *Pgt* aeciospores are disseminated from their production source in barberry bushes to their cereal host. Investigating how far away aeciospores can travel can help us understand the risk that common barberry bushes pose to initiating SR epidemics and thus enforce careful monitoring of these bushes.

3.2.2 Studying the process of pathogen dissemination is key to tackling epidemics.

The process of air-borne pathogen dissemination, from production to deposition, can be divided into four main steps: inoculum production, canopy escape, dissemination and deposition (Mahaffee & Stoll, 2016). Each one of these processes depends on a number of factors, both environmental and biological. The first step, inoculum production, depends on weather conditions and the phenology of the host and pathogen and the amount of inoculum being produced (i.e. the number of spores that will be released) that influence dispersal. Once generated and released, spores then need to escape the host canopy to be disseminated, which relies on the canopy architecture and turbulence (Andrade, Pan, Dannevik, & Zidek, 2009). The turbulence that occurs within a canopy is defined by the set of wind gusts (or eddies) that are created and that can carry spores above the canopy (Finnigan, 2000). The probability of a spore to be transported out of the canopy is affected by the velocity of these eddies and by a 'filtering factor'. This filtering factor is related to the leaf area index (LAI), i.e. large values of "leaf area" would reduce the chance that a spore would be able to escape without colliding with a leaf (Follett, Chamecki, & Nepf, 2016). This measurement of LAI represents how dense the plant canopy architecture is and can be used to estimate the vertical escape fraction with the following equation (De Jong, Bourdôt, Powell, & Goudriaan, 2002).

$$E_v = \exp\left[-\mathrm{LAI}\sqrt{\frac{v_d}{\kappa u}}\right] \tag{3.1}$$

where v_d is the deposition velocity of the spores, u is the wind speed, and κ represents the von Karman constant. This is a dimensionless constant that is often used in turbulence modelling to estimate fluxes of momentum heat and moisture from the atmosphere to the land surface and it is considered to be universal and equal to 0.4. The spores that leave the canopy would then be carried by the wind until they are deposited onto the ground or a new host. The dispersal distance will then depend on the deposition rate onto host tissue (Aylor, 2003). There are two major mechanisms of deposition: wet (in rain droplets) or dry due to

gravitational settling (sedimentation) or particle impaction (Mahaffee & Stoll, 2016). Once the pathogen has been deposited on its host, the infection process can begin if environmental factors are right for spore germination.

Many studies have been carried out taking into account environmental factors to predict infection (El Jarroudi et al., 2017, 2020). In addition, exploring how far spores can travel can give us more information about the possible risk of pathogen infection in certain areas (de Jong, Scheepens, & Zadoks, 1990). However, studying this is not easy and usually requires a deep knowledge of each step of the process. Hence, mathematical modelling can help make predictions based on basic knowledge about the system and provides a useful tool for investigating spore dispersal (McCartney & Fitt, 1985).

3.2.3 Modelling the process of spore dispersal

Dispersal models are commonly divided into two categories: empirical and physical, mechanistic models. The first ones consist of collecting data of spore (or disease) spread and fitting them into a function of the distance that spore travels from the source (Fitt, Gregory, Todd, McCartney, & Macdonald, 1987). Whereas physical models are based on turbulent dispersion theories and usually include effects of wind currents, gravitational settling and deposition. These are very informative and frequently more accurate because they model the physical factors that have an effect on the process of dispersal (Kuparinen, 2006).

Empirical models focus on finding the probability density function (dispersal kernel) that represents how the pathogen spreads from the source, which is usually defined by a negative exponential or power-law function (Fitt et al., 1987). Both of these functions seem to be able to explain dispersal relatively well, although there appears to be a preference for one or the other depending on the system. For example, air-borne spores smaller than 10 μm have been observed to fit better to power law, whereas spores dispersed in splash droplets seem to fit better in an exponential model (Fitt et al., 1987). However, most of the time the differences between dispersal kernels are minor and are rarely constant through a season. In fact, the atmospheric conditions when spores are released have been found to affect the dispersal kernel (Reynolds, 2011), with spores being released during the warmest time of the day being more likely to be dispersed over long distances (Savage, Barbetti, MacLeod, Salam, & Renton, 2012). Other factors that affect dispersal distance are spore release height, although it does not affect small spores as much as larger spores, due to their low deposition velocity (Norros et al., 2014). Empirical models have been utilised for *Pgt* aeciospores, using both power law and exponential functions to describe spore dispersal by

counting infected stems of grasses (Johnson & Dickson, 1919). Fitting the data into those functions, they obtained the following equations that described the dispersal gradients observed:

$$\ln(y) = 12.66 - 1.05x$$

for the exponential function and

$$\ln(y) = 11.97 - 3.327 \ln(x)$$

for power law, where x represents the distance downwind the source and y the concentration of spores. However, these models are an explanation of their observations and cannot always be generalised to other field and atmospheric conditions. They are not based on a mechanistic understanding of the spread of the pathogen, since they are estimated by averaging disease incidence over time at distances from a local source (Klein, Lavigne, Foueillassar, Gouyon, & Larédo, 2003). Therefore, these are statistical models that, even though they represent the observations very accurately, are not easy to extrapolate to other conditions.

For this reason, it is more realistic to include meteorological variables and information about the process. Thus, physical models can be very helpful since they allow us to include details about the system and then evaluate the dispersal process based on those parameters. Within this category, models can be based on Eulerian or Lagrangian approaches (Klein et al., 2003). Both types of models have been used within and above crops (McCartney & West, 2007). Eulerian models are generally based on the atmospheric diffusion theory and describe the dispersal of a particle by analysing the position thereof in a given area. On the other hand, Lagrangian models are based on random walk models that estimate the position of a particle at different consecutive time-steps to calculate its trajectory (Kuparinen, 2006). Even if they tend to be more accurate than the Eulerian models (especially when modelling within the plant canopy), they are usually complex and computationally very expensive.

In any case, to describe spore dispersal accurately it is crucial to incorporate the effect of wind, turbulence and deposition in the physical model. Thus, not only the meteorological conditions have to be considered, but also the biological information about the system (i.e. spore size and density). The more information we can include about the system, the more accurate our model would be. However, there is a trade-off between accuracy and complexity when building models since it is preferable to have a simpler model that is usable.

3.2.4 Gaussian Plume Models for studying spore dispersal

In Eulerian approaches, the pattern that a particle follows during dispersal is described by an advection-diffusion equation. This equation assumes that the movement of the particle is characterised by a homogeneous random walk (diffusion) around deterministic drift (advection) and can be solved by making certain assumptions (Loos, Seppelt, Meier-Bethke, Schiemann, & Richter, 2003). One of the solutions for this is the Gaussian Plume (GP) model, that omits the effects of deposition and spatial-temporal variation on the particle movement. This model assumes that the distribution of spores in the air follow a Gaussian distribution (Spijkerboer, Beniers, Jaspers, Schouten, Goudriaan, Rabbinge, & van der Werf, 2002). This type of model is very attractive to use because of their simplicity and low computational requirements (Aylor, 2003). GP models have been widely used for studying fungal spore dispersal, such as for *Fusarium graminearum* (Prussin, Marr, Schmale, Stoll, & Ross, 2015) and even pollen dispersal (McCartney & Lacey, 1991). They have also been used to assess the risk of *Chondrostereum purpureum* infection in forests (de Jong et al., 1990). Its main limitation is that it assumes that concentration in the plume remains constant and therefore cannot predict concentration in nonhomogeneous crops or within the boundary layer. Besides, it assumes a unique source point and thus it is not always applicable when investigating dispersal in fields that might have several sources of inoculum (Prussin et al., 2015). However, they have proved to produce very accurate results when studying dispersal, especially over long distances (Aylor, 1999). The classic GP model is defined by the following equation:

$$C(x,y,z,H) = \frac{Q}{u} \cdot \frac{e^{\left(-\frac{y^2}{2{\sigma_y}^2}\right)}}{\sigma_y\sqrt{2\pi}} \cdot \frac{1}{\sigma_z\sqrt{2\pi}} \left\{ e^{\left(-\frac{(H-z)^2}{2{\sigma_z}^2}\right)} + e^{\left(-\frac{(H+z)^2}{2{\sigma_z}^2}\right)} \right\} \qquad (3.2)$$

This equation contains three factors. The first one considers the number of spores released (Q, source strength) and the wind speed (u), the second is the crosswind of the shape of the plume and the third one the shape of the plume in the vertical direction. Source strength is commonly defined by the number of spores released times their escape fraction. The other two factors are going to depend on the state of the atmosphere (in particular, the planetary boundary layer). Thus, it needs information about the environmental conditions to estimate the stability of the planetary boundary layer (**Table 3.1**). The state of the atmosphere when

spores are released will have a significant effect in how far they are disseminated (Seigneur, 2019).

Table 3.1. Stability class of the planetary boundary layer depending on weather conditions. The key factors are the moment of the day (day or night), the state of the sky (clear or cloudy), the wind speed in m/s and solar radiation (Strong: Solar radiation > 600 W/m^2, Moderate: Solar radiation between 300 and 600 W/m^2, Slight: Solar radiation < 300 W/m^2) (H A McCartney & Fitt, 1985) (Turner, 1970).

Wind	Daytime Solar Radiation				Night		
(m/s)	Strong	Moderate	Slight	Overcast	< 3/8Cloud	< 4/8Cloud	Overcast
< 2	A	A - B	B	D	--	--	D
2 - 3	A - B	B	C	D	E	F	D
3 - 5	B	B - C	C	D	D	E	D
5 - 6	C	C - D	D	D	D	D	D
> 6	C	D	D	D	D	D	D

Knowing the stability class of the atmosphere, that depends on the environmental conditions, is hence key to model spore dispersal. During the day, when the temperature is high and wind speeds are low (like in a hot still day or a summer afternoon), the atmosphere is very unstable (class A-B-C), and the shape of the plume will be *looping*. This implies that the plume reaches the ground more easily and hence spores would typically be deposited closer to the source. During overcast conditions and when the wind speed is very high, the atmosphere is in a neutral state (stability class D) and the shape of the plume would resemble a cone (*conning*). The spores would then be carried fairly far from the source before they reach the ground. Finally, under stable conditions (E-F), such as still nights with clear skies or during early mornings, turbulence is suppressed, and spores could be carried longer distances (*fanning*) (**Figure 3.1**).

In this chapter, I used a GP Model to investigate how far *Pgt* aeciospores can travel after being released from a barberry bush. To do so, I first evaluated the source strength in a *Pgt*-infected barberry bush. The samples used for this purpose were collected from barberry bushes showing SR symptoms and where *Pgt* was found (Orton, Lewis, Davey, Radhakrishnan, & Saunders, 2019). As the *forma specialis* for all samples could not be confirmed and no differences between *forma specialis* are expected (Anikster, 1984), results

obtained here are assumed to be applicable for *Pgt,* for convenience. Since classification based on morphological differences can be done using urediniospores, but not at the aecial stage (Abbasi, Goodwin, & Scholler, 2005), this is a reasonable assumption. The information collected about source strength from barberry bushes was included in a GP Model alongside weather data to model *Pgt* aeciospore dispersal. In addition, I developed a user-friendly web interface that gathers real-time weather data to make the model more accessible. This provides an excellent tool for evaluating the risk that barberry bushes can pose in spreading inoculum into adjacent cereal fields.

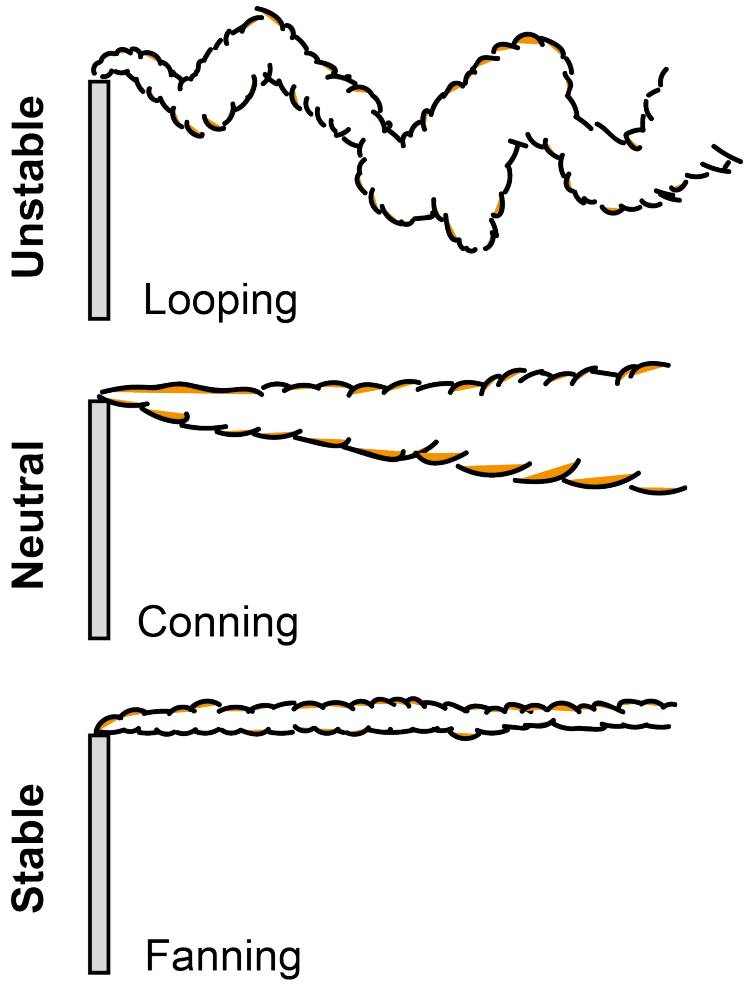

Figure 3.1. The shape of the plume changes with the state of the atmosphere. The atmosphere can be: (i) unstable (looping), under hot still conditions (stability class: A, B, C), (ii) neutral (conning) under overcast and strong winds conditions (stability class: D) or (iii) stable (fanning) with clear skies and low speed winds (stability class: E, F). Thus, spores would theoretically reach the ground earlier in unstable conditions and will reach greater lengths when the atmosphere is stable.

3.3 Methods

3.3.1 Sample collection

Barberry leaves showing SR symptoms were collected from several locations around the UK. Most analyses were done with samples collected from Brandon (Suffolk). The analysis of the number of cups per aecium was carried out with samples from Brandon and also from Pleasley Vale (Mansfield). Uninfected barberry leaves were also collected to estimate their area. All samples were collected from several barberry bushes with the help of Phoebe Davey, Morgan Gerrity, Elizabeth Orton and Clare Lewis (Saunders Lab). After collection, leaves were placed in boxes or 9 mm petri dishes and transported back to the laboratory.

3.3.2 Scanning Electron Microscopy

This was carried out as described in Chapter 2, section **2.3.6** by Kim Findley (JIC).

3.3.3 Image analysis

All measurements in images were carried out using ImageJ. To estimate the spore width in a cup and the length of the cups, the "straight" tool was used, with the scale as a reference (using Analyse > Set Scale). To calculate the area of infection (i.e. showing SR symptoms) in the leaves, both for the close-ups and for the entire leaf, the "freehand selection" tool was chosen. After selecting the region, the option Analyse > Measure was used to obtain the area. The same process was followed to quantify the area of a barberry leaf.

To quantify the number of spores per layer and the number of cups per aecia, dots were drawn on top of each element using Adobe Illustrator. This was done with the help of Morgan Gerrity (Saunders lab). To avoid mistakes, a python script was developed to quantify the dots automatically (www.github.com/vbuens/imaging/countdotspores.py).

3.3.4 Correction for potential source strength

To estimate the number of aeciospores released from aecial cups, *Pgt* aecia were attached to the wall of a square plate, above microscope slides covered with 2 % water agar. The plates were then left at 5, 10, 18, 25 and 30 ºC in the dark. After aeciospore release, pictures of the microscope slides were taken as shown in (**Figure 3.2 A**). For each picture, aeciospores were counted to obtain an estimation of the number of aeciospores that had been released "per row" (**Figure 3.2 B**) and in total. Pictures were taken at 10x or 20x, representing an area of 1x1.5 mm^2 or 0.5x0.75 mm^2 respectively. This was carried out with the help of Clare Lewis (Saunders Lab). To count the aeciospores per image, a python script was used (www.github.com/vbuens/imaging/countdotspores.py) and images were then manually checked to confirm the count was correct. Pictures that contained too many

aeciospores and could not be automatically quantified by the python script were counted manually.

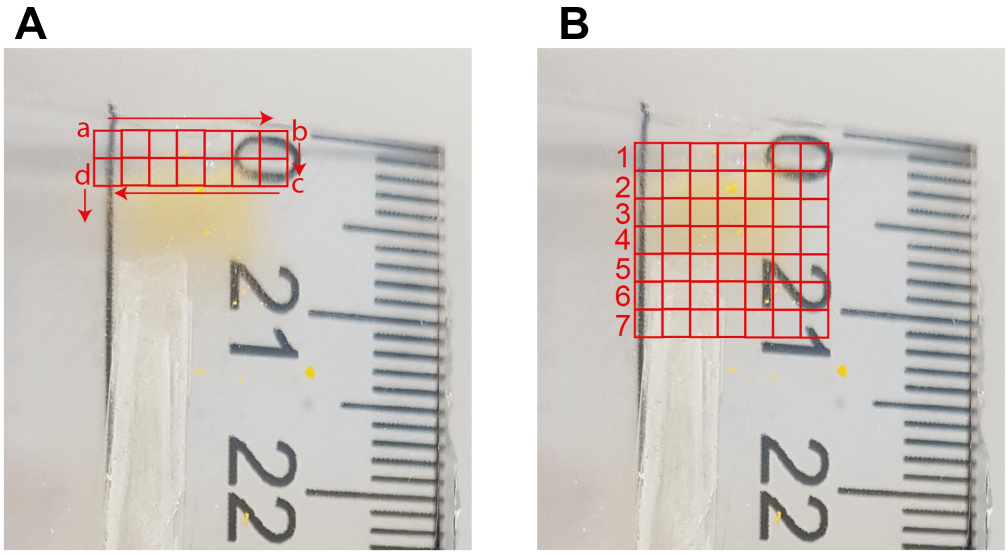

Figure 3.2. Pictures taken of the slide surface covered with aeciospores. (A) Pictures were taken as shown in the image, from a to b, and from c to d, covering all the surface with spores. Following this method, pictures were analysed in rows as shown in **(B)**, where there are 7 rows of pictures with the first being the closest to the source (i.e. the location where the aecium was placed).

3.3.5 GP Model for spore dispersal

To estimate the concentration of spores at each point downwind from the source (susceptible barberry bush) we used the following GP Model (Spijkerboer, Beniers, Jaspers, Schouten, Goudriaan, Rabbinge, & van der Werf, 2002):

$$C(x,y,z,H) = \frac{Q_{eff}}{2\pi u \sigma_{y\sigma_z}} \cdot e^{\left(-\frac{y^2}{2{\sigma_y}^2}\right)} \cdot e^{\left(-\frac{(H-z)^2}{2{\sigma_z}^2}\right)} e^{\left(-\frac{(H+z-2d)^2}{2{\sigma_z}^2}\right)} \qquad (3.2)$$

This equation contains three factors. The first one considers the number of spores released per second (Q_{eff}, effective source strength) and the wind speed in m/s (u), the second is the crosswind of the shape of the plume and the third relates to the shape of the plume in the vertical direction. The last two depend on the state of the atmosphere. Thus, information about wind speed, the time of the day and the state of the sky (solar radiation in W/m^2 and percentage of cloud cover) was used to determine the stability class of the planetary boundary layer (**Table 3.1**). This provided the values of the standard deviations σ_z and σ_y that determine the shape of the plume (**Table 3.2**), where:

$$\sigma_z = K(z_0)ax^b \quad , \quad \sigma_y = K(z_0)10^p x^q$$

Table 3.2. Values for the parameters defining σ_z and σ_y depending on the stability class. The values for *a, b, 10^p* and *q* vary depending on the stability class of the atmosphere (Spijkerboer, Beniers, Jaspers, Schouten, Goudriaan, Rabbinge, & van der Werf, 2002).

Stability Class	*a*	*b*	10^p	*q*
A	0.28	0.9	0.527	0.865
B	0.23	0.85	0.371	0.866
C	0.22	0.8	0.209	0.897
D	0.2	0.76	0.128	0.905
E	0.15	0.73	0.098	0.902
F	0.12	0.67	0.065	0.902

Here, several assumptions were made. First, an escape of 100% was assumed, since only *Pgt*-infected leaves facing the outside of the barberry bush were considered. Secondly, a scenario where all aeciospores are released at the same time and act together as a cloud was presumed. Thus, the GP model can be applied effectively. The standard GP model disregards deposition and thus here it is added in the Q factor. The effective source strength (Q_{eff}) is defined by

$$Q_{eff} = Q_{pot} \times corr \times F_d \times F_s$$

where Q_{pot} is the potential number of aeciospores that can be released, *corr* is the correction factor to calculate the aeciospores that are actually released per second, F_d is the fraction of aeciospores remaining after deposition and F_d is the fraction remaining after solar radiation (Prussin et al., 2015). The model was coded and executed using python3.

3.3.6 Web interface design

The web interface for the model was built using python3 and Django (version 3.0.2) as the web framework. To gather weather parameters, the weatherbit application programming interface (API) was used (www.weatherbit.io). A Django form was established to obtain the input values for the location (latitude and longitude), percentage of infection of the bush and leaves and height of the source. All templates were designed using HTML and CSS (bootstrap-4.0.0) for the visual aspects. The interactive options (such as the button to display the weather options, the slides and the changes in leaf pictures when selecting different levels of infection) were coded using jQuery (version 1.12.0), a JavaScript library for web animations. The specific packages included can be found in the *base.html* template on GitHub. The code for building the front-end website and back-end database is accessible on Github (www.github.com/vbuens/sr-dispersal). The web interface is hosted at the John Innes Centre and available at https://aeciospore-dispersal-model.com/.

3.4 Results

3.4.1 Potential source strength estimation

To obtain an approximation of the initial source strength, the number of aeciospores that can be produced within a barberry bush was investigated. To do so, I evaluated four parameters: (i) the number of aeciospores contained in an aecial cup, (ii) the number of cups that occur per mm^2, (iii) how many cups per leaf and (iv) the possible number of infected leaves per bush.

First, to estimate the number of aeciospores contained within an aecial cup, SEM images were evaluated to determine (i) the number of aeciospores per aeciospore layer, (ii) the length (µm) of each layer and (iii) the average length of aecial cups. The width of a layer was estimated to be 13.9 ± 0.35 (S.E.) µm per layer with an average of 265 ± 8.42 (S.E.) aeciospores found per layer. The length of aecial cups was extremely variable across all samples, since it depended on the stage of development at which they are collected, ranging from 95 µm to 680.85 µm. Significant differences ($p < 0.01$; t-test) were found between samples collected in two different years. The average for 2018 was 417.85 ± 21.32 µm and 235.14 ± 25.25 for 2019. These could due to differences in environmental conditions when samples were collected. The average value of all samples collected in 2018 and 2019 was 374.86 µm (**Figure 3.3 A**). By multiplying the number of aeciospores per layer, the length of a layer and the average length of an aecial-cup, the quantity of aeciospores inside an aecial cup can be approximated. This resulted in an average of 7,111.37 aeciospores, within a range of 1,805 to 12,916 aeciospores. Given the difficulties in assessing the length of aecial cups in each instance, the average of 7,111.37 aeciospores was used in subsequent analyses. To determine the number of cups found per mm^2, samples were collected on three different days from two different locations (Brandon, Suffolk and Pleasley Vale, Mansfield) and examined using microscopy to determine the number of cups per aecium and its area. This resulted in an average of 8.29 ± 0.42 (S.E.) cups/mm^2 and 40.05 ± 4.2 (S.E.) cups per aecium (**Figure 3.3 B**). Thus, a total of 58,953 aeciospores could be potentially contained per mm^2.

To determine the number of cups per infected leaf, the levels of infection of barberry leaves were investigated. The percentage of the leaf area covered by aecia was calculated for 85 barberry leaves with different levels of infection. Infected leaves were divided into four categories depending on the infection level: low (< 1 % of the leaf covered by aecia), medium (1-3 %), high (3-10 %) and very high (> 10 %). These categories were established based on the visual inspection of infection level in the barberry leaf, as shown in (**Figure 3.4**). Most leaves collected represented low to medium levels of infection, with only a few being highly

infected. The mean for each of the groups was estimated to be 0.54 %, 1.82 %, 5.26 % and 17.6 % for low, medium, high and very high levels respectively. These values would posteriorly be used as representative percentages of infection for each category.

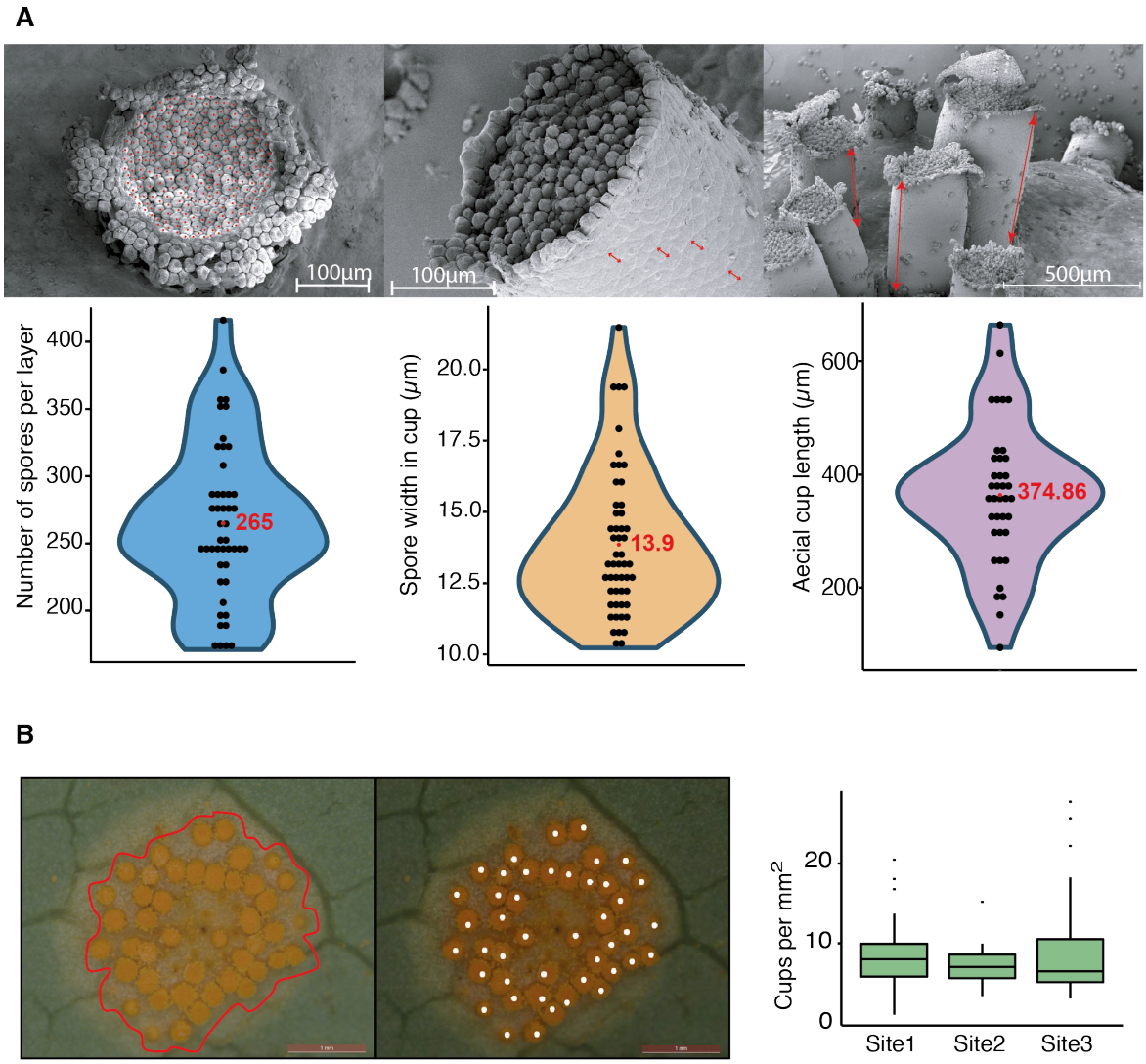

Figure 3.3 An average of 58,953 aeciospores could be found per mm². **(A)** The number of aeciospores contained in an aecial cup was determined by estimating the number of aeciospores per layer (265), the aeciospore width in a cup (13.9 µm) and the average length of an aecial cup (374.86 µm). This results in an average of 7,111 aeciospores per aecial cup. **(B)** The number of cups per aecium was calculated and divided by the area of the aecium. Using 129 measurements, an average of 8.29 aecial cups per mm² was estimated with an average of 40 aecial cups found per aecia. Site 1 and 2 corresponds to Brandon, with samples collected on the 16th and 24th of June 2019, respectively. Site 3 corresponds to Pleasey Vale, also collected in June 2019 (Manfield).

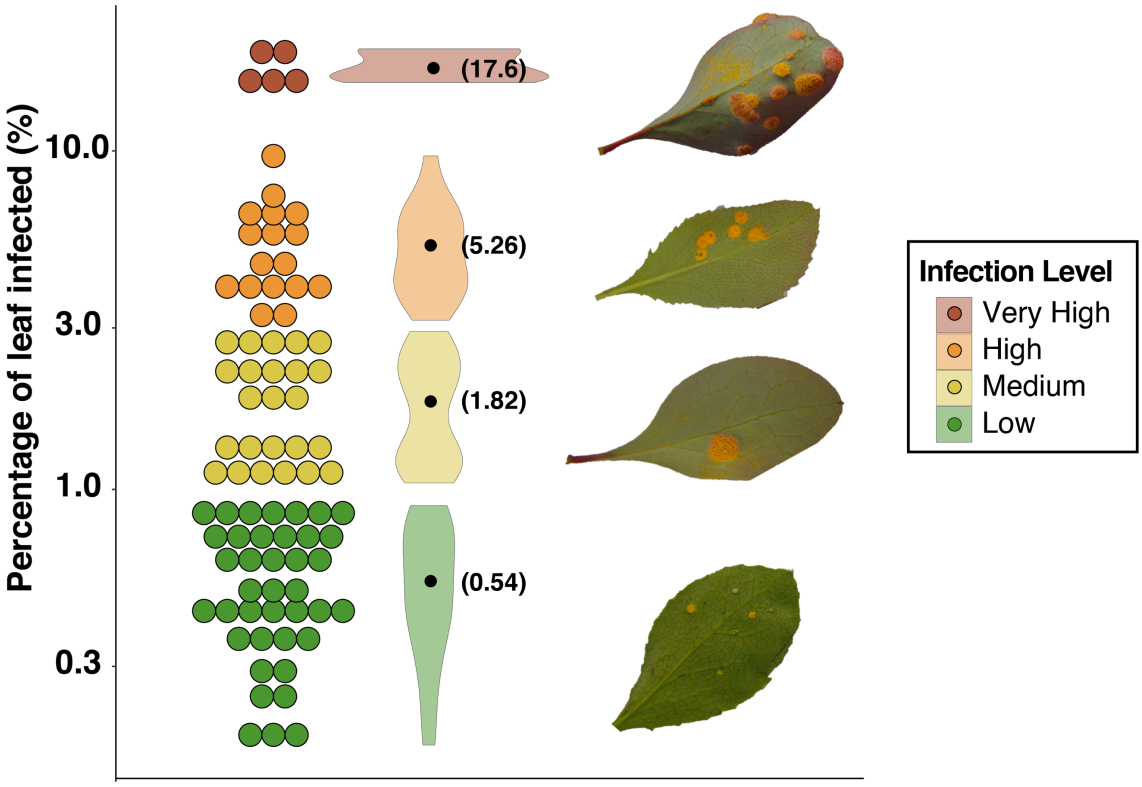

Figure 3.4. Infected leaves were classified into four categories based on infection level. The percentage of leaf covered by aecia was estimated for 85 SR-infected barberry leaves. The measurements were divided into four groups based on the observed infection level in the leaves (represented by colours). Distributions of the values included in each category are shown in the middle of the graph with the mean represented between brackets. On the right, SR-infected barberry leaves are shown as a representation for each infection level category.

To generate an estimate of the potential number of cups that can be found in an infected leaf, these values (0.54, 1.82, 5.26 and 17.6) were multiplied by the area of a mature barberry leaf. The area was calculated using 19 measurements, resulting in an average of 9.93 ± 4.04 (S.D.) cm^2. Using this value, the number of aecial cups per leaf could be approximated. For example, for a leaf with a low level of infection (average: 0.54 %), the area of infection would be:

$$\frac{0.54}{100} \times 9.93\ cm^2 = 0.054\ cm^2 = 5.36\ mm^2$$

Knowing that there are 8.29 cups/mm^2, in that area of infection there would be approximately 44.4 cups. With an average of 7,111.37 aeciospores per cup, it would mean 316,121 aeciospores being produced on a single leaf. For those leaves displaying a high level of infection they could contain:

$$\frac{17.6}{100} \times 9.93\ cm^2 = 1.75\ cm^2 = 174.77\ mm^2 \rightarrow 1448.83\ cups,$$

resulting in an estimate of 10,303,206.9 aeciospores.

To determine the total number of aeciospores that could be produced in a single bush, a count of the number of leaves in a barberry bush was needed. To determine this, measurements from the literature were obtained. Adult barberry bushes are estimated to have 58.69 ± 4.60 leaves per branch (Khan, 2014), and an average of 50-60 branches per bush (Ahmed, Anjum, Naz, Khan, & Hussain, 2013). This would imply that there could be around 3,480 leaves in a barberry bush. I also quantified the number of leaves of a barberry bush in Brandon, UK, to check the values from the literature. This revealed an approximation of 900 leaves in the side of the bush that faced a barley field and hence the side in which 100% of aeciospores could be assumed to be able to escape the canopy. This number is a quarter of the observations from the literature and thus considered a sensible approximation. To further validate this estimate, the LAI was determined using these values and compared to values in the literature. The value of LAI can be calculated using the following formula (Bréda, 2003):

$$LAI = \frac{total\ foliage\ area}{soil\ surface\ area} = \frac{leaf\ area\ \times\ number\ of\ leaves}{ground\ area} \qquad (3.3)$$

For the ground area, records were found that gave the width of a barberry shrub from 1 meter up to 1.8 meters (NH Government, n.d.), giving an average of 1.4 meters of width. That is, an area of 1.96 m^2. Substituting the values:

$$LAI = \frac{9.93 \times 10^{-4}\ (m^2) \times 3480}{1.96\ (m^2)} = 1.76$$

This value is consistent with previous reports for *Berberis* species, which ranged from 1.5 to 3.0 (Xu, Griffin, & Schuster, 2007). Therefore, it can be concluded that, even as an approximation, it is reasonable to assume that these values are a good estimate for the number of leaves in the common barberry bush.

3.4.2 Correction for the potential source strength

In section **3.4.1**, the theoretical number of aeciospores that could be released was determined based on the area of each aecium and leaf infection levels to provide a prediction of the potential source strength (Q_{pot}). The next step was to establish the actual number of aeciospores released per second (Q_0).

To assess whether temperature should be included in the model as a factor that affects source strength, the effect of temperature on the number of aeciospores released was investigated. To do so, *Pg*-infected barberry leaves were collected, and aecia left to release aeciospores on microscopy slides under an array of different temperatures. After release, the microscopy slides were observed and the number of aeciospores released was estimated in each picture and shown per row (corresponding to 1 mm), as described in the methods (**Figure 3.2**). The cumulative number of aeciospores released is shown in the graphs, where each colour represents a row, going from the closest row to the source (i.e. the first one) in a darker colour, up to the furthest row in a lighter colour (**Figure 3.5**). The cumulative number of aeciospores released has a distribution similar to a Gaussian distribution, where most of the aeciospores were deposited in the centre directly in front of the source. This was carried out at five temperatures: 5, 10, 18, 25 and 30 ºC, with three replicates per temperature. A total of 5-9 rows of pictures were captured for each replicate.

The aecium area used for each replicate was measured and the expected number of aeciospores (Q_{pot}) calculated based on estimations from the previous section. This number was then used to determine the ratio of released aeciospores vs the expected (**Figure 3.6 A**). The ratio between expected/observed was quite variable, likely due to the variations of freshness of the samples that were also collected at different stages of development. This was particularly notable for samples left at 10 ºC where ratios ranged from 0.80 % to 12.73 %. To estimate whether the temperature has an effect on the number of aeciospores that are released, t-tests were performed between pairs of temperatures that showed no significance ($p > 0.05$). This indicates that within the range of temperatures tested here, they had no effect on the total number of aeciospores released. The lack of significant

differences shows that source strength is theoretically not affected by temperatures investigated here and thus was not be included in the Q factor in the model. The ratio between expected and observed released aeciospores had an average of 2.83 % (**Figure 3.6 B**). This indicates that of the total number of aeciospores predicted in the previous section, is only a fraction of those actually released, hence a correction of 2.83 % was then included in the model.

From this, we can estimate Q_0 to be:

$$Q_0 = Q_{pot} \times 0.0283$$

Since aecial cups typically released within an hour and then were observed under the microscope, the value of Q_0 has to be divided by 3600 to estimate the number of aeciospores that would be released per second.

$$Q_0 = Q_{pot} \times \frac{0.0283}{3600}\ aeciospores\ released/s$$

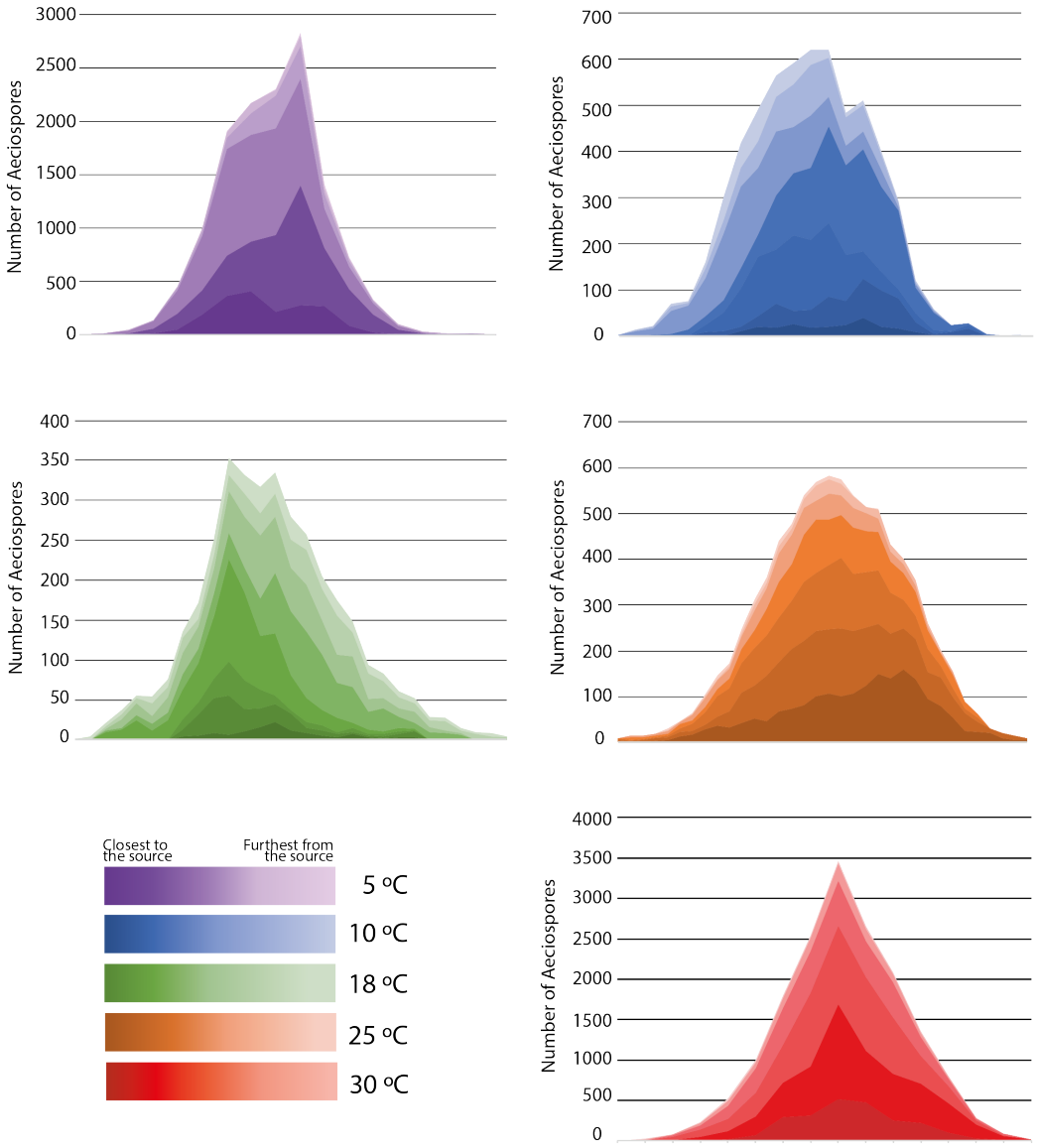

Figure 3.5. Number of aeciospores released shows a normal distribution for the range of temperatures tested (5-30 ºC). Aecial cups were left to release under different temperatures (5-30 ºC) after sprayed with water. Three replicates per temperature were carried out and aeciospores counted as described in **Figure 3.2 B**. The number of aeciospores per row were stacked, showing the shape of a Gaussian distribution. This indicates that most of the aeciospores were deposited in the centre (i.e. directly in front of the aecial cups) and fewer aeciospores were found on the sides.

A

Temperature (ºC)	Rep	Ratio
5	1	1.01
5	2	1.9
5	3	3.42
10	1	0.89
10	2	4.68
10	3	12.73
18	1	2.09
18	2	0.68
18	3	1.11
25	1	2.35
25	2	1.13
25	3	0.91
30	1	2.66
30	2	4.79
30	3	2.12

B

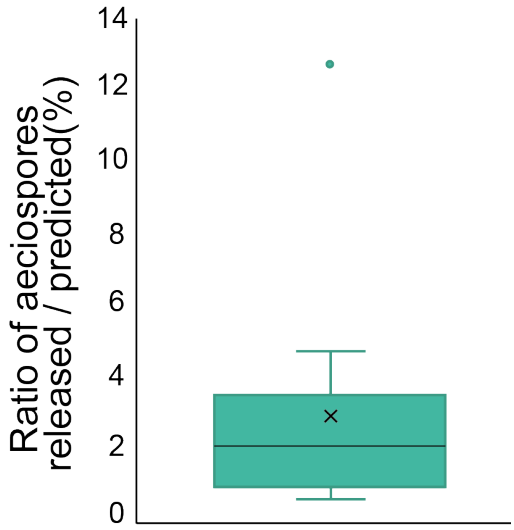

Figure 3.6. No significant differences in quantity of aeciospores released were observed under the range of temperatures tested (5-30 ºC). (A) The ratio between the observed aeciospores released and that predicted based on the area of the aecium was estimated for each temperature. No significant differences were observed between temperatures (t-test; $p > 0.05$). **(B)** Distribution of the ratios for all experiments and temperatures. The line in the boxplot represents a median of 2.1 and the 'x' represents an average of 2.83, that is, 2.83 % of the predicted aeciospores contained in the measured aecial area are actually released.

3.4.3 Aeciospore loss due to deposition and solar radiation

The basic GP model used here assumes that no aeciospores are being lost during transport. However, this assumption is not realistic since aeciospores could be lost either by deposition or by loss of viability due to solar radiation. Hence, I calculated the effective source strength as

$$Q_{eff} = Q_0 \times F_d \times F_s$$

where F_d and F_s are the fractions of the initial source strength that remain after being lost by deposition and solar radiation respectively. The fraction of aeciospores that would survive the exposure of solar deposition has the following form (Aylor, 1999):

$$F_s = \exp^{\left(\frac{-Ix}{I^* t^* u}\right)} \tag{3.4}$$

where I is the solar irradiance (W/m^2), x is the distance from the source (m), u is the wind velocity (m/s) and $I^* t^*$ is the dose of radiation that kills a fraction of 1-1/e of the spores. This dose has previously been reported to be negligible in this model for spore loss and a standard value of 20 MJ/m^2 can be adopted (Prussin et al., 2015). Although this value has not been estimated for aeciospores, but for urediniospores of *Phakopsora pachyrhizi*, 21 MJ/m2 results in a mortality of 63.2 % (i.e. the critical value) (Isard et al., 2006). Thus, this value was adopted here.

The fraction of aeciospore remaining after deposition is defined by:

$$F_d = \exp\left(\frac{-(\Gamma_w + \Gamma_d)x}{U}\right) \tag{3.5}$$

where Γ_w and Γ_d are the inverse time scales (s^{-1}) of wet and dry deposition (Aylor, 1999) that can be represented as (Prussin et al., 2015):

$$\Gamma_w = 0.000272\, R^{0.7873} \tag{3.6}$$

and

$$\Gamma_d = \sqrt{\frac{2}{\pi}} \left(\frac{v_s}{x}\right) \int_{x_0}^{x} \left[\frac{dx}{\sigma_z(x)}\right] \tag{3.7}$$

where R is the rain fall rate (mm/h), v_s is the settling velocity of aeciospores and σ_z is the standard deviation of the spread of the plume in the z direction. The integral was solved for the value of σ_z, obtaining the following expression (**Annexe 6.2**):

$$\Gamma_d = \sqrt{\frac{2}{\pi}} \left(\frac{v_s}{x}\right) \frac{1}{a} \left[\frac{(10z_0)^{0.53x^{-0.22}} x^{0.22-b+1}}{\ln(10z_0)\,(0.53 \times 0.22)} \right] \quad (3.8)$$

Since settling velocity can change depending on environmental conditions, we took a standard value of 1.13 cm/s (Pfender 2006). The roughness length (z_0) represents the effect of the surface cover on the amount of mixing. This value is thought to be related to canopy height in the form $z_0 = 0.13h$ for agricultural crops (Shaw & Pereira, 1982) where $h = 0.2$ meters.

3.4.4 *Pgt* aeciospore concentration can be estimated using a GP model

Once Q_{eff} had been determined, equation **3.2** could be used to estimate the concentration of aeciospores at each point using weather conditions to obtain values for the standard deviations σ_z and σ_y, as indicated in **Table 3.1** and **Table 3.2**. Here, we were interested in knowing how many viable aeciospores would be deposited onto the ground (i.e. z=0), thus the following equation is used to estimate the concentration at ground level:

$$C(x, y, 0, H) = \frac{Q_{eff}}{2\pi u \sigma_y \sigma_z} \cdot e^{\left(-\frac{y^2}{2\sigma_y{}^2}\right)} \cdot e^{\left(-\frac{H^2}{2\sigma_z{}^2}\right)} e^{\left(-\frac{(H-2d)^2}{2\sigma_z{}^2}\right)} \quad (3.9)$$

In the equation, H refers to the height of the source, z to the roughness length and d to the displacement height. Here, H is set at 1 m, z_0=0.026 and d=0.11, based on literature (Shaw & Pereira, 1982). The model used here assumes that the wind is coming from behind the barberry bushes and thus aeciospores are carried downwind from the source, in a straight line (**Figure 3.7 A**). Number of aeciospores at each point of the space downwind (y axis) and cross-wind (x axis) from the source are represented in a 2D graph, with colours representing the number of aeciospores deposited at each point in the x, y-axis (**Figure 3.7 B**).

To evaluate the effect that the value of Q_0 has in the estimations of the model, the number of aeciospores deposited downwind from the source was determined using different Q_0. Four different Q_0 were used: (i) 316,121, (ii)1 ,065,445, (iii) 3,079,254 and (iv) 10,303,206, assuming all aeciospores contained in a barberry leaf with the four infection levels

respectively (low, medium, high and very high) were released at the same time (in one second). The model was run using these four values of Q_0 with the environmental conditions: daylight and slightly cloudy (10 % cloud cover), no precipitation with a solar radiation of 620 W/m^2 (**Figure 3.8**). These conditions represent the meteorological conditions that can be found during an average summer (not too hot and not too cold) in England, which coincides with the time when *Pgt* aeciospores are released (May-August). The results show how for the first value of Q_0 (**Figure 3.8 A**), most aeciospores would not travel further than 40 meters, but they would travel up to 60 meters when Q_0 = 10,303,206 (**Figure 3.8 D**). This illustrates the large effect that the source strength has in where most aeciospores are likely to be deposited when they are carried by the wind.

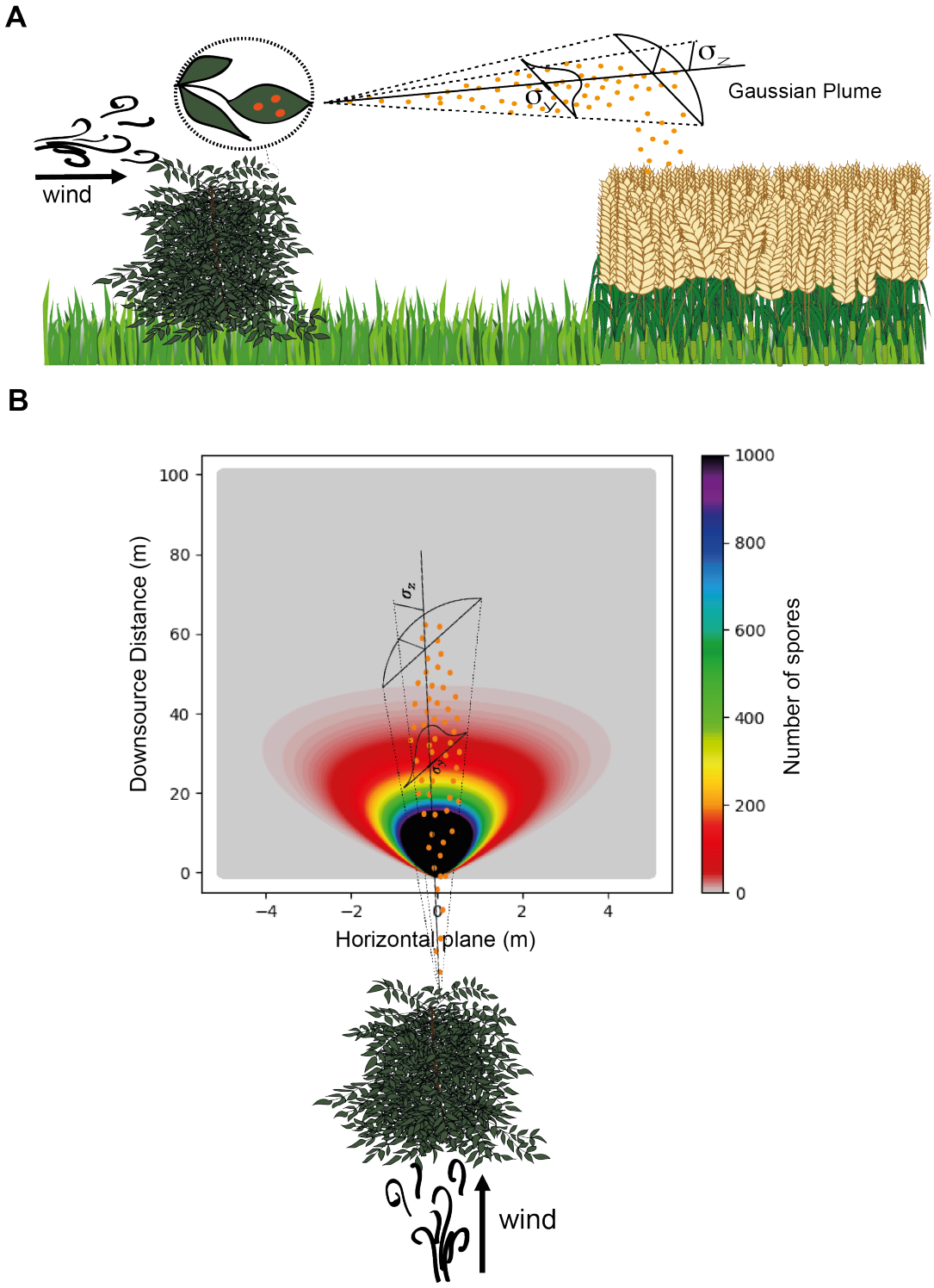

Figure 3.7. Representation of the *Pgt* aeciospore dispersal model. (A) Outline of the *Pgt* aeciospore dispersal model, where aeciospores are released in the direction of the wind and thus would travel in the shape of a GP downwind, until they get deposited onto the ground. The shape of the plume would vary according to σ_y and σ_z, shown here. **(B)** The output from the model shows graphs representing the number of aeciospores that get deposited at each point downwind from the source, as shown here. Colours represent the number of aeciospores deposited, with the scale on the right. The (0,0) point denotes the location of the SR-infected barberry bush, i.e. the source.

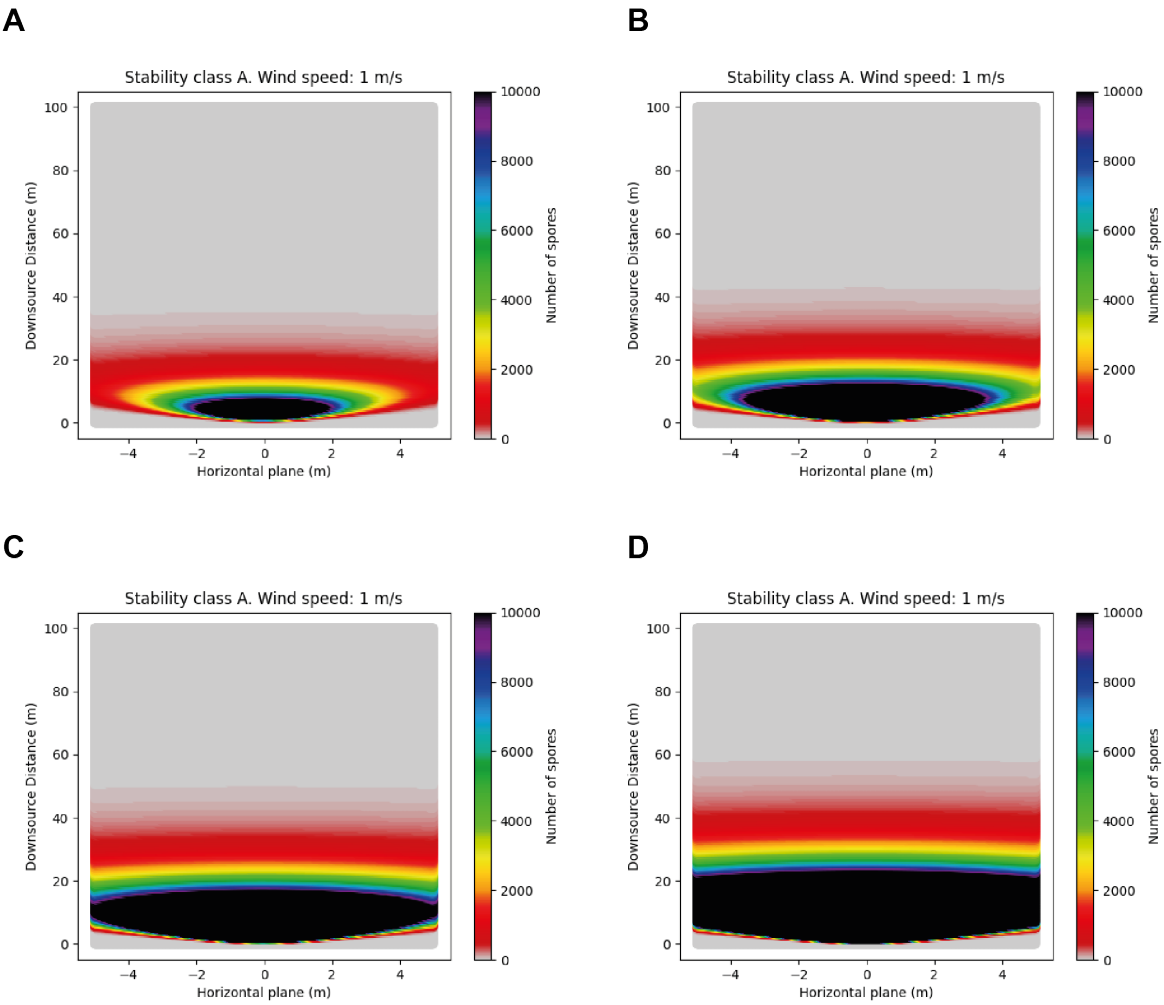

Figure 3.8. The value of the source strength (Q) has an impact on how far aeciospores can travel. The model was run with the same environmental conditions: No precipitation, 1 m/s of wind speed, 10 % cloud cover and 620 W/m^2 of solar radiation. The value of Q was assumed to be **(A)** 316,121 **(B)** 1,065,445 **(C)** 3,079,254 and **(D)** 10,303,206.9. That is, assuming that all the aeciospores contained in a leaf with an infection level low, moderate, high or very high (respectively) are released at the same time.

To evaluate the effect of weather conditions in the model, the GP model was run under different environmental conditions, using the same source strength. Since the value of Q_0 will largely vary depending on the infection level of the barberry bush, we assumed that 25 % of the bush had a medium level of infection. This resulted in a Q_0= 1,971 s^{-1}. Simulations were run under three different conditions: (i) daytime, solar radiation of 620 W/m^2, 1 m/s wind speed, no precipitation, 10 % cloud cover (**Figure 3.9 A**), (ii) as (i) but with a wind speed of 2 m/s (**Figure 3.9 B**), (iii) night-time (hence no solar radiation), 1 m/s wind speed, no precipitation, 10 % cloud cover (**Figure 3.9 C**), (iv) same as (iii) but 4 m/s of wind speed (**Figure 3.9 D**), (v) daytime, no solar radiation, 1m/s of wind speed, no precipitation and 100% cloud cover (**Figure 3.9 E**), and (vi) as (v) but with a rainfall rate of 25 mm (**Figure 3.9 F**). As mentioned in the introduction, the stability class of the atmosphere has a significant effect in how far spores are carried. When the atmosphere is stable (class E-F), spores can travel longer distances (**Figure 3.1**). This can be observed by comparing the stability class A-B (**Figure 3.9 A,B**) with F-E respectively (**Figure 3.9 C,D**). Besides, when solar radiation is high, a proportion of aeciospores would be killed, thus reducing the number of viable aeciospores being deposited. Precipitation also has an effect on aeciospore deposition, since it induces deposition, which leads to aeciospores travelling less when the rainfall rate is high. However, the effect is very small, with predictions of up to 200 aeciospores (indicated in yellow in the graph) being deposited up to 25 m without precipitation (**Figure 3.9 E**) and up to 23 m with precipitation (**Figure 3.9 F**).

As it has been shown here, how far aeciospores can travel is going to depend on two main factors. Firstly, the source strength, that is, the number of aeciospores that are being released which will depend on how infected the barberry bush is. Secondly, the environmental conditions affecting dispersal. These include: the wind speed, the percentage of cloud cover (that has an effect on the state of the atmosphere), the solar radiation (that affects the state of the atmosphere and can kill the aeciospores thus reducing the Q_{eff}) and precipitation (that helps aeciospores be deposited onto the ground). Since the maximum distance travelled by aeciospores can fluctuate depending on several factors, the recommendations for how far barberry bushes should be located from wheat fields to not pose a high risk as a source of inoculum would vary for each condition. Therefore, it would be better to assess the risk of barberry bushes based on their level of infection to try to estimate how far aeciospores could be transported under different environmental conditions.

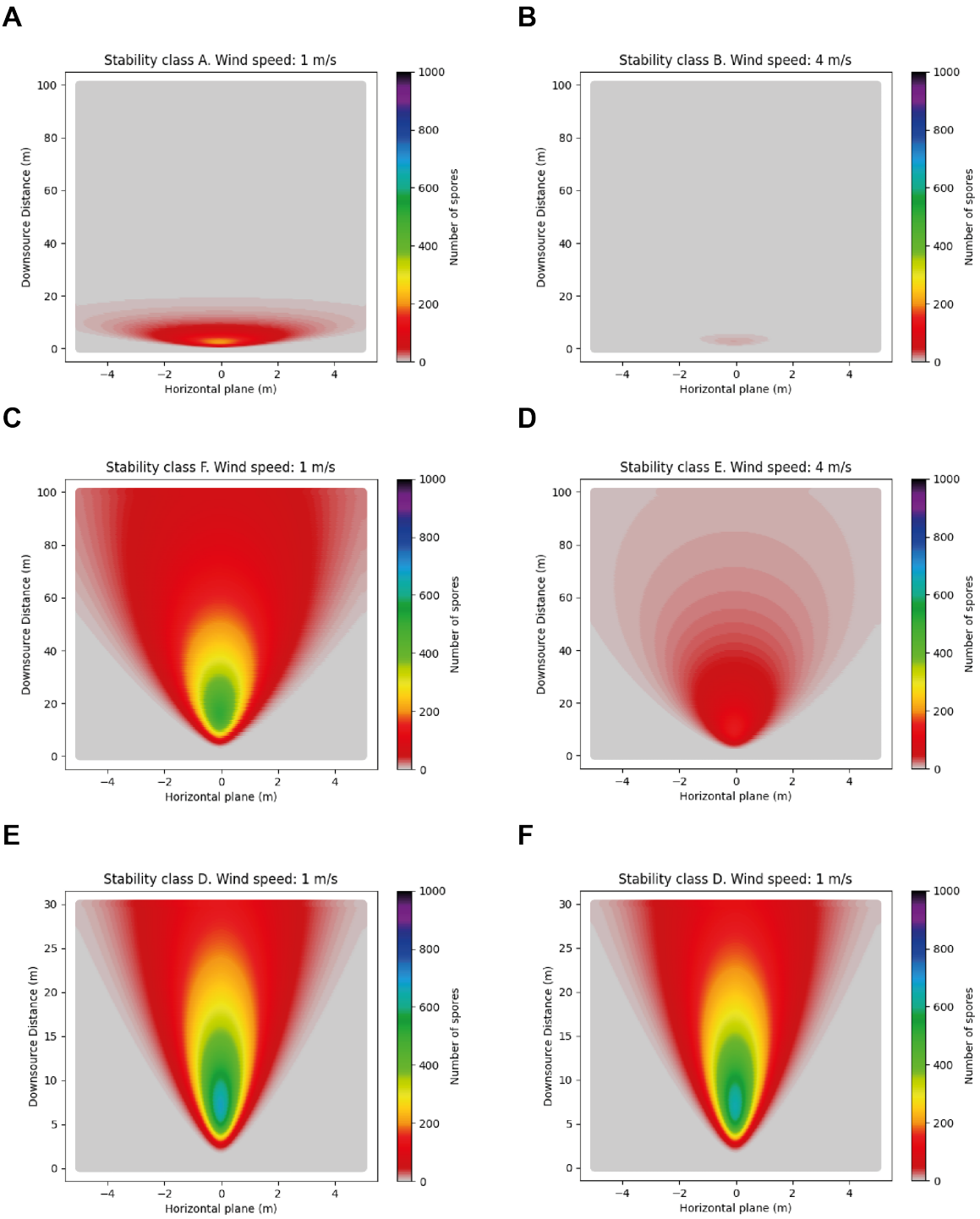

Figure 3.9. The environmental conditions affect largely spore dispersal. Simulations were ran assuming Q_0= 1,971 s^{-1}, with the following weather conditions: **(A), (B)** 620 W/m^2, no precipitation, 10 % cloud cover; **(C), (D)** night-time (no solar radiation), no precipitation, 50% cloud cover; **(E)** no precipitation, 100% cloud cover ; **(F)** rainfall rate of 25 mm, 100% cloud cover. Wind speed and stability class of the atmosphere is indicated for each graph.

3.4.5 An accessible web interface to host the aeciospore dispersal model

The *Pgt* aeciospore dispersal model developed here was included in the back end of a web interface to make it accessible for a wide range of users (**Figure 3.10**). The website is available at https://aeciospore-dispersal-model.com/. run the model, weather parameters, such as wind speed, precipitation rate and the stability class of the atmosphere, are needed. To determine the stability class, information about wind speed, percentage of cloud cover, irradiance and time of the day was collected using the weatherbit API (www.weatherbit.io). These values were then used as input into a python function to determine the stability class following the indication of **Table 3.1**. The API used here allows up to 500 calls per day with the free subscription and provides current weather data of the chosen location. The location can be specified by city name, postal code, station id or latitude and longitude. This last option was chosen since barberry bushes are unlikely to be found in cities and the specific latitude and longitude of their location is easier to find. Using these values, the API gathers information about: (i) irradiance, (ii) precipitation, (iii) RH, (iv) percentage of cloud cover, (v) wind speed and (vi) UV index. These parameters are then included in the GP model.

The infection level of the source is also needed to run the model (**Figure 3.11 A)**. The user selects the representative level of infection of the barberry leaves, choosing from Low, Medium, High or Very High, as shown in **Figure 3.4**. Using the estimation of the potential source from section **3.4.1**, the number of spores contained in each leaf can be calculated. Thus, when the user selects the level of infection, the leaves are assumed to contain the numbers of aeciospores represented in **Table 3.3**. To establish the number of leaves with that level of infection, the percentage of the bush that is infected is needed. As mentioned in section **3.4.1**, a maximum of 900 leaves are assumed to be at the front side of the barberry bush, since this is where infection mostly occurs. With the percentage provided by the user, the number of infected leaves and thus the total number of spores can be calculated. The height of the source is set as 1 meter by default, since estimations in the field showed that this height was most common, but it can also be changed by the user. The two fields highlighted in **Figure 3.11 A** are compulsory, and the model would not run without them. However, weather data can be given instead of gathered using the location by the API. This way, a user could test the model with different weather information, with three parameters needed: (1) percentage of cloud cover, (2) wind speed in m/s, (3) UV index and (4) rain fall in mm (that could be set to 0) (**Figure 3.11 B**).

Using the values provided by the user, the model runs in the background and then takes the user to a new page (**Figure 3.10**). The input values used for the model are shown at the top of the page, including rainfall rate, RH, solar radiation (irradiance), percentage cloud cover,

wind, and the percentage of infection in the barberry leaves and bush. The results show information about how far aeciospores could travel under these atmospheric conditions (**Figure 3.11 C**). First, there is a section that determines the distance of high, medium and low risk, related to the distance at which 50 %, 75 % and 99 % of the aeciospores, respectively, would land. That is, if 99 % of the aeciospores are able to reach up to 25 meters, only 1 % of the aeciospores would travel further, which presents a lower risk. The maximum distance that a single aeciospore is likely to land is also specified. Since the values estimated at each point are decimals, this maximum distance was determined by estimating the last distance at which 1 aeciospore would be found. Values lower than 1 were assumed not to be relevant. Finally, two graphs (for day and night-time conditions) showing the number of spores that would land at each point downwind from the source are included.

Table 3.3. Number of aeciospores used in the model depends on the infection level chosen. For each infection level, the percentage of infection in the leaf, the approximated number of aecial cups in the leaf and aeciospores being produced is shown.

Infection level	Assumed percentage of leaf covered by Aecia	Number of aecial cups in the leaf	Number of aeciospores produced
Low	0.54 %	44.4	316,121
Medium	1.82 %	149.8	1,065,445
High	5.26 %	433	3,079,254
Very high	17.6 %	1448.8	10,303,206.9

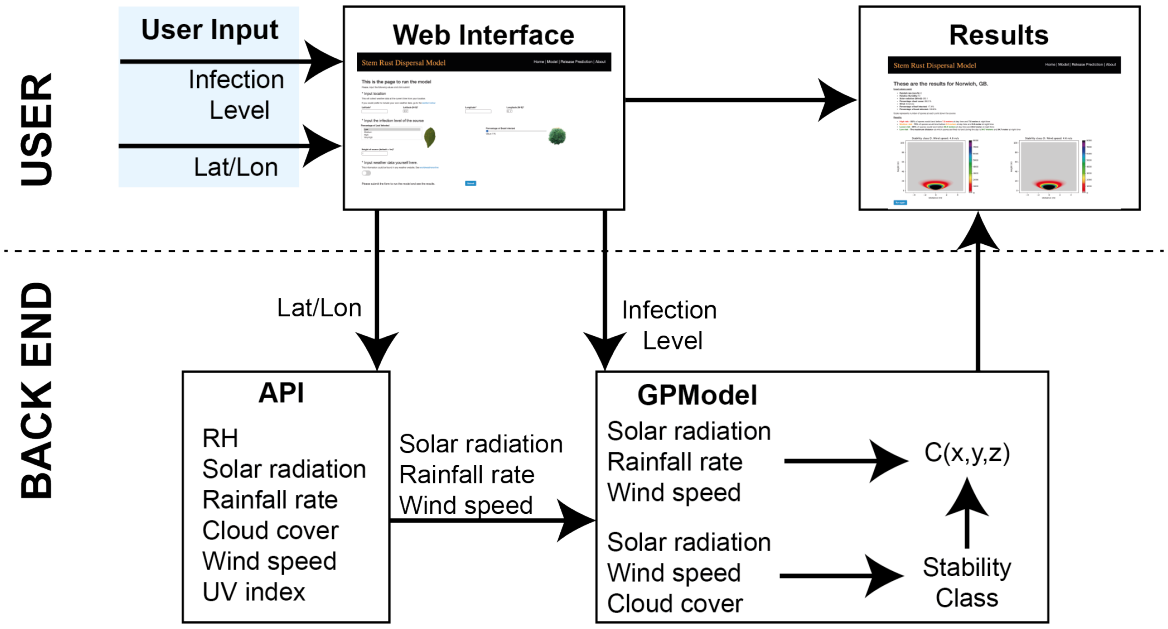

Figure 3.10 Web-app infrastructure for the aeciospore dispersal model. The user can input the required values to run the model using the web interface and these values would be taken to the backend to gather weather data and run the model. Latitude and longitude values are used by the API to collect real-time weather data that will be provided to the model, together with information about the infection level. The GP model is running in the background and values for concentration of aeciospores deposited downwards the source are calculated and displayed in the results page. The results page contains a section showing the input values used and the results for the model, including two graphs.

A

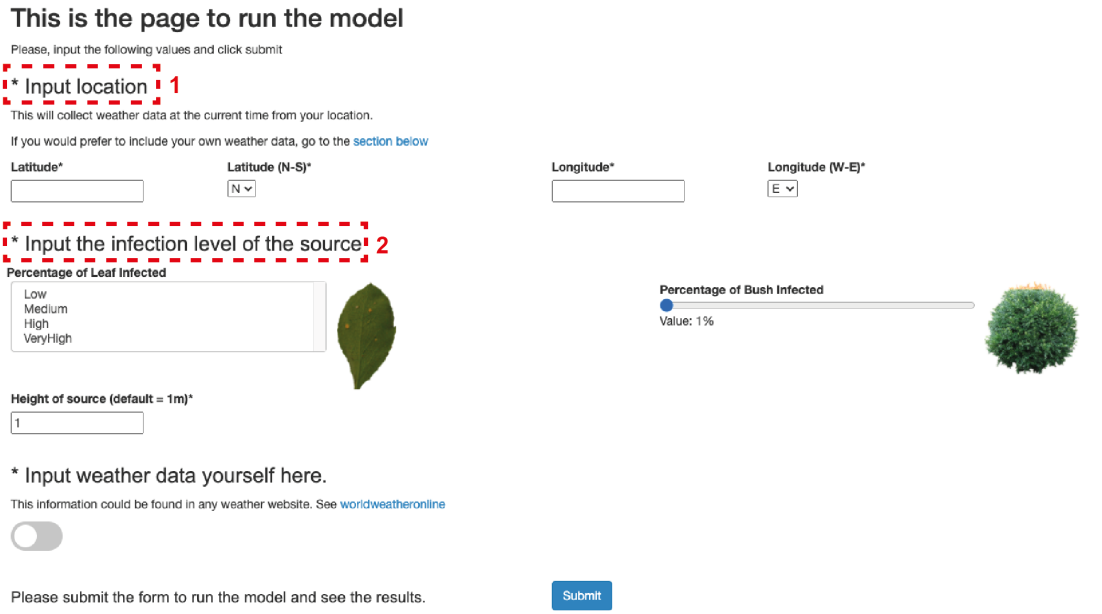

B

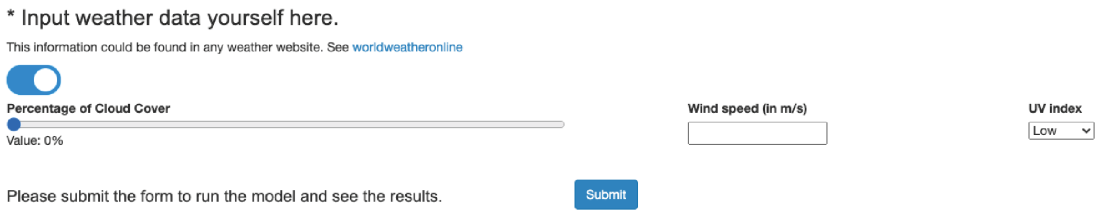

C

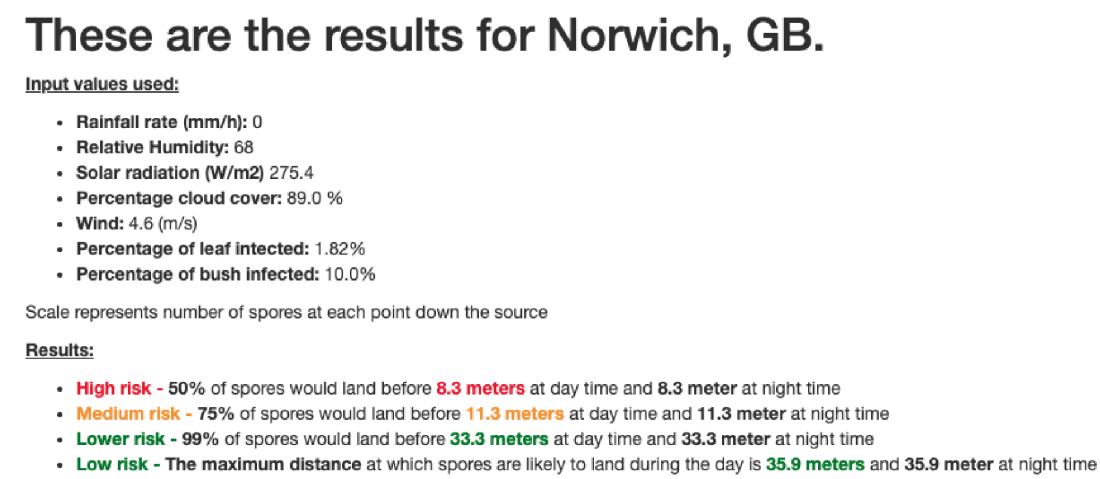

Figure 3.11. Web page for running the aeciospore release model and results display. (A) Two inputs are needed to run the model, highlighted in red: (1) the location (lat/lon) and (2) the infection level of the bush and the leaves. **(B)** Weather information can be given if the user wants to try the model with non-current weather data. This menu is displayed by selecting the button. **(C)** The results include the input values used and information about "high", "medium" and "lower" risk, showing the maximum distance that 50, 75 and 99% of aeciospores would reach. The "low risk" section shows the maximum distance that aeciospores would theoretically reach.

3.5 Discussion

3.5.1 Source strength varies depending on infection level and could be weather-dependent.

Investigating fungal spore dispersal has been an important topic for a long time, since it helps understand disease transmission and thus, much work has been done on this topic (Kuparinen, 2006). When dispersal gradients are being studied, one of the most important factors to know is the source strength (Q), i.e. the number of spores released (Gregory 1968). Here, I explored the potential source strength that can take place in a *Pgt*-infected barberry source bush. Aecial cups were found to contain an average of 7,111.37 spores, within a range of 1,805-12,916. These values are consistent with previous estimations of 11,000 aeciospores per cup (Coons, 1910). The variation between observed values is due to the difference in aecial cup length between years. This disparity could be due to the effects of random sampling or it could be a consequence of the differences in weather conditions between 2018 and 2019. Weather data from the field where samples were collected (Brandon, UK) for both years shows an increase both in rainy days and total rainfall in 2019, with respect to 2018 (**Table 3.4**). Although humidity has not been related to an increase in aeciospore production (Cotter, 1932), an increment in rain could lead to aeciospore release which could mean that the cups are emptied more often and thus do not reach a large size. Aeciospore production has been reported to not be affected by pre-inoculation temperature, although it is positively correlated to an increase in post-inoculation temperature (Kolnaar & Van Den Bosch, 2001). This could mean that an increment in temperature in the months when we find aecia (May-July), could potentially increase the number of aeciospores being produced. However, aecial cups seem to grow faster at lower temperatures. Reports show that at 31-32 ºC, aecial cups open earlier and don't grow as much as those at 7-8 ºC, when they can reach up to 2-3 mm before opening (Cotter, 1932). Average temperatures in both years fluctuated between 13-20 ºC during the season when *Pgt* is found in the field (**Table 3.4**). However, mean temperatures are not informative of periods of lower or higher temperatures during each month and thus no conclusions can be made in regard to this. Although the mean temperature in June was higher for 2019 than 2018, the opposite occurred in July. Besides, differences in mean temperatures between 2018 and 2019 were very low in general.

To our knowledge, this is the first time that the number of aecial cups/mm^2 has been estimated. Previous studies have looked at the number of aecial cups in a leaf, which was determined from examining three highly infected barberry leaves (**Table 3.5**). Using the information from (Coons, 1910) about the number of aecia per leaf and total number of

aecial cups, I estimated the average cups per aecia that would be found in these three leaves. This led to a mean of 40.02 cups per leaf, which was the same number that was obtained with the 129 measurements that were taken here (40.05). Despite this not being a definite result that 40 cups are always found per aecium; it is an indication that the observations obtained here are very consistent. By multiplying the number of aecial cups found in each leaf by the 11,000 aeciospores per cup reported, the total number of aeciospores can be determined (**Table 3.5**). The obtained numbers ranged from 3,696,000 to 8,052,000 which is also consistent with the number of aeciospores calculated herein for highly/very highly infected barberry leaves (**Table 3.3**).

Table 3.4. Differences in weather conditions for 2018 and 2019 in Brandon, UK. Temperature (ºC), rainfall (mm) and number of rainy days are shown here for both years for the months between January-August. Rainfall and rainy days were generally more abundant in 2019. Temperature is also higher for most months in 2019. Data extracted from www.metoffice.gov.uk.

	2018			2019		
	Temperature (ºC)	**Rainfall (mm)**	**Rainy days**	**Temperature (ºC)**	**Rainfall (mm)**	**Rainy days**
January	5	20.54	14	4	24.2	18
February	3	13.67	11	8	34.4	12
March	5	29.83	17	9	85.8	19
April	10	27.61	21	11	34.8	14
May	13	19.51	10	13	69.1	23
June	15	9.35	8	16	147.5	25
July	20	8.91	7	19	87.2	26
August	18	36.28	12	19	65.1	23

Table 3.5. Previous reports of number of aecial cups found in leaves agree with our observations. Reports of 3 highly SR-infected barberry leaves show an average of 40 cups per aecidia and similar number of aeciospores as the ones we estimated (Coons, 1910).

Leaf	**Pustules**	**Aecial cups**	**Cups per aecidia**	**Total aeciospores**
1	17	336	19.75	3696000
2	10	492	49.3	5423000
3	12	732	61	8052000
Total	39	1561	40.02	17171000

Estimating the number of infected leaves in a barberry bush is challenging and there is not much literature about *B. vulgaris*. Especially because the number of branches per bush and its height will also depend on the age of the shrub and environmental conditions during its growth (Cotter, 1932). Since the number of leaves per branch and number of branches per plant is very variable and changes with environmental conditions (Ahmed et al., 2013; T. Khan, 2014), calculating the exact number of leaves that are susceptible for infection to assess the source strength is not possible and informed estimations are needed. The age of the leaves in the bush could also influence the susceptibility to *Pgt* and thus affect the potential source strength being calculated. Reports show that younger leaves show infection 2-3 days earlier than older leaves (Cotter, 1932) and that leaves older than 10 days could sometimes show certain resistance to *Pgt* (Melander & Craigie, 1927). This can be an effect of the thickness of the outer epidermal wall that opposes resistance to infection. However, moderate infection can still be observed, and infection has also been observed to be equally heavy on leaves of different ages, regardless of when they were infected. This occurs especially if the weather conditions prevent barberry leaves from hardening, as happens in spring, when *Pgt* infection is more favourable (Cotter, 1932). Since *Pgt* infection, and possibly susceptibility of barberry bushes, is greatly dependent on weather, climate change could have an effect in SR epidemics. Global warming could lead to more suitable conditions for *Pgt* to spread in more geographical locations. Climate change has been reported to have caused a significant change on pathogen distribution in the past (Bebber, 2019). This has been a result of an increase in humidity and optimal temperature for pathogens to thrive. Temperature has historically played a role in wheat rust pathogens distribution, as it is the case of *Pst* (Milus et al., 2006). In fact, the first *Pgt* outbreak in Germany in 2013 was also associated to a warmer summer (Bebber, 2015). Therefore, climate change could not only affect the distribution of SR worldwide, expanding its range, but could also increment the severity of the epidemics (Launay et al., 2020; Prank et al., 2019). On the other hand, warmer conditions could also decrease the initial inoculum (Cotter, 1932) or lead to epidemics occurring earlier in the year. Besides, climate change predictions show that even though the risk of spore germination could increase, the drier climate might not allow for leaf penetration (Lewis et al., 2018).

The assessment of the source strength is one of the most important factors when modelling spore dispersal (Gregory, 1968). Due to the difficulty of measuring it accurately, getting detailed information about the source is a good approach to make an inference about the potential source strength. The observations here align with the literature and give a reasonable estimation to input into the dispersal model.

3.5.2 Gaussian Plume models can be used to estimate *Pgt* aeciospore dispersal

Empirical models such as the power law and exponential model have traditionally been the most commonly used model to describe the dispersal kernel of fungal spores (Gregory, 1968). Despite the accuracy of these model in describing specific experiments, the difficulty to extrapolate to other conditions led to the development of models that include weather conditions. In fact, exponentials and power laws have been reported to represent different environmental conditions (Reynolds, 2011). Exponential distributions have been associated to convective conditions, i.e. how days with low wind speed (unstable atmosphere), while a -2/3 inverse power law describes dispersal in stably stratified conditions, i.e. cold windy nights (neutral atmosphere). Therefore, mechanistic models that integrate weather conditions can be more general when investigating disease dispersal.

Here, I used a Gaussian Plume model to examine *Pgt* aeciospore dispersal, adapting a model previously published by including factors that are disregarded by GP models such as deposition and spore survival (Aylor, 1999; Spijkerboer, Beniers, Jaspers, Schouten, Goudriaan, Rabbinge, & van der Werf, 2002). GP models have proved accurate and useful when investigating spore dispersal (Kuparinen, 2006). Using GPs for modelling dispersal within a canopy is not appropriate due to the assumptions that this model makes (Kuparinen, 2006). However, here we assume that dispersal is taken place within an open field and thus the movement of aeciospores can be modelled as a cloud with a Gaussian distribution. The observations done here where aeciospores get released forming a normal distribution (**Figure 3.5**) indicate that this assumption is reasonable. Other mechanical models such as Lagrangian models can be more accurate than GP models, especially at local distances (Aylor & Flesch, 2001). A Lagrangian puff atmospheric dispersal model has been previously used for studying *Pgt* urediniospore dispersal (Pfender et al., 2006). However, these models are usually computationally expensive and thus making it available would be more complicated for fast simulations (Prussin et al., 2015). GP models on the other hand can be run even on a smartphone or tablet, hence making them the best choice for quick dispersal predictions. A compromise between the two also offers a good alternative and has shown good results for distances up to 100 m (P. Skelsey, Holtslag, & van der Werf, 2008). The model selected here includes parameters that describe the shape of the plume that incorporate the effect of the surface over which aeciospores are being transported, since the drag and surface roughness can have an effect on dispersal (Spijkerboer, Beniers, Jaspers, Schouten, Goudriaan, Rabbinge, & Van Der Werf, 2002). The parameters used here assume aeciospores are being transported above agricultural landscape. However, these

parameters could be changed to evaluate different situations such as dispersal over forest canopies (Shaw & Pereira, 1982).

Several improvements can be added to the GP model used here. Firstly, here we assume escape to be 100 % since only the leaves on the outer part of the bush are considered. This was done because it simplified the situation to only assess the "worst-case scenario", which would reveal the highest risk of barberry bushes. Much work has done to investigate escape of spores from canopies and it presents a great challenge in spore dispersal (Andrade et al., 2009; Follett et al., 2016; Gleicher, Chamecki, Isard, Pan, & Katul, 2014). However, a simple escape model could be built-in by including the expression mentioned in the introduction to compute the vertical escape of aeciospores from barberry bushes (De Jong et al., 2002). This would only require the LAI calculated here (section **3.4.1**). Secondly, here wind is assumed to have a constant direction which would maximise the dispersal distance. However, this is not realistic and thus wind profiles could be added to specify wind direction (Prussin et al., 2015). Thirdly, deposition here includes sedimentation based on the settling velocity assumed by one aeciospore. However, as mentioned in Chapter 2, aeciospores are observed to form clumps which thus would increase the settling velocity. (Ferrandino & Aylor, 1984) developed an equation to estimate the settling velocity based on the number of spores clustering together. This is something that could be taken into account when modelling spore deposition, especially as it was shown to have an effect on spore dispersal distance (Chamecki, Dufault, & Isard, 2012). Moreover, deposition by impaction could be included in the model to improve its precision, based on the area of the plants where it could impact (H A McCartney & Fitt, 1985). This however could complicate the model while not increasing significantly the accuracy, and when developing models, there is always a trade-off between accuracy and complexity that needs to be considered. Lastly, another important factor to consider is the viability of aeciospores. Survival rates of aeciospores will affect greatly the source strength, and even though reduction of aeciospore viability due to radiation has been taking into account in the model, the survival of aeciospores after deposition should also be considered. An estimation on this could have been done by collecting aeciospores and investigating the percentage of them that remain alive using DNA dyes techniques (Emerson et al., 2017).

Validation of the results that this model provides regarding aeciospores would be necessary. However, this presents a challenge since setting up an experiment in an open field could increase the risk of SR epidemics (Jin, 2011). Validation in a closed environment would be more appropriate, but the difficulty of working with wheat rusts and of infecting barberry bushes makes it problematic. However, the model chosen had been previously

validated (Spijkerboer, Beniers, Jaspers, Schouten, Goudriaan, Rabbinge, & van der Werf, 2002) and similar models have been experimentally validated for organisms with similar spore size, such as *F. graminearum* (~10-20 μm) (Prussin et al., 2015). Aeciospores of *Puccinia punctiformis* have been reported to reach up to 30 meters during the summer period of May-June (Berner et al., 2015). The authors used an exponential decline model to predict dispersal and found that the greatest number of infected leaves occurred at 12 meters. However, the use of an empirical model disregards the effect of the weather in spore dissemination and thus these results cannot be extrapolated to all situations. Nevertheless, the range in which aeciospores were found in their experiments is consistent with the observations obtained using the GP model here. These results are also consistent with *Pgt* urediniospores dispersal, where a single spore can be found up to 12.06 and 36.5 meters (Johnson & Dickson, 1919). The *Pgt* aeciospore dispersal model developed here presents an advantage since it can incorporate different environmental conditions and source strength levels which can then be used to evaluate the risk of barberry bushes in different situations.

3.5.3 Making the model available can help inform about the risk of *Pgt*-infected barberry bushes

Disease forecasting based on weather data is common and has been done for a number of diseases (Bourgeois et al., 2008) including rusts (Junk et al., 2016). However, many of these models remain theoretical and are not made available for use. Much information is being collected about the factors influencing crop diseases, and they need to be made easily accessible so they can inform stakeholders and farmers (Chaudhary, Bhise, Banerjee, Goyal, & Moradiya, 2015). Here, I developed a user-friendly interface to access the *Pgt* aeciospore dispersal model using Django, written in Python for the webapp (Holovaty & Kaplan-Moss, 2009). Django is one of the most popular frameworks nowadays, with a model-view-controller (MVC) architecture, that allows for a rapid development and clean design (Deacon, 2005). When compared to other popular frameworks such as Ruby on Rails or CakePHP, Django has a higher rating in user interface development, maintainability, and popularity, and scores very high in data management and testability (Plekhanova, 2009). This, together with the facility to work with Python, made it the best choice for the purpose. The current site requires the user to specify the level of infection in leaves by selecting the most representative image. When a level is chosen, a percentage of leaf covered by aecia is assumed, based on our observations (**Figure 3.4**) (**Table 3.3**). However, this is an average and could not be an exact representation of what the user is seeing in the field. Therefore, a more automatic system could be included in the webapp, adding a page to upload a picture of a leaf and estimating the exact percentage of infection (Bueno-Sancho, Corredor-Moreno,

Kangara, & Saunders, 2019). The weather API used here allows you to gather real-time data from the indicated location, which is an advantage because the model is then running with more accurate information, specific from each geographical region. This API also allows for 14-day weather predictions, which could also be included in the webapp for making future predictions. The postgres database in the backend also allows to record potential locations for barberry bushes. This could help with the Barberry Rust Explorer (BarbRE) citizen science project to track common barberry bushes across the UK (www.barbre.co.uk).

The risk that barberry bushes pose as sources of early *Pg*-inoculum to adjacent wheat fields has been known for a long time and removing them remains the most effective strategy to reduce the incidence of stem rust epidemics (Wang et al., 2015; Zhao et al., 2015). However, eradication would have ecological consequences and an impact on species that rely on barberry as a habitat or food source such as the barberry carpet moth and thus finding a balance between both systems would be ideal. Planting barberry bushes in woodlands, ensuring they are isolated far away from crops, could be a potential solution for this problem. That could guarantee a niche for the carpet moth while reducing the threat to UK agriculture.

Despite the usefulness of models, it must be noted mathematical models are theoretical and based on probabilities and even when the probability of an event occurring is low, there is still a chance of that event happening. *Pgt* uredioniospores have been modelled to be able to travel great distances in wind currents (Meyer et al., 2017) and are known to be dispersed for kilometres (Pfender et al., 2006). Even when theoretical probabilities show that most aeciospores would fall on the ground in the first few meters, the probability of an aeciospore being carried in the wind for kilometres and starting an infection further away still exists. In fact, viable *Pgt* urediniospores and aeciospores have been found up to 7,000 and 1,000 feet above the ground (Stakman, Henry, Curran, & Christopher, 1923). To avoid future epidemics of an important pathogen such as *Pgt*, risk should be reduced to a minimum. Thus, other approaches could be taken to ensure the survival of the carpet moth and other species while allowing the removal of barberry bushes. Alternatives include (i) finding another *Berberis* species resistant to *Pgt* that the carpet moth can use as its niche or (ii) planting barberry bushes in woodlands isolated from wheat fields. Although common barberry has shown resistance to certain wheat *Pgt* races in the past (Johnson 1954), *B. vulgaris* is classified as susceptible to SR. However, this is not the case for all *Berberis* spp., some such as *B. thunbergii* have been reported to present resistance to stem rust (Bartaula 2019). Unfortunately, the list of susceptible *Berberis* spp. is long and stem rust infection has been observed in several species, especially in China (Zhao 2015). Investigating the

behaviour of the carpet moth in resistant *Berberis* spp. could offer an alternative that would highly reduce the risk of SR epidemics. Planting resistant barberry bushes where the moth could survive while removing *B. vulgaris* would thus be the best possible solution for this problem. However, moths can be very delicate regarding their niche and finding other species in which they can survive might be complicated (Martin & Pullin, 2004). Besides, mass planting of non-native *Berberis* species is also not an ideal solution since the new species could be invasive and outcompete other native species. Therefore, understanding the potential risk of common barberry bushes to ensure they are located far away enough from wheat fields is our best option at the moment. Using the model developed here to guide re-planting and to create risk maps of barberry bushes that should be monitored would help manage the risk of *Pgt* in the UK.

3.6 Conclusion

A Gaussian Plume model was used to model *Pgt* aeciospore dispersal and investigate the risk of barberry bushes near wheat fields. The two main factors affecting dispersal are the source strength, i.e. the amount of initial inoculum, and the environmental conditions. Thus, I investigated the potential initial inoculum that can occur within a barberry bush by counting how many aeciospores are typically contained within an aecial cup, how many cups per mm^2 and how many cups can occur within a barberry leaf. An average of 7,111 aeciospores were found per cup, although significant differences between years were observed, possibly due to variability in weather, and an average of 8.29 aecial cups are found per mm^2. The percentage of infection in leaves based on their level was investigated, being and for a low, medium, high and very high level respectively. The potential aeciospores found in leaves is however much higher than what is released, with only 2.96 % of the predictions being observed to be released. No significant differences in the quantity of aeciospores released under different temperatures (5-30 ºC) was observed and thus temperature was not considered a factor in source strength. This information gathered about potential source strength was incorporated into the GP model with real-time weather data to predict how far aeciospores can reach from a barberry bush. Predictions show a lot of variability depending on the state of the atmosphere, with lower risk under high solar radiation. A webapp was developed with the model in the backend and a postgres database to record the entries to make the model accessible for the user. This provides an excellent tool that can be used for stem rust risk management.

Chapter 4:

Developing SNP markers to study *Pst* population dynamics in the UK

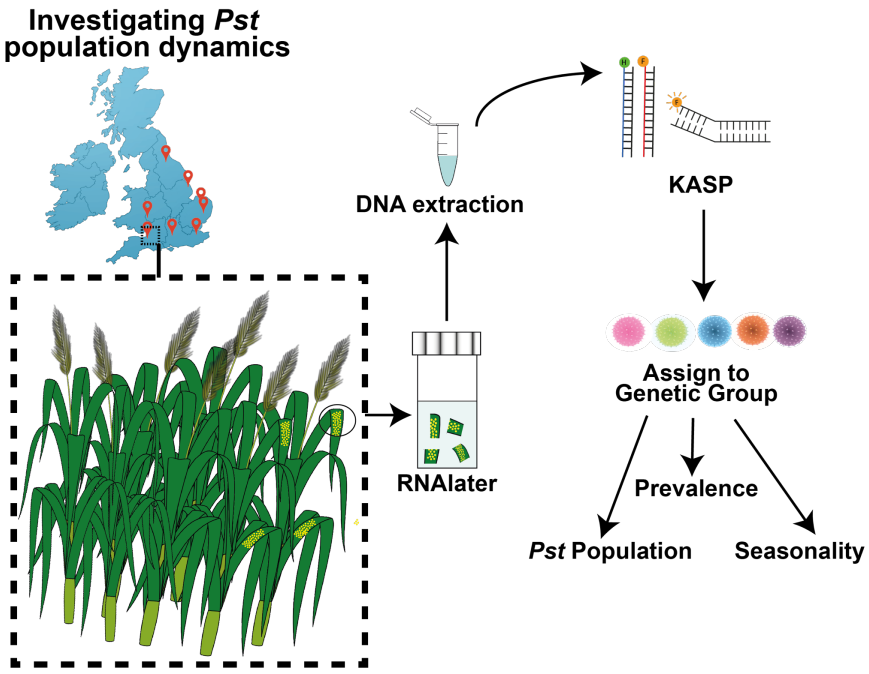

Chapter 4 Developing SNP Markers to study *Pst* population dynamics in the UK

4.1 Abstract

Yellow rust, caused by the fungus *Puccinia striiformis* f.sp *tritici (Pst)*, has been a significant threat to wheat production worldwide for centuries. Moreover, new *Pst* races have emerged recently able to adapt to new climates, evolving rapidly and being more aggressive. Much knowledge has been acquired lately about these new races and their distribution worldwide and in particular in the UK. However, the dynamics of *Pst* races at the field level still remain unknown and understanding this is essential for designing effective management programmes. Here, I have developed a quick method for genotyping field-collected *Pst*-infected wheat samples to determine which race they belong to. This consists of genotyping with Kompetitive Allele Specific PCR (KASP) using a set of Single Nucleotide Polymorphism (SNP) markers that was found to differentiate a subset of different *Pst* races identified in the UK. To study the *Pst* population dynamics, field trials were also undertaken across the UK using wheat varieties that are known to be susceptible to the disease to collect *Pst*-infected wheat samples during the 2015-2016 and 2016-2017 growing seasons. These collected samples were genotyped using the designed approach to study the distribution of *Pst* races in the UK. The results show that most samples belonged to one race named group 4 (Warrior -) that has become predominant in the UK. Besides, the seasonality of the different races was investigated, and it was concluded that the presence of *Pst* races in one season was not indicative of prevalence of the same race in following seasons.

4.2 Introduction

4.2.1 *Pst*: a threat to global agriculture

Pst has been threatening wheat for centuries, early reports of a wheat disease that is believed to be yellow rust (YR) were found in England and Sweden already in the XVIII century (Wellings, 2011). Historically, YR has been largely delimited to cool and humid environments, often located in high altitude areas (Duan et al., 2010). The origin of this pathogen was initially believed to be Transcaucasia (Chen et al., 2014), but the high level of genetic diversity and teliospore production found in isolates from the Himalayan area identified lately this zone as the most likely centre of diversity of *Pst* populations

(Hovmøller et al., 2016). Isolates from this region were thought to have travelled via wind to the rest of the world, such as East Africa, Middle East and China (Wan et al., 2004). *Pst* would have then migrated to the European continent and America (Ali et al., 2014). In 1979, *Pst* was reported for the first time in Australia, where it is known to have occurred owing to the international movement of spores from Europe and the United States on travellers' clothing (Wellings, 2007). Multiple incursions were also reported in South Africa in 1996, when this pathogen was identified for the first time in this region. The source of the isolates found was unknown but they had similarities with isolates from the Middle East and North Africa (Boshoff, Pretorius, & van Niekerk, 2002). Even though air-borne dispersion of *Pst* isolates was reported in several locations, YR was still mainly localised to cold and humid regions of the world (Duan et al., 2010).

However, *Pst* has been expanding geographically and evolving rapidly to adapt to new climates (Beddow et al., 2015). In the 2000s, new races were discovered that were more aggressive and adapted to warmer temperatures which then allowed them to colonise new regions (Chen, 2005). These races (PstS1 and PstS2) were able to spread widely into warmer regions like south eastern USA and western Australia. PstS1 caused epidemics in central USA and in Australia in 2000. PstS2 was found in NW Europe, Mediterranean region and Middle East area. *Pst* isolates belonging to these races were lately assigned to genetic groups coming from east Africa, suggesting a possible origin. These races were believed to be able to produce a higher amount of urediniospores in shorter timeframes under higher temperatures (Chen, 2005). They also germinated faster at higher temperatures (18ºC) compared to older isolates better adapted to lower temperatures (12ºC) (Milus et al., 2006). Isolates found in Australia in 2003 were also observed to be aggressive but didn't show temperature adaptation (Chen et al., 2002). The capacity of *Pst* for long-distance dispersal with its adaptability to warmer climates led to a worldwide expansion that increased the threat to global agriculture.

4.2.2 New *Pst* races have appeared in Europe

Before the 2000s, *Pst* populations in Europe had shown clonality and were believed to migrate quite frequently within the continent (Justesen, Ridout, & Hovmøller, 2002). However, in 2011 new *Pst* incursions came into Europe via long-distance wind dispersal causing the replacement of the existent clonal population (Hovmøller et al., 2016). The low genetic diversity of these populations seemed to indicate that the origin of these races was due to exotic incursions, suggesting the Himalaya region as a possible origin (Hovmøller et al., 2002). Three main races were identified in Europe in 2011: Triticale, Kranich and Warrior (named after the wheat varieties 'Kranich' and 'Warrior' where the last two were

identified). Likewise, another race called Warrior (-) was identified in Europe and found the most prevalent one in the UK in 2014 (Bueno-Sancho, Persoons, et al., 2017; Hubbard et al., 2015). Whereas the 'Triticale' and 'Kranich' races were localised in specific locations or crops, the 'Warrior' lineage was found in most countries in Europe and also showed similar levels of aggressiveness to the global races, PstS1 and PstS2 (Sørensen, Hovmøller, Leconte, Dedryver, & de Vallavieille-Pope, 2014). The high genetic diversity of the Kranich and Warrior races and their ability for teliospore production suggested that their origin could be due to the incursion of sexual recombining populations from the Himalayan area (Hovmøller et al., 2016). On the contrary, the Triticale race was not found to be similar to any populations identified so far in Asia (Hovmøller et al., 2016). Besides, these new races were able to produce more urediniospores in shorter period of time, which can lead to expansion of their geographical niche (Rodriguez-Algaba, Walter, Sørensen, Hovmøller, & Justesen, 2014). The emergence of novel races poses a high risk to agriculture globally, especially when the *Pst* population seems to be evolving constantly and quicker than before (Liu et al., 2017). Thus, managing the disease has become a priority and new surveillance programmes have been developed to study pathogen diversity.

4.2.3 Managing the disease with surveillance programmes

The appearance of new pathogen races can give rise to an epidemic that could mean the complete loss of crops and thus poses a continuous threat to food security and plant health (Dutech et al., 2012). Exotic incursions of pathogens into new areas are unpredictable and can lead to outbreaks of diseases that can produce large economical loses (Pimentel, Zuniga, & Morrison, 2005). New disease outbreaks that affect crops have thus led to an increasing necessity of improving crop protection strategies.

Monitoring systems can help us detect the disease quickly to tackle the problem before it is more widespread (Meentemeyer et al., 2004). Thus, surveillance programs to monitor YR have been taking place for a long time (Zadoks, 1961). These consist mainly of monitoring the *Pst* population through national surveys such as the United Kingdom Crop Pathogen Virulence Survey (UKCPVS) in the UK established in 1967 (Hubbard, Wilderspin, & Holdgate, 2018). Similar surveys were initiated in Germany (Hovmøller et al., 2016), Denmark (Hovmøller, Yahyaoui, & Singh, 2009) and France (de Vallavieille-Pope, Picard-Formery, Radulovic, & Johnson, 1990). This led to the creation of the Eurowheat database (www.eurowheat.org) that includes *Pst* virulence dynamics. Regular surveys have also been carried out in Australia, China, India, South Africa and more sporadically in East Africa, Middle East, western Asia, South America and the Mediterranean (Hovmøller, Sørensen, Walter, & Justesen, 2011). To enable quick responses to appearance of new races ICARDA,

CIMMYT and Aarhus university also launched in 2008 the Global Rust Reference Center (GRRC) to target YR from all countries, as part of the Borlaug Global Rust Initiative (BGRI) (Hovmøller, Walter, & Justesen, 2010). These monitoring systems help prevent big outbreaks since new races appearing can be rapidly detected, while also increasing knowledge about the pathogen.

4.2.4 Developing NGS technologies leads to better understanding of pathogens

Traditionally, surveillance of rust fungal pathogens in agroecosystems has been based on pathotype surveys to provide phenotypic information on pathogen diversity. This involves testing isolates pathogeny against several wheat varieties, which is a very time-consuming task. However, these methods only allow the analysis of a few samples and it is unlikely that a new pathotype would be detected in a timely fashion (Atkins & Clark, 2004). Newer methods are based on serological or nucleic acid assays, such as enzyme-linked immunosorbent assay (ELISA) and immunoblotting, or PCR-based and loop-mediated isothermal amplification (LAMP) assays (Mori & Notomi, 2009; Notomi et al., 2000). Although some of these methods are commonly used, they can still introduce bias by giving false positive results or have technical limitations (Lau & Botella, 2017).

Advances in Next Generation Sequencing (NGS) technologies have allowed the integration of high-resolution genotypic data in pathogen surveillance systems (Moran-Gilad, 2017). An approach called "*field pathogenomics*" was recently developed for pathogen population surveillance based on high-resolution transcriptome data acquired directly from field samples of *Pst*-infected wheat and triticale (Hubbard et al., 2015). This approach uses RNA-seq data that is generated directly from pathogen-infected leaves collected in the field, providing a unique opportunity to characterize the pathogen population and its host directly in their natural environment. Using this method, the *Pst* population form the UK was investigated in 2013 and compared to older isolates covering more than 30 years of diversity (from 1978 until 2011). The results showed a dramatic shift in the *Pst* population in the UK that was likely to have occurred due to several incursions of exotic lineages of this pathogen. When investigating this population further, four main genetic groups were found within the UK population that were observed to have different pathotypes. Some of these groups were the same as the races identified in Europe such as Warrior (group 1), Triticale (group 2) and Warrior (-) (group 4). The pathotypes were consistent with the genetic groups, as it is expected in highly clonal population (Kolmer, 2019). Another genetic group was also found (group 3) which was similar in virulence profile to a historic race but that was genotypically distinct. This group would have not been found with traditional phenotyping and happened to be part of the new European races that had emerged recently,

being genetically similar to the Warrior race (Hubbard et al., 2015). Another recent study found a new genetic group in the UK (group 5-1) similar to the Kranich race in the UK in 2014 (Bueno-Sancho, Persoons, et al., 2017). The development of this novel method has thus help us understand the genetics of this pathogen and gain a better insight into the distribution of the global *Pst* population.

4.2.5 Investigating *Pst* population dynamics in the UK

The *Pst* population in the UK has been studied in collaboration with the UKCPVS using the field pathogenomics method from 2013 and the five genetic groups have been found to infect wheat fields across the country (Bueno-Sancho, Persoons, et al., 2017; Hubbard et al., 2015). Even though a correlation between seasons and races was reported, more research is needed to confirm these observations (Bueno-Sancho, Persoons, et al., 2017). Besides, studying how the *Pst* population fluctuates and how the different races spread within a field can provide useful information to develop new management strategies that take into account these characteristics (Derevnina & Michelmore, 2015; Plantegenest et al., 2007).

Even though the field pathogenomics approach provides a great deal of information both about the host and the pathogen, it has a relatively high cost and thereby a cheaper and more rapid method would be advantageous as a first screen in regular surveillance programs. This would enable the most notable and representative samples to be quickly identified and subsequently analysed using the more comprehensive field pathogenomics method.

Genotyping by next-generation sequencing (GBS) is an emerging cost-effective method of Single Nucleotide Polymorphism (SNP) genotyping that has recently emerged and has been adopted for several applications, including breeding in wheat (*Triticum aestivum*) (Bernardo, St. Amand, Le, Su, & Bai, 2020) and studying genetic diversity in flax (*Linum usitatissimum)* (Peterson, Dong, Horbach, & Fu, 2014). Amplicon resequencing consists of amplifying regions containing useful SNPs and has been used for many species such as rice (Nasu et al., 2002), barley (Kota et al., 2008) and sugar beet (Schneider et al., 2007). Kompetitive Allele Specific PCR (KASP) is a technology based on amplifying SNPs that has been widely used in crop improvement (Dhakal et al., 2018; Tan et al., 2017). This technique offers an alternative due to its low price and high level of accuracy (Semagn, Babu, Hearne, & Olsen, 2014). Preliminary KASP assays were also developed for four of these *Pst* races, corroborating the practicality of this method (Hubbard et al., 2015).

In this chapter, I analysed samples collected from wheat field trials taking place across two growing seasons in locations susceptible to YR (14 fields in 2015-2016 and 8 fields in 2016-

2017) to study the population dynamics of *Pst* within a field. To do so, I firstly developed a quick genotyping system that I then applied to the collected samples.

4.3 Methods

4.3.1 Transcriptome sequencing of *Pst* isolates

RNA was extracted from *Pst*-infected leaf samples for transcriptome sequencing by Clare Lewis (Saunders Lab) using the Qiagen RNeasy Mini Kit (Qiagen, Germany) according to the manufacturer's instructions. RNA concentration and quality were then measured using the Agilent RNA 6000 Nano Kit on the Agilent 2100 Bioanalyzer (Agilent Technologies, United Kingdom). cDNA libraries were prepared by Nicola Cook using an Illumina TruSeq RNA Sample Preparation kit (Illumina) and libraries were sequenced on the Illumina HiSeq 2500 machine at Earlham Institute (UK) and GENEWIZ (Germany). The 101-bp paired-end reads were trimmed and filtered using FASTX-Toolkit (version 0.0.13.2) and aligned to the PST-130 assembly (Cantu et al., 2011) using TopHat (version 1.3.2.). SAMtools (Li et al., 2009) (version 0.1.19) was used to call SNPs between samples and the PST-130 genome with a minimum depth of coverage of 20x as described in (Bueno-Sancho, Bunting, Yanes, Yoshida, & Saunders, 2017). SNPeff (version 3.6) was used to identify synonymous and non-synonymous substitutions. The distribution of read counts for biallelic SNPs was analysed for all samples to confirm they had a single *Pst* genotype as described in (Hubbard et al., 2015).

4.3.2 Phylogenetic analysis of *Pst* isolates

For both phylogenetic analyses included here, a maximum likelihood approach was used. All sites, with a minimum coverage of 20x if they were different to the PST-130 reference and 2x if they were identical, were extracted for all included samples. Synthetic gene sets were generated using these sites as described in (Bueno-Sancho, Persoons, et al., 2017; Hubbard et al., 2015). Genes that contained more than 20 % of missing data for more than 20% of samples were removed from the set. The third codon position was used to build unrooted trees with RAxML 8.0.20 (Stamatakis, 2006). Phylogenetic trees were visualised using Dendroscope, version 3.5.9 (Huson et al., 2007).

4.3.3 Population analyses of *Pst* isolates

A multivariate Discriminant Analysis of Principal Components (DAPC) was performed using the Adegenet package (Jombart, 2008) to analyse the subdivision of genetic groups in the *Pst* population. This was done using a nonparametric approach without any predetermined

genetic model. To run the analysis, I generated the input file following the pipeline described in (Bueno-Sancho, Bunting, et al., 2017). First, I extracted all biallelic synonymous SNP sites for each one of the samples that had at least 20x coverage and made a list of all positions, including heterozygous sites. Then a matrix of samples was built containing the bases that they all had for each one of those positions, assigning "1", "2", "3" or "4" if there was an "A", "T"', "G" or "C" respectively. Each of the samples will appear twice (i.e. sample_1 and sample_2) in the matrix to represent each one of the nuclei, since *Pst* is dikaryotic. If a position was missing, then a -9 was assigned to that site. This matrix was then used to run DAPC analysis. The optimum number of genetic groups was assessed based on decreasing Bayesian information criterion (BIC) values, as explained in (Jombart, Devillard, & Balloux, 2010) and the results were used to assign *Pst* isolates into population clusters.

4.3.4 Development of a pipeline for finding markers

To find a list of appropriate SNP markers to identify *Pst* genetic groups, I selected a set of 295 *Pst*-infected wheat samples that were previously sequenced for the analysis and built a matrix of synonymous sites as described in the previous section. Samples representing each nuclei of the same isolate in the matrix were treated as a single sample that was heterozygous if the nuclei were different and homozygous if they were identical. I then developed a pipeline using python3 (github.com/vbuens/ShortScripts/get_markers.py) to find markers to define genetic groups that had the following requirements:

1. SNP can be found in all genetic groups
2. SNP should (ideally) be found in all isolates
3. SNP is the same for all the isolates within a genetic group
4. SNP is different between genetic groups

The script takes four inputs: (1) the matrix previously described, (2) a file with information about the samples and their genetic groups (separated by tabs), (3) a percentage (1-100) of missing data allowed and (4) a percentage (1-100) of error within a group permitted (**Figure 4.3**). The script then evaluates all the SNPs, clustering the samples by groups and comparing them within a group and between groups. First, it filters positions that have more missing data than the input value, by checking that all SNPs are found in at least a certain percentage of the samples. That is, if a threshold of 20 % missing data is allowed, it will remove all SNP positions that are not found in at least 80 % of the samples. This filtering is important since missing data could be due to lack of coverage when sequencing but the position could still be present in the isolate. Secondly, it filters based on consistency within a genetic group, allowing a certain percentage of error. For example, allowing a 10 % of

error would mean that if at least 90% of samples within a group have the same SNP for a certain position, it would be accepted. But it would be rejected if more than 10% of the libraries have a different SNP for the same position.

The script was executed with different combinations of thresholds to find appropriate markers for each genetic group. Firstly a 0 % of error within a group was allowed while varying the percentage of missing data permitted from 10 % up to 40 %. Then, the same was repeated but with a 10 % of variability within a group.

4.3.5 Wheat inoculation with *Pst* isolates from different genetic groups

To obtain *Pst*-infected wheat samples from isolates from different genetic groups, I infected wheat plants with four different isolates, one for each of the four genetic groups (**Table 4.1**). This was done with the help of Francesca Minter (Saunders lab). Wheat seedlings from the susceptible cultivar Vuka were grown in 9 x 9 cm pots which contained a peat and sand compost mix (85 % fine peat, 15 % Gri 2.7 Kg/m^3 Osmocote, wetting agent, 4 Kg/m^3 Malime and 1 Kg/m^3 PG mix). A total of ten wheat seeds were planted per pot and were treated with 25 mL of growth regulator (Maleic Hydrozide 0.2 g/L) four days after sowing. After 14 days, wheat plants were spray-inoculated with *Pst* spores. To facilitate inoculation, spores were heat-activated at 40 ºC for 5 minutes and then resuspended in Novec 7100 (3M™, MN, USA) at a concentration of 1 mg/mL, prior to inoculation. After inoculation, plants were kept in the dark at 10 ºC for two days under high humidity conditions to promote spore germination. The wheat seedlings were then placed in cellulose bags to prevent contamination from other isolates and returned to controlled environment conditions. Infected tissue was collected 14 days post-inoculation and stored in RNA later solution at 4 ºC (Life technologies, UK). DNA was then extracted from these samples, as described below, to be used in the subsequent KASP assays as positive controls.

Table 4.1. *Pst* isolates used for wheat seedling inoculation. Four UK isolates from the four selected genetic groups were used to inoculate wheat plants.

GENETIC GROUP	ISOLATE NAME	YEAR OF COLLECTION	ORIGIN
1	F18	2014	UK
3	15/151	2015	UK
4	14/7	2014	UK
5-1	14/106	2014	UK

4.3.6 Computational testing of the SNP markers

Transcriptome data from 475 *Pst*-infected wheat and triticale samples collected from 2013, 2014, 2015 and 2016 was used to test the SNP makers. These samples had been analysed previously by following the method described in (Bueno-Sancho, Persoons, et al., 2017; Hubbard et al., 2015) and their genetic group was known. First, positions that had ≥ 20 x coverage if they were different to the reference and 2 x if they were identical were extracted for each sample. Then, a python3 script (was developed that looked at the bases that each sample had for the 96 SNP markers defined. The script then assigned the *Pst*-infected sample to a genetic group based on those positions. The assigned genetic group was compared to the known genetic group for each sample to confirm whether the markers worked. The same process was followed when the set of 4 markers was tested. The script used is on GitHub: https://github.com/vbuens/ShortScripts/blob/master/get_markers.py.

4.3.7 DNA extraction of *Pst* infected leaf samples

DNA was extracted from *Pst* infected wheat samples using the MyTaq™ Extract-PCR kit, as described by the manufacturer (Bioline). In short, 20 µL of Buffer A, 10 µL of Buffer B and 70 µL of water was added to a total of 10-20 mg of tissue that was disrupted using a homogenizer. Samples were then incubated for 5 minutes at 75 ºC followed by 10 minutes at 95 ºC. After extraction, DNA was purified using Agencourt® XP magnetic beads (Beckman Coulter). The AMPure XP beads use solid-phase reversible immobilisation (SPRI) paramagnetic beads which selectively bind to DNA fragments that are larger than 100 bp. Impurities such as primers, nucleotides, salts and enzymes can be removed by repeated washing of bead-bound DNA. For each purification, an equal volume of AMPure XP beads and DNA solution were combined, mixed thoroughly and incubated for 15 minutes at room temperature. The resulting solution was then placed in a magnetic rack to allow the DNA-bound AMPure XP beads to aggregate to the tube wall out of the solution and incubated for a further 5 minutes until the supernatant became clear. Following removal of the supernatant, two washes were performed with 200 µL of 80% Ethanol. Finally, samples were placed outside of the magnetic rack for 5-15 minutes until dry and then resuspended in 52 µL of nuclease-free water. The samples were then mixed thoroughly and further incubated for 2 minutes at room temperature. Samples were then placed in the magnetic rack for 2 minutes and the supernatant containing DNA was transferred into a new collection 1.5 mL collection tube.

4.3.8 Quantification of DNA concentration using the Qubit

DNA concentration was quantified using the Qubit™ dsDNA HS Assay Kit (ThermoFisher Scientific, Paisley, UK). To quantify the concentrations of DNA within a sample, this assay uses a fluorescent dye that intercalates within the DNA molecules. Upon excitation, the relative fluorescence correlates directly with the quantity of DNA that the sample contains. A master mix was made with 1 µL of dye and 199 µL of buffer per sample. Two DNA standards (containing 0 ng/µL and 100 ng/µL) are needed to create a standard curve that is used to accurately quantify the DNA within a sample. For each control sample, 190 µL of master mix was added to 10 µL of standard DNA. For each DNA sample to quantify, 199 µL of master mix was added to 1 µL of DNA sample. All samples and standards were mixed thoroughly and incubated for two minutes at room temperature. DNA concentrations were then determined using the Qubit™ 3.0 Fluorometer (ThermoFisher Scientific, Paisley, UK).

4.3.9 TruSeq Custom Amplicon Library preparation

A total of 91 *Pst*-infected samples were selected for sequencing with the TruSeq Custom Amplicon method. Illumina designed primers that would amplify the set of 96 designed SNP markers in 200-250 bp amplicons and combined those primers into a Custom Amplicon Oligo Pool. This pool was included in the TruSeq Custom Amplicon Library Preparation Kit (Illumina, CA, USA). For each of the 91 samples, 1-100 ng (25 ng/µL) of DNA were entered into the library preparation. The 96 amplicons were amplified and prepared for sequencing using the TruSeq Custom Amplicon v1.5 Library Preparation Kit following the manufacturer's instructions (Illumina, CA, USA).

The primers in the pool were hybridised to the DNA from each sample with an initial denaturation step at 95 ºC for 1 minute followed by 58 cycles of 90 ºC for 30 seconds with a decrease of 0.5 ºC per cycle; 20 cycles of 60 ºC for 1 minute with a decrease of 0.5 ºC per cycle; 10 cycles of 50 ºC for 2 minutes with a reduction of 1 ºC per cycle and a final extension of 40 ºC for 10 minutes. DNA with the primers was then bound to a membrane and washed twice with wash buffer to remove primers that had not bound. The target regions then amplified using the bound primers by incubating the samples at 37 ºC with the Extension Ligation Mix for 45 minutes. A unique identifying barcode (adapter) was added to each sample before the amplicons were amplified with an initial denaturisation of 95 ºC for 3 minutes, then 26-33 cycles of 98 ºC for 30 seconds, 67 ºC for 30 seconds and 72 ºC for 1 minute with a final elongation step of 72 ºC for 5 minutes. The number of cycles of PCR performed depended on the input DNA quantity of the sample.

Finally, a clean-up with Agencourt AMPure XP magnetic beads, as previously described for DNA extraction, was performed and each sample eluted in 25 µL elution buffer. To quantify the concentration of the DNA the Qubit™ was used as previously described. To quantify the insert size of each library, each sample was run on the Agilent 2100 Bioanalyzer (Agilent Technologies, CA, USA) using the High Sensitivity DNA Kit. The resulting concentration of 91 DNA libraries ranged from 0.2 ng/µL to 55.2 ng/µL with insert sizes between 176 and 560 bp (**Table 6.4**).

4.3.10 Sequencing on the MiSeq platform

The 91 libraries constructed with the TruSeq Custom Amplicon method were pooled and loaded onto the MiSeq sequencer (Illumina, CA, USA) at the Earlham Institute (Norwich, United Kingdom) with a final concentration of 580 pM. Before sequencing, the pool was denatured with 0.1 M sodium hydroxide for 5 minutes and then neutralised using 200 µM Tris-HCl, pH 7. The denatured libraries were sequenced with 20 % PhiX and a cluster density of 70 % using the 500 cycle MiSeq v2 Reagent Kit (Illumina, CA, USA) on the MiSeq sequencer which generated 251 bp paired-end reads. The resulting data were de-multiplexed on the sequencer to produce fastq files for each sample.

4.3.11 Data analysis of samples sequenced on the MiSeq platform

The quality of the 251-bp paired-end reads for each of the 91 samples was examined using fastqc (version 0.11.8) (Andrews, 2010) and trimmed to remove adapter sequences using trimmomatic (version 0.33) (Bolger, Lohse, & Usadel, 2014). The trimmed reads were aligned to the PST-130 assembly (Cantu et al., 2011) using bwa mem (version 0.7.5) with default parameters. SAMtools (Li et al., 2009) (version 0.1.19) was used to call SNPs between samples and the PST-130 genome with a minimum depth of coverage of 20X as described in (Bueno-Sancho, Bunting, et al., 2017). The same script used for the computational test of the markers was used here to look at the bases of the set of 96 SNP sites for each sample and then assign each sample to a genetic group based on the list of markers.

4.3.12 KASP genotyping

For each marker, three primers were designed using Primer3plus software (version 4.0.0.), one specific for each possible base at that position and a third common primer. KASP primers were designed by Francesca Minter (Saunders Lab) under my supervision and by Clare Lewis (Saunders Lab). Each of the specific primers was designed carrying standard FAM (5' GAAGGTGACCAAGTTCATGCT 3') or HEX (5' GAAGGTCGGAGTCAACGGATT 3') compatible tails and with the target SNP at the 3' end. Oligonucleotides were ordered from

Sigma-Aldrich (USA) and primer pools prepared as recommended by the manufacturer (LGC, UK): 12 µL of each tailed primer (100 µM), 30 µL of the common primer (100 µM) and 46 µL of dH_2O. The reaction was prepared mixing 2.5 µL 2x KASP MasterMix (Kaspar mix), 0.07 µL of primer pool and 2.5 µL of DNA (5-30 ng/µL). KASP genotyping was carried out as described previously (Bueno-Sancho, Persoons, et al., 2017). PCR reactions were prepared in a 384-well clear plates (Roche, Switzerland) and the PCR was performed using an Eppendorf Mastercycler pro 384 using the following protocol: hot start at 94 ºC for 15 minutes, followed by ten touchdown cycles (95 ºC for 20 seconds, touchdown 65 ºC for 60 seconds, -1 ºC per cycle, for 25 seconds), followed by 35 cycles of amplification (94 ºC for 20 seconds; 57 ºC for 60 seconds). As KASP amplicons are smaller than 120 bp, an extension step is unnecessary in the PCR protocol. Reaction plates were then assessed on a Tecan Safire plate reader at ambient temperature. Additional amplification cycles (up to 40-45 cycles) were performed if genotyping clusters were not clear after 35 cycles. Data analysis was performed manually using Klustercaller software (version 2.22.0.5, LGC Genomics).

4.3.13 Field trials

To study the *Pst* population in the UK, field trials were established by Jane Thomas and Sarah Holdgate (NIAB, Cambridge, UK) in locations that are known to be frequented by YR infection. Each field contained two wheat varieties that were previously known to be highly susceptible to the disease: Solstice and KWS Kielder. The varieties were planted in two separated areas but within the same field for two consecutive wheat growing seasons.

For the first year of the study (2015-16), a total of 14 different locations across the UK were selected: Aby, Cambridge, Cirencester, Colchester, Croft, Driffield, Harper Adams, Hereford, Morley, Stonham, Sutten Scotney, Trull, Warwick and Wye (**Figure 4.8A**). For the 2016-2017 wheat growing season, the study is focused on just 8 of these sites in order to be able to monitor the disease in each field more frequently within the limitations of time constraints (**Figure 4.8B**). Four of these sites were larger sites than the previous year to enhance the space to monitor the spread of disease foci: Morley, Hereford, Stonham and Sutton. The other four sites are the same size as those used in first year: Aby, Croft, Taunton (Trull) and Kent (Wye).

The fields were monitored monthly during the wheat growing season (from December until June) by Christopher Judge and he collected samples of wheat leaves each time infected plants were spotted in the field. After collecting a sample, it was stored in RNAlater and labelled with: (i) exact location, (ii) name of the field and spatial information within the field, (iii) date and (iv) wheat variety.

4.4 Results

4.4.1 Finding SNP markers to identify *Pst* genetic groups

4.4.1.1 Selection of *Pst* samples to identify genetic markers

A total of five main *Pst* genetic groups were recently identified in the UK. Four of them were found in 2013 (Hubbard et al., 2015) and in 2014 a fifth race that was previously identified in Europe, called the Kranich race, was also found in the UK for the first time (Bueno-Sancho et al., 2017). To identify genetic markers that would enable us to classify the five *Pst* genetic groups, I first studied the *Pst* population during 2013, 2014 and 2015 to find SNP markers that were specific for each population. This would allow us to rapidly differentiate them using just these limited set of positions, instead of carrying out full transcriptomics of each sample.

To identify a set of appropriate markers, the first step was to select representative *Pst* isolates to include in the analysis. During the field pathogenomics BBSRC-funded project, more than 600 samples were sequenced from 2013 – 2016 from all over the world. To carry out a precise analysis, I only chose isolates for which we had good quality data and that were known to be very well assigned to each genetic group. Samples were chosen to be representative of the five genetic groups and with a high enough number of samples to capture all the diversity within each genetic group. A set of 295 representative *Pst* isolates collected from 2013, 2014 and 2015 was selected from 24 countries. The number of samples from each genetic group varied due to availability, having included more samples from group 4 (198) since it was the most abundant group and less for Kranich (8) and group 2 (10). Most of the included samples were originally collected from the UK, Germany and France, particularly for 2013 for which we only had samples from the UK (**Figure 4.1**).

Phylogenetic analysis was carried out using these 295 *Pst*-infected samples using the third codon position of 2,329 PST-130 gene models via maximum-likelihood model (679,350 nucleotide sites; **Figure 4.2**). These 295 isolates had been previously analysed and assigned to a genetic group (Adams, Neher, & Saunders, 2020; Bueno-Sancho, et al., 2017; Hubbard et al., 2015). Isolates clustered well phylogenetically into their respective genetic group and are highlighted in the tree in the colour of their group. Thus, I could confirm that these samples were appropriate for identifying representative markers that were specific for each one of the five populations.

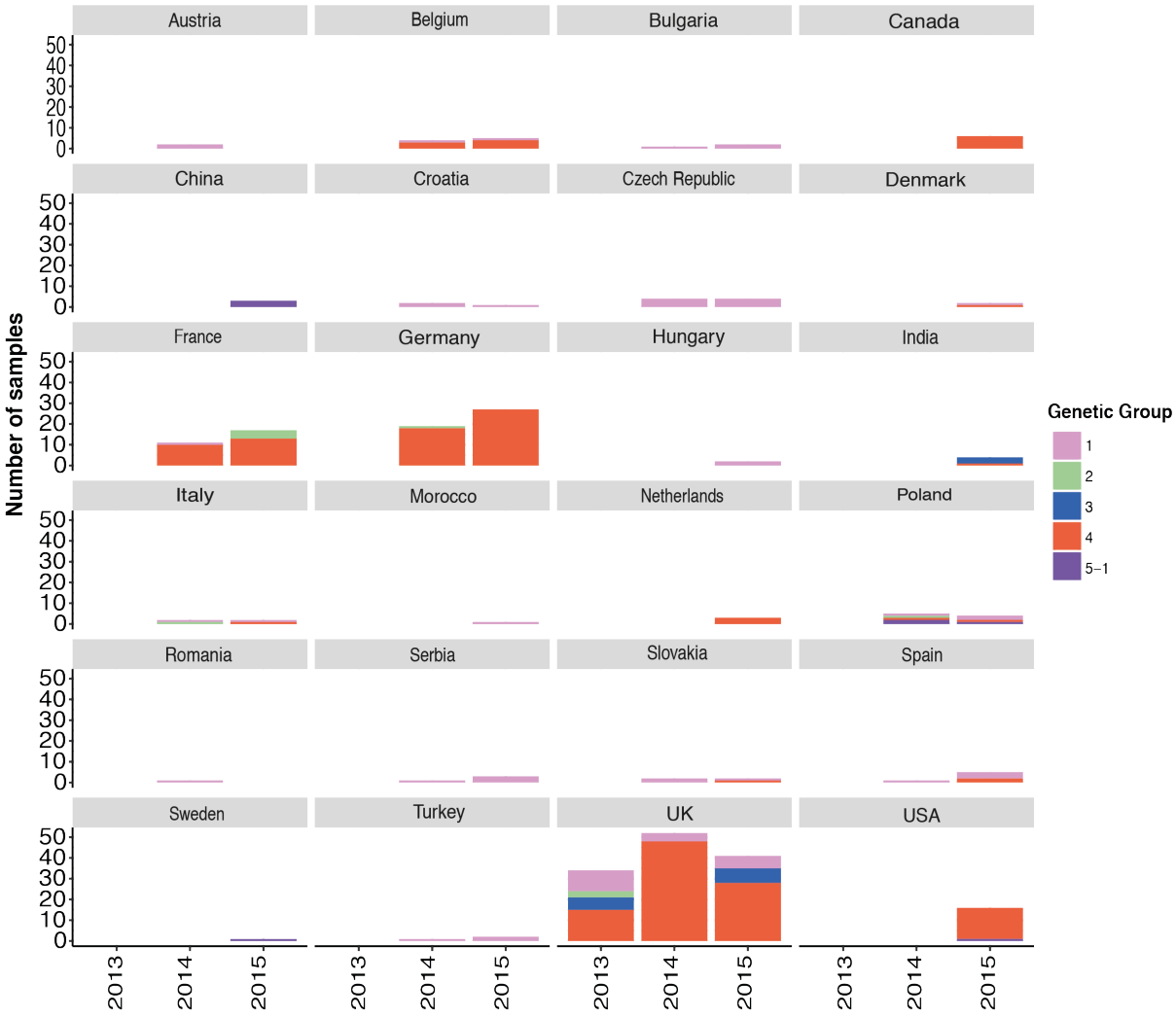

Figure 4.1. The 295 selected samples were collected from different locations and different years. The samples chosen for the analysis were originally collected from different locations around Europe, USA, China, India and Canada during three different years (2013, 2014 and 2015). All samples included from 2013 were collected from the UK and belonged to groups 1, 2, 3 or 4. Samples included from 2014 and 2015 were from all five genetic groups. Most of the included samples were collected form the UK, Germany and France.

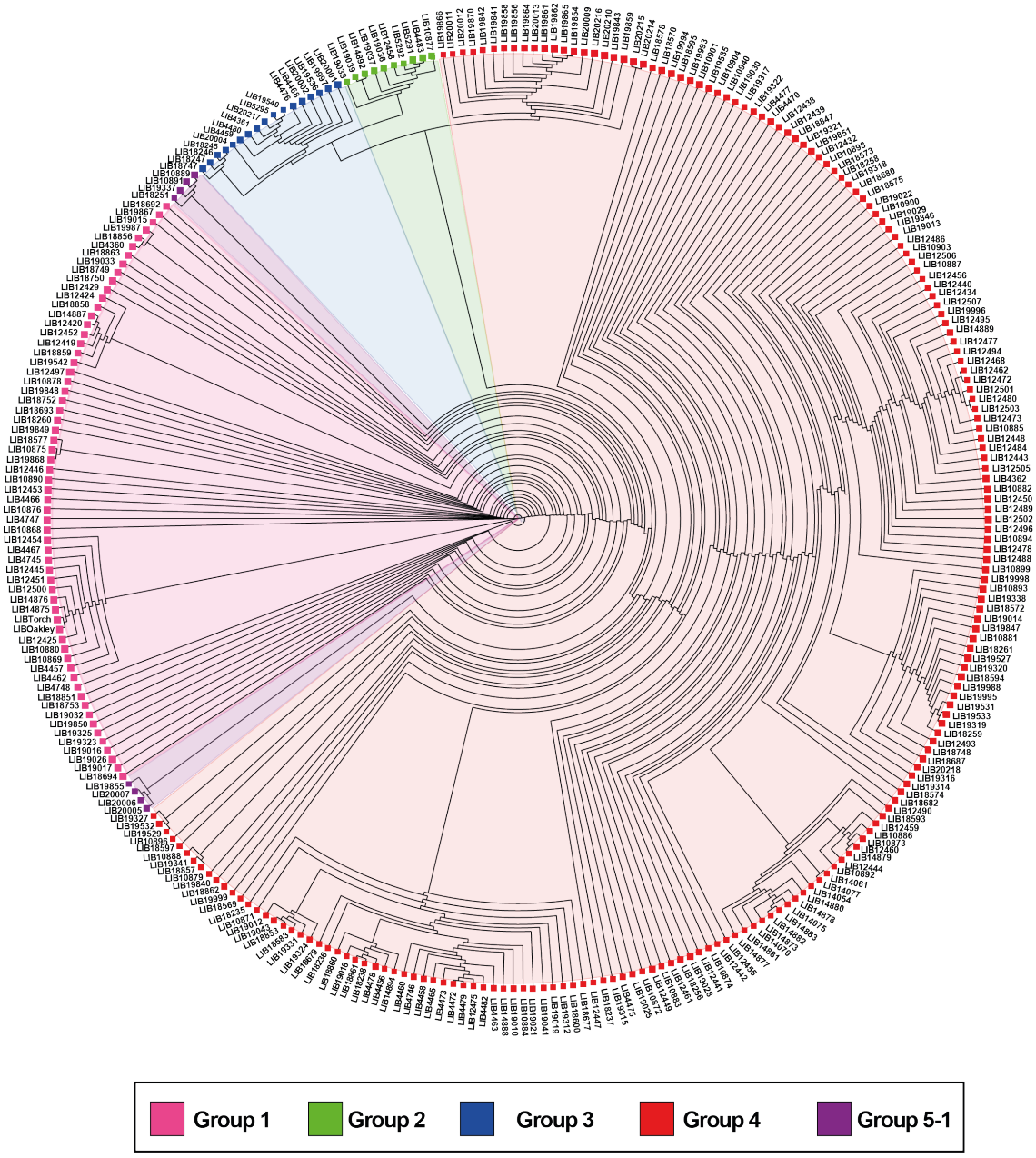

Figure 4.2. The selected 295 *Pst* samples are a good representation of the five *Pst* genetic groups. Phylogenetic tree of the 295 samples using the third codon position of 2,329 PST-130 gene models (679,350 sites). Isolates are clustered into five genetic groups, represented by colours. The background colour represents the genetic clustering assigned, as previously seen in (Adams et al., 2020; Bueno-Sancho, Persoons, et al., 2017; Hubbard et al., 2015).

4.4.1.2 A set of 96 SNP markers was found that could differentiate the five *Pst* genetic groups

Using 295 *Pst*-infected samples, all synonymous SNP sites were extracted for each isolate and then compared to each other to extract specific markers for each genetic group as described in the methods (**Figure 4.3**). The high variability that exists between isolates within a single genetic group (Bueno-Sancho et al., 2017; Hubbard et al., 2015) made it very difficult to define consensus markers within and between genetic groups. Besides, sequencing errors and missing data complicated this analysis further. Thus, I had to include a margin of error in the analysis in order to gain a set of markers, while setting a threshold to make sure that they were sufficiently reliable.

A vast number of markers was initially found for group 2, which was expected since a low number of samples was included. Identification of markers for the genetic groups 1, 3 and 5-1 (Kranich) was relatively easy, however group 4 (with the highest genetic variability) was more challenging. Only a small number of consensus markers could be identified that were conserved across all *Pst* isolates in this genetic group, which limited marker identification for this group (**Figure 4.4**). Nonetheless, markers were found to be specific for group 2 and group 4 (i.e. 7582_7250) or group 3 and group 4 (i.e. 8552_2672) and thus group 4 could be differentiated by using these markers and group3-specific (26014_8757) and group 2-specific (i.e. 10129_723). Due to similarity between group 1 and 5-1, several markers were found to be specific for those two groups and different for the rest of the groups. Overall, a set of 96 markers were obtained that could allow us to differentiate genetic groups. Out of these 96, 37 markers were specific for group 2 (that were found with an allowance of 10 % missing data and 0% of error) and 24 were useful for differentiating all genetic groups (**Table 6.3**). Since group 2 *Pst* isolates had been consistently identified only on triticale and rye (Hubbard et al., 2015), this group was excluded from subsequent analyses.

4.4.2 Markers were successfully tested using three different methods

To test that the selected set of markers were able to identify the different *Pst* genetic groups, three different methods were used. First, we took a computational approach with samples that were already sequenced, then a sequencing-based approach with samples with a known genetic group and thirdly using KASP assays to quickly genotype samples by amplifying single SNPs.

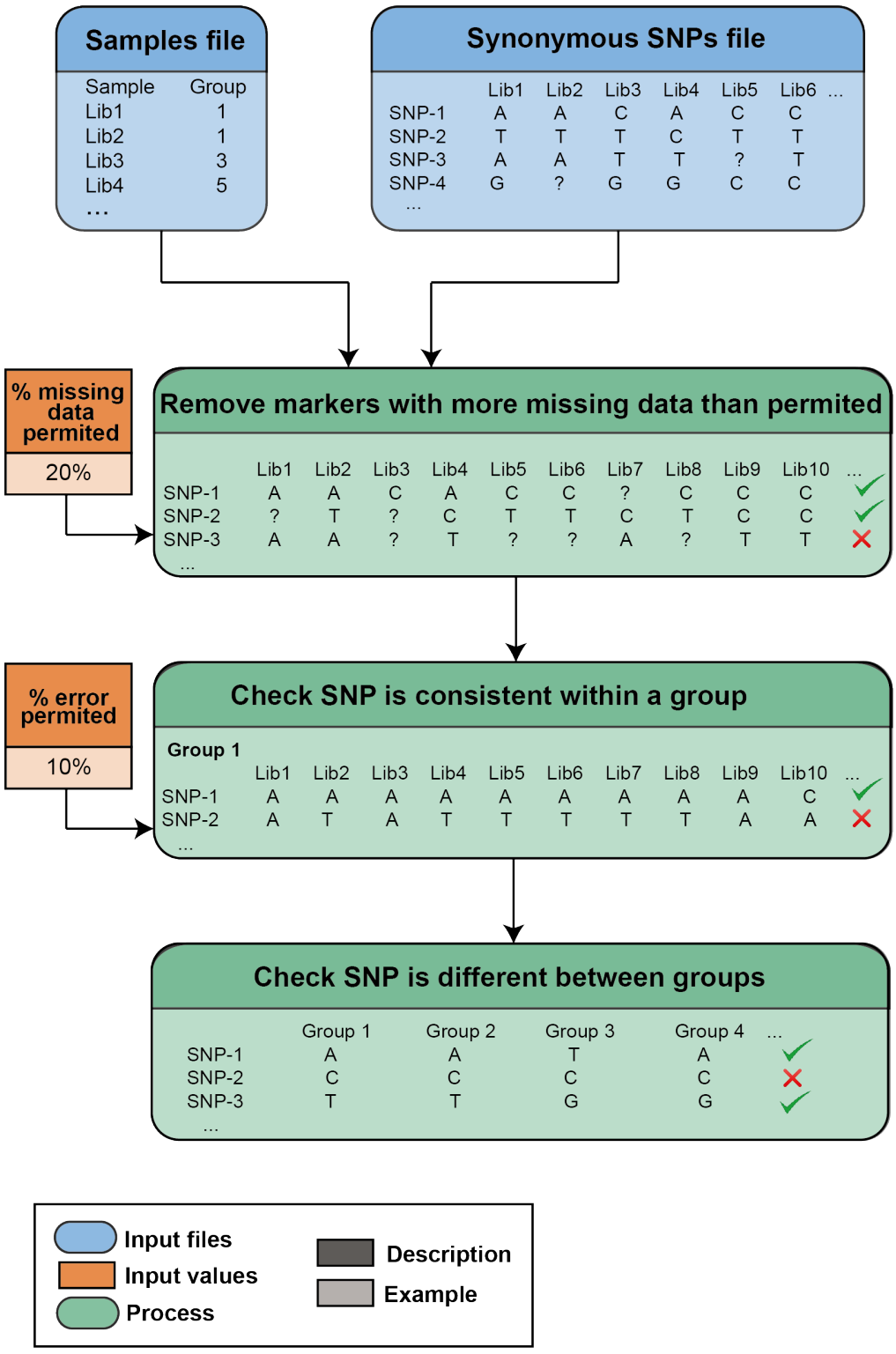

Figure 4.3. Workflow of the python script used for identifying markers. Two input files were required: (1) a file with the synonymous SNP positions for each sample and (2) a file with the group each sample had been assigned to. Two input values are also needed to use as thresholds: (1) Maximum percentage of missing data permitted and (2) maximum percentage of errors permitted. The synonymous SNPs file was used to find positions that were consistent within a group, different between groups and followed the specified thresholds.

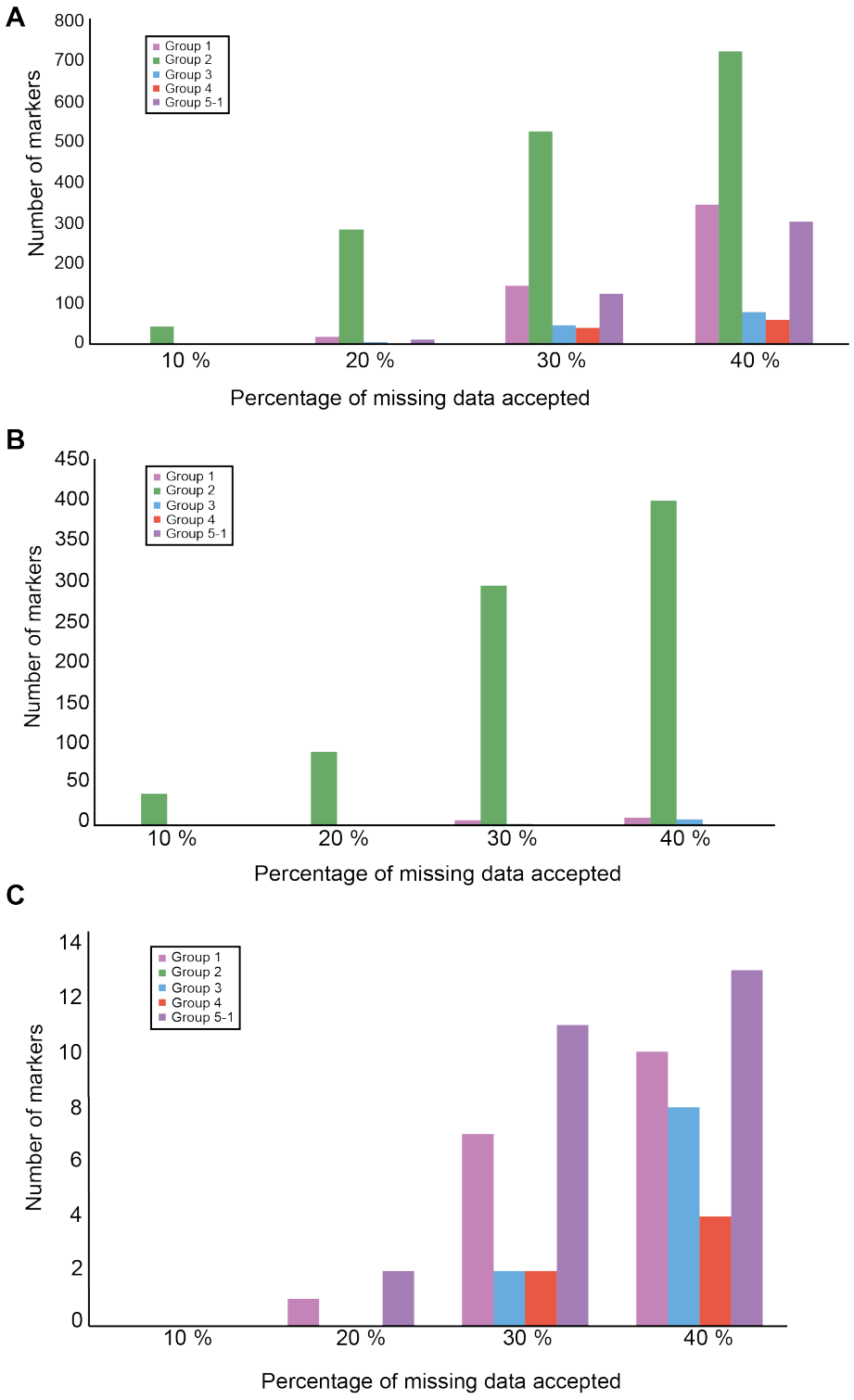

Figure 4.4. Number of markers varied greatly for each genetic group depending on the specified thresholds. Number of markers found with a threshold of 10%, 20%, 30% and 40% of missing data permitted and **(A)** 10 % of error permitted or **(B)**, **(C)** 0 % of error permitted. **(C)** shows the same analysis than **(B)** but without including genetic group 2.

4.4.2.1 Computational tests revealed markers were suitable for differentiating *Pst* genetic groups

To determine that the list of selected markers was suitable for identifying genetic groups, I initially took a computational approach to see if I could assign the genetic group of samples that had been previously sequenced by assessing the base at these 96 positions. I utilised transcriptome data from 475 *Pst*-infected samples collected across four years: 2013, 2014, 2015 and 2016, including the 295 samples that were used to define the set of markers. Using a python script, I assessed the nucleotides at each SNP position for each of the 96 positions and assigned a score to classify each sample into one of the five genetic groups. Using this approach, I was able to classify 98.95 % of the samples into their previously defined genetic groups, determined through full transcriptome sequencing. Only five samples were not successfully assigned and were those with poor quality data or that were not very well assigned to their genetic group. Therefore, these results were very promising and showed how analysing just 96 SNP positions was sufficient to assign *Pst* isolates to one of the four *Pst* genetic groups assessed herein.

4.4.2.2 Amplicon resequencing confirmed the efficacy of the 96 markers

To evaluate the SNP markers using the TruSeq Illumina custom amplicon method, a pool of primers was designed by Illumina that amplified 200 bp surrounding the SNP site of interest. A total of 91 libraries were prepared, of which 43 were *Pst* -infected samples that had been previously genotyped using transcriptomic analysis and thus their genetic group was known. The other 48 were samples collected during 2016 from field trials. To test how well this method worked, I firstly explored the number of contigs containing the SNP markers that were sequenced for each sample (**Figure 4.5**). Most of the samples contained around half of the contigs, showing that the designed primers were not able to amplify all the SNP markers as expected. Markers contained in the contigs located at the bottom of **Figure 4.5**, such as 10095_1765, 11587_2433 and 19742_674 were not present for any of the samples. Markers at the top, coloured in light blue, such as 9827_1344, 8286_876, 8069_1156 and 7753_15395 were found in most of the samples. Three samples (14/113, 14/7 and 16.0392) did not contain most contigs, showing that the amplification of SNP markers was not very consistent and did not work with high accuracy, possibly due to low initial DNA concentration for these samples.

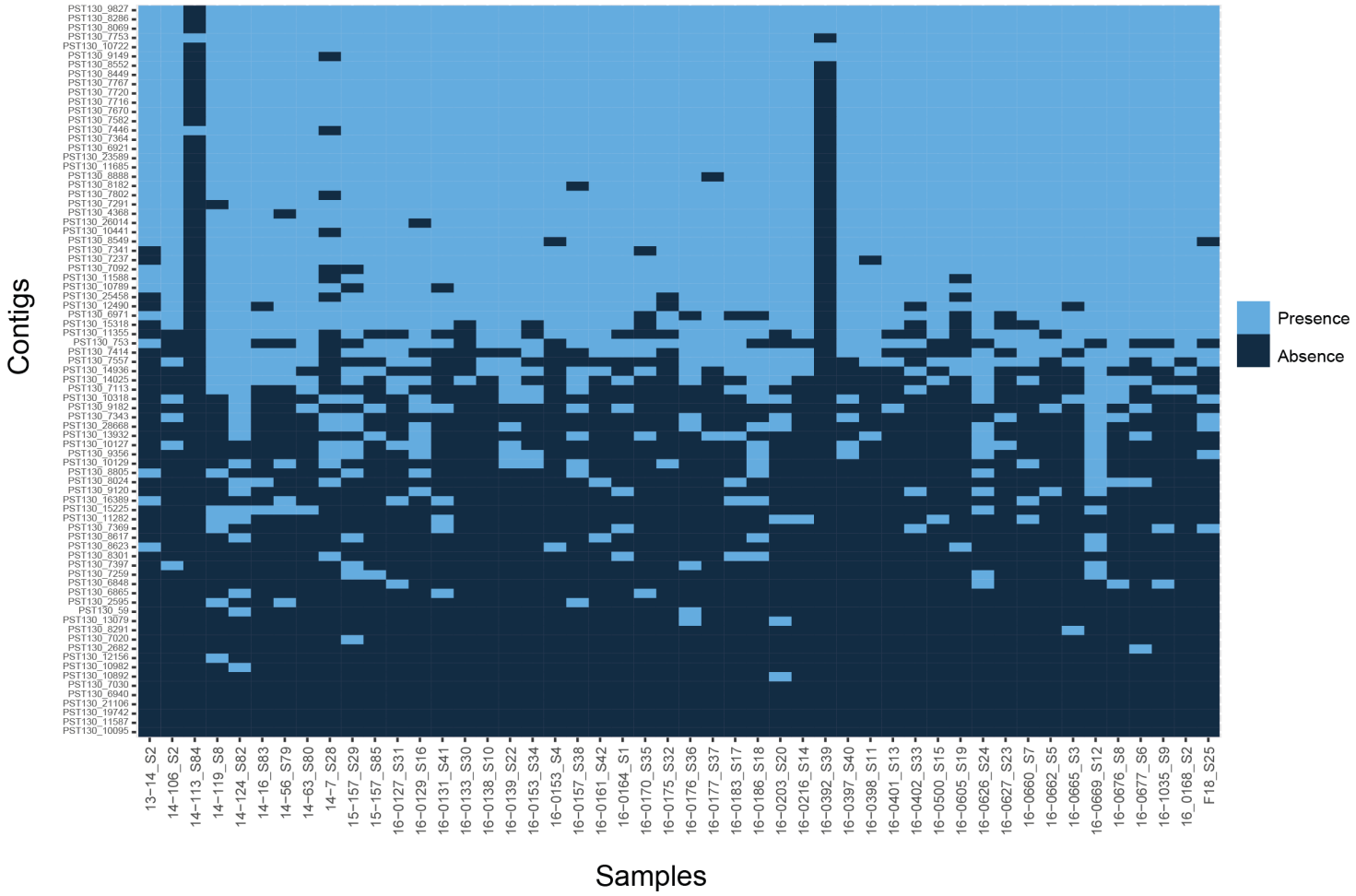

Figure 4.5. Around half of the contigs that contained the selected markers were found in almost all samples. The 96 selected positions from a total of 48 *Pst*-infected samples collected during the 'field pathogenomics' project from 2013-2016 were sequenced to test the markers. All samples apart from two contained around half of the positions, the other half of the positions were missing. Markers are coloured in dark blue if they were missing in a sample and light blue if they were found. Markers are sorted in the y-axis by prevalence, showing the markers found in mostly all samples at the top.

		GROUP 1				GROUP 3				GROUP 4				GROUP 5_1 (KRANICH)			
Marker	Group	Expected	16.0164	F18	16.0127	Expected	16.0676	16.0401	16.0402	Expected	16.0669	16.0203	15/157	Expected	16.0183	16.0186	14/106
6921_3712	2, 3	TT	TT	TT	TT	CT	CT	CT	CT	TT	TT	TT	TT	TT	TT	TT	TT
6971_19720	ALL	GG	GG	GG	GG	AA	AA	AA	AA	AG	AG	AG	AG	GG	-	-	GG
7237_8357	ALL	GG	GG	GG	GG	CC	CC	CC	CC	CG	CG	CG	CG	GG	GG	GG	CG
7291_1846	1, 2	AA	AA	AA	AA	AG	AG	AG	AG	AG	AG	AG	AG	AG	AG	AG	AG
7341_4368	1,5_1	AT	AT	AT	AT	TT	TT	TT	TT	TT	-	TT	TT	AT	AT	AT	AT
7341_4770	3	CT	CT	-	CT	TT	TT	TT	-	CT	CT	CT	CT	CT	-	CT	-
7364_28843	1	AT	AT	AT	AT	TT	TT	TT	TT	TT	TT	TT	TT	TT	TT	TT	TT
7446_5852	2,5_1	GG	GG	GG	GG	GG	GG	GG	GG	GG	GG	GG	GG	AG	AG	AG	AG
7582_7250	2,4	CT	CT	CT	CT	CT	CT	CT	CT	CC	CC	CC	CC	CT	CT	CT	CT
7582_8369	2,4	AG	AG	AG	AG	AG	AG	AG	AG	GG	GG	GG	GG	GG	GG	GG	GG
8552_2672	ALL	AA	AA	AA	AA	AG	AG	AG	AG	AG	AG	AG	AG	AA	AA	AA	AA
9827_1344	2, 3	CC	CC	CC	CC	CC	CC	CC	CC	CC	CC	CC	CC	CC	CC	CC	CC
10441_476	1,5_1	TT	TT	TT	TT	CT	CT	CT	-	CT	CT	CT	CT	TT	TT	TT	TT
10441_749	1,5_1	TT	TT	TT	TT	CT	CT	-	CT	CT	CT	CT	CT	TT	TT	TT	TT
26014_8757	3	CT	CT	CT	CT	TT	TT	TT	TT	CT	CT	CT	CT	CT	CT	CT	CT

Figure 4.6. The selected 96 SNP markers were able to correctly assign the genetic group of the control *Pst*-infected samples that were sequenced. Three samples of each genetic group (1, 3, 4 and 5-1) are shown here, with their bases for each one of 15 markers. The "expected" column shows the bases that a sample from each genetic group would typically have. The control samples resembled the expected bases and thus were assigned to their genetic group successfully. Some of the samples showed missing data for some of the markers but the assignment of the genetic group was still possible.

Using this technique, we could identify the genetic group correctly for 40 out of the 43 *Pst*-infected samples tested that had previously been assigned to genetic groups and produced sufficient data for analysis (**Figure 4.6**). The remaining three samples had very low DNA concentrations and therefore failed to generate sufficient transcriptomic data. However, despite the low data acquired for one of the samples (14/7), I was still able to assign the sample to its corresponding genetic group. Out of the 48 *Pst*-infected samples that had not been previously characterised, four of them did not produce data of sufficient quality to assign genetic groups. The remaining 44 *Pst*-infected samples all produced sufficient data and were assigned to group 4. For most samples, we used between 40-50 of the 96 markers to identify their genetic group, with an average of 47.87 markers (± 8.6 S.D.) used per sample. This indicates that not all the primers were very effective in all cases and thus for almost half of the markers we had no data available. As primers were designed and pooled by Illumina, optimisation of the technique to increase the coverage for all markers was not possible. This adds a limitation to this method because it is harder to implement and will rely on Illumina to add more markers or optimise the method. However, even with half of the SNP positions with missing data, we could still successfully identify the genetic group. This suggests that this method is not very effective to amplify all 96 positions but also that not all 96 positions are needed to assign *Pst*-infected samples to a genetic group.

4.4.2.3 KASP assays can be used to identify populations with the set of markers

To further test the aforementioned markers, I carried out KASP assays and designed specific primers for a subset of 36 of the initial 96 markers (**Table 6.5**). The high level of GC content and repeat content in certain regions prevented primer design for the remaining markers.

To test these KASP primers, a total of 5 samples were utilised as positive controls to represent the four genetic groups of *Pst* that infect wheat: *Pst* isolates F18 and F22 (both from group 1), *Pst* isolate 15/151 (group 3), *Pst* isolate 14/7 (group 4) and isolate 14/106 (group 5-1). Initial analysis revealed that many of the KASP assays were not very consistent for all the primers (**Figure 4.7**). KASP results using these control samples differed greatly from the expected results in some cases. Therefore, we selected four primer triplets that could be used to reliably differentiate between the four genetic groups: CLPST163, CLPST167, PST-16 and PST-18 (**Table 4.2**). These four primers allowed us to differentiate between the four genetic groups very easily and gave consistent results when tested with several samples (**Figure 4.11**).

	Primer	CLPST160	CLPST163	CLPST167	CLPST171	PST-16	PST-17	PST-18	PST-23	PST-29	PST-19
	Marker	7670_3437	10982_2778	7291_1846	11355_649	7364_28843	753_1139	8291_7564	19742_674	7237_13346	8552_2672
	Contig	PST130_7670	PST130_10982	PST130_7291	PST130_11355	PST130_7364	PST130_753	PST130_8291	PST130_19742	PST130_7237	PST130_8552
	SNP	C3524T	G2778A	G1846A	A649C	t28843a	c1139a	a7564g	c674t	g13346c	A2672G
	Specific	ALL	ALL	Group 1	ALL	Group 1	Group 1, 5-1	Group 5-1	ALL	ALL	Group 3
Expected	Group 4	XY	XY	XY	XY	XX	XY	XX	XY	XY	XY
	Group 3	XX	YY	XY	YY	XX	XY	XX	YY	YY	XY
	Group 1	YY	XX	YY	XX	XY	XX	XX	XX	XX	XX
	Group 1	YY	XX	YY	XX	XY	XX	XX	XX	XX	XX
KASP results	Group 4	XX	XY	XY	XX	XX	XX	XX	XX	XY	-
	Group 3	YY	YY	XY	XY	XX	XX	XX	XX	XX	-
	Group 1	XX	XX	YY	XX	XY	XX	XX	XX	XY	-
	Group 1	XX	XX	YY	XX	XY	XX	XX	XX	XY	-

Figure 4.7. KASP primers were tested with control *Pst*-infected samples fom different genetic groups. Example of 10 of the tested primers and the results observed running KASP vs the expected results. For a given marker, each primer would give a signal: XX, XY or YY (represented in blue, green or red to mirror KASP results), depending on the genetic group of the sample that is amplifying. Many primers did not give the expected results (the expected and observed results did not match) and thus were not chosen for further analysis. Only four of the primers (highlighted in light orange) worked well for the samples consistently and were selected.

Once primers had been validated using positive controls, the four primers were further evaluated using additional *Pst* infected samples that had also been subjected to full transcriptome sequencing and whose genetic group was known. The four KASP primers were very effective in distinguishing *Pst* genetic groups, with identical results compared to the Illumina sequencing. Out of the 43 samples sequenced using the amplicon Illumina sequencing method, 10 were also tested in KASP, giving the same result. Also, the 48 samples collected from the 2016 field trials were tested with KASP resulting in an identical conclusion. This indicates that KASP is a quick and effective method to genotype samples using this limited set of markers. By focusing on just four markers, we can therefore genotype samples rapidly and with a low cost.

Table 4.2. Four primer triplets were selected for amplifying four SNP markers that allow us to differentiate *Pst* genetic groups. Five isolates from four genetic groups were chosen as positive controls. The expected bases that would be amplified by each primer triplet depending on the genetic group are shown here, with the corresponding KASP results within brackets. Colours represent the fluorescence given by KASP primers when amplifying each corresponding nucleotide (**Figure 4.11**).

	Group 1		Group 3	Group 4	Group 5-1
	F18	F22	15/151	14/7	14/109
CLPST163	GG (XX)	GG (XX)	AA (YY)	AG (XY)	GG (XX)
CLPST167	AA (YY)	AA (YY)	AG (XY)	AG (XY)	AG (XY)
PST-16	AT (XY)	AT (XY)	TT (XX)	TT (XX)	TT (XX)
PST-18	AA (XX)	AA (XX)	AA (XX)	AA (XX)	AG (XY)

4.4.2.4 Computational analysis revealed samples can be assigned to genetic groups using just four markers.

To further check that the four selected markers were sufficient to assign *Pst*-infected samples to genetic groups, I performed the same computational test previously described in section 4.4.2.1. Out of the 475 *Pst*-infected samples tested, 405 were successfully assigned to their correct genetic group (85.26 %) and 47 had missing data for some of these positions and thus could not be assigned to a genetic group. The remaining 23 samples also had missing data for some positions thus leading to confusing results. These were all samples that were previously described as belonging to group 4 but due to the missing data I was unable to infer whether they belonged to group 3 or group 4. These results showed that the

genetic group of *Pst*-infected samples can be successfully identified using these four positions as long as data is available for all four nucleotide positions.

4.4.3 Studying the *Pst* population in the UK across two wheat growing seasons

4.4.3.1 Field trials were carried out for two wheat growing seasons to study *Pst* population dynamics in the UK

To study the *Pst* population in the UK, field trials were carried out across the UK for two consecutive wheat growing seasons. For the 2015-2016 wheat growing season 14 fields were monitored and due to time constraint only 8 were chosen for the 2016-2017 wheat growing season (**Figure 4.8**). These 8 fields were still located all across the UK in order to get a good representation of the *Pst* population in different areas.

A total of 757 *Pst*-infected samples were collected by Christopher Judge (NIAB) in the first year and 539 *Pst*-infected samples collected in the following year. During the first year, YR was found for the first time in November in a field in Harper, and it remained more or less constant across the entire year (**Figure 4.9**). In Taunton, the disease appeared at the beginning of January 2016 and then seemed to withdraw during March and April and appeared again in May. A similar case was observed for Cirencester, where infected samples were collected in December 2015 but then no disease was found in March and April, and Callow, where disease was only observed in December and then in April. For the field in Cambridge, infected samples were only collected in February, March and April. In all other fields, YR disease was constant across the wheat growing season, starting mostly in December-January, with samples regularly taken to get a representation of *Pst* in each field.

For the 2016-2017 wheat growing season, YR was found later than the previous year. *Pst*-infected plants were only found at the beginning of the year in Stonham, Taunton, Croft and Morley fields (**Figure 4.10**). In these last two, disease seemed to disappear to only appear again in March-April. This was particularly noticeable in Morley, where only a few infected plants were observed in December and then disease withdrew until April. In Stonham and Taunton, diseased plants were observed all across the season. In the other four fields, *Pst*-infected plants were not found until March-April and then remained mostly constant until the end of the season in June.

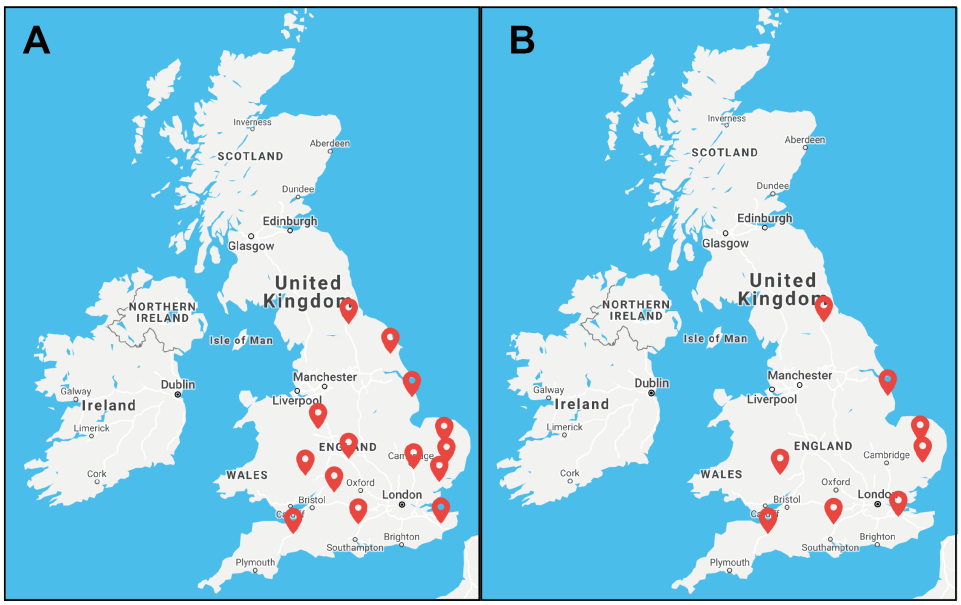

Figure 4.8. Field trials were carried out all over the UK for two years. A total of 14 sites were monitored during the wheat growing season of 2015-2016 **(A)** and 8 were monitored during 2016-2017 **(B)**. Fields were located in positions that are known to be susceptible to YR.

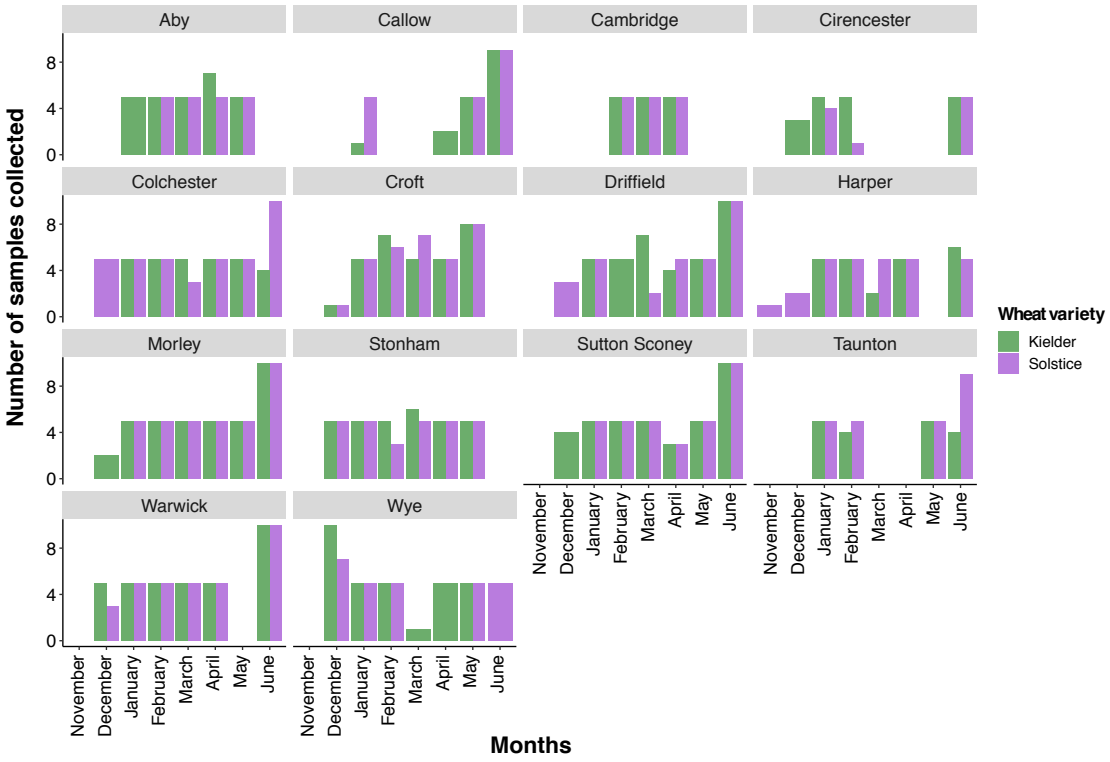

Figure 4.9. A total of 757 *Pst*-infected samples were collected during the 2015-2016 wheat growing season from 14 different fields across the UK. YR disease was found in most fields around December and then it remained constant for the rest of the growing season. In Taunton and Cirencester, YR disease withdrew during March and April. Similarly, in Callow disease was found in January and then again in April, with no symptoms found in February and March. For the field in Cambridge, infected samples were only collected during February, March and April.

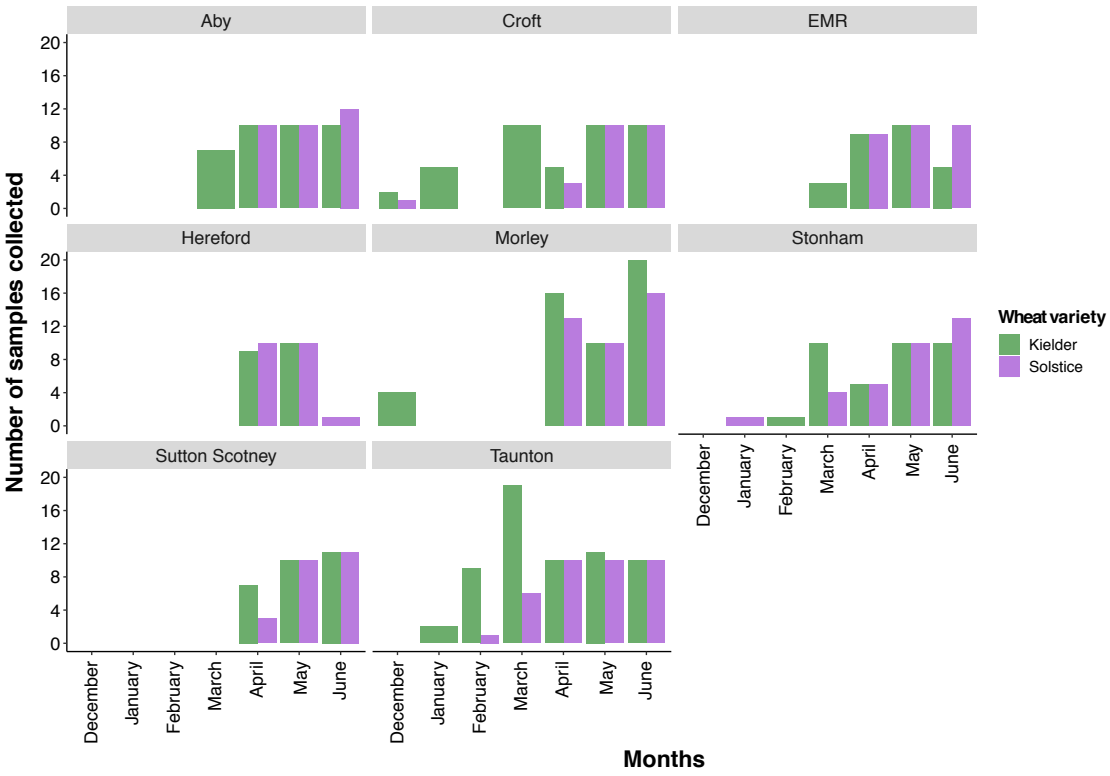

Figure 4.10. A total of 539 *Pst*-infected samples were collected during the 2015-2016 wheat growing season from 8 different fields across the UK. YR disease was only found in December-January in Croft, Morley, Stonham and Taunton. In Croft, disease was not found in February and in Morley, YR-infected plants were not found again until April. In Taunton and Stonham, disease was found all across the year and thus samples were collected accordingly. In the other four fields (Aby, EMR, Hereford and Sutton Scotney) disease was firstly observed in March-April and remained mostly constant until the end of the season in June.

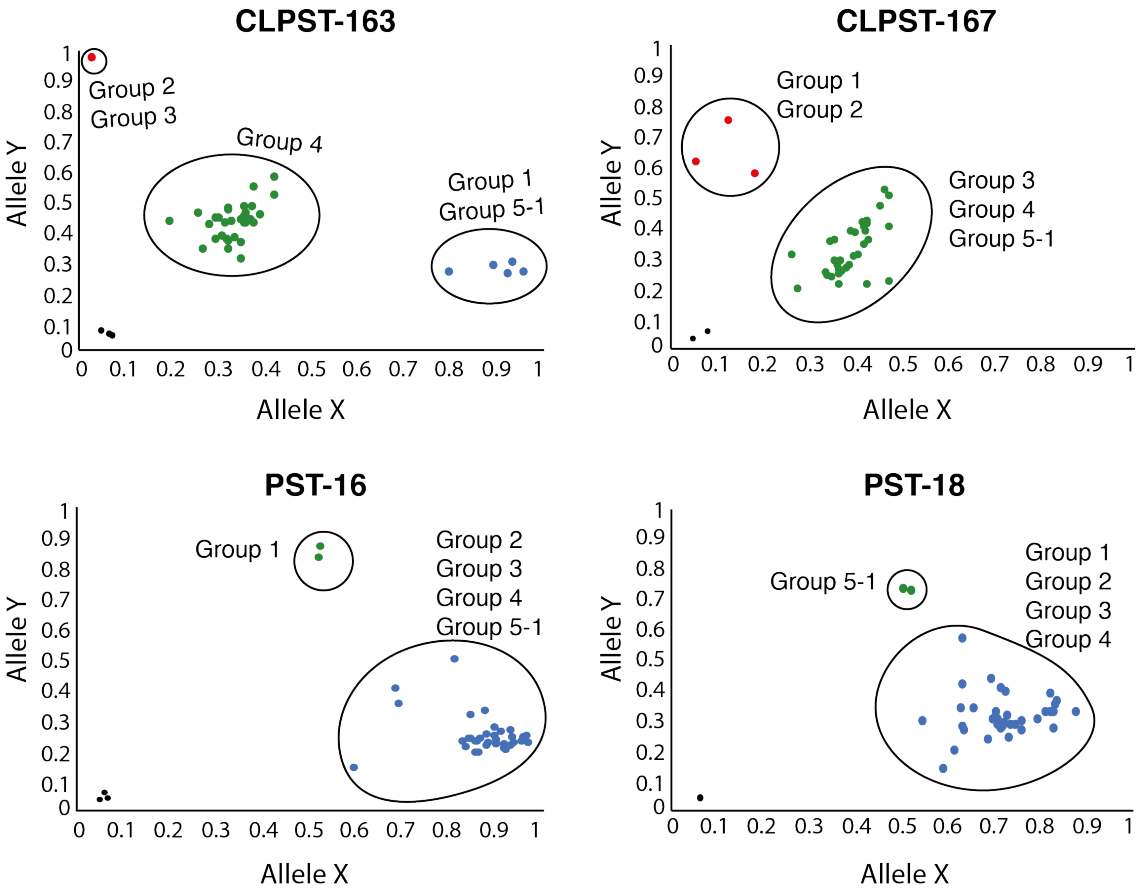

Figure 4.11. *Pst*-infected field samples were genotyped using four KASP assays. Four primer triplets were chosen for genotyping the field-collected samples: CLPST-163, CLPST-167, PST-16 and PST-18. These primers amplify four SNPs: 10982_2778, 7291_1846, 7364_28843 and 8291_7564 respectively. These SNPs can be used to differentiate the *Pst* genetic groups as shown in the figure.

4.4.3.2 Field samples can be successfully genotyped using KASP assays

As the Illumina amplicon strategy and KASP assays were both effective in assigning *Pst* genetic groups, I chose to genotype a wider range of field samples using the quicker and more economical KASP method (**Figure 4.11**). I selected a total of five samples to use as positive controls in each assay representing each of the four *Pst* genetic groups, as previously mentioned, and two negative controls: one with water and another with wheat DNA, to ensure that the primers were not amplifying wheat DNA. Therefore, the four validated KASP assays were used to examine 85 *Pst*-infected field samples from the 2015-2016 season and 379 *Pst*-infected field samples from the 2016-2017 season to evaluate the distribution of *Pst* genetic groups in a field across the wheat growing season.

For the first year of field trials, we selected 53 *Pst*-infected samples collected from the wheat variety Solstice and 32 from KWS Kielder to try to get an equal representation of both varieties. Three fields were studied: Aby (19 samples), Hereford (32 samples) and Taunton (34 samples). Out of the 85 *Pst*-infected samples, 76 were identified as belonging to group 4, 6 were from group Kranich (5-1) and only one was assigned to group 1 (**Figure 4.12**). There were two samples for which the DNA concentration was too low and thus the KASP primer did not amplify. Interestingly, group 4 and Kranich were found all through the season, whereas group 1 was only found in May.

During the following wheat growing season, out of the 379 *Pst*-infected samples that were analysed, 175 were collected from the wheat cultivar Solstice, and 204 were from KWS Kielder. Samples from all eight fields were selected for genotyping to get a better representation of *Pst* genetic groups found across the UK (**Figure 4.13**). Out of the 379 *Pst*-infected samples that were selected for KASP, we could identify the genetic group for 336. The remaining 43 had very low DNA concentration and thus not all the four KASP assays were successful. This low concentration can be due to the small quantity of initial material used. To make sure sampling did not interfere in the natural process of dispersal in the field trials, small samples (≈ 1 cm) were taken which made it difficult to extract large concentrations of DNA. All 336 *Pst*-infected samples were assigned to the genetic group 4 and no other genetic group was identified.

The dynamics of the *Pst* population across both consecutive years was studied in the field located in Taunton, Hereford and Aby. **Figure 4.14** illustrates how the *Pst* genetic groups identified throughout the growing season changed in the fields for both years. Even though both group 5-1 and group 1 were found in Taunton field in 2016, all collected *Pst*-infected

samples were analysed from the same field for the following season and none of these genetic groups were found that year. For Hereford and Aby, all samples collected both in 2016 and 2017 belonged to genetic group 4 and thus no conclusion can be drawn regarding dynamics in *Pst* races. In summary, despite different genetic groups found in 2016, I observed that in 2017 all 374 genotyped samples belonged to the genetic group 4 (**Figure 4.13**). This further supports that genetic group 4 is the predominant one in the UK.

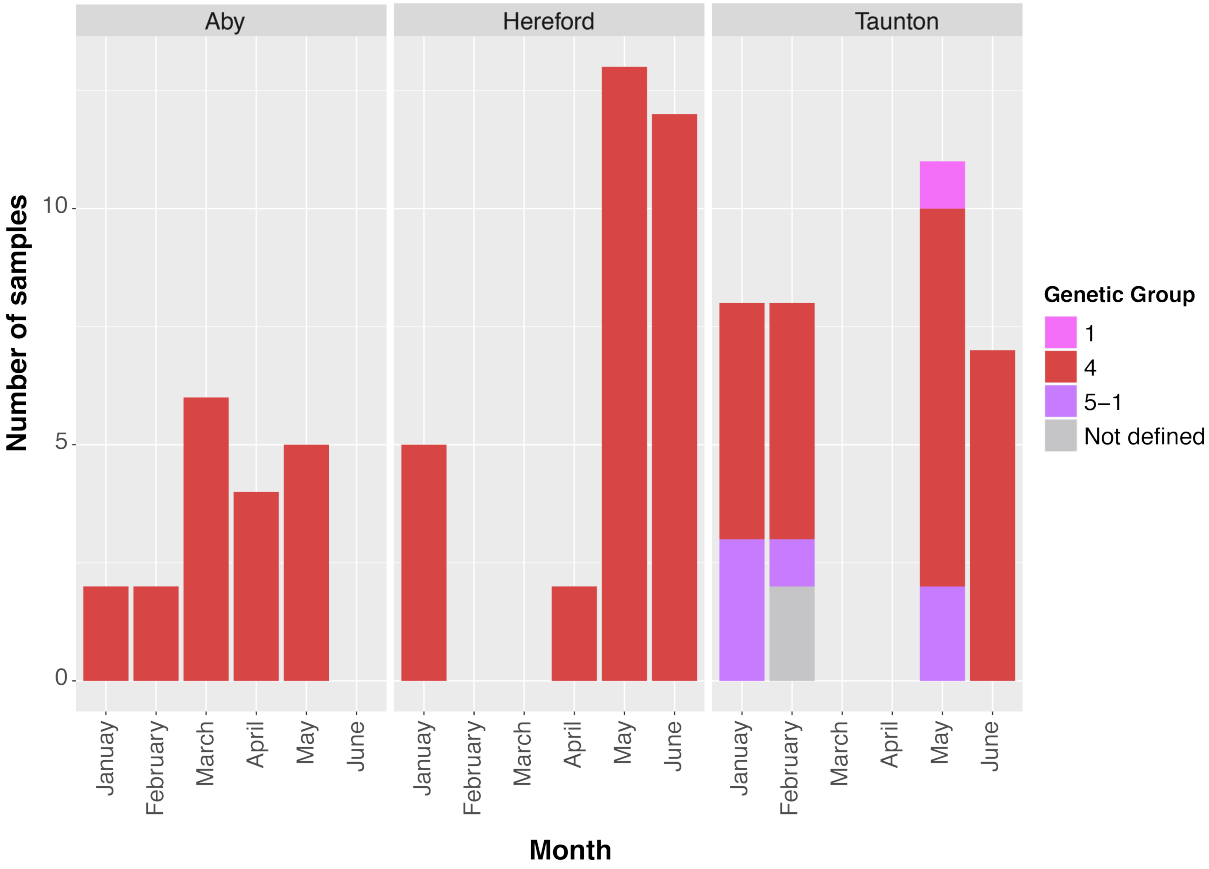

Figure 4.12. Three different *Pst* genetic groups were found in 2016. A total of 85 *Pst*-infected samples from 2016 were genotyped using KASP from three different fields: Aby, Hereford and Taunton. Most of the samples found belonged to genetic group 4. A few samples from group 5-1 were found at Taunton in January, February and May, and only one from group 1 was found in May at the same field.

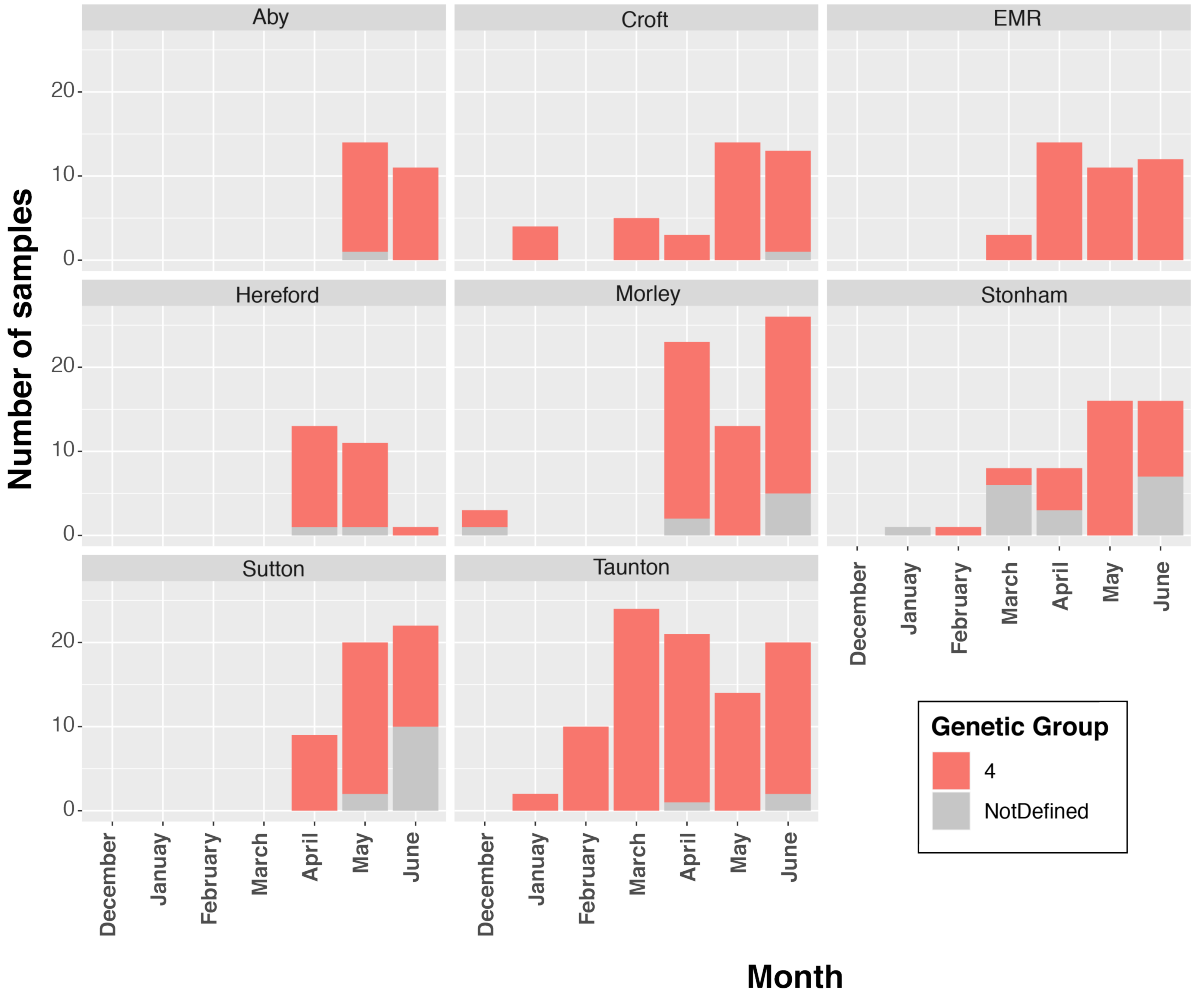

Figure 4.13. *Pst* genetic group 4 was prevalent in 2017. A total of 379 *Pst*-infected samples from 2016-2017 were genotyped using KASP from eight fields across the UK. All samples that were successfully genotyped were assigned to genetic group 4. A subset of samples that could not be identified due to low DNA concentration in the original sample.

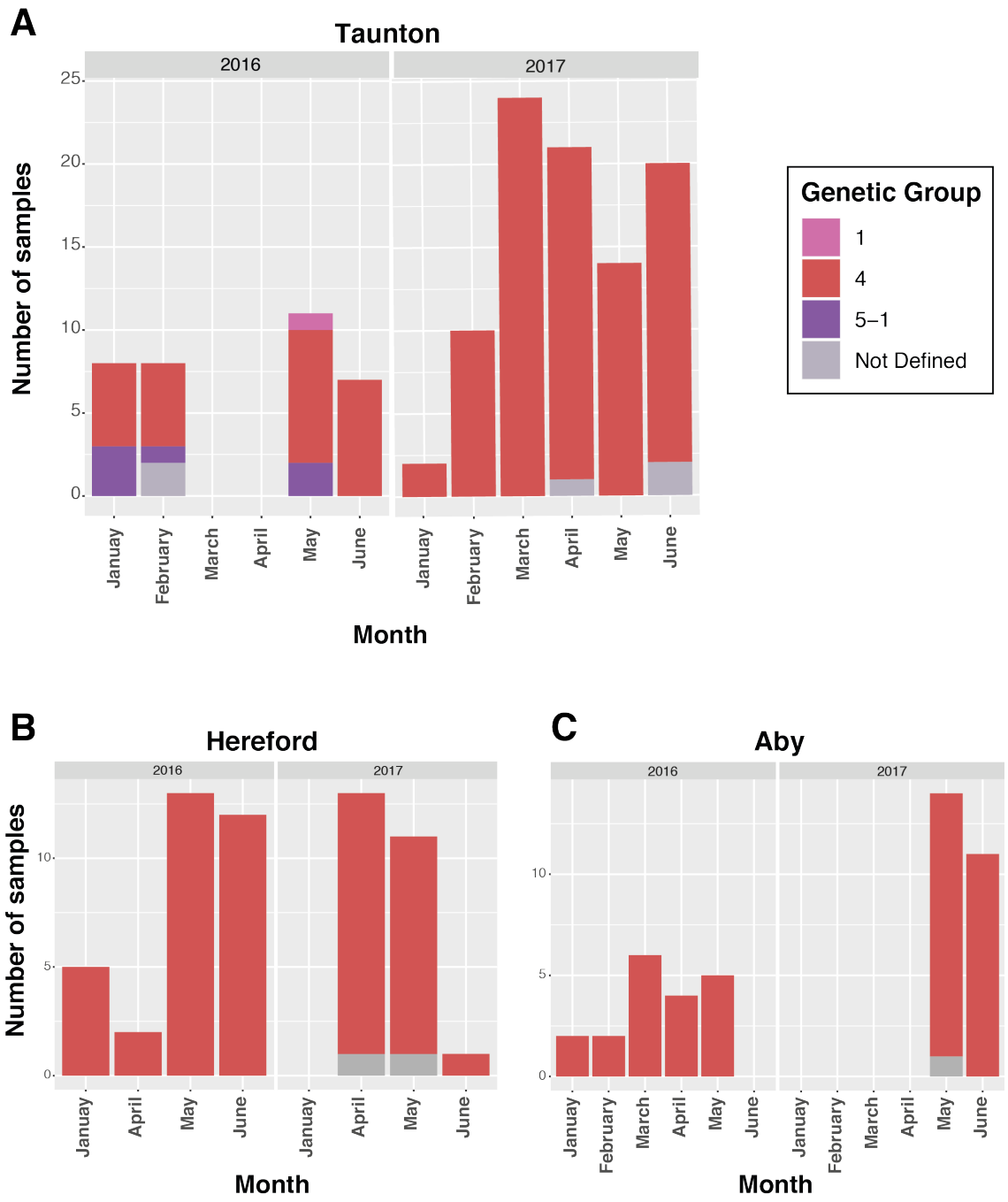

Figure 4.14. *Pst* genotypes found in one year cannot predict the prominent genotypes for the following year. *Pst*-infected field samples collected from three field in **(A)** Taunton, **(B)** Hereford and **(C)** Aby were genotyped for two years to find their genetic group. In the first year, samples from three different *Pst* genetic groups were identified (1, 4 and 5-1) in Taunton but the following year all samples belonged to a single genetic group (group 4). In Hereford and Aby, only one genetic group was found both years. The results from Taunton show how prediction of genotypes based on results early in the year or the previous year is not possible.

4.4.3.3 Transcriptomic analysis of *Pst*-infected samples confirms the results obtained with KASP assays.

To evaluate whether the results obtained using KASP marker analysis were consistent with the original field pathogenomics method, a subset of 15 field *Pst*-infected samples were selected for full transcriptome sequencing. All the selected samples were collected during the 2016-2017 growing season from different fields: Aby (3 samples), Croft (2), EMR (6), Hereford (1), Morley (1), Stonham (1) and Sutton (1). A total of 11 *Pst*-infected samples were obtained from the Solstice cultivar and 4 to from KWS Kielder. Out of these 15 samples, 7 were also genotyped by KASP and assigned to group 4.

Phylogenetic analysis was performed on all 15 *Pst*-infected samples plus 31 representative *Pst*-infected samples from all five genetic groups (Bueno-Sancho, Persoons, et al., 2017). Phylogenetic analysis revealed that all 15 *Pst*-infected samples clustered well with isolates from group 4 (**Figure 4.15**). DAPC analysis also clustered the field samples with group 4 isolates (**Figure 4.16**). Three of the *Pst*-infected field samples: He-4-17-S6, CT-1-17-K2 and CT-1-17-K5 clustered together further away from the other samples. Further examination of the distribution of read counts for these three samples showed that they did not contain sufficient data for analysis. Moreover, the distribution of biallelic SNPs for a dikaryon is expected to have a peak at 0.5, representing each one of the two haploid nuclei (**Figure 4.17 A**). However, the distribution for CT-1-17-K2 did not follow the pattern expected of a dikaryon which suggest the sample might not contain a single *Pst* genotype and thus conclusions cannot be drawn for this sample (**Figure 4.17 B**).

Next, I examined the full 96 SNP sites to determine if I could assign the samples to their genetic group and thus confirm the KASP results. Using the list of 96 markers, I was able to assign all *Pst*-infected samples (apart from the three previously mentioned that did not have enough data) to the *Pst* genetic group 4. Thus, I could confirm that these samples belong to *Pst* genetic group 4 as was observed with KASP analysis. This provides further validation for the utility of these 4 KASP markers. This also further supports that *Pst* genetic group 4 seems to be the predominant group in the UK and the only one that was found in the field trials during the 2016-2017 wheat growing season.

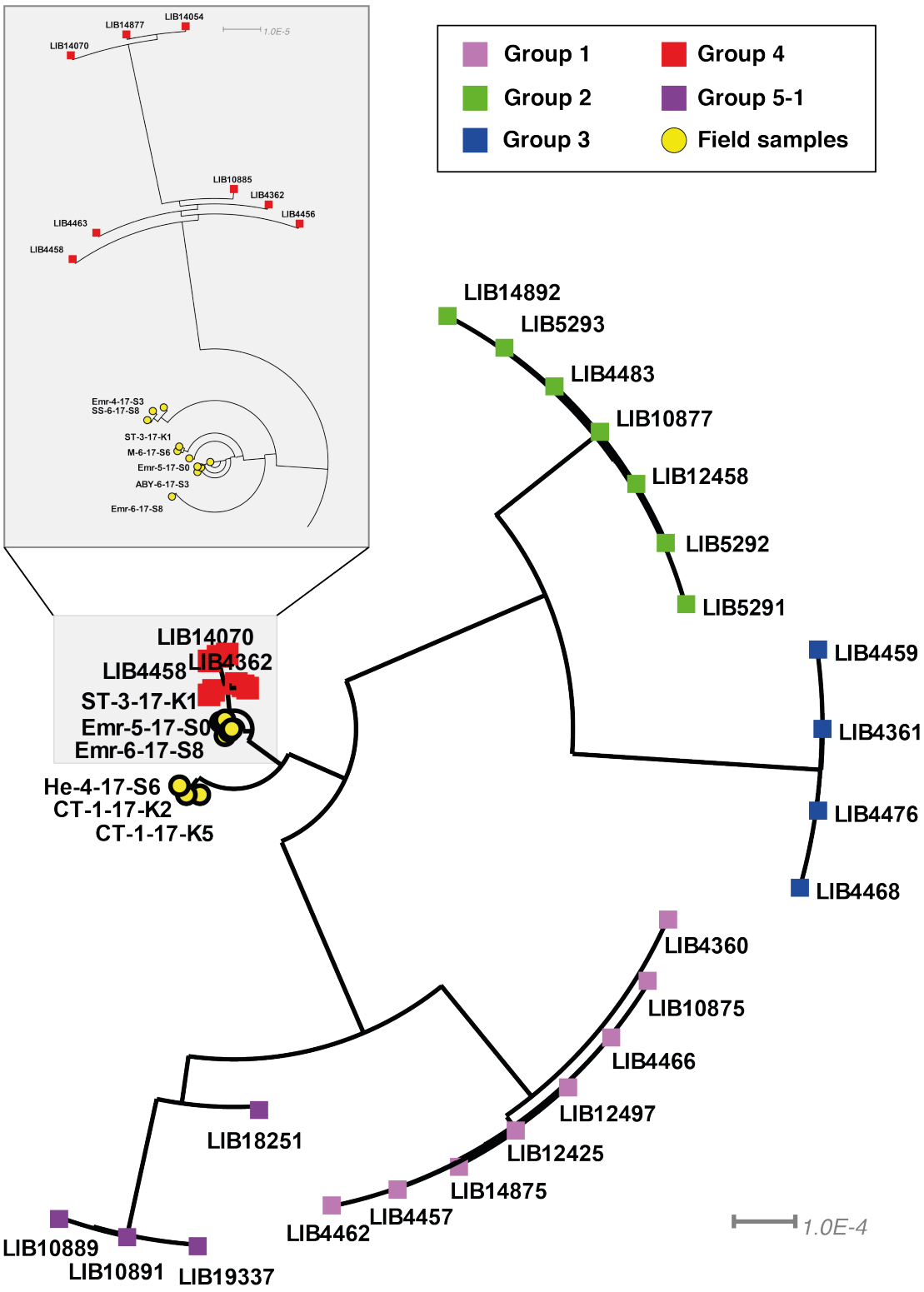

Figure 4.15. All 15 *Pst*-infected field samples clustered with representative samples from genetic group 4. A set of 3,363,961 sites (8,179 PST-130 gene sets) were used for phylogenetic analysis of 15 *Pst*-infected field samples with a set of 33 representative *Pst*-infected samples from all give genetic groups to investigate the diversity of the field samples. All *Pst*-infected field samples clustered well with representative samples from group 4.

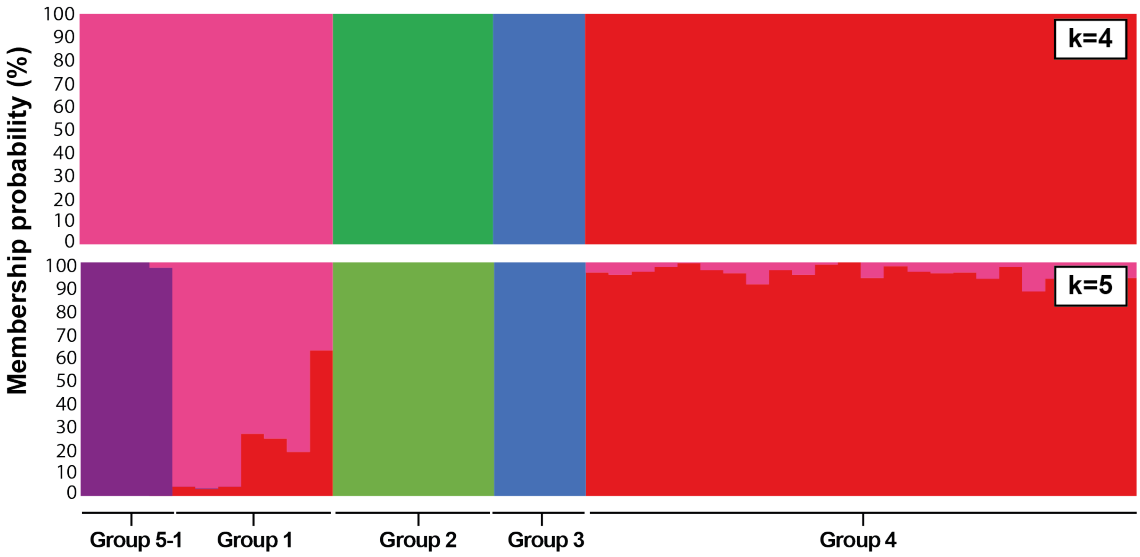

Figure 4.16. DAPC results *Pst*-infected show field samples cluster well with group 4 isolates. For k=4, group 5-1 isolates clustered with group 1, as expected. However, group 5-1 is found when k=5. In both cases, all field-collected samples were grouped with genetic group 4.

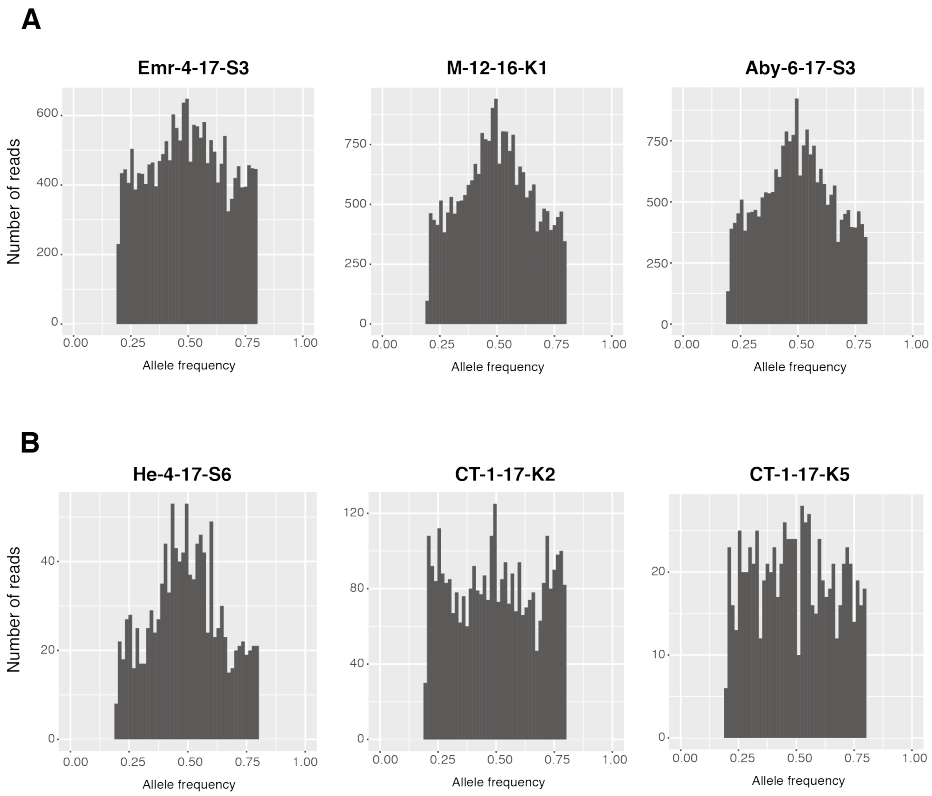

Figure 4.17. Distribution of biallelic single nucleotide polymorphism (SNP) read frequencies of *Pst*-infected field samples. (A) Read frequency at biallelic SNPs for *Pst*-infected field samples that clustered with represtative isolates from group 4 in the tree. These graphs represent that these samples consist of a single *Pst* genotype and got a high amount of reads. **(B)** Read frequency at biallelic SNPs for the three field samples that did not cluster well in the tree. Samples show to have a low amount of reads and thus their analysis is not reliable.

4.5 Discussion

4.5.1 Limitations in SNP discovery for genotyping

Single nucleotide polymorphisms are the most common way of variation in organisms and have been used for differentiating populations since the development of high-throughput sequencing technologies (Fischer, Stolze-Rybczynski, Cui, et al., 2010). For this reason, molecular markers based on SNPs have been shown to be an effective approach for evaluating diversity (Helyar et al., 2011; Mboup, Bahri, Leconte, Vallavieille-pope, & Kaltz, 2012). However, finding representative SNP markers for genotyping has certain limitations, partly linked to the challenges of SNP calling in NGS technologies, which can cause errors and missing data (Chan, 2009).

To find the set of 96 SNP markers to differentiate *Pst* populations described here, a large percentage of missing data in the samples had to be accepted in some cases (**Table 6.3**). This can be justified because of low quality samples and the expected missing data within samples, since loss of data that can occur in NGS technologies (Ferretti, Raineri, & Ramos-Onsins, 2012). The transcriptome data obtained when sequencing *Pst*-infected samples included here contained both the pathogen (*Pst*) and the host (wheat). As level of infection in the sequenced samples could vary, the percentage of pathogen reads obtained varied between 30-40% (Bueno-Sancho, Persoons, et al., 2017; Hubbard et al., 2015) which implies that the amount of data for each sample varies and missing data is expected. Besides, removing loci that include missing data has been observed to lead to biases in the results (Huang & Lacey Knowles, 2016). Therefore, accepting missing data for finding markers here is adequate considering the difficulty of the analysis.

Regarding errors within groups, a maximum of 10% of samples with different genotype to the rest of the genetic group was used. NGS technologies are known to produce sequencing errors that can bias the results (Fox & Reid-Bayliss, 2014; Kanagawa, 2003; Metzker, 2010). Therefore, I considered it important to expect a certain amount of error within the included samples. The high variability within genetic groups could also hinder the discovery of conserved sites across all samples (Hovmøller et al., 2011). A lower percentage of missing data and errors would have been required for markers if less samples had been used, but a good representation of the variability within groups was prioritised to avoid false positives. There will always be a threshold between including all variability and the difficulty of finding SNP markers and this is a limitation in the method to consider.

Many pipelines for SNP discovery have been established for multiple organisms and technologies, with different applications (Hyten et al., 2010; Rafalski, 2002; You et al., 2012). The pipeline developed here to find specific SNP markers to differentiate *Pst* genetic groups could also be easily applied to any other organism, as long as the genetic groups were previously known, or using additional *Pst* genetic groups (Hovmøller, 2019). The python script would only need a matrix of biallelic SNPs for the samples to study and a file with the information about the grouping of each sample (www.github.com/vbuens/ShortScripts/get_markers.py).

The challenges regarding SNP discovery are mainly associated to the drawbacks of NGS technologies and variation among individuals. Therefore, this entails a need for subsequently validating the SNPs to make sure they are robust enough for your purpose (Seeb et al., 2011; Shirasawa et al., 2010).

4.5.2 Genomic variations can affect virulence

Investigating genomic structural differences can help us not only understand evolution and the pathogen population, but also gain information about virulence. In particular, SNPs play an important role in virulence gain. The emergence of point mutations in avirulence proteins can give place to isolates that are able to avoid recognition by R proteins (Ellis, Lagudah, Spielmeyer, & Dodds, 2014). Due to the homogeneity in wheat varieties as a consequence of breeding for disease resistance, there is a high selection pressure on pathogens to overcome resistance genes (Schwessinger, 2016).

Pst isolates are highly heterozygous and contain a high percentage of regions with mobile elements and repeats (Cuomo et al., 2017). Transposable elements are also known to have a significant effect on virulence gain, as it is the case of the effector *AvrSr35* of *Pgt* (Li et al., 2019). Several *Pgt* isolates have been reported to have a large insertion disruption in this effector, likely due to multiple transposable elements insertions. Moreover, structural variation by asexual chromosomal recombination can also lead to gain of virulence, as for *AvrSr50* (Chen et al., 2017). Finding avirulence alleles is however very challenging precisely due to this genomic structural variation. Large deletions would just show as missing data, repetitive regions would map equally to multiple regions of the genome and high heterozygosity could cause mismapping (Pfeifer, 2017). Besides, accessory chromosomes are often not found in genome references and thus occurring SNPs are rarely detected (Pfeifer, 2017). Despite these challenges, much information can be obtained from investigating genomic variations and thus its study is of highly importance.

Here, SNP variations between *Pst* genetic groups was investigated which could open the opportunity of finding biological answers that explain the differences between these races. However, the SNPs used to differentiate between genetic groups were synonymous mutations, and thus are less likely to have a significant role in virulence. The same analysis done here could be repeated with non-synonymous mutations in the hope of finding structural differences between *Pst* genetic groups. Another interesting future line of work would be to compute differential expression analyses between the genetic groups selected here and focusing on the genes that contain more SNP differences between genetic groups. This could give us a hint on the importance of the conserved mutations within a group.

4.5.3 Amplicon resequencing and KASP are both viable for assigning genetic groups with the 96 set of markers

To assign samples to a genetic group using these 96 SNP markers, two methods were tested: Amplicon resequencing and KASP genotyping. Both technologies have been widely used for genotyping in several species, especially in crop improvement (Malik et al., 2016; Semagn et al., 2014). Amplicon resequencing and KASP were both able to successfully genotype samples, despite not being able to include all 96 markers. SNPs provide great resolution when studying diversity in populations, but a large number of them is usually needed (Singh et al., 2013). Here, genotyping of field samples was possible with just a small set of markers, which is reasonable considering the genetic groups were previously identified.

The TruSeq technique is slower in comparison to KASP, since after extracting the DNA, libraries have to be made using the standard TruSeq protocol that takes a day and then sequencing needs to be performed which takes around 48 hours (Illumina, 2015). After obtaining reads, the data has to be processed which would potentially require certain bioinformatic skills. The posterior data analysis would also take a few days which means that from collecting a sample to getting the results, a minimum of a week would be needed for 96 samples. For KASP on the other hand, after DNA extraction the analysis is direct and thus is faster than amplicon resequencing. KASP also allows the genotyping of fewer samples if necessary, whereas for TruSeq 96 samples should be analysed at the same time to make it cost-effective (Semagn et al., 2014). Regarding costs, TruSeq has a substantially higher cost than KASP (Ganal, Altmann, & Röder, 2009). Taking into account all the advantages and disadvantages of each method, KASP was chosen as the best method for genotyping a high number of samples, quickly and at a low price. Comparisons of both methods agree with these conclusions (Ertiro et al., 2015).

Many methods have been widely used for *Pst* surveillance to classify samples into the different race groups (Ali et al., 2014; Atkins & Clark, 2004). KASP genotyping offers an advance against other methods in terms of low cost and speed of processing (Semagn et al., 2014). When compared to the Field Pathogenomics approach (Hubbard et al., 2015), this method also generates less unnecessary data when the aim is to genotype. However, doing full transcriptomics of a *Pst* infected wheat sample also provides information about the host (Bueno-Sancho, Persoons, et al., 2017; Hubbard et al., 2015). Besides, both amplicon resequencing and KASP would not be able to find new genetic groups. Undertaking full transcriptomics of samples could indeed be used to identify new genetic groups, however the relatively high cost of the method makes it not very adequate for routine surveillance (Bräutigam & Gowik, 2010). A new method was recently developed that consists of sequencing a set of polymorphic genes that captures all *Pst* diversity to genotype samples using the MinIon sequencer (Radhakrishnan et al., 2019). This technique also allows the discovery of new genetic groups and permits analysis almost *in situ*. However, it is still highly expensive for regular surveillance. Therefore, the approach developed here offers an alternative for quick surveillance of *Pst*. Although it has limitations, it can be used as a way of preliminary screening many samples along with another method for those samples that cannot be genotyped with KASP. This would be a way of reducing the cost of management systems while increasing the number of samples that can be analysed.

4.5.4 Group 4 seems to be more prevalent in the UK

Managing plant diseases presents a great challenge because the resources are usually limited and determining when, where and how to invest these precious resources typically requires a high knowledge of epidemic dynamics (Cunniffe et al., 2016). However, there is still a lack of knowledge in terms of *Pst* race dynamics.

The results obtained here show how group 4 has become the most predominant group in the UK. These results are consistent with what was observed by the UKCPVS in the last few years (**Table 4.3**). Since the beginning of the field pathogenomics project (Hubbard et al., 2015), group 4 has been increasing its prevalence in the UK with a very clear tendency. The competitive exclusion principle states that when different populations occupy the same niche, if one of them is even slightly more fit or aggressive, it will end up displacing the other populations completely until they become extinct (Gause, 1936; Hardin, 1960). This can explain the increasing prevalence of the Warrior (-) race in the UK, causing the others to almost disappear. A few samples from group 3 were actually found in 2017 which were not seen in the field trials carried out here. This can also be an effect of sampling randomisation

which could lead to other genetic groups being left undetected in the field (Stephen Parnell, van den Bosch, Gottwald, & Gilligan, 2017). Sampling here was carried out randomly, collecting around 10-20 samples every month. This entails that when there were less infected plants, samples can capture well the *Pst* population in the field, but as the number of *Pst*-infected plants increases, capturing all the diversity becomes more complicated. To appreciate this concept, I estimated the probability of finding a sample that did not belong to group 4, considering different proportions of genetic groups in the field. To do so, I used the frequencies found (**Table 4.3**) to simulate conditions in the field and different quantities of samples being taken from said field. This simulation was done 1000 times to estimate the probability with more accuracy (**Figure 4.18 A**). The same process was done, simulating several proportions of genetic groups, and the probability of finding an isolate that does not belong to group 4 but is present in the field gets bellow 0.2 only when the proportion of group 4 is greater than 70 % (**Figure 4.18 B**). Thus, it can be concluded that, even if other isolates might have been in the field, the proportion of them must have been very low, otherwise they would have been found.

Table 4.3. Pathotype group frequencies from 2014-2018. Samples found from each genetic group in the UK since 2014. Group 4 is becoming more prevalent and the other groups are not as frequent as in later years. A group outside of the four main genetic groups is also found in 2017 and 2018. Table adapted from 2019 UKCPVS report (Hubbard, Wilderspin, & Holdgate, 2019).

Genetic group	Frequency of Isolates Found (%)				
	2014	2015	2016	2017	2018
1 (Warrior)	19	3	8	0	0
3	8	28	29	3	0
4 (Warrior -)	69	66	63	93	93
5-1 (Kranich)	4	3	0	0	3
Other	0	0	0	4	4

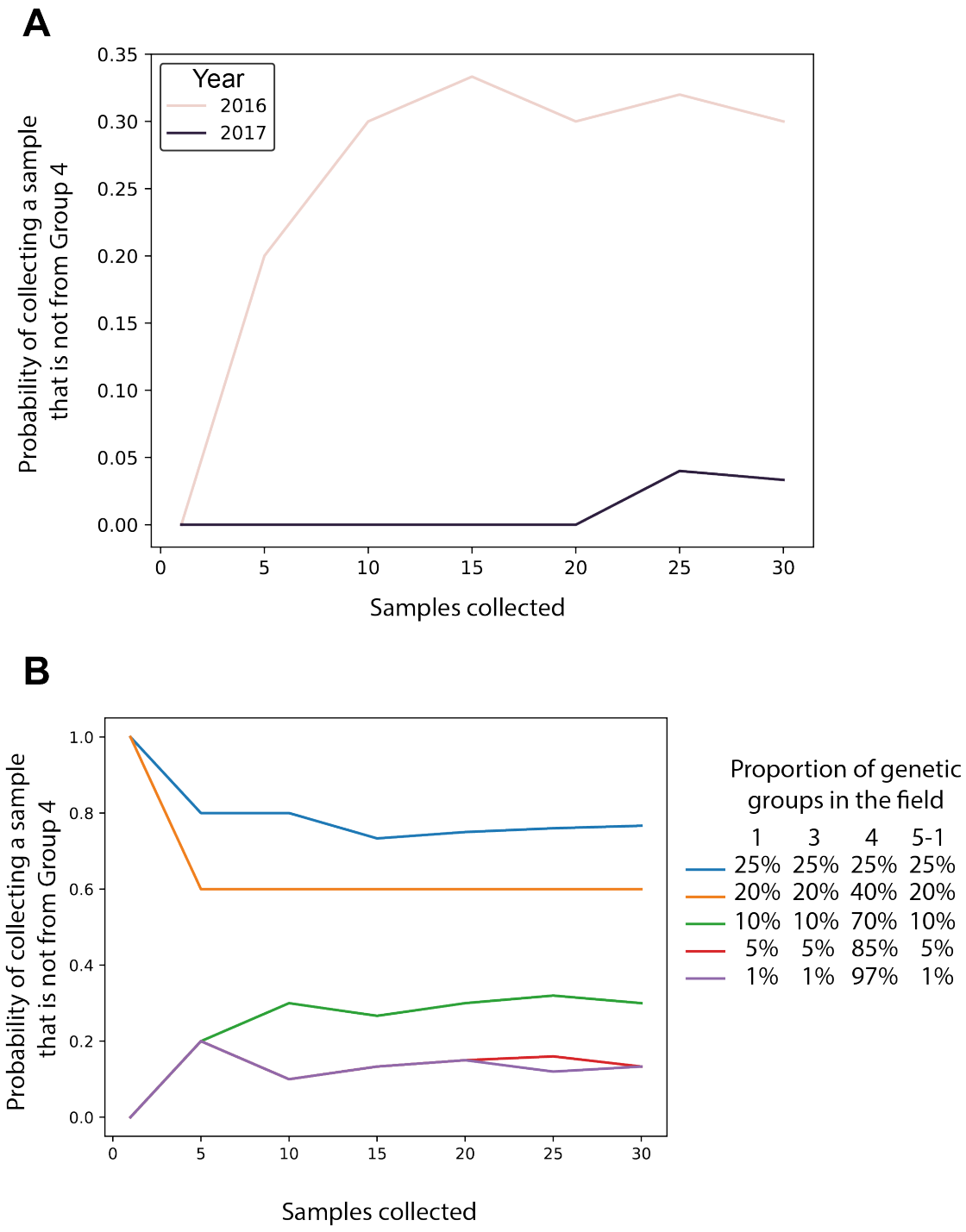

Figure 4.18. Probability of finding an isolate that was not from group 4 reduces to 0.2 when the proportion of group 4 in the field is above 70%. Probability of finding a *Pst* isolate that belongs to a group different to group 4 was investigated by considering scenarios with different proportions of groups occurring in the field. **(A)** Proportions seen by NIAB (**Table 4.3**) were used to investigate probability, and we saw that the probability increased when collecting 5 samples in 2016 and 25 in 2017. **(B)** Different proportions of *Pst* genetic groups in the field were used and it was observed that, if 10 samples were taken, probability of finding an isolate that was not from group 4 is only very low when group 4 is the most prevalent in the field (more than 70 %).

Even though the wheat varieties used here (Solstice and KWS Kielder) were previously seen to only be infected with group 4 *Pst* isolates in 2014 (Bueno-Sancho, Persoons, et al., 2017), here it is shown how other groups can infect these varieties. However, it has been observed how group 4 is more aggressive in certain varieties, including Solstice (Corredor-Moreno, unpublished). If group 4 could indeed infect these two varieties more easily, that could also explain the results obtained here. Furthermore, in 2016, group 4 was found throughout the year whereas group 1 was only found in summer. This genetic group has also been found to occur more frequently in southern Europe (Bueno-Sancho, Persoons, et al., 2017) and evidence shows how temperature adaptation can occur in certain *Pst* races (Mboup et al., 2012). Thus, it could mean that either group 4 is better adapted to lower temperatures, which could help isolates spread quickly early in the season, or group 1 is adapted to warmer climates.

Group 5-1 was found all across the year in Taunton, thus showing that this group can also occur during the entire season and not only summer months. Besides, group 5-1 has been frequently found in colder areas like Poland and Denmark, thus showing this group can be adapted to lower temperatures (Ali et al., 2014). Seasonality in pathogen populations is a well-studied phenomenon in pathogen populations (Altizer et al., 2006; Estrada-Pena, 2009) although further experiments would need to be done to determine if that is the case for these *Pst* races.

These results could also indicate that group 4 is more aggressive and it can infect more easily when the plant is healthier. When later in the season the host immune system is already compromised by one pathogen race, other races could infect more easily and thus more groups are observed towards the end of the season (Lamichhane & Venturi, 2015).

4.5.5 Races prevalence cannot be predicted based on previous data

The field trials were carried out here with the aim of answering key questions regarding *Pst* population dynamics within a field, such as how pathogen composition can affect disease spread and whether early genotypes can predict genotypes later in the season. Different races of the pathogen can influence the spread of each other, and this information is key to predict disease dynamics.

Different races can have different behaviours in the same host and therefore competition between them affects the dispersal of the disease (Hamelin et al., 2016). Multi-pathogen infections can have either antagonistic or synergistic results, meaning that they can either compete for a host, slowing down the epidemics, or cooperate in the infection by coexisting

in the same host, which could increase the speed of spread of the disease and cause susceptibility to other pathogens (Belhaj et al., 2016). Results obtained from genotyping samples collected from field trials for two years are unfortunately not very informative regarding how pathogen population dynamics affect disease spread. Previous studies have shown that pathogen population composition can affect disease spread (Bonsall, 2004). Here, there is only data from one field that contains more than one *Pst* race. Therefore, differences in disease dynamics between *Pst* races could not be well studied since only one genetic group was mostly found. In principle, no substantial differences can be noted when comparing disease level and infection between a field containing more than one race and the fields that are in principle infected with only one genetic group. However, more testing should be done to conclude this, and it is possible that other genetic groups are in the field affecting disease spread and remained undetected.

Genotypes that appear early in the season are likely to remain within the field all through the season and hence be found later in the year. However, new genotypes that had not been seen at the beginning can emerge towards the end of the season, as it has been observed in Taunton field in 2016. Consequently, it can be concluded that early *Pst* genotypes cannot predict genotypes later in the season. Besides, here we could get information about the genetic group of the collected samples, but individual information about each isolate could not be obtained. This makes it impossible to determine whether different pathogens from the same genetic group were appearing later in the season or whether it was the same isolate that spread within the field. The most likely scenario is the coexistence of several isolates from the same genetic group that stayed in the field across all season.

4.6 Conclusion

New disease outbreaks that affect crops have led to an increasing necessity of improving crop protection strategies. Economic losses are often due to a lack of surveillance programs or early warning systems. Studying how current pathogens are spreading is key to understanding their dispersal dynamics to design better informed disease management systems. Here, I developed a quick genotyping method for *Pst* samples that consist of using KASP to amplify four SNP markers to determine the race. This could be used to rapidly monitor YR disease by analysing a high number of samples in a cheap manner. The markers developed here were also given to our industrial partners that implemented them in their own laboratories for disease monitoring. At the minute, these markers are very specific to the UK *Pst* population but could be expanded to include more races. The simplicity of this method allowed me to genotype a vast number of samples quickly and at a low price in

order to study *Pst* dynamics in the UK. This investigation led us to reach the following conclusions: (i) one main genetic group was found across both years, which indicates that it could have become the predominant race in the UK, (ii) early *Pst* genotypes cannot predict genotypes appearing later in the season and (iii) temporal niche partitioning could be occurring in the UK. Further research is however necessary to confirm these conclusions since the scope of the study contained some limitations that could be influencing the observations.

Chapter 5:
General Discussion

Chapter 5 General Discussion

5.1 Investigating wheat rust pathogen transmission

Wheat rust pathogens have been threatening agriculture all throughout history (McIntosh, 2009) and today, these pathogens cause loses of more than £4 billion in the UK alone (Figueroa et al., 2018). Investigating how these pathogens are able to spread and the key aspects of the dynamics between these pathogens and their host is vital for the design of appropriate control strategies (Meentemeyer et al., 2011). Modelling of pathogen dispersal has been carried out for many pathogens in the past and has proved helpful in managing disease, such as the sudden oak death in the US (Cunniffe et al., 2016), ash dieback in the UK (National Statistics, 2015) or grapevine leafroll disease (Atallah, Gómez, Conrad, & Nyrop, 2015). When transmission and disease development is well understood, this enables much better targeted control, which can reduce the cost of management and increase its efficiency (Donatelli et al., 2017). The objective of this thesis was to improve our understanding of wheat rust pathogen transmission to apply the acquired knowledge to wheat rust management. To achieve this, I focused on three main aspects: (i) *Pgt* aeciospore release to understand the beginning of the dispersal process, (ii) dispersal of *Pgt* aeciospores in an open landscape and (iii) dynamics of *Pst* population in the UK.

5.1.1 Initial inoculum and weather are significant factors in disease epidemics

Inoculum production is the first step in the dispersal process and has been observed to play an important role in epidemics (Filho et al., 2016). A larger amount of initial inoculum causes a greater probability of secondary infection and further dispersal. In fact, an increase in disease severity has been linked to the sporulation rate, i.e. spores produced per lesion per day (Xu & Ridout, 1998). In particular for stem rust, initial inoculum levels have been observed to determine disease severity in epidemics (Dill-Macky, Rees, & Platz, 1991). The same has been observed for brown rust, where high levels of initial inoculum hastened disease progression (Rao, Snow, & Berggren, 1989). Understanding how inoculum is produced and released is thus important when studying the process of disease development and pathogen dispersal (Gregory 1968). Here, I investigated the release of *Pgt* aeciospores and the effect that different levels of inoculum can have in aeciospore dispersal.

Observations using high-speed videography confirmed that aeciospores are actively released, allowing them to surpass the boundary layer and enter the free stream that can carry them long distances (Chapter 2). Although the release speeds observed were slightly

slower than previously observed for other basidiomycetes (Norros et al., 2014), distance experiments indicate they can reach up to 7 cm, especially when clustering together (**Figure 2.12**). The clustering would affect posterior deposition, by incrementing the settling velocity of aeciospores as discussed in Chapter 3, following the equation by (Ferrandino & Aylor, 1984). However, separation of spore clusters after release has been previously observed (Pringle et al. 2017) and this could well occur for *Pgt* aeciospores. Once aeciospores are deposited further from the initial source, if conditions are right, they could start an infection on a new host. A single spore could theoretically provide an infection, although different levels of efficiency have been observed for different pathogens (Pei, Ruiz, Hunter, Arnold, & Bayon, 2002). For example, observations on *P. triticina* indicated that up to 50 % of single-spore inoculations can produce uredinia (Zadoks 1979). For *Pgt* a linear correlation between inoculum density and posterior uredinia numbers has been observed (Petersen, 1958). The amount of inoculum that can be produced in a standard barberry bush has been examined in Chapter 3 and dispersal of said inoculum was calculated using a Gaussian Plume Model (**Figure 3.8**). This model also evidenced the crucial effect that weather conditions have in the process of dispersal.

Simulation studies have shown that weather and initial disease level (i.e. initial inoculum) have the largest effect in final disease incidence (Hong & Hwang, 1998; Luo & Zeng, 1995). Both inoculum production and dispersal are highly affected by environmental conditions. Even though no significant effect was observed in the quantity of aeciospore release and how far they could reach after release under the range of temperatures tested here (5-30 ºC), temperature is known to have a direct effect in the development of aecia (Kolnaar & Van Den Bosch, 2001). At lower temperatures, aecia can reach larger dimensions which would increase the level of inoculum. A vital factor in aeciospore release is humidity. A mathematical model that only involves the need for water and subsequent rounding-off of the aeciospores was developed in this thesis (Chapter 2). This model proved to be consistent with observations and contributes to the hypothesis that water availability is the major factor in aeciospore release. This information is important for understanding aeciospore dispersal.

Investigating the environmental factors required for spores to be released gives us an indication of when release and thus dispersal and posterior infection are likely to occur. The periodicity of aeciospore release was discussed in Chapter 2, although a strong correlation with water availability was observed (Pady et al., 1969). Periodicity has however been observed to have an effect in how far spores can be dispersed (Schmale, Bergstrom, &

Shields, 2006). This is due to the effect that atmospheric conditions have on dispersal (Oneto, Golan, Mazzino, Pringle, & Seminara, 2020). Spores released at night are more likely to be deposited onto the ground whereas spores release during the day can fly for days. However, sun exposure reduces the survival rate of spores and thus many fungi tend to release at night (Rotem & Aust, 1991). Sometimes, fungi with spores more resistant to radiation predominantly release during the day to increment the distance travelled due to turbulence (Oneto et al., 2020).The link of *Pgt* aeciospore release with high RH is consistent with the need of aeciospores for moisture for germination and subsequent infection (Powell, 1974; Truxall, Travis, & Hickey, 1995). The link between periodicity on spore release and weather has been well studied for several fungi and disease patterns are associated with it (Chastagner et al., 1978; Langenberg, 1977; van Niekerk, Calitz, Halleen, & Fourie, 2010).

Wheat rusts are highly influenced by environmental conditions, not only in the process of spore release and dispersal. Temperature affects the pathogen life cycle, infection rates and the length of the latency period (Papastamati & Van Den Bosch, 2007). Germination is also highly dependent on temperature, with different rusts having different ranges of temperatures (de Vallavieille-Pope, Huber, Leconte, & Goyeau, 1995; Singh et al., 2002). Therefore, climate change could have an effect in several aspects, including (i) increasing inoculum production, (ii) reducing the effect of resistance genes, since these can be affected by temperature and crop age, (iii) shifting the geographical distribution of rusts (Chakraborty, Luck, Hollaway, Fitzgerald, & White, 2011). An increment in inoculum production can give rise to larger pathogen populations which accelerates the evolution of the pathogen and can increase the probability of pathogens overcoming host resistance and/or reducing sensitivity to fungicides. Regarding dispersal and disease incidence, climate change can also have an effect on migration routes and deposition (Prank et al., 2019). Epidemics are expected to vary as climate changes, becoming more severe for *Pst* (Lyon & Broders, 2017), and changing the infection season for *P. triticina* (Launay et al., 2020). In the case of *Pgt*, stem rust epidemics could occur in regions that were previously unsuitable as temperatures increase (Saunders et al., 2019).

5.1.2 Landscape composition affects pathogen dispersal dynamics

Investigating the dynamics of a plant disease is important to comprehend how epidemics occur and thus try to stop them. Host composition in the agriculture landscape has a significant role in epidemics, since host genetic homogeneity in the field leads to an increase

in pathogen virulence (Stukenbrock & McDonald, 2008). Thus, it is generally advised to sown both resistant and susceptible cultivars within the same field since this has been observed to reduce the risk of epidemics (Bhardwaj, Prasad, Gangwar, Khan, & Kumar, 2016). The frequencies of the host composition are reported to have an effect in the pathogen population, as it was observed for *P. triticina* which leads to a decrease in adaptation (Papaïx et al., 2011). Host mixtures are known to decrease disease incidence and their use is more effective for race-specific pathogens than for race-nonspecific pathogens (Xu & Ridout, 2000). Mixing hosts in square blocks has been reported to be more effective than in strips, which is likely due to the decrease efficacy in dispersal (Xu & Ridout, 2000).

The effect of landscape is very obvious in heteroecious pathogens, such as wheat rusts, that the presence of the alternate host can lead to higher genetic variability and thus an increment in the likelihood of epidemics (Zhao, Wang, Chen, & Kang, 2016). That is the case that was investigated here, where the risk of barberry bushes near wheat fields was evaluated in Chapter 3. The risk that barberry bushes pose to wheat production has been known for a while and removal of bushes has proved to be an effective way of reducing epidemics (Peterson, 2018). Nevertheless, there could be other ways of managing the risk while still allowing the planting of barberry bushes that form essential habitat for various species, as long as they are at a safe distance from wheat fields. Disease incidence can decrease when fragmentation in the agricultural landscape increases, i.e. when crop patches are more isolated, due to a reduction in the probability of spread (Carlsson-Granér & Thrall, 2002; Perkins & Matlack, 2002). However, fragmentation can also lead to an increment in the edge effect that can rise the probability of infection (Kelly & Meentemeyer, 2002; Rizzo & Garbelotto, 2003). In the case of *Pgt* aeciospore dispersal studied here, the location of barberry bushes in an open landscape not only can increase the probability of them getting infected, but also the posterior dispersal. Planting barberry bushes in the interior of forests could thus decrease the continuity of the pathogen dispersal chain while still allowing for a natural habitat for insects that rely on barberry as a habitat and/or food source such as the barberry carpet moth (Tischendorf & Fahrig, 2000). Investigating the landscape where barberry bushes are planted could also help decrease the probability of dispersal by including elements that act as a barrier, such as windbreaks (Marrou et al., 1979; Plantegenest et al., 2007).

Despite the array of studies on the effect that host composition has on pathogen populations and how pathogen populations vary due to competition, few studies have investigated the effect of pathogen populations in disease spread. Besides, most disease transmission

models ignore the pathogen population which can be a key factor in dispersal (Papaïx et al., 2011). This was one of the aims of this PhD thesis, but the lack of variability in the *Pst* races found meant that it could not be investigated, as discussed in Chapter 4. The pathogen population composition can affect how disease progresses, since different pathogens can have either antagonistic or synergistic effect in disease incidence (Belhaj et al., 2016). An example of this is the reduction in *P. triticina* pustule density due to endophytic fungi in wheat (Dingle & McGee, 2003). However, the effect of different races of the same pathogen remains unknown. Different races of the same pathogen are known to behave differently in the same host, due to susceptibility, aggressiveness of the race or fitness. Thus, competition between races could also affect disease progression in a field (Bonsall, 2004). More aggressive pathogen strains also tend to occur more frequently in resistant host populations (Pariaud, Robert, Goyeau, & Lannou, 2009; Thrall & Burdon, 2003). The occurrence of mainly one *Pst* race in the UK during the 2016-2017 wheat growing season is an indication that this Warrior (-) race (referred as Group 4 in Chapter 4) could have replaced others. Considering that this race was observed to infect a wider range of wheat cultivars, it is reasonable to believe that this race could be more aggressive (Bueno-Sancho, Persoons, et al., 2017).

Considering the landscape and the pathogen races composition can provide an advantage in disease management. Observations show that managing fungicide application considering dispersal between fields can be more effective than just considering 'within-field' spread (Parnell, Van Den Bosch, & Gilligan, 2006). Strains resistant and sensitive to a given fungicide can coexist in the field and their coexistence depends on their competitive relationship and not on the fungicide spray heterogeneity (Parnell, Gilligan, & Van Den Bosch, 2005). Understanding the global *Pst* population could help reduce the risk of emergence of new races in other geographical locations by isolating pathogen populations (Plantegenest et al., 2007). Population genetics could also be integrated with landscape ecology to facilitate the understanding of gene flow, genetic drift and selection (Manel, Schwartz, Luikart, & Taberlet, 2003). Had I found more than one *Pst* race in the field trials carried out in Chapter 4, investigating the effect of landscape composition in *Pst* race dynamics would have been interesting.

5.2 Tools to manage diseases

5.2.1 Surveillance systems can help manage wheat rusts

Wheat diseases have been traditionally managed by the use of R genes that give resistance to pathogens and fungicide application to avoid infection (Chaves et al., 2013). However, fungal pathogens are known to be able to overcome host resistance and to develop resistance to fungicide treatments (Ayliffe et al., 2008). In the case of wheat rusts, this was observed when the virulent Ug99 race overcame resistance of the wheat varieties being grown and caused severe stem rust epidemics in many parts of the world (Bhavani, Hodson, Huerta-Espino, Randhawa, & Singh, 2019). Mutations in genes targeted by fungicides have also been recently found in *Pst* that could lead to a decrease in fungicide sensitivity (Tian et al., 2019) (Cook et al., unpublished). Thus, even if resistant cultivars are sown in the field, active monitoring is important to detect diseases early on.

One of the main questions in surveillance programs is how to optimise sampling resources and detect unanticipated pathogens (Cunniffe, Koskella, et al., 2015). Investigating sampling strategies is key towards an optimised monitoring system that ensures all the variability in pathogen virulence is detected. For example, regular or 'equal-stratified' sampling strategies are reported to be more robust than random sampling, and including data about disease dispersal and environmental information can improve accuracy (Hirzel & Guisan, 2002). Sampling fewer fields but collecting more samples per field, instead of more fields but few samples, has also been observed to help capture the full representation of pathogen diversity in disease fields (Jochua, Amane, Steadman, Xue, & Eskridge, 2008). Simulations have also shown how spreading sampling resources evenly in time can optimise the early detection of disease (Parnell, Gottwald, Gilks, & van den Bosch, 2012). Using spatially-explicit models that explain disease dispersal can be of great help when optimising surveillance programs (Parnell, Gottwald, Irey, Luo, & Van Den Bosch, 2011).

Advances in molecular techniques have helped improve diagnosis and study of fungal pathogens unsuitable for culture (Martin, James, & Levesque, 2000). From traditional pathology or genetic markers up to more sophisticated sequencing such as Field Pathogenomics, all these methodologies have provided a useful insight into the wheat rust pathogens, as discussed in Chapter 4. Within this thesis, I developed a quick system that could help monitoring large volumes of *Pst* samples in an inexpensive manner (Chapter 4). This could improve the capacity for sampling while still keeping the costs low. Sampling to monitor races has allowed the identification of the origin and evolution of *Pst* races (Ali et al., 2014). The distribution of *Pst* races has been changing quickly over the past decade and

new races are being found (Hovmøller, 2019). Despite the diversity in races found globally, in the UK there seems to be a predominant race (Hubbard et al., 2019). This was also observed in the present study (Chapter 4) where mainly one *Pst* race was found all over the UK across two wheat-growing seasons. As discussed in Chapter 4, this is likely a consequence of the exclusion principle where a race can displace others due to competition (Hardin, 1960).

Surveillance is usually carried out at a local or national scale, which limits the information about the worldwide pathogen population. Sharing the data globally in a coordinated manner is key to track pathogens at the global level and avoid the emergence of epidemics (Islam et al., 2016). Investigating wind dispersal patterns can also help predict where new races could be travelling and going next (Meyer et al., 2017). Besides information about races, about host resistance and disease severity can be useful. Standard procedures about how to sample, score and track these pathogens have been developed by the BGRI community (Ali & Hodson, 2017). Currently, there are monitoring systems in place that investigate the evolution of both *Pst* and *Pgt* races globally (Hodson, 2011). The development of these platforms occurred as a consequence of the creation of BGRI, which emerged as a way of allowing collaboration among rust scientists worldwide (McIntosh & Pretorius, 2011). The Global Cereal Rust Monitoring System (GCRMS) has allowed information to be collected globally for the wheat stem rust pathogen (Hodson, Cressman, Nazari, Park, & Yahyaoui, 2009). This platform contains information about rust diseases, survey routines, visualisation tools, such as RustMapper and a pathogen tracker (Park et al., 2011). This was created when the Ug99 race appeared to be able to track the dispersal of this race across the world and improve monitoring (Hodson et al., 2012). Several websites were developed, including rust surveillance data in RustTracker.org via which the Wheat Rust Toolbox, that includes maps and data visualisation (Hansen & Lassen, 2013). Host information is still limited, although some advances have been made towards including more data (Hodson et al., 2012). For example, surveys of Barberry bushes are currently being carried out as part of the Wheat Rust ToolBox, to develop a diagnosis system for *Puccinia* spp. from aecial samples (Hansen & Lassen, 2013). A disease monitoring system was also developed in Ethiopia to control the development of *Pst*. The Ethiopian Early Warning System integrates field surveillance data, spore dispersal modelling and weather data to forecast disease and inform wheat rust advisories and policymakers (Allen-Sader et al., 2019).

Information about pathogen races collected from surveillance programmes can be included in models about disease forecasting or pathogen dispersal to have a full picture of the state of the disease globally. These models, if made available in the form of platforms, can be used to inform farmers and advisors worldwide. The existence of a community that shares information about the races found in different locations can accelerate the response to new threats in other parts of the world.

5.2.2 Developing tools and using new technologies for wheat rust management

Developing new technologies and strategies that can help improve management is a key step in the process of protecting agriculture from devastating crop diseases. More and more, websites are being developed to include models that can help farmers make decisions. For example, a website was developed to allow users to utilise the Strawberry Advisory System to get predictions of disease incidence (Pavan, Fraisse, & Peres, 2011). This AgroClimate website helped reduce unnecessary fungicide usage by providing recommendations of application based on predictions (www.agroclimate.org). Similar web-based diagnosis systems have been developed for oilseed-crops oilseed-crops (Kolhe, Kamal, Saini, & Gupta, 2011) and for banana plant diseases (Budiyanto et al., 2018). These user-friendly interfaces have also helped stakeholders optimise control of invasive plant diseases using culling strategies (Cunniffe, Stutt, et al., 2015). Forecasting models based on weather have also been made available through website development (Kang et al., 2010). These can help farmers decide when to spray fungicides by creating risk maps. Similar tools have been developed for potato late blight, using RH and temperature data to predict the risk and make recommendations on fungicide application (Wharton, Kirk, Baker, & Duynslager, 2008) and also for wheat yellow rust, with risks maps that use WebGIS technologies (Kuang, Liu, Ma, & Wang, 2013). A similar framework to help farmers was developed for *P. triticina* called Injury Profile SIMulation (IPSIM). This platform predicts disease risk based on weather, soil information and cropping systems (Robin et al., 2018). The improvement on the accessibility of weather forecasts thanks to the use of APIs has led to the emergence of several web-based tools that can provide disease predictions in real time for the user (Fernandes, Del Ponte, Pavan, & Cunha, 2007). Here, I developed a user-friendly interface to run the *Pgt* aeciospore dispersal model to evaluate the risk that barberry bushes pose near wheat fields (Chapter 3, **Figure 3.10**). This website allows users to input the location of a barberry bush and gather real-time weather data to predict the risk of aeciospores being carried long distances by the wind. To my knowledge, this is the first time that an open source and user-friendly website has been developed for *Pgt* aeciospores. Ideally,

citizens could also use this website to run the model and thus record the position of barberry bushes, which would allow us to map the occurrence of these bushes in the UK. However, public engagement in citizen science projects is challenging (Newman et al., 2010) and hence the website developed here provides an interface very easy to use that does not require much input from the user.

Disease diagnosis has also moved forward thanks to the development of new technologies, with web-based systems being developed for diagnosing, such as *Dr. wheat* for wheat pests in Pakistan (Khan et al., 2008). Many of these diagnosis systems rely on Artificial Intelligence methodologies for image recognition (Selvaraj et al., 2019). Indeed, the use of machine learning (ML) algorithms for detecting diseases is not new and it has provided a great tool for quick phenotyping (Singh, Ganapathysubramanian, Singh, & Sarkar, 2016; Wang, Sun, & Wang, 2017). These technologies have also been used for estimating infection levels in leaves for several crops (Bueno-Sancho et al., 2019; Sethy, Negi, Barpanda, Behera, & Rath, 2018). Thanks to the use of Unmanned Aerial Vehicles (UAV), the use of these technologies has been escalated to the field level (Duarte-Carvajalino et al., 2018). UAV imaging has been applied to yellow rust detection to assist disease monitoring using high resolution multispectral and hyperspectral imagery (Su et al., 2018; Zhang et al., 2019). For brown rust, disease severity levels at different canopy scales have been estimated using both ML and spectral data (Azadbakht, Ashourloo, Aghighi, Radiom, & Alimohammadi, 2019). Using spectral data to identify patches of infected crops can thus be applied to targeted control to reduce fungicide application (West et al., 2003). Hyperspectral data also allows for detection of wheat diseases remotely with high accuracy (Mewes, Franke, & Menz, 2011). These technologies create a great advantage when identifying diseases or measuring infection levels since they allow for high accuracy at a much quicker speed than the human eye ever could, without bias (Bock, Poole, Parker, & Gottwald, 2010).

To tackle plant diseases, and in particular wheat rusts, first, basic knowledge about the disease is needed. This includes the environmental conditions conductive for the disease, host-pathogen dynamics and how disease spreads. Once information about the disease has been obtained, effective tools can be developed to predict and stop epidemics. With computer power doubling every year over the past two decades, computational capacity allows for much better systems that can and should be used to manage plant diseases. Much knowledge about wheat rusts has been acquired over the years that is now being applied to manage diseases worldwide. Recent advances in technologies can help improve rust management at all levels. Firstly, regular disease diagnosis checks using UAV technologies

with image recognition can be used for quick surveillance (Bohnenkamp, Behmann, & Mahlein, 2019). Secondly, sampling effectively when disease is found, making use of models for best sampling strategies, and genotyping to identify pathogens in a cost-effective manner. Thirdly, this information can be integrated into a global platform that contains already developed models while gathering real-time weather data. This system could then give recommendations about what to do in the field in terms of fungicide application or even removal of certain plants/patches in the field to decrease pathogen inoculum. Recent model-based frameworks have already been developed that integrate satellite imagery with airborne inoculum information and weather data to control crop diseases (Newlands, 2018). Moreover, platforms could make use of GIS technologies that include information about landscape composition incorporating surveillance data to create risks maps. Better management of crop diseases is needed and the technology to achieve this is already out there. Creating survey protocols that integrate all different aspects and developing platforms to share the data would highly improve plant disease management and it only requires global collaboration to reach such an apparent utopia.

5.3 Concluding statement

After the emergence of the virulent stem rust Ug99 strain in Uganda, Norman Borlaug declared his famous quote: "*Rust never sleeps*" (Borlaug, 2008). Thus, as (rust) scientists, neither should we [1]. Plant diseases are frequently disregarded when they are not a significant problem, but a potential threat should not be ignored until it is too late. Mathematical modelling can help us increase our knowledge about plant diseases and prevent epidemics before they occur. Investigating plant diseases at different levels and integrating them into open-source platforms that can help inform stakeholders and make better decisions is key in the path towards global food security. It has reached a point where the lack of scientific collaboration and data sharing is restraining progress. Current technology advances are giving us the opportunity for global collaboration and I believe it is our duty as scientists to develop systems that integrate worldwide multi-level data for better management. This thesis is one step further towards trying to prevent future epidemics by improving our understanding of wheat rusts and providing useful and inexpensive tools for rust management.

[1] Figurately speaking. Lack of sleep has shown to reduce productivity and is thus not recommended (Rosekind et al., 2010).

References

Abbasi, M., Goodwin, S. B., & Scholler, M. (2005). Taxonomy, phylogeny, and distribution of Puccinia graminis, the black stem rust: New insights based on rDNA sequence data. *Mycoscience*. https://doi.org/10.1007/s10267-005-0244-x

Adams, T. M., Neher, R. A., & Saunders, D. G. O. (2020). Tracking wheat yellow rust: near real-time data sharing with Nextstrain. https://doi.org/10.5281/ZENODO.3758079

Ahmed, M., Anjum, M. A., Naz, R. M. M., Khan, M. R., & Hussain, S. (2013). Characterization of indigenous barberry germplasm in Pakistan: Variability in morphological characteristics and nutritional composition. *Fruits*. https://doi.org/10.1051/fruits/2013085

Alexander, D. E. (2017). Fluid Biomechanics. In *Nature's Machines*. https://doi.org/10.1016/b978-0-12-804404-9.00003-7

Ali, S., Gladieux, P., Leconte, M., Gautier, A., Justesen, A. F., Hovmøller, M. S., … de Vallavieille-Pope, C. (2014). Origin, Migration Routes and Worldwide Population Genetic Structure of the Wheat Yellow Rust Pathogen Puccinia striiformis f.sp. tritici. *PLoS Pathogens*, *10*(1). https://doi.org/10.1371/journal.ppat.1003903

Ali, S., & Hodson, D. (2017). Wheat rust surveillance: Field disease scoring and sample collection for phenotyping and molecular genotyping. In *Methods in Molecular Biology*. https://doi.org/10.1007/978-1-4939-7249-4_1

Allen-Sader, C., Thurston, W., Meyer, M., Nure, E., Bacha, N., Alemayehu, Y., … Gilligan, C. A. (2019). An early warning system to predict and mitigate wheat rust diseases in Ethiopia. *Environmental Research Letters*. https://doi.org/10.1088/1748-9326/ab4034

Altizer, S., Dobson, A., Hosseini, P., Hudson, P., Pascual, M., & Rohani, P. (2006). Seasonality and the dynamics of infectious diseases. *Ecology Letters*. https://doi.org/10.1111/j.1461-0248.2005.00879.x

Andrade, D., Pan, Z., Dannevik, W., & Zidek, J. (2009). Modeling soybean rust spore escape from infected canopies: Model description and preliminary results. *Journal of Applied Meteorology and Climatology*. https://doi.org/10.1175/2008JAMC1917.1

Andrews, S. (2010). FastQC - A quality control tool for high throughput sequence data. *Babraham Bioinformatics*. https://doi.org/10.1016/0038-0717(73)90093-X

Anikster, Y. (1984). The formae speciales. *The Cereal Rusts*, *1*, 115–130.

Aoun, M., Kolmer, J. A., Breiland, M., Richards, J., Brueggeman, R. S., Szabo, L. J., & Acevedo, M. (2020). Genotyping-by-sequencing for the study of genetic diversity in puccinia triticina. *Plant Disease*. https://doi.org/10.1094/PDIS-09-19-1890-RE

Arya, A., & Perelló, A. E. (2010). Management of Fungal Plant Pathogens. In A. Arya & A. E. Perelló (Eds.) (pp. 364–366). Preston, UK: MPG Books Group.

Atallah, S. S., Gómez, M. I., Conrad, J. M., & Nyrop, J. P. (2015). A plant-level, spatial,

bioeconomic model of plant disease diffusion and control: Grapevine leafroll disease. *American Journal of Agricultural Economics*. https://doi.org/10.1093/ajae/aau032

Atkins, S. D., & Clark, I. M. (2004). Fungal molecular diagnostics: A mini review. *Journal of Applied Genetics*.

Ayliffe, M., Singh, R., & Lagudah, E. (2008). Durable resistance to wheat stem rust needed. *Current Opinion in Plant Biology*. https://doi.org/10.1016/j.pbi.2008.02.001

Aylor, D. E. (1999). Biophysical scaling and the passive dispersal of fungus spores: Relationship to integrated pest management strategies. *Agricultural and Forest Meteorology*. https://doi.org/10.1016/S0168-1923(99)00072-6

Aylor, D. E. (2003). Spread of plant disease on a continental scale: Role of aerial dispersal of pathogens. *Ecology*. https://doi.org/10.1890/01-0619

Aylor, D. E., & Flesch, T. K. (2001). Estimating spore release rates using a lagrangian stochastic simulation model. *Journal of Applied Meteorology*.

Azadbakht, M., Ashourloo, D., Aghighi, H., Radiom, S., & Alimohammadi, A. (2019). Wheat leaf rust detection at canopy scale under different LAI levels using machine learning techniques. *Computers and Electronics in Agriculture*. https://doi.org/10.1016/j.compag.2018.11.016

Barnes, G., Saunders, D. G. O., & Williamson, T. (2020). Banishing barberry: The history of Berberis vulgaris prevalence and wheat stem rust incidence across Britain. *Plant Pathology*. https://doi.org/10.1111/ppa.13231

Bebber, Daniel P. (2019). Climate change effects on Black Sigatoka disease of banana. *Philosophical Transactions of the Royal Society B: Biological Sciences*. https://doi.org/10.1098/rstb.2018.0269

Bebber, Daniel P., & Gurr, S. J. (2015). Crop-destroying fungal and oomycete pathogens challenge food security. *Fungal Genetics and Biology*. https://doi.org/10.1016/j.fgb.2014.10.012

Bebber, Daniel Patrick. (2015). Range-Expanding Pests and Pathogens in a Warming World. *Annual Review of Phytopathology*. https://doi.org/10.1146/annurev-phyto-080614-120207

Beddow, J. M., Pardey, P. G., Chai, Y., Hurley, T. M., Kriticos, D. J., Braun, H.-J., … Yonow, T. (2015). Research investment implications of shifts in the global geography of wheat stripe rust. *Nature Plants*, *1*, 15132. Retrieved from https://doi.org/10.1038/nplants.2015.132

Belhaj, K., Cano, L. M., Prince, D. C., Kemen, A., Yoshida, K., Dagdas, Y. F., … Schornack, S. (2016). Arabidopsis late blight: Infection of a nonhost plant by Albugo laibachii enables full colonization by Phytophthora infestans. *Cellular Microbiology*, *19*(July 2016). https://doi.org/10.1111/cmi.12628

Berlin, A. (2017). *Stem rust attacks in Sweden heralds the return of a previously vanquished foe*.

Berlin, A., Djurle, A., Samils, B., & Yuen, J. (2012). Genetic Variation in Puccinia graminis Collected from Oats, Rye, and Barberry . *Phytopathology*. https://doi.org/10.1094/phyto-03-12-0041-r

Berlin, A., Samils, B., & Andersson, B. (2017). Multiple genotypes within aecial clusters in Puccinia graminis and Puccinia coronata: improved understanding of the biology of cereal rust fungi. *Fungal Biology and Biotechnology*.

https://doi.org/10.1186/s40694-017-0032-3
Bernardo, A., St. Amand, P., Le, H. Q., Su, Z., & Bai, G. (2020). Multiplex restriction amplicon sequencing: a novel next-generation sequencing-based marker platform for high-throughput genotyping. *Plant Biotechnology Journal*. https://doi.org/10.1111/pbi.13192
Berner, D. K., Smallwood, E. L., Vanrenterghem, M., Cavin, C. A., Michael, J. L., Shelley, B. A., … Mukhina, Z. (2015). Some dynamics of spread and infection by aeciospores of Puccinia punctiformis, a biological control pathogen of Cirsium arvense. *Biological Control*. https://doi.org/10.1016/j.biocontrol.2015.05.001
Bhardwaj, S. C., Prasad, P., Gangwar, O. P., Khan, H., & Kumar, S. (2016). Wheat rust research-then and now. *Indian J. Agric. Sci*, *86*(10), 1231–1244.
Bhavani, S., Hodson, D. P., Huerta-Espino, J., Randhawa, M. S., & Singh, R. P. (2019). Progress in breeding for resistance to Ug99 and other races of the stem rust fungus in CIMMYT wheat germplasm. *Frontiers of Agricultural Science and Engineering*.
Bock, C. H., Poole, G. H., Parker, P. E., & Gottwald, T. R. (2010). Plant disease severity estimated visually, by digital photography and image analysis, and by hyperspectral imaging. *Critical Reviews in Plant Sciences*. https://doi.org/10.1080/07352681003617285
Bohnenkamp, D., Behmann, J., & Mahlein, A. K. (2019). In-field detection of Yellow Rust in Wheat on the Ground Canopy and UAV Scale. *Remote Sensing*. https://doi.org/10.3390/rs11212495
Bolger, A. M., Lohse, M., & Usadel, B. (2014). Trimmomatic: A flexible trimmer for Illumina sequence data. *Bioinformatics*. https://doi.org/10.1093/bioinformatics/btu170
Bonsall, M. B. (2004). The impact of diseases and pathogens on insect population dynamics. In *Physiological Entomology*. https://doi.org/10.1111/j.0307-6962.2004.00389.x
Borlaug, N. E. (2008). Stem rust never sleeps. *The New York Times*.
Boshoff, W. H. P., Pretorius, Z. A., & van Niekerk, B. D. (2002). Establishment, Distribution and Pathogenecity of Puccinia striiformis f . sp . tritici in South Africa, (May), 485–492.
Bourgeois, G., Plouffe, D., Chouinard, G., Beaudry, N., Choquette, D., Carisse, O., & DeEll, J. (2008). THE APPLE CIPRA NETWORK IN CANADA: USING REAL-TIME WEATHER INFORMATION TO FORECAST APPLE PHENOLOGY, INSECTS, DISEASES AND PHYSIOLOGICAL DISORDERS. *Acta Horticulturae*. https://doi.org/10.17660/actahortic.2008.803.2
Bräutigam, A., & Gowik, U. (2010). What can next generation sequencing do for you? Next generation sequencing as a valuable tool in plant research. *Plant Biology*. https://doi.org/10.1111/j.1438-8677.2010.00373.x
Breckling, B. (2002). Individual-based modelling: potentials and limitations. *TheScientificWorldJournal*. https://doi.org/10.1100/tsw.2002.179
Bréda, N. J. J. (2003). Ground-based measurements of leaf area index: A review of methods, instruments and current controversies. *Journal of Experimental Botany*. https://doi.org/10.1093/jxb/erg263
Brook, P. J. (1969). Effects of Light, Temperature, and Moisture on Release of Ascospores by Venturia Inaequalis (Cke.) Wint. *New Zealand Journal of*

Agricultural Research. https://doi.org/10.1080/00288233.1969.10427090
Budiyanto, G., Ipnuwati, S., Al Gifari, S. A., Huda, M., Jalal, B., Latif, A. A., … Hananto, A. L. (2018). Web based expert system for diagnosing disease pest on banana plant. *International Journal of Engineering and Technology(UAE)*.
Bueno-Sancho, V., Bunting, D. C. E., Yanes, L. J., Yoshida, K., & Saunders, D. G. O. (2017). Field Pathogenomics: An Advanced Tool for Wheat Rust Surveillance BT - Wheat Rust Diseases: Methods and Protocols. In S. Periyannan (Ed.) (pp. 13–28). New York, NY: Springer New York. https://doi.org/10.1007/978-1-4939-7249-4_2
Bueno-Sancho, V., Corredor-Moreno, P., Kangara, N., & Saunders, D. G. O. (2019). K-PIE: using K-means algorithm for Percentage Infection symptoms Estimation. https://doi.org/10.5281/ZENODO.3584148
Bueno-Sancho, V., Lewis, C. M., & Saunders, D. G. O. (2020). Advances in understanding the biology and epidemiology of rust diseases of cereals. In *Achieving durable disease resistance in cereals*.
Bueno-Sancho, V., Persoons, A., Hubbard, A., Cabrera-Quio, L. E., Lewis, C. M., Corredor-Moreno, P., … Saunders, D. G. O. (2017). Pathogenomic Analysis of Wheat Yellow Rust Lineages Detects Seasonal Variation and Host Specificity. *Genome Biology and Evolution*. https://doi.org/10.1093/gbe/evx241
Buller, A. H. R. (1909). *Researches on Fungi ...* (Vol. 1). London, New York [etc.]: Longmans, Green and co.,. Retrieved from https://www.biodiversitylibrary.org/item/34820
Buller, A. H. R. (1950). *Researches on fungi, Vol. VII: the sexual process in the Uredinales*. University of Toronto Press.
Buller, A. H. R. (1958). *Researches on Fungi ...* (Vol. 3). London, New York [etc.]: Longmans, Green and co.,. Retrieved from https://www.biodiversitylibrary.org/item/26509
Burk, W. R., Flegler, S. L., & Hess, W. M. (1982). Ultrastructural Studies of Clathraceae and Phallaceae (Gasteromycetes) Spores. *Mycologia*. https://doi.org/10.2307/3792646
Caffi, T., & Rossi, V. (2018). Fungicide models are key components of multiple modelling approaches for decision-making in crop protection. *Phytopathologia Mediterranea*. https://doi.org/10.14601/Phytopathol_Mediterr-22471
Cantu, D., Govindarajulu, M., Kozik, A., Wang, M., Chen, X., Kojima, K. K., … Dubcovsky, J. (2011). Next generation sequencing provides rapid access to the genome of Puccinia striiformis f. sp. tritici, the causal agent of wheat stripe rust. *PLoS ONE*. https://doi.org/10.1371/journal.pone.0024230
Carlsson-Granér, U., & Thrall, P. H. (2002). The spatial distribution of plant populations, disease dynamics and evolution of resistance. *Oikos*. https://doi.org/10.1034/j.1600-0706.2002.970110.x
Carter, M. (1963). Mycosphaerella Pinodes II. The Phenology of Ascospore Release. *Australian Journal of Biological Sciences*. https://doi.org/10.1071/bi9630800
Chakraborty, S., Luck, J., Hollaway, G., Fitzgerald, G., & White, N. (2011). Rust-proofing wheat for a changing climate. *Euphytica*. https://doi.org/10.1007/s10681-010-0324-7
Chamecki, M., Dufault, N. S., & Isard, S. A. (2012). Atmospheric dispersion of wheat rust spores: A new theoretical framework to interpret field data and estimate

downwind dispersion. *Journal of Applied Meteorology and Climatology*. https://doi.org/10.1175/JAMC-D-11-0172.1

Chan, E. Y. (2009). Next-Generation Sequencing Methods: Impact of Sequencing Accuracy on SNP Discovery. In A. A. Komar (Ed.), *Single Nucleotide Polymorphisms: Methods and Protocols* (pp. 95–111). Totowa, NJ: Humana Press. https://doi.org/10.1007/978-1-60327-411-1_5

Chang, K. F., Blenis, P. V., & Hiratsuka, Y. (1989). Mechanism and pattern of spore release by Endocronartium harknessii. *Canadian Journal of Botany*. https://doi.org/10.1139/b89-015

Chastagner, G. A., Ogawa, J. M., & Manji, B. T. (1978). Dispersal of Conidia of Botrytis cinerea in Tomato Fields. *Phytopathology*, *68*, 1172–1176. Retrieved from https://www.apsnet.org/publications/phytopathology/backissues/Documents/1978Articles/Phyto68n08_1172.PDF

Chaudhary, S., Bhise, M., Banerjee, A., Goyal, A., & Moradiya, C. (2015). Agro advisory system for cotton crop. In *2015 7th International Conference on Communication Systems and Networks, COMSNETS 2015 - Proceedings*. https://doi.org/10.1109/COMSNETS.2015.7098701

Chaves, M. S., Martinelli, J. A., Wesp-Guterres, C., Graichen, F. A. S., Brammer, S. P., Scagliusi, S. M., … Chaves, A. L. S. (2013). The importance for food security of maintaining rust resistance in wheat. *Food Security*. https://doi.org/10.1007/s12571-013-0248-x

Chen, J., Upadhyaya, N. M., Ortiz, D., Sperschneider, J., Li, F., Bouton, C., … Dodds, P. N. (2017). Loss of AvrSr50 by somatic exchange in stem rust leads to virulence for Sr50 resistance in wheat. *Science*. https://doi.org/10.1126/science.aao4810

Chen, W., Wellings, C., Chen, X., Kang, Z., & Liu, T. (2014). Wheat stripe (yellow) rust caused by Puccinia striiformis f. sp. tritici. *Molecular Plant Pathology*, *15*(5), 433–446. https://doi.org/10.1111/mpp.12116

Chen, X. M. (2005). Epidemiology and control of stripe rust [Puccinia striiformis f . sp . tritici] on wheat. *Canadian Journal of Botany*, *27*, 314–337. https://doi.org/10.1071/ar07045

Chen, X., More, M., Milus, E. a., Long, D. L., Line, R. F., Marshall, D., & Jackson, L. (2002). Wheat Stripe Rust Epidemics and Races of Puccinia striiformis f . sp . tritici in the United States in 2000. *The American Phytapathological Society*, 28–30. https://doi.org/10.1094/PDIS.2002.86.1.39

Clark, J. S., Lewis, M., McLachlan, J. S., & HilleRisLambers, J. (2003). Estimating Population Spread : What Can We Forecast and How Well ? *Ecology*, *84*(8), 1979–1988.

Coons, G. H. (1910). Researches on Fungi. *Science*. https://doi.org/10.1126/science.32.814.179

Cooper, M., Podlich, D. W., Micallef, K. P., Smith, O. S., Jensen, N. M., Chapman, S. C., & Kruger, N. L. (2009). Complexity, quantitative traits and plant breeding: a role for simulation modelling in the genetic improvement of crops. In *Quantitative genetics, genomics and plant breeding*. https://doi.org/10.1079/9780851996011.0143

Cotter, R. U. (1932). *Factors Affecting the Development of the Aerial Stage of Puccinia Graminis*. U.S. Department of Agriculture. Retrieved from

https://books.google.co.uk/books?id=2JBHAQAAMAAJ
Cunniffe, N. J., Cobb, R. C., Meentemeyer, R. K., Rizzo, D. M., & Gilligan, C. A. (2016). Modeling when, where, and how to manage a forest epidemic, motivated by sudden oak death in California. *Proceedings of the National Academy of Sciences*, *113*(20), 201602153. https://doi.org/10.1073/pnas.1602153113
Cunniffe, N. J., Koskella, B., E. Metcalf, C. J., Parnell, S., Gottwald, T. R., & Gilligan, C. A. (2015). Thirteen challenges in modelling plant diseases. *Epidemics*, *10*, 6–10. https://doi.org/10.1016/j.epidem.2014.06.002
Cunniffe, N. J., Stutt, R. O. J. H., DeSimone, R. E., Gottwald, T. R., & Gilligan, C. A. (2015). Optimising and Communicating Options for the Control of Invasive Plant Disease When There Is Epidemiological Uncertainty. *PLoS Computational Biology*, *11*(4), 1–24. https://doi.org/10.1371/journal.pcbi.1004211
Cuomo, C. A., Bakkeren, G., Khalil, H. B., Panwar, V., Joly, D., Linning, R., … Fellers, J. P. (2017). Comparative analysis highlights variable genome content of wheat rusts and divergence of the mating loci. *G3: Genes, Genomes, Genetics*. https://doi.org/10.1534/g3.116.032797
Dammer, K. H., Wollny, J., & Giebel, A. (2008). Estimation of the Leaf Area Index in cereal crops for variable rate fungicide spraying. *European Journal of Agronomy*. https://doi.org/10.1016/j.eja.2007.11.001
De Jong, M. D., Bourdôt, G. W., Powell, J., & Goudriaan, J. (2002). A model of the escape of Sclerotinia sclerotiorum ascospores from pasture. *Ecological Modelling*. https://doi.org/10.1016/S0304-3800(01)00462-8
de Jong, M. D., Scheepens, P. C., & Zadoks, J. C. (1990). Risk analysis applied to biological control of a forest weed, using the gaussian plume model. *Grana*, *29*(2), 139–145. https://doi.org/10.1080/00173139009427744
de Vallavieille-Pope, C., Huber, L., Leconte, M., & Goyeau, H. (1995). Comparative effects of temperature and interrupted wet periods on germination, penetration, and infection of Puccinia recondita f. sp. tritici and P.striiformis on wheat seedlings. *Phytopathology*. https://doi.org/10.1094/phyto-85-409
de Vallavieille-Pope, C., Picard-Formery, H., Radulovic, S., & Johnson, R. (1990). Specific resistance factors to yellow rust in seedlings of some French wheat varieties and races of Puccinia striiformis Westend in France. *Agronomie*. https://doi.org/10.1051/agro:19900202
Deacon, J. (2005). Model-view-controller (mvc) architecture. *Computer Systems Development*.
DEFRA. (2016). DEFRA Farming Statistics.
Derevnina, L., & Michelmore, R. W. (2015). Wheat rusts never sleep but neither do sequencers: Will pathogenomics transform the way plant diseases are managed? *Genome Biology*. https://doi.org/10.1186/s13059-015-0615-3
Dhakal, S., Tan, C. T., Anderson, V., Yu, H., Fuentealba, M. P., Rudd, J. C., … Liu, S. (2018). Mapping and KASP marker development for wheat curl mite resistance in "TAM 112" wheat using linkage and association analysis. *Molecular Breeding*. https://doi.org/10.1007/s11032-018-0879-x
Dill-Macky, R., Rees, R. G., & Platz, G. J. (1991). Inoculum pressure and the development of stem rust epidemics in barley. *Australian Journal of Agricultural Research*. https://doi.org/10.1071/AR9910769
Dingle, J., & McGee, P. A. (2003). Some endophytic fungi reduce the density of

pustules of Puccinia recondita f. sp. tritici in wheat. *Mycological Research*. https://doi.org/10.1017/S0953756203007512

Dixon, P. A. (1963). Spore liberation by water drops in some myxomycetes. *Transactions of the British Mycological Society*. https://doi.org/10.1016/s0007-1536(63)80065-0

Dizlek, H., & Özer, M. S. (2016). Effects of sunn pest (Eurygaster integriceps) damage ratio on physical, chemical, and technological characteristics of wheat. *Quality Assurance and Safety of Crops and Foods*. https://doi.org/10.3920/QAS2015.0622

Dobbs, C. G. (1942). On the primary dispersal and isolation of fungal spores. *New Phytologist*, *41*(1), 63–69. https://doi.org/10.1111/j.1469-8137.1942.tb07060.x

Donatelli, M., Magarey, R. D., Bregaglio, S., Willocquet, L., Whish, J. P. M., & Savary, S. (2017). Modelling the impacts of pests and diseases on agricultural systems. *Agricultural Systems*. https://doi.org/10.1016/j.agsy.2017.01.019

Dressaire, E., Yamada, L., Song, B., & Roper, M. (2016). Mushrooms use convectively created airflows to disperse their spores. *Proceedings of the National Academy of Sciences of the United States of America*. https://doi.org/10.1073/pnas.1509612113

Duan, X., Tellier, A., Wan, A., Leconte, M., de Vallavieille-Pope, C., & Enjalbert, J. (2010). Puccinia striiformis f.sp. tritici presents high diversity and recombination in the over-summering zone of Gansu, China. *Mycologia*, *102*(1), 44–53. https://doi.org/10.3852/08-098

Duarte-Carvajalino, J. M., Alzate, D. F., Ramirez, A. A., Santa-Sepulveda, J. D., Fajardo-Rojas, A. E., & Soto-Suárez, M. (2018). Evaluating late blight severity in potato crops using unmanned aerial vehicles and machine learning algorithms. *Remote Sensing*. https://doi.org/10.3390/rs10101513

Dutech, C., BarrÈs, B., Bridier, J., Robin, C., Milgroom, M. G., & RavignÉ, V. (2012). The chestnut blight fungus world tour: Successive introduction events from diverse origins in an invasive plant fungal pathogen. *Molecular Ecology*. https://doi.org/10.1111/j.1365-294X.2012.05575.x

El Jarroudi, M., Kouadio, L., Bock, C. H., El Jarroudi, M. E., Junk, J., Pasquali, M., … Delfosse, P. (2017). A threshold-based weather model for predicting stripe rust infection in winter wheat. *Plant Disease*. https://doi.org/10.1094/PDIS-12-16-1766-RE

El Jarroudi, M., Lahlali, R., Kouadio, L., Denis, A., Belleflamme, A., El Jarroudi, M., … Tychon, B. (2020). Weather-based predictive modeling of wheat stripe rust infection in Morocco. *Agronomy*. https://doi.org/10.3390/agronomy10020280

Elderfield, J. A. D., Lopez-Ruiz, F. J., Van Den Bosch, F., & Cunniffe, N. J. (2018). Using epidemiological principles to explain fungicide resistance management tactics: Why do mixtures outperform alternations? *Phytopathology*. https://doi.org/10.1094/PHYTO-08-17-0277-R

Ellis, J. G., Lagudah, E. S., Spielmeyer, W., & Dodds, P. N. (2014). The past, present and future of breeding rust resistant wheat. *Front Plant Sci*, *5*(November), 641. https://doi.org/10.3389/fpls.2014.00641

Emerson, J. B., Adams, R. I., Román, C. M. B., Brooks, B., Coil, D. A., Dahlhausen, K., …

Rothschild, L. J. (2017). Schrödinger's microbes: Tools for distinguishing the living from the dead in microbial ecosystems. *Microbiome*. https://doi.org/10.1186/s40168-017-0285-3

Ertiro, B. T., Ogugo, V., Worku, M., Das, B., Olsen, M., Labuschagne, M., & Semagn, K. (2015). Comparison of Kompetitive Allele Specific PCR (KASP) and genotyping by sequencing (GBS) for quality control analysis in maize. *BMC Genomics*. https://doi.org/10.1186/s12864-015-2180-2

Estrada-Pena, A. (2009). Tick-borne pathogens, transmission rates and climate change. *Frontiers in Bioscience*. https://doi.org/10.2741/3405

FAO. (2019). *The State of Food and Agriculture 2019. Moving forward on food loss and waste reduction*.

Fernandes, J. M. C., Del Ponte, E. M., Pavan, W., & Cunha, G. R. (2007). Web-based system to true-forecast disease epidemics - Case study for fusarium head blight of wheat. In *Climate Prediction and Agriculture: Advances and Challenges*. https://doi.org/10.1007/978-3-540-44650-7_25

Ferrandino, F. J., & Aylor, D. E. (1984). Settling Speed of Cluster of Spores. *Phytopathology*, *74*(8), 969–972.

Ferretti, L., Raineri, E., & Ramos-Onsins, S. (2012). Neutrality tests for sequences with missing data. *Genetics*. https://doi.org/10.1534/genetics.112.139949

Figueroa, M., Hammond-Kosack, K. E., & Solomon, P. S. (2018). A review of wheat diseases—a field perspective. *Molecular Plant Pathology*. https://doi.org/10.1111/mpp.12618

Filho, A. B., Inoue-Nagata, A. K., Bassanezi, R. B., Belasque, J., Amorim, L., Macedo, M. A., … Savary, S. (2016). The importance of primary inoculum and area-wide disease management to crop health and food security. *Food Security*. https://doi.org/10.1007/s12571-015-0544-8

Finnigan, J. (2000). Turbulence in Plant Canopies. *Annual Review of Fluid Mechanics*, *32*(1), 519–571. https://doi.org/10.1146/annurev.fluid.32.1.519

Fischer, M., Cox, J., Davis, D. J., Wagner, A., Taylor, R., Huerta, A. J., & Money, N. P. (2004). New information on the mechanism of forcible ascospore discharge from Ascobolus immersus. *Fungal Genetics and Biology*, *41*(7), 698–707.

Fischer, M. W. F., Stolze-Rybczynski, J. L., Cui, Y., & Money, N. P. (2010). How far and how fast can mushroom spores fly? Physical limits on ballistospore size and discharge distance in the Basidiomycota. *Fungal Biology*. https://doi.org/10.1016/j.funbio.2010.06.002

Fischer, M. W. F., Stolze-Rybczynski, J. L., Davis, D. J., Cui, Y., & Money, N. P. (2010). Solving the aerodynamics of fungal flight: How air viscosity slows spore motion. *Fungal Biology*. https://doi.org/10.1016/j.funbio.2010.09.003

Fitt, B. D. L., Gregory, P. H., Todd, A. D., McCartney, H. A., & Macdonald, O. C. (1987). Spore Dispersal and Plant Disease Gradients; a Comparison between two Empirical Models. *Journal of Phytopathology*. https://doi.org/10.1111/j.1439-0434.1987.tb00452.x

Follett, E., Chamecki, M., & Nepf, H. (2016). Evaluation of a random displacement model for predicting particle escape from canopies using a simple eddy diffusivity model. *Agricultural and Forest Meteorology*. https://doi.org/10.1016/j.agrformet.2016.04.004

Fones, H., & Gurr, S. (2015). The impact of Septoria tritici Blotch disease on wheat:

An EU perspective. *Fungal Genetics and Biology*. https://doi.org/10.1016/j.fgb.2015.04.004

Fourie, P., Schutte, T., Serfontein, S., & Swart, F. (2013). Modeling the effect of temperature and wetness on Guignardia pseudothecium maturation and ascospore release in citrus orchards. *Phytopathology*. https://doi.org/10.1094/PHYTO-07-11-0194

Fox, E. J., & Reid-Bayliss, K. S. (2014). Accuracy of Next Generation Sequencing Platforms. *Journal of Next Generation Sequencing & Applications*. https://doi.org/10.4172/2469-9853.1000106

Fox, R. W., & McDonald, A. T. (1994). Introduction to Fluid Mechanics. *European Journal of Engineering Education*. https://doi.org/10.1080/03043799408928334

Fritz, J. A., Seminara, A., Roper, M., Pringle, A., & Brenner, M. P. (2013). A natural O-ring optimizes the dispersal of fungal spores. *Journal of the Royal Society Interface*. https://doi.org/10.1098/rsif.2013.0187

Galante, T. E., Horton, T. R., & Swaney, D. P. (2011). 95% of basidiospores fall within 1 m of the cap: A field- and modeling-based study. *Mycologia*. https://doi.org/10.3852/10-388

Ganal, M. W., Altmann, T., & Röder, M. S. (2009). SNP identification in crop plants. *Current Opinion in Plant Biology*. https://doi.org/10.1016/j.pbi.2008.12.009

Gause, G. F. (1936). The Struggle for Existence. *Soil Science*. https://doi.org/10.1097/00010694-193602000-00018

Gaydos, D. A., Petrasova, A., Cobb, R. C., & Meentemeyer, R. K. (2019). Forecasting and control of emerging infectious forest disease through participatory modelling. *Philosophical Transactions of the Royal Society B: Biological Sciences*. https://doi.org/10.1098/rstb.2018.0283

Geagea, L., Huber, L., Sache, I., Flura, D., McCartney, H. A., & Fitt, B. D. L. (2000). Influence of simulated rain on dispersal of rust spores from infected wheat seedlings. *Agricultural and Forest Meteorology*, *101*(1), 53–66. https://doi.org/10.1016/S0168-1923(99)00155-0

Gérard, P. R., Husson, C., Pinon, J., & Frey, P. (2006). Comparison of Genetic and Virulence Diversity of Melampsora larici-populina Populations on Wild and Cultivated Poplar and Influence of the Alternate Host. *Phytopathology*, *96*(9), 1027–1036. https://doi.org/10.1094/PHYTO-96-1027

Gilligan, C. A., & Van Den Bosch, F. (2008). Epidemiological Models for Invasion and Persistence of Pathogens. *Annu. Rev. Phytopathol*, *46*, 385–418. https://doi.org/10.1146/annurev.phyto.45.062806.094357

Gilligan, C. a, Truscott, J. E., & Stacey, A. J. (2007). Impact of scale on the effectiveness of disease control strategies for epidemics with cryptic infection in a dynamical landscape: an example for a crop disease. *Journal of the Royal Society, Interface / the Royal Society*, *4*(16), 925–934. https://doi.org/10.1098/rsif.2007.1019

Gleicher, S. C., Chamecki, M., Isard, S. A., Pan, Y., & Katul, G. G. (2014). Interpreting three-dimensional spore concentration measurements and escape fraction in a crop canopy using a coupled Eulerian-Lagrangian stochastic model. *Agricultural and Forest Meteorology*. https://doi.org/10.1016/j.agrformet.2014.03.020

Gold, R. E., Littlefield, L. J., & Statler, G. D. (1979). Ultrastructure of the pycnial and

aecial stages of Puccinia recondita . *Canadian Journal of Botany*. https://doi.org/10.1139/b79-015
Gregory, P. H. (1949). The operation of the puff-ball mechanism of Lycoperdon perlatum by raindrops shown by ultra-high-speed Schlieren cinematography. *Transactions of the British Mycological Society*. https://doi.org/10.1016/s0007-1536(49)80030-1
Gregory, P. H. (1961). *The microbiology of the atmosphere*. (P. N. Polunin, Ed.). London: Leonard Hill [books] limited.
Gregory, P. H. (1968). Interpreting Plant Disease Dispersal Gradients. *Annual Review of Phytopathology*. https://doi.org/10.1146/annurev.py.06.090168.001201
Grove, G. G. (1991). Powdery Mildew of Sweet Cherry: Influence of Temperature and Wetness Duration on Release and Germination of Ascospores of Podosphaera clandestina . *Phytopathology*. https://doi.org/10.1094/phyto-81-1271
Hamelin, F. M., Bisson, A., Desprez-Loustau, M. L., Fabre, F., & Mailleret, L. (2016). Temporal niche differentiation of parasites sharing the same plant host: Oak powdery mildew as a case study. *Ecosphere*, *7*(11). https://doi.org/10.1002/ecs2.1517
Hansen, J. G., & Lassen, P. (2013). Managing global crop disease data. In *EFITA-WCCA-CIGR Conference - Sustainable Agriculture through ICT Innovation*.
Hardin, G. (1960). The competitive exclusion principle. *Science*. https://doi.org/10.1126/science.131.3409.1292
Helfer, S. (2014). Rust fungi and global change. *New Phytologist*. https://doi.org/10.1111/nph.12570
Helyar, S. J., Hemmer-Hansen, J., Bekkevold, D., Taylor, M. I., Ogden, R., Limborg, M. T., … Nielsen, E. E. (2011). Application of SNPs for population genetics of nonmodel organisms: New opportunities and challenges. *Molecular Ecology Resources*. https://doi.org/10.1111/j.1755-0998.2010.02943.x
Hernandez Nopsa, J. F., & Pfender, W. F. (2014). A latent period duration model for wheat stem rust. *Plant Disease*. https://doi.org/10.1094/PDIS-11-13-1128-RE
Hess, G. R., Randolph, S. E., Arneberg, P., Chemini, C., Furlanello, C., Harwood, J., … Swinton, J. (2002). Spatial aspects of disease dynamics. *The Ecology of Wildlife Disease*, (6), 102–118.
Hirooka, T., & Ishii, H. (2013). Chemical control of plant diseases. *Journal of General Plant Pathology*. https://doi.org/10.1007/s10327-013-0470-6
Hirst, J. M. (1953). Changes in atmospheric spore content: Diurnal periodicity and the effects of weather. *Transactions of the British Mycological Society*. https://doi.org/10.1016/s0007-1536(53)80034-3
Hirzel, A., & Guisan, A. (2002). Which is the optimal sampling strategy for habitat suitability modelling. *Ecological Modelling*. https://doi.org/10.1016/S0304-3800(02)00203-X
Hobbelen, P. H. F., Paveley, N. D., Oliver, R. P., & Van Den Bosch, F. (2013). The usefulness of fungicide mixtures and alternation for delaying the selection for resistance in populations of Mycosphaerella graminicola on winter wheat: A modeling analysis. *Phytopathology*. https://doi.org/10.1094/PHYTO-06-12-0142-R
Hodson, D. P. (2011). Shifting boundaries: Challenges for rust monitoring. *Euphytica*.

https://doi.org/10.1007/s10681-010-0335-4
Hodson, D. P., Cressman, K., Nazari, K., Park, R. F., & Yahyaoui, A. (2009). The global cereal rust monitoring system. In *Proceedings of Oral Papers and Posters, 2009 Technical Workshop, BGRI, Cd. Obregón, Sonora Mexico* (pp. 35–46).
Hodson, D. P., Grønbech-Hansen, J., Lassen, P., Alemayeh, Y., Arista, J., Sonder, K., … Jin, Y. (2012). Tracking the wheat rust pathogens. In *Proceedings Borlaug Global Rust Initiative Technical Workshop; Oral Presentations; Beijing (China); 1-4 Sep. 2012*.
Holovaty, A., & Kaplan-Moss, J. (2009). *The Definitive Guide to Django: Web Development Done Right*. *Development*.
Hong, J. K., & Hwang, B. K. (1998). Influence of inoculum density, wetness duration, plant age, inoculation method, and cultivar resistance on infection of pepper plants by Colletotrichum coccodes. *Plant Disease*. https://doi.org/10.1094/PDIS.1998.82.10.1079
Hovmøller, M. S. (2019). GRRC annual report 2019: Stem-and yellow rust genotyping and race analyses. *GRRC Glob. Rust Ref. Cent*. Retrieved from https://agro.au.dk/fileadmin/www.grcc.au.dk/International_Services/Pathotype_YR_results/GRRC_annual_report_2019.pdf
Hovmøller, M. S., Justesen, A. F., & Brown, J. K. M. (2002). Clonality and long-distance migration of Puccinia striiformis f.sp. tritici in north-west Europe. *Plant Pathology*, *51*(1), 24–32. https://doi.org/10.1046/j.1365-3059.2002.00652.x
Hovmøller, M. S., Walter, S., Bayles, R. A., Hubbard, A., Flath, K., Sommerfeldt, N., … de Vallavieille-Pope, C. (2016). Replacement of the European wheat yellow rust population by new races from the centre of diversity in the near-Himalayan region. *Plant Pathology*, *65*(3), 402–411. https://doi.org/10.1111/ppa.12433
Hovmøller, Mogens S., Sørensen, C. K., Walter, S., & Justesen, A. F. (2011a). Diversity of Puccinia striiformis on Cereals and Grasses . *Annual Review of Phytopathology*. https://doi.org/10.1146/annurev-phyto-072910-095230
Hovmøller, Mogens S, Sørensen, C. K., Walter, S., & Justesen, A. F. (2011). Diversity of Puccinia striiformis on cereals and grasses. *Annual Review of Phytopathology*, *49*, 197–217. https://doi.org/10.1146/annurev-phyto-072910-095230
Hovmøller, Mogens Støvring, Walter, S., & Justesen, A. F. (2010). Escalating threat of wheat rusts. *Science (New York, N.Y.)*, *329*(5990), 369. https://doi.org/10.1126/science.1194925
Hovmøller, Mogens Støvring, Yahyaoui, A., & Singh, R. P. (2009). A Global Reference Centre for Wheat Yellow Rust: Pathogen Variability, Evolution and Dispersal Pathways at Regional and Global Levels. In *Full Papers and abstracts for the presented talks* (p. 91).
Huang, H., & Lacey Knowles, L. (2016). Unforeseen consequences of excluding missing data from next-generation sequences: Simulation study of rad sequences. *Systematic Biology*. https://doi.org/10.1093/sysbio/syu046
Hubbard, A., Lewis, C. M., Yoshida, K., Ramirez-Gonzalez, R. H., de Vallavieille-Pope, C., Thomas, J., … Saunders, D. G. O. (2015). Field pathogenomics reveals the emergence of a diverse wheat yellow rust population. *Genome Biology*, *16*(1), 23. https://doi.org/10.1186/s13059-015-0590-8
Hubbard, A., Wilderspin, S., & Holdgate, S. (2018). United Kingdom Cereal Pathogen Virulence Survey 2017 Annual Report. *Ahdb*, (September), 61. Retrieved from

http://www.niab.com/uploads/files/ukcpvs-annual-report-2017.pdf%0Ahttps://cereals.ahdb.org.uk/media/1304707/ukcpvs-annual-report-2017.pdf
Hubbard, A., Wilderspin, S., & Holdgate, S. (2019). *United Kingdom Cereal Pathogen Virulence Survey (UKCPVS)*. Cambridge.
Hughes, S. J., Cole, G. T., & Kendrick, B. (2007). Biology of Conidial Fungi. *Mycologia*. https://doi.org/10.2307/3792982
Huson, D. H., Richter, D. C., Rausch, C., Dezulian, T., Franz, M., & Rupp, R. (2007). Dendroscope: An interactive viewer for large phylogenetic trees. *BMC Bioinformatics*. https://doi.org/10.1186/1471-2105-8-460
Hyten, D. L., Song, Q., Fickus, E. W., Quigley, C. V., Lim, J. S., Choi, I. Y., … Cregan, P. B. (2010). High-throughput SNP discovery and assay development in common bean. *BMC Genomics*. https://doi.org/10.1186/1471-2164-11-475
Illumina. (2015). TruSeq RNA Sample Preparation v2 Guide. *Illumina*. https://doi.org/10.1016/j.canlet.2015.06.003
Ilton, M., Saad Bhamla, M., Ma, X., Cox, S. M., Fitchett, L. L., Kim, Y., … Patek, S. N. (2018). The principles of cascading power limits in small, fast biological and engineered systems. *Science*. https://doi.org/10.1126/science.aao1082
Ingold, C. T. (1928). Spore discharge in Podospora curvula. *Annals of Botany*, (2), 567–570.
Ingold, C. T. (1934). The spore discharge mechanism in Basidiobolus Ranarum. *New Phytologist*. https://doi.org/10.1111/j.1469-8137.1934.tb06814.x
Ingold, C. T. (1939). Spore discharge in land plants. *Spore Discharge in Land Plants.*
Ingold, C. T. (1999). Active liberation of reproductive units in terrestrial fungi. *Mycologist*. https://doi.org/10.1016/S0269-915X(99)80040-8
Ingold, C. T., & Hadland, S. A. (1959). The ballistics of Sordaria. *New Phytologist*. https://doi.org/10.1111/j.1469-8137.1959.tb05333.x
Isard, S. A., Dufault, N. S., Miles, M. R., Hartman, G. L., Russo, J. M., De Wolf, E. D., & Morel, W. (2006). The effect of solar irradiance on the mortality of Phakopsora pachyrhizi urediniospores. *Plant Disease*. https://doi.org/10.1094/PD-90-0941
Isard, Scott A., & Chamecki, M. (2015). A Physically Based Theoretical Model of Spore Deposition for Predicting Spread of Plant Diseases. *Phytopathology*. https://doi.org/10.1094/phyto-10-15-0275-r
Islam, M. T., Croll, D., Gladieux, P., Soanes, D. M., Persoons, A., Bhattacharjee, P., … Kamoun, S. (2016). Emergence of wheat blast in Bangladesh was caused by a South American lineage of Magnaporthe oryzae. *BMC Biology*. https://doi.org/10.1186/s12915-016-0309-7
Jin, Y. (2011). Role of Berberis spp. as alternate hosts in generating new races of Puccinia graminis and P. striiformis. *Euphytica*. https://doi.org/10.1007/s10681-010-0328-3
Jochua, C., Amane, M. I. V., Steadman, J. R., Xue, X., & Eskridge, K. M. (2008). Virulence diversity of the common bean rust pathogen within and among individual bean fields and development of sampling strategies. *Plant Disease*. https://doi.org/10.1094/PDIS-92-3-0401
Johansson, V., Lönnell, N., Rannik, Ü., Sundberg, S., & Hylander, K. (2016). Air humidity thresholds trigger active moss spore release to extend dispersal in

space and time. *Functional Ecology*. https://doi.org/10.1111/1365-2435.12606

Johnson, A. G., & Dickson, J. G. (1919). *Stem rust of grains and the barberry in Wisconsin*. Wisconsin: Madison : Agricultural Experiment Station of the University of Wisconsin.

Jombart, T. (2008). Adegenet: A R package for the multivariate analysis of genetic markers. *Bioinformatics*. https://doi.org/10.1093/bioinformatics/btn129

Jombart, T., Devillard, S., & Balloux, F. (2010). Discriminant analysis of principal components: A new method for the analysis of genetically structured populations. *BMC Genetics*. https://doi.org/10.1186/1471-2156-11-94

Jones, D. R. (2003). The distribution and importance of the Mycosphaerellaleaf spot diseases of banana. *Mycosphaerella Leaf Spot Diseases of Bananas: Present Status and Outlook. Proceedings of the 2nd International Workshop on Mycosphaerella Leaf Spot Diseases Held in San Jose, Costa Rica on 20-23 May 2002.*

Junk, J., Kouadio, L., Delfosse, P., & El Jarroudi, M. (2016). Effects of regional climate change on brown rust disease in winter wheat. *Climatic Change*. https://doi.org/10.1007/s10584-015-1587-8

Justesen, A. F., Ridout, C. J., & Hovmøller, M. S. (2002). The recent history of Puccinia striiformis f. sp. tritici in Denmark as revealed by disease incidence and AFLP markers. *Plant Pathology*, *51*(1), 13–23.

Kadowaki, K., Leschen, R. A. B., & Beggs, J. R. (2010). Periodicity of spore release from individual Ganoderma fruiting bodies in a natural forest. *Society*.

Kanagawa, T. (2003). Bias and Artifacts in Multitemplate Polymerase Chain Reactions (PCR). *Journal of Bioscience and Bioengineering*. https://doi.org/10.1263/jbb.96.317

Kang, W. S., Hong, S. S., Han, Y. K., Kim, K. R., Kim, S. G., & Park, E. W. (2010). A web-based information system for plant disease forecast based on weather data at high spatial resolution. *Plant Pathology Journal*. https://doi.org/10.5423/PPJ.2010.26.1.037

Kelly, M., & Meentemeyer, R. K. (2002). Landscape dynamics of the spread of Sudden Oak Death. *Photogrammetric Engineering and Remote Sensing*.

Khan, F. S., Razzaq, S., Irfan, K., Maqbool, F., Farid, A., Illahi, I., & Amin, T. U. (2008). Dr. Wheat: A Web-based Expert System for Diagnosis of Diseases and Pests in Pakistani Wheat. *Lecture Notes in Engineering and Computer Science*.

Khan, T. (2014). Estimation of genetic diversity among Berberis spp . from Karakoram Mountain Ranges using morpho - pathological and floral characters. *Journal of Biodiversity and Environmental Sciences*, *5*(2), 286–295.

Kim, S., Park, H., Gruszewski, H. A., Schmale, D. G., & Jung, S. (2019). Vortex-induced dispersal of a plant pathogen by raindrop impact. *Proceedings of the National Academy of Sciences of the United States of America*. https://doi.org/10.1073/pnas.1820318116

Kinjo, N., & Zang, M. (2001). Morphological and phylogenetic studies on Cordyceps sinensis distributed in southwestern China. *Mycoscience*. https://doi.org/10.1007/BF02460956

Klein, E. K., Lavigne, C., Foueillassar, X., Gouyon, P. H., & Larédo, C. (2003). Corn pollen dispersal: Quasi-mechanistic models and field experiments. *Ecological*

Monographs. https://doi.org/10.1890/0012-9615(2003)073[0131:CPDQMM]2.0.CO;2
Kolhe, S., Kamal, R., Saini, H. S., & Gupta, G. K. (2011). A web-based intelligent disease-diagnosis system using a new fuzzy-logic based approach for drawing the inferences in crops. *Computers and Electronics in Agriculture*. https://doi.org/10.1016/j.compag.2011.01.002
Kolmer, J. (2013). Leaf rust of wheat: Pathogen biology, variation and host resistance. *Forests*. https://doi.org/10.3390/f4010070
Kolmer, J. A. (2019). Virulence of puccinia triticina, the wheat leaf rust fungus, in the United States in 2017. *Plant Disease*. https://doi.org/10.1094/PDIS-09-18-1638-SR
Kolnaar, R. W., & Van Den Bosch, F. (2001). Effect of temperature on epidemiological parameters of Puccinia lagenophorae. *Plant Pathology*. https://doi.org/10.1046/j.1365-3059.2001.00533.x
Kot, M., Lewis, M. A., & Driessche, P. Van Den. (1996). Dispersal Data and the Spread of Invading Organisms. *Ecological Society of America*, *77*(7), 2027–2042. https://doi.org/10.2307/2265698
Kota, R., Varshney, R. K., Prasad, M., Zhang, H., Stein, N., & Graner, A. (2008). EST-derived single nucleotide polymorphism markers for assembling genetic and physical maps of the barley genome. *Functional and Integrative Genomics*. https://doi.org/10.1007/s10142-007-0060-9
Kramer, C. L., Pady, S. M., Clary, R., & Haard, R. (1968). Diurnal periodicity in aeciospore release of certain rusts. *Transactions of the British Mycological Society*, *51*(5), 679-IN6. https://doi.org/10.1016/s0007-1536(68)80150-0
Kuang, W., Liu, W., Ma, Z., & Wang, H. (2013). Development of a Web-Based Prediction System for Wheat Stripe Rust BT - Computer and Computing Technologies in Agriculture VI. In D. Li & Y. Chen (Eds.) (pp. 324–335). Berlin, Heidelberg: Springer Berlin Heidelberg.
Kuparinen, A. (2006). Mechanistic models for wind dispersal. *Trends in Plant Science*. https://doi.org/10.1016/j.tplants.2006.04.006
Lamichhane, J. R., & Venturi, V. (2015). Synergisms between microbial pathogens in plant disease complexes: A growing trend. *Frontiers in Plant Science*. https://doi.org/10.3389/fpls.2015.00385
Langenberg, W. J. (1977). Relation of Weather Variables and Periodicities of Airborne Spores of Alternaria dauci. *Phytopathology*. https://doi.org/10.1094/phyto-67-879
Lau, H. Y., & Botella, J. R. (2017). Advanced DNA-based point-of-care diagnostic methods for plant diseases detection. *Frontiers in Plant Science*. https://doi.org/10.3389/fpls.2017.02016
Launay, M., Zurfluh, O., Huard, F., Buis, S., Bourgeois, G., Caubel, J., … Bancal, M. O. (2020). Robustness of crop disease response to climate change signal under modeling uncertainties. *Agricultural Systems*. https://doi.org/10.1016/j.agsy.2019.102733
Lee, S. K., & Kakishima, M. (1999). Aeciospore surface structures of Gymnosporangium and Roestelia (Uredinales). *Mycoscience*. https://doi.org/10.1007/bf02464289
Leff, B., Ramankutty, N., & Foley, J. a. (2004). Geographic distribution of major crops

across the world. *Global Biogeochemical Cycles*, *18*(1), n/a--n/a. https://doi.org/10.1029/2003GB002108

Lewis, C., Persoons, A., P. Bebber, D., Kigathi, R., Maintz, J., Findlay, K., … G. O. Saunders, D. (2018). *Potential for re-emergence of wheat stem rust in the United Kingdom*. *Communications Biology* (Vol. 1). https://doi.org/10.1038/s42003-018-0013-y

Li, F., Upadhyaya, N. M., Sperschneider, J., Matny, O., Nguyen-Phuc, H., Mago, R., … Figueroa, M. (2019). Emergence of the Ug99 lineage of the wheat stem rust pathogen through somatic hybridisation. *Nature Communications*, *10*(1), 5068. https://doi.org/10.1038/s41467-019-12927-7

Li, H., Handsaker, B., Wysoker, A., Fennell, T., Ruan, J., Homer, N., … Durbin, R. (2009). The Sequence Alignment/Map format and SAMtools. *Bioinformatics*. https://doi.org/10.1093/bioinformatics/btp352

Liu, M., Rodrigue, N., & Kolmer, J. (2014). Population divergence in the wheat leaf rust fungus Puccinia triticina is correlated with wheat evolution. *Heredity*. https://doi.org/10.1038/hdy.2013.123

Liu, W., Maccaferri, M., Bulli, P., Rynearson, S., Tuberosa, R., Chen, X., & Pumphrey, M. (2017). Genome-wide association mapping for seedling and field resistance to Puccinia striiformis f. sp. tritici in elite durum wheat. *Theoretical and Applied Genetics*. https://doi.org/10.1007/s00122-016-2841-9

Loos, C., Seppelt, R., Meier-Bethke, S., Schiemann, J., & Richter, O. (2003). Spatially explicit modelling of transgenic maize pollen dispersal and cross-pollination. *Journal of Theoretical Biology*. https://doi.org/10.1016/S0022-5193(03)00243-1

Luo, Y., & Zeng, S. M. (1995). Simulation studies on epidemics of wheat stripe rust (Puccinia striiformis) on slow-rusting cultivars and analysis of effects of resistance components. *Plant Pathology*. https://doi.org/10.1111/j.1365-3059.1995.tb02786.x

Lyon, B., & Broders, K. (2017). Impact of climate change and race evolution on the epidemiology and ecology of stripe rust in central and eastern USA and Canada. *Canadian Journal of Plant Pathology*. https://doi.org/10.1080/07060661.2017.1368713

Mahaffee, W. F., & Stoll, R. (2016). The ebb and flow of airborne pathogens: monitoring and use in disease management decisions. *Phytopathology*, *106*(5). https://doi.org/10.1094/PHYTO-02-16-0060-RVW

Malik, N., Dwivedi, N., Singh, A. K., Parida, S. K., Agarwal, P., Thakur, J. K., & Tyagi, A. K. (2016). An Integrated Genomic Strategy Delineates Candidate Mediator Genes Regulating Grain Size and Weight in Rice. *Scientific Reports*. https://doi.org/10.1038/srep23253

Manel, S., Schwartz, M. K., Luikart, G., & Taberlet, P. (2003). Landscape genetics: Combining landscape ecology and population genetics. *Trends in Ecology and Evolution*. https://doi.org/10.1016/S0169-5347(03)00008-9

Marrou, J., Duteil, M., Quiot, J. B., Labonne, G., Leclant, F., & Renoust, M. (1979). Ecology and epidemiology of cucumber mosaic virus [in the south-east of France], 8: Effects of natural wind-breaks and surrounding vegetable crops on cucumber mosaic virus (CMV) epidemics [aphids]. *Annales de Phytopathologie (France)*.

Martin, L. A., & Pullin, A. S. (2004). Host-plant specialisation and habitat restriction in an endangered insect, Lycaena dispar batavus (Lepidoptera: Lycaenidae) I. Larval feeding and oviposition preferences. *European Journal of Entomology*. https://doi.org/10.14411/eje.2004.012

Martin, R. R., James, D., & Levesque, C. A. (2000). Impacts of molecular diagnostic technologies on plant disease management. *Annual Review of Phytopathology*. https://doi.org/10.1146/annurev.phyto.38.1.207

Mboup, M., Bahri, B., Leconte, M., Vallavieille-pope, C. De, & Kaltz, O. (2012). Genetic structure and local adaptation of European wheat yellow rust populations : the role of temperature-specific adaptation, *5*, 341–352. https://doi.org/10.1111/j.1752-4571.2011.00228.x

McCallum, B. D., Seto-Goh, P., & Xue, A. (2017). Physiological specialization of Puccinia triticina, the causal agent of wheat leaf rust, in Canada in 2011. *Canadian Journal of Plant Pathology*. https://doi.org/10.1080/07060661.2017.1386715

McCartney, A., & West, J. (2007). Dispersal of fungal spores through the air. *Mycology Series*, *25*, 65.

McCartney, H. A., & Lacey, M. E. (1991). Wind dispersal of pollen from crops of oilseed rape (Brassica napus L.). *Journal of Aerosol Science*. https://doi.org/10.1016/0021-8502(91)90005-3

McCartney, H A, & Fitt, B. D. L. (1985). Advances in Plant Pathology: Mathematical Modelling of Crop Disease. Academic Press, London.

McCartney, H Alastair. (1994). Dispersal of spores and pollen from crops. *Grana*, *33*(2), 76–80.

McCracken, F. I. (1987). Observations on the spore release of Paxillus panuoides. *Grana*. https://doi.org/10.1080/00173138709429947

McIntosh, R. A., & Pretorius, Z. A. (2011). Borlaug Global Rust Initiative provides momentum for wheat rust research. *Euphytica*. https://doi.org/10.1007/s10681-011-0389-y

McIntosh, Robert A. (2009). History and status of the wheat rusts. In *Proceedings of the 2009 Technical Workshop Borlaug Global Rust Initiative, Cd. Obregon, Sonora, Mexico, March* (pp. 17–20).

Meentemeyer, R. K., Cunniffe, N. J., Cook, A. R., Filipe, J. a. N., Hunter, R. D., Rizzo, D. M., & Gilligan, C. A. (2011). Epidemiological modeling of invasion in heterogeneous landscapes: spread of sudden oak death in California (1990–2030). *Ecosphere*, *2*(2), art17. https://doi.org/10.1890/ES10-00192.1

Meentemeyer, R., Rizzo, D., Mark, W., & Lotz, E. (2004). Mapping the risk of establishment and spread of sudden oak death in California, *200*, 195–214. https://doi.org/10.1016/j.foreco.2004.06.021

Melander, L. W., & Craigie, J. H. (1927). Nature of resistance of Berberis spp. to Puccinia graminis. *Phytopathology*, *17*, 95-114 (99).

Meredith, D. S. (1963). Violent Spore Release in Some Fungi Imperfecti. *Annals of Botany*. https://doi.org/10.1093/oxfordjournals.aob.a083833

Meredith, D. S. (1973). Significance of Spore Release and Dispersal Mechanisms in Plant Disease Epidemiology. *Annual Review of Phytopathology*. https://doi.org/10.1146/annurev.py.11.090173.001525

Metzker, M. L. (2010). Sequencing technologies the next generation. *Nature Reviews*

Genetics. https://doi.org/10.1038/nrg2626
Mewes, T., Franke, J., & Menz, G. (2011). Spectral requirements on airborne hyperspectral remote sensing data for wheat disease detection. *Precision Agriculture*. https://doi.org/10.1007/s11119-011-9222-9
Meyer, M., Burgin, L., Hort, M. C., Hodson, D. P., & Gilligan, C. A. (2017). Large-scale atmospheric dispersal simulations identify likely airborne incursion routes of wheat stem rust into Ethiopia. *Phytopathology*. https://doi.org/10.1094/PHYTO-01-17-0035-FI
Micheli, P. A. (1729). Nova plantarum genera juxta Tournefortii methodum disposita quibus plantae. *Bernardi Paperini*.
Milus, E. A., Seyran, E., & McNew, R. (2006). Aggressiveness of Puccinia striiformis f. sp. tritici isolates in the south-central United States. *Plant Disease*, *90*(7), 847–852.
Mims, C. W., Littlefield, L. J., & Heath, M. C. (1980). Ultrastructure of Rust Fungi. *Mycologia*. https://doi.org/10.2307/3759550
Money, N. P. (1994). Osmotic Adjustment and the role of turgor in Mycelial Fungi. In J. G. H. Wessels & F. Meinhardt (Eds.), *The Mycota Vol 1: Growth, Differentiation and Sexuality* (pp. 67–88). Berlin: Springer-Verlag.
Money, N. P., & Webster, J. (1989). Mechanism of sporangial emptying in Saprolegnia. *Mycological Research*. https://doi.org/10.1016/S0953-7562(89)80094-2
Moran-Gilad, J. (2017). Whole genome sequencing (WGS) for food-borne pathogen surveillance and control – Taking the pulse. *Eurosurveillance*. https://doi.org/10.2807/1560-7917.ES.2017.22.23.30547
Mori, Y., & Notomi, T. (2009). Loop-mediated isothermal amplification (LAMP): a rapid, accurate, and cost-effective diagnostic method for infectious diseases. *Journal of Infection and Chemotherapy*, *15*(2), 62–69.
NASA. (n.d.). Boundary Layer. Retrieved from https://www.grc.nasa.gov/WWW/K-12/airplane/boundlay.html
Nasu, S., Suzuki, J., Ohta, R., Hasegawa, K., Yui, R., Kitazawa, N., … Minobe, Y. (2002). Search for and analysis of single nucleotide polymorphisms (SNPS) in rice (Oryza sativa, Oryza rufipogon) and establishment of SNP markers. *DNA Research*. https://doi.org/10.1093/dnares/9.5.163
Nathan, R., Getz, W. M., Revilla, E., Holyoak, M., Kadmon, R., Saltz, D., & Smouse, P. E. (2008). A movement ecology paradigm for unifying organismal movement research. *Proceedings of the National Academy of Sciences*, *105*(49), 19052–19059. https://doi.org/10.1073/pnas.0800375105
Nathan, R., Klein, E. K., Robledo-Arnuncio, J. J., & Revilla, E. (2012). Dispersal kernels : review . Chapter 15. *Dispersal Ecology and Evolution*, *First Edit*.
National Statistics. (2015). *Agriculture in the United Kingdom*.
Newlands, N. K. (2018). Model-Based Forecasting of Agricultural Crop Disease Risk at the Regional Scale, Integrating Airborne Inoculum, Environmental, and Satellite-Based Monitoring Data. *Frontiers in Environmental Science*. https://doi.org/10.3389/fenvs.2018.00063
Newman, G., Zimmerman, D., Crall, A., Laituri, M., Graham, J., & Stapel, L. (2010). User-friendly web mapping: Lessons from a citizen science website. *International Journal of Geographical Information Science*.

https://doi.org/10.1080/13658816.2010.490532
NH Government. (n.d.). European barberry. Retrieved from https://www.agriculture.nh.gov/publications-forms/documents/european-barberry.pdf
Noblin, X., Yang, S., & Dumais, J. (2009). Surface tension propulsion of fungal spores. *Journal of Experimental Biology*. https://doi.org/10.1242/jeb.029975
Nobliri, X., Yang, S., & Dumais, J. (2009). Surface tension propulsion of fungal spores. *Journal of Experimental Biology*. https://doi.org/10.1242/jeb.029975
Norros, V., Rannik, Ü., Hussein, T., Petäjä, T., Vesala, T., & Ovaskainen, O. (2014). Do small spores disperse further than large spores? *Ecology*. https://doi.org/10.1890/13-0877.1
Notomi, T., Okayama, H., Masubuchi, H., Yonekawa, T., Watanabe, K., Amino, N., & Hase, T. (2000). Loop-mediated isothermal amplification of DNA. *Nucleic Acids Research*. https://doi.org/10.1093/nar/28.12.e63
Oerke, E. C., & Dehne, H. W. (2004). Safeguarding production - Losses in major crops and the role of crop protection. *Crop Protection*, *23*(4), 275–285. https://doi.org/10.1016/j.cropro.2003.10.001
Oliver, R. P., & Hewitt, H. G. (2014). *Fungicides in crop protection: Second edition*. *Fungicides in Crop Protection: Second Edition*.
Olivera Firpo, P. D., Newcomb, M., Flath, K., Sommerfeldt-Impe, N., Szabo, L. J., Carter, M., … Jin, Y. (2017). Characterization of Puccinia graminis f. sp. tritici isolates derived from an unusual wheat stem rust outbreak in Germany in 2013. *Plant Pathology*. https://doi.org/10.1111/ppa.12674
Olivera, P., Newcomb, M., Szabo, L. J., Rouse, M., Johnson, J., Gale, S., … Jin, Y. (2015). Phenotypic and genotypic characterization of race TKTTF of Puccinia graminis f. sp. tritici that caused a wheat stem rust epidemic in southern Ethiopia in 2013-14. *Phytopathology*. https://doi.org/10.1094/PHYTO-11-14-0302-FI
Oneto, D. L., Golan, J., Mazzino, A., Pringle, A., & Seminara, A. (2020). Timing of fungal spore release dictates survival during atmospheric transport. *Proceedings of the National Academy of Sciences of the United States of America*. https://doi.org/10.1073/pnas.1913752117
Orton, E., Lewis, C., Davey, P., Radhakrishnan, G., & Saunders, D. (2019). *Stem rust (Puccina graminis) identified on spring barley in the UK adjacent to infected Berberis vulgaris*. https://doi.org/http://dx.doi.org/10.5197/j.2044-0588.2019.040.011
Otten, W., & Gilligan, C. A. (2006). Soil structure and soil-borne diseases: Using epidemiological concepts to scale from fungal spread to plant epidemics. *European Journal of Soil Science*, *57*(1), 26–37. https://doi.org/10.1111/j.1365-2389.2006.00766.x
Pady, S. M., Kramer, C. L., & Clary, R. (1967). Diurnal periodicity in airborne fungi in an orchard. *Journal of Allergy*. https://doi.org/10.1016/0021-8707(67)90094-9
Pady, S. M., Kramer, C. L., & Clary, R. (1969). Aeciospore release in Gymnosporangium . *Canadian Journal of Botany*. https://doi.org/10.1139/b69-146
Page, R. M., & Kennedy, D. (1964). Studies on the Velocity of Discharged Sporangia of Pilobolus kleinii. *Mycologia*. https://doi.org/10.2307/3756678

Panstruga, R., & Dodds, P. N. (2009). Terrifie protein traffic: The mystery of effector protein delivery by filamentous plant pathogens. *Science*. https://doi.org/10.1126/science.1171652

Papaïx, J., Goyeau, H., Du Cheyron, P., Monod, H., & Lannou, C. (2011). Influence of cultivated landscape composition on variety resistance: An assessment based on wheat leaf rust epidemics. *New Phytologist*, *191*(4), 1095–1107. https://doi.org/10.1111/j.1469-8137.2011.03764.x

Papastamati, K., & Van Den Bosch, F. (2007). The sensitivity of the epidemic growth rate to weather variables, with an application to yellow rust on wheat. *Phytopathology*. https://doi.org/10.1094/PHYTO-97-2-0202

Pariaud, B., Robert, C., Goyeau, H., & Lannou, C. (2009). Aggressiveness components and adaptation to a host cultivar in wheat leaf rust. *Phytopathology*. https://doi.org/10.1094/PHYTO-99-7-0869

Park, R., Fetch, T., Hodson, D., Jin, Y., Nazari, K., Prashar, M., & Pretorius, Z. (2011). International surveillance of wheat rust pathogens: Progress and challenges. *Euphytica*. https://doi.org/10.1007/s10681-011-0375-4

Parnell, S., Gilligan, C. A., & Van Den Bosch, F. (2005). Small-scale fungicide spray heterogeneity and the coexistence of resistant and sensitive pathogen strains. *Phytopathology*. https://doi.org/10.1094/PHYTO-95-0632

Parnell, S., Gottwald, T. R., Gilks, W. R., & van den Bosch, F. (2012). Estimating the incidence of an epidemic when it is first discovered and the design of early detection monitoring. *Journal of Theoretical Biology*, *305*, 30–36. https://doi.org/10.1016/j.jtbi.2012.03.009

Parnell, S., Gottwald, T. R., Irey, M. S., Luo, W., & Van Den Bosch, F. (2011). A stochastic optimization method to estimate the spatial distribution of a pathogen from a sample. *Phytopathology*. https://doi.org/10.1094/PHYTO-11-10-0311

Parnell, S., Van Den Bosch, F., & Gilligan, C. A. (2006). Large-scale fungicide spray heterogeneity and the regional spread of resistant pathogen strains. *Phytopathology*. https://doi.org/10.1094/PHYTO-96-0549

Parnell, Stephen, van den Bosch, F., Gottwald, T., & Gilligan, C. A. (2017). Surveillance to Inform Control of Emerging Plant Diseases: An Epidemiological Perspective. *Annual Review of Phytopathology*. https://doi.org/10.1146/annurev-phyto-080516-035334

Pasquill, F. (1962). *Atmospheric Diffusion: The Dispersion of Windborne Material from Industrial and Other Sources*. Van Nostrand. Retrieved from https://books.google.co.uk/books?id=9X4aAAAAMAAJ

Pavan, W., Fraisse, C. W., & Peres, N. A. (2011). Development of a web-based disease forecasting system for strawberries. *Computers and Electronics in Agriculture*. https://doi.org/10.1016/j.compag.2010.10.013

Pei, M. H., Ruiz, C., Hunter, T., Arnold, G. M., & Bayon, C. (2002). Quantitative relationships between inoculum of Melampsora larici-epitea and corresponding disease on Salix. *Plant Pathology*. https://doi.org/10.1046/j.1365-3059.2002.00739.x

Perkins, T. E., & Matlack, G. R. (2002). Human-generated pattern in commercial forests of southern Mississippi and consequences for the spread of pests and pathogens. *Forest Ecology and Management*. https://doi.org/10.1016/S0378-

1127(00)00645-9
Petersen, L. J. (1958). Studies on the relationship between inoculum density and infection of wheat by uredospores of Puccinia gramminis var. tritici.
Peterson, G. W., Dong, Y., Horbach, C., & Fu, Y. B. (2014). Genotyping-by-sequencing for plant genetic diversity analysis: A lab guide for SNP genotyping. *Diversity*. https://doi.org/10.3390/d6040665
Peterson, P. D. (2018). The Barberry Eradication Program in Minnesota for Stem Rust Control: A Case Study. *Annual Review of Phytopathology*. https://doi.org/10.1146/annurev-phyto-080417-050133
Pfeifer, S. P. (2017). From next-generation resequencing reads to a high-quality variant data set. *Heredity*. https://doi.org/10.1038/hdy.2016.102
Pfender, W., Graw, R., Bradley, W., Carney, M., & Maxwell, L. (2006). Use of a complex air pollution model to estimate dispersal and deposition of grass stem rust urediniospores at landscape scale. *Handbook of Environmental Chemistry, Volume 5: Water Pollution*. https://doi.org/10.1016/j.agrformet.2006.06.007
Piattoni, F., Oir, F., Morara, M., Iotti, M., & Zambonelli, A. (2013). The role of wild boars in spore dispersal of hypogeous fungi. *Acta Mycologica*. https://doi.org/10.5586/am.2012.017
Pimentel, D., Zuniga, R., & Morrison, D. (2005). Update on the environmental and economic costs associated with alien-invasive species in the United States. *Ecological Economics*. https://doi.org/10.1016/j.ecolecon.2004.10.002
Pipal, F. J. (1918). The Barberry and its Relation to the Stem Rust of Wheat in Indiana. *Proceedings of the Indiana Academy of Science*.
Plantegenest, M., Le May, C., & Fabre, F. (2007). Landscape epidemiology of plant diseases. *Journal of the Royal Society, Interface / the Royal Society*, *4*(16), 963–972. https://doi.org/10.1098/rsif.2007.1114
Plekhanova, J. (2009). Evaluating web development frameworks: Django, Ruby on Rails and CakePHP. *Institute for Business and Information Technology*.
Poppinga, S., Haushahn, T., Warnke, M., Masselter, T., & Speck, T. (2015). Sporangium exposure and spore release in the peruvian maidenhair fern (Adiantum peruvianum, Pteridaceae). *PLoS ONE*. https://doi.org/10.1371/journal.pone.0138495
Powell, J. M. (1974). Environmental factors affecting germination of Cronartium comandrae aeciospores . *Canadian Journal of Botany*. https://doi.org/10.1139/b74-083
Prank, M., Kenaley, S. C., Bergstrom, G. C., Acevedo, M., & Mahowald, N. M. (2019). Climate change impacts the spread potential of wheat stem rust, a significant crop disease. *Environmental Research Letters*. https://doi.org/10.1088/1748-9326/ab57de
Pringle, A., Brenner, M., Fritz, J., Roper, M., & Seminara, A. (2017a). Chapter 20 Reaching the Wind. https://doi.org/10.1201/9781315119496-21
Pringle, A., Brenner, M., Fritz, J., Roper, M., & Seminara, A. (2017b). Chapter 20 Reaching the Wind. https://doi.org/10.1201/9781315119496-21
Prussin, A. J., Marr, L. C., Schmale, D. G., Stoll, R., & Ross, S. D. (2015). Experimental validation of a long-distance transport model for plant pathogens: Application to Fusarium graminearum. *Agricultural and Forest Meteorology*. https://doi.org/10.1016/j.agrformet.2014.12.009

Purcell, E. M. (1977). Life at low Reynolds number. *American Journal of Physics*, *45*(1), 3–11.

Radhakrishnan, G. V., Cook, N. M., Bueno-Sancho, V., Lewis, C. M., Persoons, A., Mitiku, A. D., … Saunders, D. G. O. (2019). MARPLE, a point-of-care, strain-level disease diagnostics and surveillance tool for complex fungal pathogens. *BMC Biology*. https://doi.org/10.1186/s12915-019-0684-y

Rafalski, A. (2002). Applications of single nucleotide polymorphisms in crop genetics. *Current Opinion in Plant Biology*. https://doi.org/10.1016/S1369-5266(02)00240-6

Raguso, R. A., & Roy, B. A. (1998). "Floral" scent production by Puccinia rust fungi that mimic flowers. *Molecular Ecology*. https://doi.org/10.1046/j.1365-294x.1998.00426.x

Rapilly, F. (1979). Yellow rust epidemiology. *Annual Review of Phytopathology*, *17*, 59–73.

Ray, D. K., Mueller, N. D., West, P. C., & Foley, J. A. (2013). Yield Trends Are Insufficient to Double Global Crop Production by 2050. *PLoS ONE*. https://doi.org/10.1371/journal.pone.0066428

Ray, D. K., Ramankutty, N., Mueller, N. D., West, P. C., & Foley, J. A. (2012). Recent patterns of crop yield growth and stagnation. *Nature Communications*. https://doi.org/10.1038/ncomms2296

Reynolds, A. M. (2011). Exponential and power-law contact distributions represent different atmospheric conditions. *Phytopathology*. https://doi.org/10.1094/PHYTO-01-11-0001

Rieux, A., Soubeyrand, S., Bonnot, F., Klein, E. K., Ngando, J. E., Mehl, A., … De Lapeyre De Bellaire, L. (2014). Long-distance wind-dispersal of spores in a fungal plant pathogen: Estimation of anisotropic dispersal kernels from an extensive field experiment. *PLoS ONE*, *9*(8). https://doi.org/10.1371/journal.pone.0103225

Rijkenberg, F. H. J., & Truter, S. J. (1974). The ultrastructure of the Puccinia sorghi aecial stage. *Protoplasma*. https://doi.org/10.1007/BF01275814

Rizzo, D. M., & Garbelotto, M. (2003). Sudden Oak Death: Endangering California and Oregon Forest Ecosystems. *Frontiers in Ecology and the Environment*. https://doi.org/10.2307/3868064

Robin, M. H., Bancal, M. O., Cellier, V., Délos, M., Felix, I., Launay, M., … Aubertot, J. N. (2018). IPSIM-Web, an online resource for promoting qualitative aggregative hierarchical network models to predict plant disease risk: Application to brown rust on wheat. *Plant Disease*. https://doi.org/10.1094/PDIS-12-16-1816-SR

Rodriguez-Algaba, J., Walter, S., Sørensen, C. K., Hovmøller, M. S., & Justesen, A. F. (2014). Sexual structures and recombination of the wheat rust fungus Puccinia striiformis on Berberis vulgaris. *Fungal Genetics and Biology*, *70*. https://doi.org/10.1016/j.fgb.2014.07.005

Rodríguez-Moreno, V. M., Jiménez-Lagunes, A., Estrada-Avalos, J., Mauricio-Ruvalcaba, J. E., & Padilla-Ramírez, J. S. (2020). Weather-data-based model: an approach for forecasting leaf and stripe rust on winter wheat. *Meteorological Applications*. https://doi.org/10.1002/met.1896

Roelfs, A P, Singh, R. P., & Saari, E. E. (1992). Rust Diseases of Wheat, 81. https://doi.org/FSA7547-PD-11-06N

Roelfs, Alan P. (2010). Effects of Barberry Eradication on Stem Rust in the United

States. *Plant Disease*. https://doi.org/10.1094/pd-66-177
Roper, M., Pepper, R. E., Brenner, M. P., & Pringle, A. (2008). Explosively launched spores of ascomycete fungi have drag-minimizing shapes. *Proceedings of the National Academy of Sciences of the United States of America*. https://doi.org/10.1073/pnas.0805017105
Roper, M., Seminara, A., Bandi, M. M., Cobb, A., Dillard, H. R., & Pringle, A. (2010). Dispersal of fungal spores on a cooperatively generated wind. *Proceedings of the National Academy of Sciences*. https://doi.org/10.1073/pnas.1003577107
Rosekind, M. R., Gregory, K. B., Mallis, M. M., Brandt, S. L., Seal, B., & Lerner, D. (2010). The cost of poor sleep: Workplace productivity loss and associated costs. *Journal of Occupational and Environmental Medicine*. https://doi.org/10.1097/JOM.0b013e3181c78c30
Rossi, V., Racca, P., Giosue', S., Pancaldi, D., & Alberti, I. (1997). A simulation model for the development of brown rust epidemics in winter wheat. *European Journal of Plant Pathology*. https://doi.org/10.1023/A:1008677407661
Rotem, J., & Aust, H. J. (1991). The Effect of Ultraviolet and Solar Radiation and Temperature on Survival of Fungal Propagules. *Journal of Phytopathology*. https://doi.org/10.1111/j.1439-0434.1991.tb00139.x
Sakes, A., Van Wiel, M. Der, Henselmans, P. W. J., Van Leeuwen, J. L., Dodou, D., & Breedveld, P. (2016). Shooting mechanisms in nature: A systematic review. *PLoS ONE*. https://doi.org/10.1371/journal.pone.0158277
Samborski, D. J. (1985). Wheat leaf rust. In *Diseases, Distribution, Epidemiology, and Control* (pp. 39–59). Elsevier.
Sandeep, C. S., Luo, L., & Senetakis, K. (2020). Effect of grain size and surface roughness on the normal coefficient of restitution of single grains. *Materials*. https://doi.org/10.3390/ma13040814
Sato, T., & Sato, S. (1985). Morphology of aecia of the rust fungi. *Transactions of the British Mycological Society*, *85*(2), 223–238.
Saunders, D. G. O., Pretorius, Z. A., & Hovmøller, M. S. (2019). Tackling the re-emergence of wheat stem rust in Western Europe. *Communications Biology*. https://doi.org/10.1038/s42003-019-0294-9
Savage, D., Barbetti, M. J., MacLeod, W. J., Salam, M. U., & Renton, M. (2012). Seasonal and Diurnal Patterns of Spore Release Can Significantly Affect the Proportion of Spores Expected to Undergo Long-Distance Dispersal. *Microbial Ecology*. https://doi.org/10.1007/s00248-011-9949-x
Savary, S., Willocquet, L., Pethybridge, S. J., Esker, P., McRoberts, N., & Nelson, A. (2019). The global burden of pathogens and pests on major food crops. *Nature Ecology and Evolution*. https://doi.org/10.1038/s41559-018-0793-y
Savile, D. B. O. (1954). Cellular Mechanics, Taxonomy and Evolution in the Uredinales and Ustilaginales. *Mycologia*. https://doi.org/10.1080/00275514.1954.12024412
Schlichting, H., & Gersten, K. (2000). Fundamentals of Boundary-Layer Theory. In *Boundary-Layer Theory*. https://doi.org/10.1007/978-3-642-85829-1_2
Schmale, D. G., Bergstrom, G. C., & Shields, E. J. (2006). Night-time spore deposition of the fusarium head blight pathogen, Gibberella zeae, in rotational wheat fields. *Canadian Journal of Plant Pathology*. https://doi.org/10.1080/07060660609507276

Schneider, K., Kulosa, D., Soerensen, T. R., Möhring, S., Heine, M., Durstewitz, G., … Ganal, M. (2007). Analysis of DNA polymorphisms in sugar beet (Beta vulgaris L.) and development of an SNP-based map of expressed genes. *Theoretical and Applied Genetics*. https://doi.org/10.1007/s00122-007-0591-4

Schneller, J., Gerber, H., & Zuppiger, A. (2008). Speed and force of spore ejection in Selaginella martensii. *Botanica Helvetica*. https://doi.org/10.1007/s00035-008-0814-6

Schwessinger, B. (2016). Fundamental wheat stripe rust research in the 21st century. *New Phytologist*, 1625–1631. https://doi.org/10.1111/nph.14159

Seeb, J. E., Carvalho, G., Hauser, L., Naish, K., Roberts, S., & Seeb, L. W. (2011). Single-nucleotide polymorphism (SNP) discovery and applications of SNP genotyping in nonmodel organisms. *Molecular Ecology Resources*. https://doi.org/10.1111/j.1755-0998.2010.02979.x

Seigneur, C. (2019). Atmospheric Dispersion. In C. Seigneur (Ed.), *Air Pollution: Concepts, Theory, and Applications* (pp. 95–124). Cambridge: Cambridge University Press. https://doi.org/DOI: 10.1017/9781108674614.006

Selvaraj, M. G., Vergara, A., Ruiz, H., Safari, N., Elayabalan, S., Ocimati, W., & Blomme, G. (2019). AI-powered banana diseases and pest detection. *Plant Methods*. https://doi.org/10.1186/s13007-019-0475-z

Semagn, K., Babu, R., Hearne, S., & Olsen, M. (2014). Single nucleotide polymorphism genotyping using Kompetitive Allele Specific PCR (KASP): Overview of the technology and its application in crop improvement. *Molecular Breeding*. https://doi.org/10.1007/s11032-013-9917-x

Sethy, P. K., Negi, B., Barpanda, N. K., Behera, S. K., & Rath, A. K. (2018). Measurement of disease severity of rice crop using machine learning and computational intelligence. In *SpringerBriefs in Applied Sciences and Technology*. https://doi.org/10.1007/978-981-10-6698-6_1

Shah, D. A., Paul, P. A., De Wolf, E. D., & Madden, L. V. (2019). Predicting plant disease epidemics from functionally represented weather series. *Philosophical Transactions of the Royal Society B: Biological Sciences*. https://doi.org/10.1098/rstb.2018.0273

Sharma-Poudyal, D., Chen, X., & Rupp, R. A. (2014). Potential oversummering and overwintering regions for the wheat stripe rust pathogen in the contiguous United States. *International Journal of Biometeorology*, *58*(5), 987–997. https://doi.org/10.1007/s00484-013-0683-6

Shaw, R. H., & Pereira, A. R. (1982). Aerodynamic roughness of a plant canopy: A numerical experiment. *Agricultural Meteorology*. https://doi.org/10.1016/0002-1571(82)90057-7

Shirasawa, K., Isobe, S., Hirakawa, H., Asamizu, E., Fukuoka, H., Just, D., … Tabata, S. (2010). SNP discovery and linkage map construction in cultivated tomato. *DNA Research*. https://doi.org/10.1093/dnares/dsq024

Silva Junior, G. J., Scapin, M. da S., Silva, F. P., Silva, A. R. P., Behlau, F., & Ramos, H. H. (2016). Spray volume and fungicide rates for citrus black spot control based on tree canopy volume. *Crop Protection*. https://doi.org/10.1016/j.cropro.2016.03.014

Singh, A., Ganapathysubramanian, B., Singh, A. K., & Sarkar, S. (2016). Machine Learning for High-Throughput Stress Phenotyping in Plants. *Trends in Plant*

Science. https://doi.org/10.1016/j.tplants.2015.10.015
Singh, K., Wegulo, S. N., Skoracka, A., & Kundu, J. K. (2018). Wheat streak mosaic virus: a century old virus with rising importance worldwide. *Molecular Plant Pathology*. https://doi.org/10.1111/mpp.12683
Singh, N., Choudhury, D. R., Singh, A. K., Kumar, S., Srinivasan, K., Tyagi, R. K., … Singh, R. (2013). Comparison of SSR and SNP markers in estimation of genetic diversity and population structure of Indian rice varieties. *PLoS ONE*. https://doi.org/10.1371/journal.pone.0084136
Singh, R., Mahmoudpour, A., Rajkumar, M., & Narayana, R. (2017). A review on stripe rust of wheat, its spread, identification and management at field level. *Research on Crops*. https://doi.org/10.5958/2348-7542.2017.00091.2
Singh, R P, Huerta-Espino, J., & Roelfs, A. P. (2002). The wheat rusts. Retrieved from http://www.fao.org/docrep/006/Y4011E/y4011e0g.htm
Singh, Ravi P., Hodson, D. P., Huerta-Espino, J., Jin, Y., Bhavani, S., Njau, P., … Govindan, V. (2011). The Emergence of Ug99 Races of the Stem Rust Fungus is a Threat to World Wheat Production. *Annual Review of Phytopathology*. https://doi.org/10.1146/annurev-phyto-072910-095423
Singh, Ravi P., Hodson, D. P., Huerta-Espino, J., Jin, Y., Njau, P., Wanyera, R., … Ward, R. W. (2008). Will Stem Rust Destroy the World's Wheat Crop? *Advances in Agronomy*. https://doi.org/10.1016/S0065-2113(08)00205-8
Singh, B. V. (1969). Studies on aecial development in rust fungi: Puccinia polliniae . *Canadian Journal of Botany*. https://doi.org/10.1139/b69-106
Skelsey, P., Holtslag, A. A. M., & van der Werf, W. (2008). Development and validation of a quasi-Gaussian plume model for the transport of botanical spores. *Agricultural and Forest Meteorology*. https://doi.org/10.1016/j.agrformet.2008.04.006
Skelsey, Peter, Rossing, W. a H., Kessel, G. J. T., & van der Werf, W. (2010). Invasion of Phytophthora infestans at the landscape level: how do spatial scale and weather modulate the consequences of spatial heterogeneity in host resistance? *Phytopathology*, *100*(11), 1146–1161. https://doi.org/10.1094/PHYTO-06-09-0148
Sørensen, C., Hovmøller, M., Leconte, M., Dedryver, F., & de Vallavieille-Pope, C. (2014). New races of Puccinia striiformis found in Europe reveal race-specificity of long-term effective adult plant resistance in wheat. *Phytopathology*, *2011*, 1–37. https://doi.org/10.1094/PHYTO-12-13-0337-R
Spiers, A. G. (1985). Factors affecting basidiospore release by Chondrostereum purpureum in New Zealand. *European Journal of Forest Pathology*. https://doi.org/10.1111/j.1439-0329.1985.tb00874.x
Spijkerboer, H. P., Beniers, J. E., Jaspers, D., Schouten, H. J., Goudriaan, J., Rabbinge, R., & van der Werf, W. (2002). Ability of the Gaussian plume model to predict and describe spore dispersal over a potato crop. *Ecological Modelling*, *155*(1), 1–18. https://doi.org/10.1016/S0304-3800(01)00475-6
Spijkerboer, H. P., Beniers, J. E., Jaspers, D., Schouten, H. J., Goudriaan, J., Rabbinge, R., & Van Der Werf, W. (2002). Ability of the Gaussian plume model to predict and describe spore dispersal over a potato crop. *Ecological Modelling*. https://doi.org/10.1016/S0304-3800(01)00475-6
Stakman, E. C., Henry, A. W., Curran, G. C., & Christopher, W. N. (1923). Spores in the

Upper Air. *Scientific American*. https://doi.org/10.1038/scientificamerican0824-108a
Stamatakis, A. (2006). RAxML-VI-HPC: Maximum likelihood-based phylogenetic analyses with thousands of taxa and mixed models. *Bioinformatics*. https://doi.org/10.1093/bioinformatics/btl446
Stanaway, M. A., Mengersen, K. L., & Reeves, R. (2011). Hierarchical Bayesian modelling of early detection surveillance for plant pest invasions. *Environmental and Ecological Statistics*. https://doi.org/10.1007/s10651-010-0152-x
Stępalska, D., & Wołek, J. (2009). Intradiurnal periodicity of fungal spore concentrations (Alternaria, Botrytis, Cladosporium, Didymella, Ganoderma) in Cracow, Poland. *Aerobiologia*. https://doi.org/10.1007/s10453-009-9137-3
Stolze-rybczynski, J. L., Cui, Y., Stevens, M. H. H., Davis, D. J., Fischer, M. W. F., & Money, N. P. (2009). Adaptation of the Spore Discharge Mechanism in the Basidiomycota, *4*(1), 1–6. https://doi.org/10.1371/journal.pone.0004163
Stukenbrock, E. H., & McDonald, B. A. (2008). The origins of plant pathogens in agro-ecosystems. *Annual Review of Phytopathology*. https://doi.org/10.1146/annurev.phyto.010708.154114
Su, J., Liu, C., Coombes, M., Hu, X., Wang, C., Xu, X., … Chen, W. H. (2018). Wheat yellow rust monitoring by learning from multispectral UAV aerial imagery. *Computers and Electronics in Agriculture*. https://doi.org/10.1016/j.compag.2018.10.017
Subba Rao, K. V., Snow, J. P., & Berggren, G. T. (1989). Effect of Growth Stage and Initial Inoculum Level on Leaf Rust Development and Yield Loss Caused by Puccinia recondita f. sp. tritici. *Journal of Phytopathology*. https://doi.org/10.1111/j.1439-0434.1989.tb01130.x
Sundberg, S. (2010). Size matters for violent discharge height and settling speed of Sphagnum spores: Important attributes for dispersal potential. *Annals of Botany*. https://doi.org/10.1093/aob/mcp288
Tan, C. T., Assanga, S., Zhang, G., Rudd, J. C., Haley, S. D., Xue, Q., … Liu, S. (2017). Development and validation of kasp markers for wheat streak mosaic virus resistance gene wsm2. *Crop Science*. https://doi.org/10.2135/cropsci2016.04.0234
Teng, P. S., Blackie, M. J., & Close, R. C. (1978). Simulation modelling of plant diseases to rationalize fungicide use. *Outlook on Agriculture*. https://doi.org/10.1177/003072707800900603
Thach, T., Ali, S., de Vallavieille-Pope, C., Justesen, A. F., & Hovmøller, M. S. (2016). Worldwide population structure of the wheat rust fungus Puccinia striiformis in the past. *Fungal Genetics and Biology*, *87*. https://doi.org/10.1016/j.fgb.2015.12.014
Thiessen, L. D., Neill, T. M., & Mahaffee, W. F. (2017). Timing fungicide application intervals based on airborne erysiphe necator concentrations. *Plant Disease*. https://doi.org/10.1094/PDIS-12-16-1727-RE
Thrall, P. H., & Burdon, J. J. (2003). Evolution of virulence in a plant host-pathogen metapopulation. *Science*. https://doi.org/10.1126/science.1080070
Tian, Y., Meng, Y., Zhao, X., Chen, X., Ma, H., Xu, S., … Zhan, G. (2019). Trade-Off Between Triadimefon Sensitivity and Pathogenicity in a Selfed Sexual Population of Puccinia striiformis f. sp. Tritici. *Frontiers in Microbiology*.

https://doi.org/10.3389/fmicb.2019.02729
Tischendorf, L., & Fahrig, L. (2000). On the usage and measurement of landscape connectivity. *Oikos*. https://doi.org/10.1034/j.1600-0706.2000.900102.x
Trail, F. (2007). Fungal cannons: Explosive spore discharge in the Ascomycota. *FEMS Microbiology Letters*. https://doi.org/10.1111/j.1574-6968.2007.00900.x
Trail, F., Gaffoor, I., & Vogel, S. (2005). Ejection mechanics and trajectory of the ascospores of Gibberella zeae (anamorph Fuarium graminearum). *Fungal Genetics and Biology*, *42*(6), 528–533.
Truxall, D. L., Travis, J. W., & Hickey, K. D. (1995). Effect of temperature and wetness on infection of black raspberry by aeciospores of Arthuriomyces peckianus. *Plant Disease*. https://doi.org/10.1094/PD-79-0805
Turner, D. B. (1970). Workbook of atmospheric dispersion estimates. US Department of Health, Education, and Welfare. *Environmental Health Service, Cincinnati, OH*.
Tuthill, J. (2005). Evaluating the explosive spore discharge mechanism of Pilobolus Crystallinus using mechanical measurements and mathematical modeling. *Biomechanics*.
van den Bosch, F., & Gilligan, C. A. (2008). Models of Fungicide Resistance Dynamics. *Annual Review of Phytopathology*. https://doi.org/10.1146/annurev.phyto.011108.135838
van Maanen, A., & Xu, X.-M. (2003). Modelling Plant Disease Epidemics. *European Journal of Plant Pathology*. https://doi.org/10.1023/A:1026018005613
van Niekerk, J. M., Calitz, F. J., Halleen, F., & Fourie, P. H. (2010). Temporal spore dispersal patterns of grapevine trunk pathogens in South Africa. *European Journal of Plant Pathology*. https://doi.org/10.1007/s10658-010-9604-2
Viljanen-Rollinson, S. L. H., Parr, E. L., & Marroni, M. V. (2007). Monitoring long-distance spore dispersal by wind-a review. *New Zealand Plant Protection*.
Vogel, S. (2005). Living in a physical world II. The bio-ballistics of small projectiles. *Journal of Biosciences*, *30*(2), 167–175.
Wahyuno, D., Kakishima, M., & Ono, Y. (2002). Aeciospore-surface structures of Phragmidium species parasitic on roses. *Mycoscience*. https://doi.org/10.1007/S102670200023
Wan, A., Zhao, Z., Chen, X., He, Z., Jin, S., Jia, Q., … Yuan, Z. (2004). Wheat Stripe Rust Epidemic and Virulence of Puccinia striiformis f. sp. tritici in China in 2002. *Plant Disease*, *88*(8), 896–904. https://doi.org/10.1094/PDIS.2004.88.8.896
Wang, G., Sun, Y., & Wang, J. (2017). Automatic Image-Based Plant Disease Severity Estimation Using Deep Learning. *Computational Intelligence and Neuroscience*. https://doi.org/10.1155/2017/2917536
Wang, M. N., Wan, A. M., & Chen, X. M. (2015). Barberry as alternate host is important for puccinia graminis f. Sp. Tritici but not for puccinia striiformis f. Sp. Tritici in the U.S. Pacific Northwest. *Plant Disease*. https://doi.org/10.1094/PDIS-12-14-1279-RE
Waring, P. (2004). Successes in conserving the Barberry Carpet moth Pareulype berberata (D. & S.) (Geometridae) in England. *Journal of Insect Conservation*. https://doi.org/10.1007/s10841-004-1341-4
Wellings, C. R. (2007). Puccinia striiformis in Australia: A review of the incursion, evolution, and adaptation of stripe rust in the period 1979-2006. In *Australian*

Journal of Agricultural Research. https://doi.org/10.1071/AR07130
Wellings, Colin R. (2011). Global status of stripe rust: A review of historical and current threats. *Euphytica*, *179*(1), 129–141. https://doi.org/10.1007/s10681-011-0360-y
West, J. S., Fitt, B. D. L., Leech, P. K., Biddulph, J. E., Huang, Y. J., & Balesdent, M. H. (2002). Effects of timing of Leptosphaeria maculans ascospore release and fungicide regime on phoma leaf spot and phoma stem canker development on winter oilseed rape (Brassica napus) in southern England. *Plant Pathology*. https://doi.org/10.1046/j.1365-3059.2002.00726.x
West, Jon S., Townsend, J. A., Stevens, M., & Fitt, B. D. L. (2012). Comparative biology of different plant pathogens to estimate effects of climate change on crop diseases in Europe. *European Journal of Plant Pathology*, *133*(1), 315–331. https://doi.org/10.1007/s10658-011-9932-x
West, Jonathan S., Bravo, C., Oberti, R., Lemaire, D., Moshou, D., & McCartney, H. A. (2003). The Potential of Optical Canopy Measurement for Targeted Control of Field Crop Diseases. *Annual Review of Phytopathology*. https://doi.org/10.1146/annurev.phyto.41.121702.103726
Weston, W. H. (1923). Production and dispersal of conidia in the Philippine Sclerosporas of maize. *J. Agr. Res*, *23*, 239–277.
Wharton, P. S., Kirk, W. W., Baker, K. M., & Duynslager, L. (2008). A web-based interactive system for risk management of potato late blight in Michigan. *Computers and Electronics in Agriculture*. https://doi.org/10.1016/j.compag.2007.10.002
White, J. K. A., & Gilligan, C. A. (2006). The role of initial inoculum on epidemic dynamics. *Journal of Theoretical Biology*. https://doi.org/10.1016/j.jtbi.2006.04.004
Wilson, R., Dini, D., & Van Wachem, B. (2017). The influence of surface roughness and adhesion on particle rolling. *Powder Technology*. https://doi.org/10.1016/j.powtec.2017.01.080
Wulft, B. B. H., & Moscou, M. J. (2014). Strategies for transferring resistance into wheat: From wide crosses to GM cassettes. *Frontiers in Plant Science*. https://doi.org/10.3389/fpls.2014.00692
Xu, C. Y., Griffin, K. L., & Schuster, W. S. F. (2007). Leaf phenology and seasonal variation of photosynthesis of invasive Berberis thunbergii (Japanese barberry) and two co-occurring native understory shrubs in a northeastern United States deciduous forest. *Oecologia*. https://doi.org/10.1007/s00442-007-0807-y
Xu, X. M., & Ridout, M. S. (1998). Effects of initial epidemic conditions, sporulation rate, and spore dispersal gradient on the spatio-temporal dynamics of plant disease epidemics. *Phytopathology*. https://doi.org/10.1094/PHYTO.1998.88.10.1000
Xu, X. M., & Ridout, M. S. (2000). Stochastic simulation of the spread of race-specific and race-nonspecific aerial fungal pathogens in cultivar mixtures. *Plant Pathology*. https://doi.org/10.1046/j.1365-3059.2000.00444.x
Xue, A. G., Chi, D. T., Shu-zhen, Z., & Zuo-fu, L. (2012). Wheat Production and Wheat Rust Management in Canada. *Journal of Northeast Agricultural University (English Edition)*, *19*(1), 1–14. https://doi.org/10.1016/S1006-

8104(12)60032-4
Yafetto, L., Carroll, L., Cui, Y., Davis, D. J., Fischer, M. W. F., Henterly, A. C., … Money, N. P. (2008). The fastest flights in nature: High-speed spore discharge mechanisms among fungi. *PLoS ONE*. https://doi.org/10.1371/journal.pone.0003237
You, F. M., Deal, K. R., Wang, J., Britton, M. T., Fass, J. N., Lin, D., … Dvorak, J. (2012). Genome-wide SNP discovery in walnut with an AGSNP pipeline updated for SNP discovery in allogamous organisms. *BMC Genomics*. https://doi.org/10.1186/1471-2164-13-354
Zadoks, J. C. (1961). Yellow rust on wheat in epidemiology and physiologic specialization. *Tijdschrift Over Plantenziekten*. https://doi.org/10.1007/BF01984044
Zhang, X., Han, L., Dong, Y., Shi, Y., Huang, W., Han, L., … Sobeih, T. (2019). A deep learning-based approach for automated yellow rust disease detection from high-resolution hyperspectral UAV images. *Remote Sensing*. https://doi.org/10.3390/rs11131554
Zhao, J., Wang, M., Chen, X., & Kang, Z. (2016). Role of Alternate Hosts in Epidemiology and Pathogen Variation of Cereal Rusts. *Annual Review of Phytopathology*, *54*(1). https://doi.org/10.1146/annurev-phyto-080615-095851
Zhao, J., Zhao, S., Chen, X., Wang, Z., Wang, L., Yao, J., … Kang, Z. (2015). Determination of the role of berberis spp. in wheat stem rust in China. *Plant Disease*. https://doi.org/10.1094/PDIS-09-14-0928-RE
Zhao, L., Schaefer, D., & Marten, M. R. (2005). Assessment of elasticity and topography of Aspergillus nidulans spores via atomic force microscopy. *Applied and Environmental Microbiology*. https://doi.org/10.1128/AEM.71.2.955-960.2005
Zwetko, P., & Blanz, P. (2012). Aeciospore types in rusts on Ranunculus and allied genera, *96*, 105–121.

Chapter 6 Annexe

6.1 Lubrication model for aeciospore release

The aeciospore release mechanism will be modelled as shown in (**Figure 6.1 A**), where an aeciospore, surrounded by neighbouring spores, will expand after hydration. This expansion in aeciospore volume after water intake will decrease the interspore gap which will intensify the lubrication force. For mathematical simplicity, this squeezing shut of the interspore gap will be modelled by assuming that the sides of the aeciospores remain parallel or in a fixed orientation so that the distance between the spore and the wall is purely a function of time, i.e. it is independent of *x*. In this way the angle between the walls, α, is assumed to be constant. During squeezing, the aeciospore pushes on the film creating a strong lubrication force in the direction normal to the wall. Since the walls are inclined, this generates a component of force in the direction of the axis of symmetry. The aeciospore is thus propelled forwards in the positive *x* direction (**Figure 6.1 A**). The z axis is the axis of symmetry (**Figure 6.1 B**), so that the walls are located at

$$z = \pm \tan \propto$$

We assume that the gap between the aeciospore and the walls of the neighbouring aeciospores is small so that the lubrication theory can be used. Let the aeciospore occupy the portion of the *z* axis covering $0 \le z \le L$ at $t=0$. Let *h(x,t)* be the gap between the aeciospore and the walls, assumed uniform (i.e. it does not depend on *z*). The Reynolds lubrication equation can then be applied here

$$\frac{1}{12\mu}(h^3 p_z)_z = V^{(n)} - \frac{1}{2}V^{(t)}h_z \qquad (1)$$

where

- *p(z,t)* is the pressure in the liquid film
- $V^{(n)}$ is the velocity of the spore in the *y* direction (90º to the wall)
- $V^{(t)}$ is the velocity of the spore in the *x* direction
- μ is the dynamic viscosity of the liquid in the film, assumed to be water

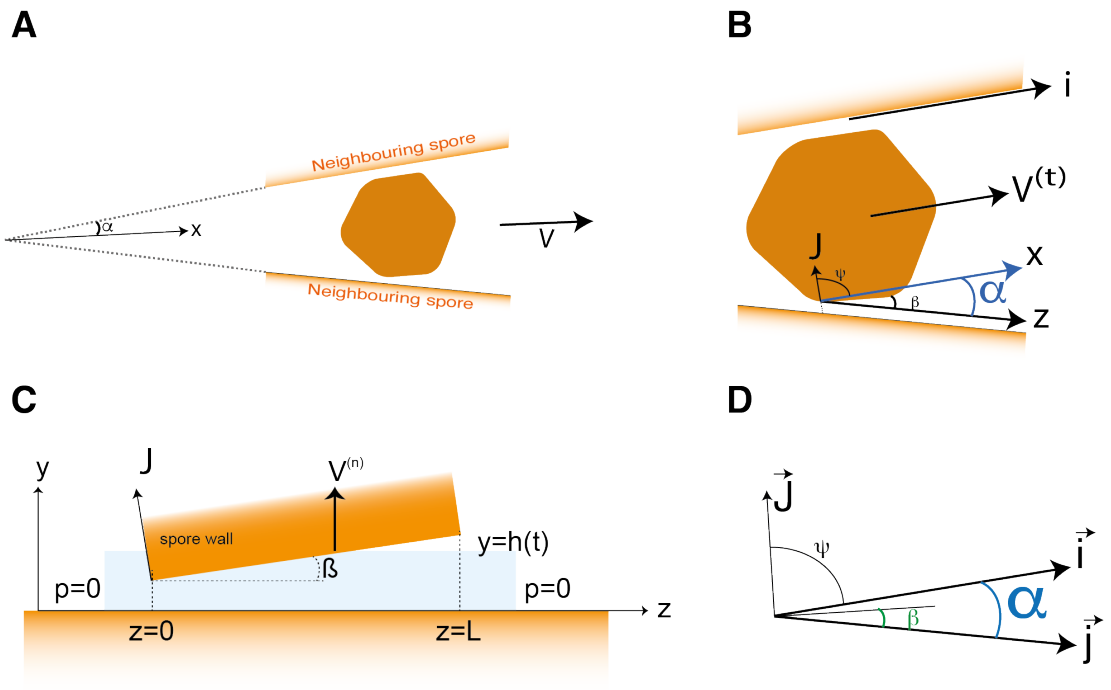

Figure 6.1. Description of the *Pg* aeciospore release model. (A) Aeciospores are surrounded by neighbouring spores, forming an angle of a between their direction of release and the neighbouring aeciospore wall. **(B)** There is a force in the **J** direction acting on the spore. **(C)** At z=0, L; p=0 (i.e. atmospheric pressure). The wall of the modelled aeciospore is in an angle b with respect to the wall of the neighbouring aeciospore. **(D)** The vector **J** indicates the direction of the force that acts on the aeciospore and that will force it to be released in the *i* direction.

The equation describing the edge of the aeciospore would be

$$h(z,t) = H(t) + z\tan\beta, \qquad 0 \le z \le L \tag{2}$$

assuming that β remains constant during the motion and restricted to the range

$$0 < \beta < \frac{\pi}{2}$$

It must be that case that $h_t = H_t = V^{(n)}$ and that $X_t = V^{(t)}$, where $x = X(t)$ is the location of the centre of mass of the aeciospore. So (1) becomes

$$\frac{1}{12\mu}(h^3 p_z)_z = H_t - \frac{1}{2}X_t\tan\beta \tag{3}$$

Integrating with respect to z twice, substituting $h(z, t)$ from (2) and assuming that p is zero (i.e. atmospheric pressure) at z=0, L (**Figure 6.1 C**), we obtain

$$p = -\frac{12\mu}{(2H + L\tan\beta)}\frac{z(L-z)}{(H + z\tan\beta)^2}\left(H_t - \frac{1}{2}X_t\tan\beta\right) \tag{4}$$

We now compute the pressure force per unit length (in the transverse direction, i.e. into the paper) on the aeciospore in the *y* direction normal to the wall. The magnitude of this force per unit length is given by

$$f = \int_0^L p\, dz = \frac{12\mu}{\tan^3\beta} g(\omega)\left(H_t - \frac{1}{2}X_t \tan\beta\right) \tag{5}$$

where

$$g(\omega) = \log(1+\omega) - \frac{2\omega}{(2+\omega)}, \qquad \omega = \frac{L}{H}\tan\beta \tag{6}$$

Note that from (2), in order for $H \geq 0$ everywhere, we need

$$H + L\tan\beta > 0 \quad \rightarrow \qquad -1 < \omega < \infty \tag{7}$$

Thus, the function $g(\omega)$ will have the form shown in **Figure 6.2.**

The force per unit length calculated here (5) is defined as the vector J, whose magnitude is $|\mathbf{J}| = f$. We are interested in finding the component of **J** in the *x* direction, that is along the axis of symmetry (**Figure 6.1 A**). This component is given by

$$\boldsymbol{J} \cdot \boldsymbol{i} = |\boldsymbol{J}| \cos\psi$$

where ψ is the angle between **J** and **i** (**Figure 6.1 D**), and $\psi = \pi/2 - (\alpha - \beta)$. Thus

$$\boldsymbol{J} \cdot \boldsymbol{i} = |\boldsymbol{J}| \cos\psi = f\cos\left(\frac{\pi}{2} - (\alpha - \beta)\right) = f\sin(\alpha - \beta)$$

The equation (5) represents the force per unit length, but we are interested in knowing the force acting on the entire surface of the aeciospore. Assuming that the cuboid aeciospore extends for a length λ in the transverse direction, the total magnitude of force on one side of the aeciospore acting in the *x* direction is then

$$F = f\lambda\sin(\alpha - \beta) \tag{8}$$

The parameter λ represents the length of the aeciospore, while *L* previously defined in (**2**) can then be used to represent an individual aeciospore or a row of spores. Both parameters are thus kept separated so we can vary *L* without varying the extent of a single spore in the transversal direction.

Using (**6**) we write the previous expression (**8**) as

$$F = -\frac{12\mu\lambda}{\tan^3\beta} g(\omega)\sin(\alpha - \beta)\left(H_t - \frac{1}{2}X_t\tan\beta\right) \tag{9}$$

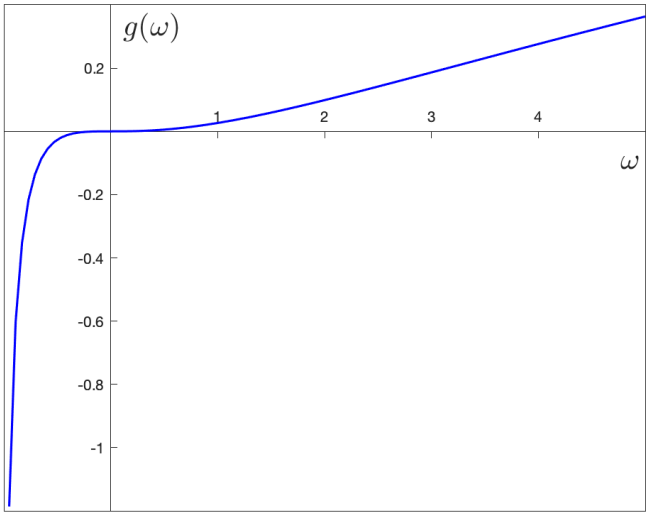

Figure 6.2. Function g (ω) defined in (6) over the allowable range [-1, ∞] (7). The value of g (ω) varies from -∞ when ω ⟶ -1, up to +∞ when ω ⟶ ∞. The value of g (ω) is close to 0 when ω is near 0.

Assuming that the cuboid spore has four of its faces pressurised by the neighbouring spores, Newton's second law can be applied to obtain

$$4F = mX_{tt}$$

where m is the mass of the spore. Substituting for F from (**9**) we obtain the differential equation for the spore's centre of mass,

$$X_{tt} = 4\frac{F}{m} = 4m^{-1}\left[\frac{12\mu\lambda}{\tan^3\beta}g(\omega)\sin(\beta-\alpha)\left(H_t - \frac{1}{2}X_t\tan\beta\right)\right]$$

Thus

$$X_{tt} = 4m^{-1}ag(\omega)\sin(\beta-\alpha)\,H_t - 4m^{-1}ag(\omega)\sin(\beta-\alpha)\frac{1}{2}X_t\tan\beta$$

Rearranging the terms, we can write the above equation as

$$X_{tt} + AX_t - B(t) = 0\,, \qquad (10)$$

where

$$A = -\frac{24\mu\lambda}{m}\frac{\sin(\beta-\alpha)}{tan^2\beta}g(\omega), \qquad B(t) = \frac{48\mu\lambda}{m}(-H_t)\left(\frac{g(\omega)}{tan^3\beta}\right)\sin(\alpha-\beta)$$

The terms in the curved brackets in *B(t)* are both positive since ($H_t < 0$).

The value of β will determine whether the aeciospore side is parallel to the neighbouring aeciospore (if β = 0) or not (β ≠ 0), as shown in **Figure 6.3**. Thus, we will examine both possibilities in the two following sections.

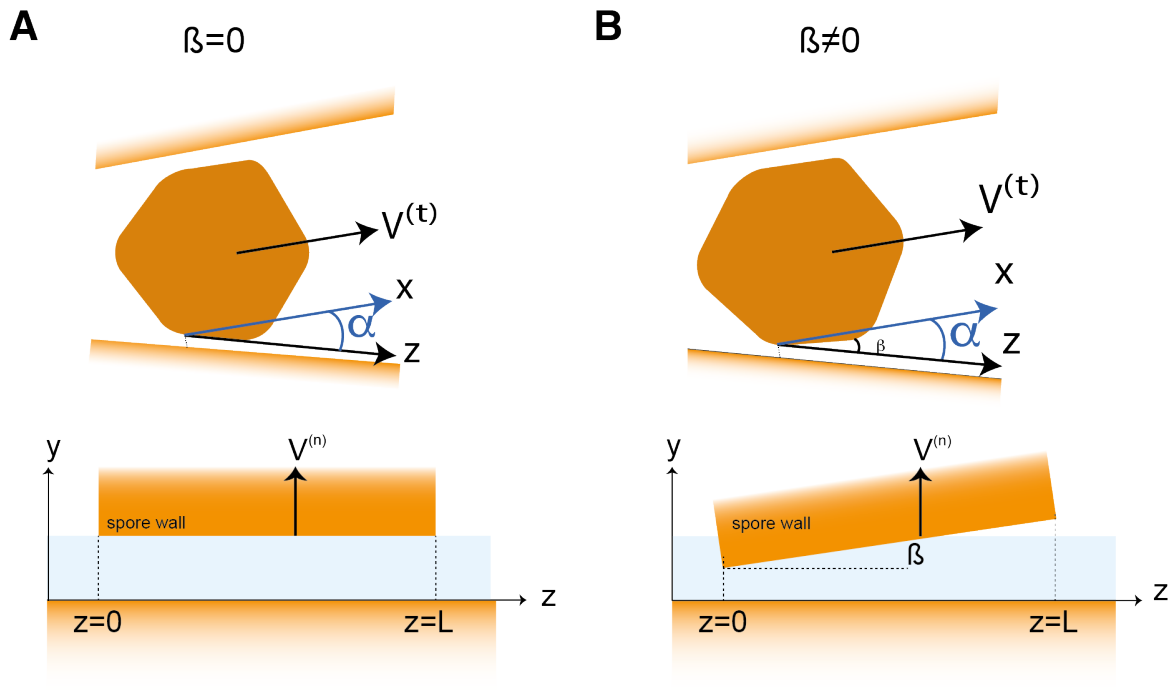

Figure 6.3. The value of b will determine the position of the aeciospore wall regarding its neighbouring spore. (A) If β = *0*, the wall of the aeciospore will be parallel to the *z* axis. **(B)** If β ≠*0*, the aeciospore wall will be inclined with respect to *z* in an angle β.

6.1.1 Predictions when β = 0

When β = 0, the term A=0 and equation (10) reduces to the following form

$$X_{tt} = -\frac{4\mu\lambda L^3}{m}\frac{H_t}{H^3}\sin\alpha$$

Integrating the above equation, we can get an expression for the spore speed

$$X_t = \frac{\gamma}{m}\left(\frac{1}{H^2} - \frac{1}{H_0^2}\right), \qquad (11)$$

where $\gamma = 2\mu\lambda L^3\sin\alpha$, and $H_0 = H(0)$ is the initial gap before the spore starts moving.

The formula from (**11**) assumes that the aeciospore is at rest at $t = 0$. This expression applies regardless of the particular form of $H(t)$, i.e., the way in which the gap closes is irrelevant.

To get an expression for the location of the aeciospore at any time *t*, we must integrate (**11**). To do so, we assume *H(t)* to take the simplest possible form

$$H(t) = H_0(1 - \delta t),$$

which implies that the gap closes linearly in time, with δ being the rate at which the gap closes. Hence, using the above expression, we can integrate (**11**) to obtain

$$X(t) = \frac{\gamma}{mH_0^2}\left(\frac{\delta t^2}{1 - \delta t}\right), \qquad (12)$$

assuming *X(0)* = 0.

We want to estimate the aeciospore velocity after travelling the distance required to exit the aecial cup. Defining the distance travelled as *D*, then the aeciospore would leave the aecial-cup at time *t = T,* where *T* satisfies the quadratic equation:

$$\delta T^2 + \nu\delta T - \nu = 0$$

where ν = $mDH_0^2\gamma$. This can be solved to find T and then substituting in the following expression to calculate the speed of the spore at the point of ejection:

$$V = X_t(T) = \frac{\gamma}{m}\left(\frac{1}{H(T)^2} - \frac{1}{H_0^2}\right)$$

The ejection velocities predicted, using different values of D, are lower than the observed velocities using the HS camera (**Figure 6.4**). Velocities observed with HS videography ranged from 0.1-0.7, with the average around 0.2 m/s, as shown in Chapter 2, section **2.4.1**. This indicates that if we assume β = 0, the model does not fit our observations.

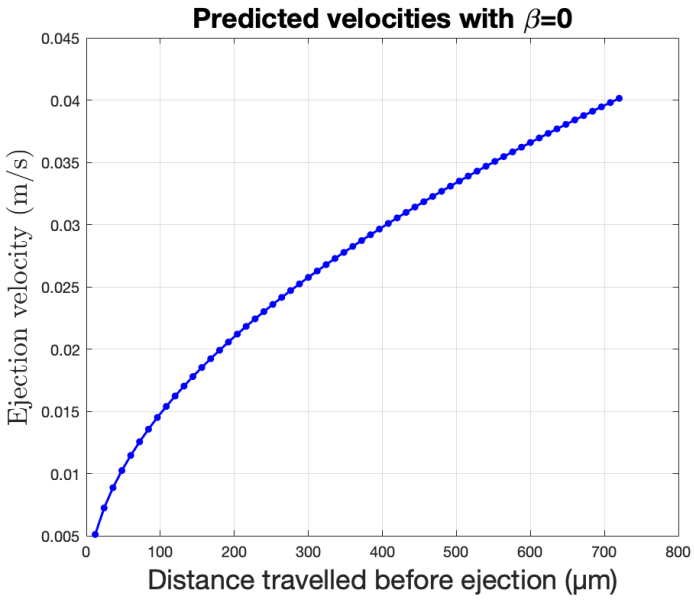

Figure 6.4. Predicted velocities when β=0. Velocities were estimated using the parameters from **Table 6.1**, with a value of α = 0.2. The ejection velocity estimated remains bellow 0.045 m/s for values of D up to 800 μm.

6.1.2 Predictions when β ≠ 0

When β ≠0, A≠0 and thus, we must consider the first term (-AX_t) in (9). This term represents an additional acceleration effect resulting from the spore edge not being parallel to the wall. To get a higher predicted ejection velocity, the term -AX_t must be greater than zero. Thus

$$-AX_t = \frac{24\mu\lambda}{m}\frac{\sin(\beta-\alpha)}{tan^2\beta}g(\omega)X_t > 0$$

Since $X_t > 0$, in order for -AX_t to be greater than zero, we need

$$\sin(\beta-\alpha)\,g(\omega) > 0 \qquad (13)$$

The description of the function g(ω) indicates that g > 0 when ω > 0 (**Figure 6.2**), and thus when β > 0, since

$$\omega = \frac{L}{H}\tan\beta,$$

as indicated in (**6**). Therefore, to meet the condition in (**13**), either (i) α > 0 and β > α, or (ii) α < 0 and β < 0. The latter requires α < 0 which is physically nonsensical, and hence, for an additional positive acceleration effect, we need

$$\alpha > 0 \quad \text{and} \quad \beta > \alpha$$

As long as both of these conditions hold, the aeciospore will be accelerated more than if it were parallel to the wall.

To identify the important scales in the problem, we carry out a dimensional analysis. The parameters included in the model have the following dimensions,

$$[\lambda] = L, \qquad [h_0] = L, \qquad [\mu] = ML^{-1}T^{-1}, \qquad [\rho] = ML^{-3}, \qquad [\delta] = T^{-1}$$

Where M, L and T represent fundamental units of mass, length and time.

Combining these parameters, it is possible to identify two important timescales in the problem

$$\tau_1 = \frac{1}{\delta} \quad \text{and} \quad \tau_2 = \left(\frac{\lambda^2 \rho}{\mu}\right)$$

The first one, τ_1, is the timescale on which the gap between the aeciospore and the wall closes. Using the values from **Table 6.1**, we calculate

$$\tau_1 = 1.85 \text{ s} \quad \text{and} \quad \tau_2 = 1.42 \text{ x } 10^{-4} \text{s}$$

In this model, the aeciospore is assumed to be a cube of dimension λ with its mass given by

$$m = \rho\lambda^3,$$

where ρ is the density of the aeciospore.

The computer programming software Matlab determines the speed of the aeciospore once it has travelled a certain distance, X* after a time t* has elapsed. In particular, the release velocity is calculated when

$$X^* = n\lambda$$

for an integer n, that represents the number of aeciospore lengths (i.e. λ) that the aeciospore has travelled before exiting the aecial cup. Based on observation from videography, n is expected to be small, with a maximum of 2 or 3. Once the aeciospore has travelled a distance X*, the time that has elapsed, t*, is on the order of few τ_2 units, and it is only a very small fraction of τ_1 units (typically 10^{-4}). Thus, it can be concluded that τ_2 is the important time scale for the aeciospore ejection. Furthermore, while it is the squeezing effect due to aeciospore rounding-off after water absorption that accelerates the aeciospore, by the time of ejection the initial gap h_0 has only closed by a very small amount.

Table 6.1. Physical values included in the aeciospore release model. The value of ρ has been extracted from (Pasquill, 1962). The values of H_0 and λ have been estimated from SEM images and the value of δ from videography from Chapter 2 **(2.4.7)**. Values for α,β need to be estimated (TBC: To Be Confirmed).

Parameter	Value	Parameter	Value
μ	8.9 x 10^{-4} Pa s	ρ	882 kg m^{-3}
d	0.46 µm/s	λ	12 x 10^{-6} m
H_0	2 x 10^{-6} m	α, β	TBC

6.1.2.1 Velocity calculations

Using Matlab, with the in-built ode integrator ode45, the following equation is solved,

$$X_{tt} = -AX_t + B(t)$$

assuming that the aeciospore starts at rest at X=0 and time t=0, i.e.:

$$X(0) = 0, \qquad X_t(0) = 0$$

In the numerical calculation, for the known parameters (μ, ρ, δ, λ, H_0), the values from **Table 6.1** are used. The values of μ and ρ has been extracted from the literature (Pasquill, 1962) and the values of H_0 and λ have been estimated from SEM images. The value of δ was estimated from videos as indicated in Chapter 2 (**section 2.4.6**). The value of α and β are difficult to estimate and thus a range of values are considered (**Figure 6.5**). As previously mentioned, to meet the condition from (12), α must be larger than β. However, the release velocity is not very sensitive to changes in α and β. Ejection speed would change depending on the values used, but estimated velocities remain within the range of observations (0.094 – 0.754 m/s).

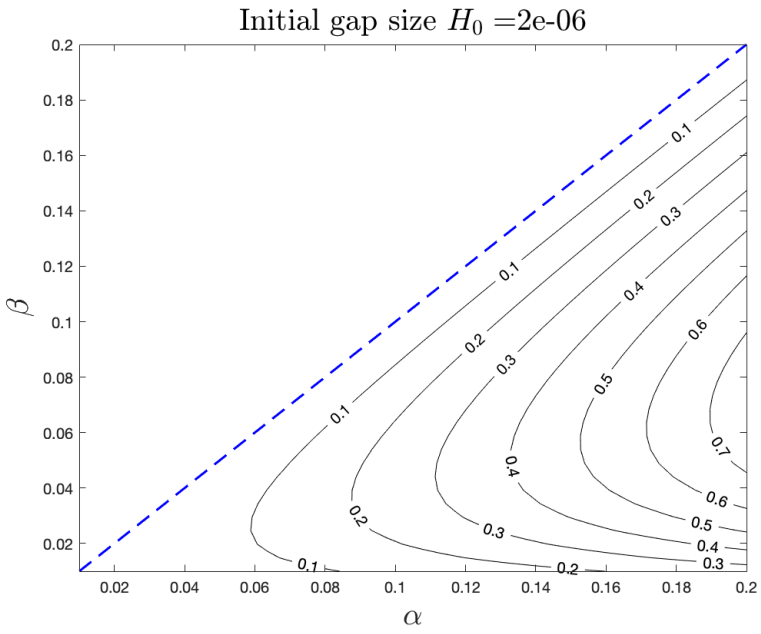

Figure 6.5 *Pg* aeciospore predicted velocity of release (m/s). Using a value of H_0= 2x10^{-6} m for the initial gap size between neighbouring aeciospores, the ejection velocities were estimated for different values of α and β, keeping in mind that α must always be greater than β. Values in the contour lines are given in m/s. The dashed blue line delineates the region where α> β. Predicted velocities were in the same range as observed using HS videography (0.1-0.7 m/s).

6.2 Estimation of the dry deposition rate

The inverse time scale (s^{-1}) of dry deposition that can be represented as (Aylor, 1999):

$$\Gamma_d = \sqrt{\frac{2}{\pi}} \left(\frac{v_s}{x}\right) \int_{x_0}^{x} \left[\frac{dx}{\sigma_z(x)}\right] \tag{14}$$

where v_s is the settling velocity of aeciospores and σ_z is the standard deviation of the spread of the plume in the z direction.

$$\int_{x_0}^{x} \left[\frac{dx}{\sigma_z(x)}\right] = \frac{dx}{\sigma_z(x)} = \int_{x_0}^{x} \frac{dx}{K(z_0)ax^b} \tag{15}$$

$$\int_{x_0}^{x} \frac{dx}{K(z_0)ax^b} = \int_{x_0}^{x} \frac{dx}{(10z_0)^{0.53x^{-0.22}}ax^b} = \frac{1}{a}\int_{x_0}^{x} \frac{dx}{(10z_0)^{0.53x^{-0.22}}x^b} \tag{16}$$

The integral that needs to be solved, thus, is:

$$\int \frac{dx}{(10z_0)^{0.53x^{-0.22}}x^b} = \int (10z_0)^{-0.53x^{-0.22}} x^{-b}\, dx \tag{17}$$

which can be solved by steps, with the following principle:

$$\int udv = u \times v - \int v\, du \tag{18}$$

where

$u = x^{-b} \quad \rightarrow \quad du = -bx^{-b-1}\, dx$

$dv = (10z_0)^{-0.53x^{-0.22}} dx \quad \rightarrow \quad v = \frac{(10z_0)^{-0.53x^{-0.22}}}{\ln(10z_0)\,(0.53 \times 0.22)x^{-0.22-1}}$

For simplicity, we will substitute the constants $10z_0$, 0.53 and 0.22 by *p*, *c*, and *q* respectively. Hence,

$$\int (p)^{-ax^{-b}} x^{-b}\, dx = x^{-b} \times \frac{(p)^{-cx^{-q}}}{\ln(p)\,(cq)x^{-q-1}} - \int \frac{(p)^{-cx^{-q}}}{\ln(p)\,(cq)x^{-q-1}} \times (-b)x^{-b-1} dx$$

$$= x^{-b} \times \frac{(p)^{-cx^{-q}}}{\ln(p)\,(cq)x^{-q-1}} + \frac{b}{\ln(p)\,(cq)} \int (p)^{-cx^{-q}} \times x^{q-b} dx$$

The principle from (**18**) can be used again to solve the integral:

$$\int (p)^{-cx^{-q}} \times x^{q-b} dx \tag{19}$$

Thus,

$u = (p)^{-cx^{-q}} \quad \rightarrow \quad du = \ln(p)\,(p)^{-cx^{-q}} cex^{-q-1}\, dx$

$dv = x^{q-b} dx \quad \rightarrow \quad v = \frac{x^{q-b+1}}{q-b+1}$

Using the above terms, we can solve integral (**19**) using (**18**):

$$\int (p)^{-cx^{-q}} \times x^{q-b} dx = (p)^{-cx^{-q}} \times \frac{x^{q-b+1}}{q-b+1} - \int \frac{x^{q-b+1}}{q-b+1} \ln(p)\,(p)^{-cx^{-q}} cqx^{-q-1}\, dx$$

$$= (p)^{-cx^{-q}} \times \frac{x^{q-b+1}}{q-b+1} - \frac{cq\ln(p)}{q-b+1} \int x^{-b}\,(p)^{-cx^{-q}}\, dx$$

The integral in the above expression is the same one that needed to be solved. Therefore:

$$\int (p)^{-cx^{-q}} x^{-b}\, dx =$$

$$= \frac{x^{q-b+1}\,(p)^{-cx^{-q}}}{\ln(p)\,(cq)}$$

$$+ \frac{b}{\ln(p)\,(cq)} \left[(p)^{-cx^{-q}} \times \frac{x^{q-b+1}}{q-b+1} - \frac{cq\ln(p)}{q-b+1} \int x^{-b}\,(p)^{-cx^{-q}}\, dx \right]$$

This can be simplified as

$$\int (p)^{-cx^{-q}} x^{-b}\, dx =$$

$$= \frac{x^{q-b+1}(p)^{-cx^{-q}}}{\ln(p)\,(cq)} + \frac{q\,(p)^{-cx^{-q}} x^{q-b+1}}{\ln(p)\,(cq)(q-b+1)}$$

$$- \frac{b}{\ln(p)\,(cq)} \frac{cq\ln(p)}{(q-b+1)} \int x^{-b}\ (p)^{-cx^{-q}}\, dx$$

$$= \frac{x^{q-b+1}(p)^{-cx^{-q}}}{\ln(p)\,(cq)} + \frac{q\,(p)^{-cx^{-q}} x^{q-b+1}}{\ln(p)\,(cq)(q-b+1)}$$

$$- \frac{b}{(q-b+1)} \int x^{-b}\ (p)^{-cx^{-q}}\, dx$$

$$= \frac{\left(x^{q-b+1}(p)^{-cx^{-q}}\right)(q-b+1) + \left(b\,(p)^{-cx^{-q}} x^{q-b+1}\right)}{\ln(p)\,(cq)(q-b+1)}$$

$$- \frac{b}{(q-b+1)} \int x^{-b}\ (p)^{-cx^{-q}}\, dx$$

Since the integral in the last factor is the same as the initial integrals, they can be grouped:

$$\int (p)^{-cx^{-q}} x^{-b}\, dx \left(1 + \frac{b}{(q-b+1)}\right)$$

$$= \frac{\left(x^{q-b+1}(p)^{-cx^{-q}}\right)(q-b+1) + \left(b(p)^{-cx^{-q}} x^{q-b+1}\right)}{\ln(p)\,(cq)(q-b+1)}$$

Thus,

$$\int (p)^{-cx^{-q}} x^{-b}\, dx \left(\frac{q-b+1+b}{(q-b+1)}\right) = \int (p)^{-cx^{-q}} x^{-b}\, dx \left(\frac{q+1}{(q-b+1)}\right)$$

$$= \frac{(p)^{-cx^{-q}} x^{q-b+1}(q-b+1) + b\,(p)^{-cx^{-q}} x^{q-b+1}}{\ln(p)\,(cq)(q-b+1)}$$

This expression can be simplified

$$\int (p)^{-cx^{-q}} x^{-b}\, dx \left(\frac{q+1}{(q-b+1)}\right) = \frac{(q-b+1+b)\,(p)^{-cx^{-q}} x^{q-b+1}}{\ln(p)\,(cq)(q-b+1)}$$

$$= \frac{(q+1)\,(p)^{-cx^{-q}} x^{q-b+1}}{\ln(p)\,(cq)(q-b+1)}$$

Resulting in

$$\int (p)^{-cx^{-q}} x^{-b}\, dx = \frac{(p)^{-cx^{-q}} x^{q-b+1}}{\ln(p)\,(cq)}$$

Placing the original values, we obtain

$$\int (10z_0)^{-0.53x^{-0.22}} x^{-q}\, dx = \frac{(10z_0)^{0.53x^{-0.22}} x^{0.22-b+1}}{\ln(10z_0)\,(0.53 \times 0.22)}$$

Substituting back to the initial integral

$$\int_{x_0}^{x} \left[\frac{dx}{\sigma_z(x)}\right] = \frac{1}{a}\int_{x_0}^{x} (10z_0)^{-0.53x^{-0.22}} x^{-q}\, dx$$

Where x_0 is 0 meters and x will vary and thus have to be calculated at each point downwind from the source. Therefore, the integral between those two points would be:

$$\int_{x_0}^{x} \left[\frac{dx}{\sigma_z(x)}\right] = \frac{1}{a}\left[\frac{(10z_0)^{-0.53x^{-0.22}} x^{0.22-b+1}}{\ln(10z_0)\,(0.53 \times 0.22)}\right]$$

Since at x_0=0, the term will cancel. Therefore, the deposition rate will be given by

$$\Gamma_d = \sqrt{\frac{2}{\pi}} \left(\frac{v_s}{x}\right) \frac{1}{a}\left[\frac{(10z_0)^{-0.53x^{-0.22}} x^{0.22-b+1}}{\ln(10z_0)\,(0.53 \times 0.22)}\right] \qquad (20)$$

Table 6.2. Results of the mathematical operations used in this section.

Operation	Result
$(af(x))'$	$\ln(a) a^{f(x)} f'(x)$
$\int a^{f(x)} dx$	$\frac{1}{f'(x)\ln(a)} a^{f(x)}\, dx$

6.3 Developing SNP markers to identify the *Pst* population

Table 6.3. Set of 96 SNP markers to identify *Pst* genetic groups, corresponding to Chapter 4 . Base pairs found for each population at each one of the positions for the 96 markers. Two columns indicating the % of error and the % of missing data used to find that marker are included. The last column shows which genetic group can be identified using the given marker.

SNP Marker	Group 1	Group 2	Group 3	Group 4	Group 5-1	% Error	% Missing data	Specific for:
10129_723	AA	AC	AA	AA	AA	0	10	Group 2
10318_2684	GG	CG	GG	GG	GG	0	10	Group 2
10318_2718	AA	AG	AA	AA	AA	0	10	Group 2
10722_2542	CC	CT	CC	CC	CC	0	10	Group 2
10722_2596	AA	AG	AA	AA	AA	0	10	Group 2
10789_3220	CC	CT	CC	CC	CC	0	10	Group 2
10892_3852	TT	CT	TT	TT	TT	0	10	Group 2
11282_5071	TT	AT	TT	TT	TT	0	10	Group 2
11282_5335	TT	CT	TT	TT	TT	0	10	Group 2
11587_2433	CC	CT	CC	CC	CC	0	10	Group 2
11588_391	AA	AG	AA	AA	AA	0	10	Group 2
12490_380	GG	TG	GG	GG	GG	0	10	Group 2
14936_554	GG	AG	GG	GG	GG	0	10	Group 2
15318_606	AA	AC	AA	AA	AA	0	10	Group 2
16389_951	AA	AG	AA	AA	AA	0	10	Group 2
23589_132	AA	AG	AA	AA	AA	0	10	Group 2
25458_2613	AA	AC	AA	AA	AA	0	10	Group 2
28668_2280	TT	CT	TT	TT	TT	0	10	Group 2
4368_396	TT	CT	TT	TT	TT	0	10	Group 2
6848_15952	CC	CT	CC	CC	CC	0	10	Group 2
6865_3945	TT	CT	TT	TT	TT	0	10	Group 2
7343_3422	TT	TG	TT	TT	TT	0	10	Group 2
7414_9882	CC	CT	CC	CC	CC	0	10	Group 2
7720_2763	GG	CG	GG	GG	GG	0	10	Group 2
7767_6171	AA	AT	AA	AA	AA	0	10	Group 2
8024_3203	GG	AG	GG	GG	GG	0	10	Group 2
8069_1156	AA	AG	AA	AA	AA	0	10	Group 2
8286_876	TT	CT	TT	TT	TT	0	10	Group 2
8449_1451	TT	CT	TT	TT	TT	0	10	Group 2
8449_1544	TT	CT	TT	TT	TT	0	10	Group 2
8549_13444	CC	CT	CC	CC	CC	0	10	Group 2
8623_4151	TT	AT	TT	TT	TT	0	10	Group 2
8805_7906	AA	AG	AA	AA	AA	0	10	Group 2

8888_2680	AA	AG	AA	AA	AA	0	10	Group 2
9149_1708	TT	CT	TT	TT	TT	0	10	Group 2
9827_1344	CC	CG	CC	CC	CC	0	10	Group 2
10127_1130	AA	AG	AG	AG	AA	0	20	Group 1 and Group 5-1
10441_749	TT	CT	CT	CT	TT	0	20	Group 1 and Group 5-1
2682_3747	CC	CC	CC	CC	CG	0	20	Group 5-1
7113_7055	GG	GG	GG	GG	CG	0	20	Group 5-1
10095_1765	CC	CC	CC	CC	CT	0	30	Group 5-1
15225_2855	AA	AA	AA	AA	AG	0	30	Group 5-1
6921_3712	TT	CT	CT	TT	TT	0	30	Group 2 and Group 3
7020_2447	CC	CC	CC	CC	CG	0	30	Group 5-1
7341_4368	AT	TT	TT	TT	AT	0	30	Group 1 and Group 5-1
7364_28843	AT	TT	TT	TT	TT	0	30	Group 1
7446_5852	GG	AG	GG	GG	AG	0	30	Group 2 and Group 5-1
7557_5505	GG	AG	AG	AG	GG	0	30	Group 1 and Group 5-1
7670_3524	CC	CT	TT	CT	CC	0	30	ALL
7716_4224	GG	AG	AG	AG	GG	0	30	Group 1 and Group 5-1
7802_6182	CC	CT	CT	CT	CC	0	30	Group 1 and Group 5-1
8291_7564	AA	AA	AA	AA	AG	0	30	Group 5-1
8552_2672	AA	AA	AG	AG	AA	0	30	Group 3 and Group 4
11685_2070	CC	CT	CC	CC	CC	10	10	Group 2
7753_15395	AG	GG	GG	GG	GG	10	20	Group 1

10441_476	TT	CT	CT	CT	TT	10	20	Group 1 and Group 5-1
13079_219	TT	CC	CC	CT	TT	10	30	ALL
2595_1398	CC	CT	CT	CT	CC	10	30	Group 1 and Group 5-1
59_4161	TT	AT	AT	AT	TT	10	30	Group 1 and Group 5-1
753_1139	CC	AC	AC	AC	CC	10	30	Group 1 and Group 5-1
10982_2778	GG	AA	AA	AG	GG	10	40	ALL
7802_6449	AA	AG	AG	AG	AA	10	30	Group 1 and Group 5-1
8182_11012	CC	AC	AC	AC	CC	10	30	Group 1 and Group 5-1
8301_20194	TT	CT	CT	CT	TT	10	30	Group 1 and Group 5-1
9120_5942	AT	TT	AA	AT	TT	10	40	ALL
9182_3916	GG	AG	AG	AG	GG	10	40	Group 1 and Group 5-1
7291_1846	AA	AA	AG	AG	AG	10	10	Group 1 and Group 2
14025_4585	TG	TT	TT	TG	GG	10	20	Group 2 and Group 3
26014_8757	CT	CT	TT	CT	CT	10	20	Group 3
7092_712	CC	CC	CT	CC	CC	10	20	Group 3
7092_715	TT	TT	CT	TT	TT	10	20	Group 3
7341_4770	CT	CT	TT	CT	CT	10	20	Group 3
7670_3437	TT	CT	CC	CT	TT	10	20	ALL
11355_1370	CC	CG	GG	CG	CC	10	30	ALL
11355_649	AA	AC	CC	AC	AA	10	40	ALL
11355_934	TT	CT	CC	CT	TT	10	30	ALL
12156_2790	TT	CT	CT	TT	CT	10	20	ALL
13932_495	CT	CT	CC	CT	CT	10	20	Group 3
19742_674	CC	CT	TT	CT	CC	10	30	ALL

21106_873	AA	AT	TT	AT	AA	10	30	ALL
6940_13038	AA	AG	GG	AG	AA	10	30	ALL
6940_13850	CC	CT	TT	CT	CC	10	30	ALL
6940_13871	GG	AG	AA	AG	GG	10	30	ALL
6940_13871	GG	AG	AA	AG	GG	10	30	ALL
7030_3696	AA	AA	AG	AA	AA	10	30	Group 3
7237_13346	GG	CC	CC	CG	GG	10	30	ALL
7237_8357	GG	CC	CC	CG	GG	10	30	ALL
7259_1082	CC	CT	TT	CT	CT	10	30	ALL
7369_14359	GG	TG	TT	TG	GG	10	30	ALL
7397_14343	TT	TG	GG	TG	TT	10	30	ALL
7582_7250	CT	CC	CT	CC	CT	10	30	Group 2 and Group 4
7582_8369	AG	GG	AG	GG	AG	10	30	ALL
7582_8747	CT	TT	CT	TT	CT	10	30	Group 2 and Group 4
7670_3586	TT	AT	AA	AT	TT	10	30	ALL
8617_14756	TT	CT	CC	CT	TT	10	30	ALL
9356_4561	TG	TG	GG	TG	TT	10	30	ALL

Table 6.4. Libraries sequenced using TruSeq Custom Amplicon Illumina method. Insert size and concentration for each one of the samples included is shown here.

Sample	Insert size	Concentration (ng/µl)	Norm (nM)
16.0164	307	8.62	43.26
16.0168	371	4.5	18.69
16.0665	320	7.78	37.46
16.0153	340	0.8	3.63
16.0662	309	7.52	37.5
16.0677	307	4.68	23.49
16.0660.	343	10.9	48.97
16.0676	317	9.56	46.47
16.0135	278	2.6	14.41
16.0138	310	2.16	10.74
16.0398	319	22.6	109.16
16.0669	350	3.26	14.35
16.0401	289	16.2	86.37
16.0216	304	25.2	127.73
16.0500.	289	5.88	31.35

16.0129	310	21.2	105.37
16.0183	285	18	97.32
16.0186	330	26.2	122.33
16.0605	303	4.02	20.44
16.0203	290	1.7	9.03
14/106	284	21.6	117.19
16.0139	306	19.9	100.2
16.0627	279	24.4	134.75
16.0626	298	6.5	33.61
F18	286	3.92	21.12
F22	289	8.56	45.64
13/14	291	0.548	2.9
14//7	328	0.242	1.14
15/157	319	0.512	2.47
16.0133	288	3.68	19.69
16.0127	383	29	116.67
16.0175	176	24.8	217.12
16.0402	290	37.2	197.65
16.0153	275	1.35	7.56
16.0170.	293	55.2	290.29
16.0176	288	33.8	180.83
16.0177	302	33.2	169.39
16.0157	312	25.6	126.43
16.0392	296	5.56	28.94
16.0397	304	28.6	144.96
16.0131	281	53	290.62
16.0161	289	50.2	267.65
Aby_2/16_S2	268	0.254	1.46
Aby_2/16_K1	284	6.74	36.57
Aby_3/16_K0	279	2.92	16.13
Aby_3/16_K1	293	8.36	43.96
Aby_3/16_S1	354	0.406	1.77
Aby_3/16_S1	242	0.252	1.6
Aby_5/16_K1	254	2.36	14.32
He_1/16_S0	252	6.96	42.56
He_1/16_S1	270	0.488	2.78
He_1/16_S2	282	6.36	34.75
He_1/16_S3	268	14.2	81.64
He_1/16_K0	288	21	112.35
He_4/16_K1	283	2.04	11.11
He_4/16_K2	281	9.24	50.67
He_5/16_K0	306	1.26	6.34

He_5/16_K1	284	3	16.28
He_5/16_K2A	337	0.894	4.09
He_5/16_K2B	343	3.38	15.18
He_5/16_K2C	289	41	218.6
He_5/16_K3	313	0.267	1.31
He_5/16_K4A	344	0.79	3.54
He_5/16_K4B	295	1.8	9.4
He_5/16_S1	284	1.07	5.81
He_5/16_S2	321	0.302	1.45
He_5/16_S3	288	4.24	22.68
He_5/16_S4	291	1.66	8.79
He_5/16_S5	286	0.554	2.98
He_6/16_S1	304	0.312	1.58
He_6/16_S2	324	0.482	2.29
He_6/16_S3	345	1.12	5
He_6/16_S6	320	1.2	5.78
He_6/16_S7	259	0.32	1.9
He_6/16_S8	423	0.654	2.38
He_6/16_S9	254	21.4	129.82
He_6/16_K1	288	1.15	6.15
He_6/16_K8	302	9.58	48.88
14/56	269	16	91.65
14/63	280	17.1	94.1
14/119	259	3.56	21.18
14/124	275	17.3	96.93
14/16	275	15.4	86.29
14/113	305	2.88	14.55
15/157	285	1.1	5.95
T_1/16_K3	277	2.86	15.91
T_2/16_K2	266	6.1	35.33
T_6/16_S3A	272	5.18	29.34
T_5/16_K3B	276	7.34	40.98
T_6/16_S6	271	7.02	39.91
T_6/16_S8	271	11.8	67.09

Table 6.5. List of FAM, HEX, and Common primers for the 36 markers. The fluorescence tail is coloured as blue (FAM) or green (HEX) and the last base that will amplified is highlighted in red. For each primer, the marker, its name, the specific SNP are indicated. A column showing the group that each primer triplet can differentiate is also included.

Marker	Name	SNP	Group	FAM (X-axis)	HEX (Y-axis)	Common	Orientation
10127_1130	CLPST153	G1130A	1 and 5-1	GAAGGTGACCAAGTTCATGCTGCAAGTTCAGCCTCGACg	GAAGGTCGGAGTCAACGGATTGCAAGTTCAGCCTCGACa	CAAGCGAAACAACAAAGCAG	
10441_476	CLPST154	C476T	1 and 5-1	GAAGGTGACCAAGTTCATGCTGGTGCTGCCAAGGCTGTc	GAAGGTCGGAGTCAACGGATTGGTGCTGCCAAGGCTGTt	TGAGGGCAGGGATAACTTTG	
7670_3524	CLPST160	C3524T	ALL	GAAGGTGACCAAGTTCATGCTCTGAATATGATTTTGATGGATCg	GAAGGTCGGAGTCAACGGATTCTGAATATGATTTTGATGGATCa	GCTCACAAGGCTTCGTTTG	REVERSE
10982_2778	CLPST163	G2778A	ALL	GAAGGTGACCAAGTTCATGCTACCAGCAGGTTTCGATCTTTc	GAAGGTCGGAGTCAACGGATTACCAGCAGGTTTCGATCTTTt	CTTGTCCCCGCTGTATCATC	REVERSE
7291_1846	CLPST167	G1846A	1 and 2	GAAGGTGACCAAGTTCATGCTTCTCGACATAAGAGCCACCAg	GAAGGTCGGAGTCAACGGATTTCTCGACATAAGAGCCACCAa	ATGTGGCTATCCCAACCAAC	
11355_649	CLPST171	A649C	All	GAAGGTGACCAAGTTCATGCTTTCAGTGCCAAAAACGTCa	GAAGGTCGGAGTCAACGGATTTTCAGTGCCAAAAACGTCc	CACATGGACATCAGGGTGAG	
10129_723	PST-1	C723A	2	GAAGGTGACCAAGTTCATGCTTCGTCAGTACATGTTCAAAAGAATg	GAAGGTCGGAGTCAACGGATTTCGTCAGTACATGTTCAAAAGAATt	TAGTAGCGCCCACAGATGAC	REVERSE
11282_5335	PST-2	t5355c	2	GAAGGTGACCAAGTTCATGCTCAGAGAGAGCGTGGAGGAt	GAAGGTCGGAGTCAACGGATTCAGAGAGAGCGTGGAGGAc	CAACCCATCTCACAACCACG	
11685_2070	PST-3	C2027T	2	GAAGGTGACCAAGTTCATGCTGGATTTCATTCGATTGCTGCg	GAAGGTCGGAGTCAACGGATTGGATTTCATTCGATTGCTGCa	CAGTTGCTGGAATCCGATCA	REVERSE
4368_396	PST-4	T396C	2	GAAGGTGACCAAGTTCATGCTCCCATTGTCAAATCCTTCCTGa	GAAGGTCGGAGTCAACGGATTCCCATTGTCAAATCCTTCCTGg	CACCCGATTAGCTGAACAGT	REVERSE
6848_15952	PST-5	C15952T	2	GAAGGTGACCAAGTTCATGCTCGTATTCACATTCTCTTCTGCTTTg	GAAGGTCGGAGTCAACGGATTCGTATTCACATTCTCTTCTGCTTTa	GATGTAAACCTCCTCTTCCACT	REVERSE
7414_9882	PST-6	c9882t	2	GAAGGTGACCAAGTTCATGCTGAGAGACGGTTCCTGGTGc	GAAGGTCGGAGTCAACGGATTGAGAGACGGTTCCTGGTGt	CATGGTTAGTAAGTCAAGCCACA	
7720_2763	PST-7	g2763c	2	GAAGGTGACCAAGTTCATGCTTGGTCGATATTCTCTCCTCTCg	GAAGGTCGGAGTCAACGGATTTGGTCGATATTCTCTCCTCTCc	TGGCTTCAGTATTCGAACAAGT	
8069_1156	PST-8	A1156G	2	GAAGGTGACCAAGTTCATGCTGAACCTTTCTCGAGACATCATTATt	GAAGGTCGGAGTCAACGGATTGAACCTTTCTCGAGACATCATTATc	TCCATGGCAAGAGACGAATT	REVERSE
8286_876	PST-9	t876c	2	GAAGGTGACCAAGTTCATGCTAATCAAGGTTCATTCCGCCt	GAAGGTCGGAGTCAACGGATTAATCAAGGTTCATTCCGCCc	ACCAACGTCCGGAACTGAAA	
8805_7906	PST-10	a7906g	2	GAAGGTGACCAAGTTCATGCTTCTCGAGTACTTGGAAATCTGAa	GAAGGTCGGAGTCAACGGATTTCTCGAGTACTTGGAAATCTGAg	GTCCACTCCACCAACTACCA	
10441_749	PST-11	C749T	1 and 5-1	GAAGGTGACCAAGTTCATGCTGAGTCCCCAATAAAGTCGGTg	GAAGGTCGGAGTCAACGGATTGAGTCCCCAATAAAGTCGGTa	GTATCCATACTCACACGCGC	REVERSE
2682_3747	PST-12	c3747g	5-1	GAAGGTGACCAAGTTCATGCTAGACCGAGTTCAGCGAGAc	GAAGGTCGGAGTCAACGGATTAGACCGAGTTCAGCGAGAg	TTGGTTGGCGTGAGGTGAT	
15225_2855	PST-13	a2855g	5-1	GAAGGTGACCAAGTTCATGCTGCTTCCATTGGTCAGGTTGa	GAAGGTCGGAGTCAACGGATTGCTTCCATTGGTCAGGTTGg	TACGTACTTACCCCGGATCG	
6921_3712	PST-14	T3712C	2 and 3	GAAGGTGACCAAGTTCATGCTCAAGCAGCAGAAGTAGTAATCCTa	GAAGGTCGGAGTCAACGGATTCAAGCAGCAGAAGTAGTAATCCTg	AGGATGACTCGGAAGCTGAT	REVERSE
7341_4368	PST-15	a4368t	1 and 5-1	GAAGGTGACCAAGTTCATGCTGTCCAGTTGCAGAGATTGGa	GAAGGTCGGAGTCAACGGATTGTCCAGTTGCAGAGATTGGt	TGGCTATACAGTGGATCGCT	
7364_28843	PST-16	T28843A	1	GAAGGTGACCAAGTTCATGCTCGCTCTTGGGGTAGATGGa	GAAGGTCGGAGTCAACGGATTCGCTCTTGGGGTAGATGGt	ACACCCCTCCACTCTCCTC	REVERSE
753_1139	PST-17	c1139a	1 and 5-1	GAAGGTGACCAAGTTCATGCTTGTTCTCGGGCAGGTTGAc	GAAGGTCGGAGTCAACGGATTTGTTCTCGGGCAGGTTGAa	AGAGTTTGGTTTGAAGGTGGT	
8291_7564	PST-18	A7564G	5-1	GAAGGTGACCAAGTTCATGCTGGAAGGGGTATCTTACAAGTTGATt	GAAGGTCGGAGTCAACGGATTGGAAGGGGTATCTTACAAGTTGATc	CCCCACTCTCTCCTGAAATTG	REVERSE
8552_2672	PST-19	A2672G	3 and 4	GAAGGTGACCAAGTTCATGCTCTCCTTACCCACTCCTACGt	GAAGGTCGGAGTCAACGGATTCTCCTTACCCACTCCTACGc	CCTCAGTCGTTCCTCCACTT	REVERSE
9182_3916	PST-20	g3916a	1 and 5-1	GAAGGTGACCAAGTTCATGCTGCGTCATCATCGGTAGTCTg	GAAGGTCGGAGTCAACGGATTGCGTCATCATCGGTAGTCTa	TTGAAAGCAGCGTAACCCAG	
7291_1846	PST-21	g1846a	1 and 2	GAAGGTGACCAAGTTCATGCTCTCGACATAAGAGCCACCAg	GAAGGTCGGAGTCAACGGATTCTCGACATAAGAGCCACCAa	TGGTCAATCACAGCTGGTAAC	
7670_3524	PST-22	C3437T	ALL	GAAGGTGACCAAGTTCATGCTTGCTGAATATGATTTTGATGGATCg	GAAGGTCGGAGTCAACGGATTTGCTGAATATGATTTTGATGGATCa	TCCAACCCAAGATTGCGATC	REVERSE
19742_674	PST-23	c674t	ALL	GAAGGTGACCAAGTTCATGCTTCTCCTGGATATGCGCTTCc	GAAGGTCGGAGTCAACGGATTTCTCCTGGATATGCGCTTCt	GGGTTTTGGATTGGCTGGAA	
6940_13850	PST-24	C13850T	ALL	GAAGGTGACCAAGTTCATGCTGTCCCTTGGTCCTGAACTTTg	GAAGGTCGGAGTCAACGGATTGTCCCTTGGTCCTGAACTTTa	TGGTGAGTGGTACTATTCGGT	REVERSE
7582_8369	PST-25	g8369a	2 and 4	GAAGGTGACCAAGTTCATGCTAAGGACAAGGCGAGGTTCAg	GAAGGTCGGAGTCAACGGATTAAGGACAAGGCGAGGTTCAa	ACGTCCACCACCTCGATATC	
7341_4770	PST-26	c4770t	ALL	GAAGGTGACCAAGTTCATGCTGGTCTTGGCTTATCTCGTCc	GAAGGTCGGAGTCAACGGATTGGTCTTGGCTTATCTCGTCt	TGGCCCTTGGGTGGAAAA	
7582_8747	PST-27	t8747c	ALL	GAAGGTGACCAAGTTCATGCTGGATATCGACCTAGAGCAGATTAt	GAAGGTCGGAGTCAACGGATTGGATATCGACCTAGAGCAGATTAc	GTCCACCACGATGTCCCC	
6940_13871	PST-28	a13871g	ALL	GAAGGTGACCAAGTTCATGCTTCGGTCAAACAAACGATCTc	GAAGGTCGGAGTCAACGGATTTCGGTCAAACAAACGATCTt	ACCGTCGTTCCAGCTATCTT	REVERSE
7237_13346	PST-29	g13346c	ALL	GAAGGTGACCAAGTTCATGCTACTTCTACTCTTCGACTGACCg	GAAGGTCGGAGTCAACGGATTACTTCTACTCTTCGACTGACCc	CGGCAGATTGTGTGGATGAA	
7397_14343	PST-30	t14343g	ALL	GAAGGTGACCAAGTTCATGCTGGGGATCCGAGAAATGTGTTa	GAAGGTCGGAGTCAACGGATTGGGGATCCGAGAAATGTGTTc	GCTGGTAATTGGTAAGCTTTGT	REVERSE